Layer-by-Layer Spin-Assembly of Carbon Nanotube Incorporated H-Bonded Multilayer Films

by

Hüseyin Enis KARAHAN

A Thesis Submitted to the

Graduate School of Engineering

in Partial Fulfillment of the Requirements for

the Degree of

Master of Science

in

Materials Science and Engineering

Koç University

September 2012

Koç University

Graduate School of Sciences and Engineering

This is to certify that I have examined this copy of a master's thesis by

Hüseyin Enis KARAHAN

and have found that it is complete and satisfactory in all respects,

and that any and all revisions required by the final

examining committee have been made.

Committee Members:

_____

A. Levent DEMİREL, Ph. D. (Advisor)

_____

F. Seniha GÜNER, Ph. D.

_____

Fevzi Çakmak CEBECİ, Ph. D.

_____

Özgür BİRER, Ph. D.

_____

Annamaria MİKO, Ph. D.

Date: _____

Ubi materia, ibi geometria.

[Where there is matter, there is geometry.]

Johannes KEPLER (1571 – 1630)

This thesis is dedicated to my brilliant nephew Tuna Kaan KAYA and to my lifelong guide Prof. Dr. Şerife Birgül TANTEKİN.

ABSTRACT

Various inorganic materials have been incorporated in organic multilayers using electrostatically-driven layer-by-layer (LbL) nanotechnology. However, weak interactions such as H-bondings, pi-pi stackings, and hydrophobic effects have not been employed as much as electrostatic forces in organic-inorganic hybrid LbL systems. This thesis introduces new procedures to prepare pristine carbon nanotube (CNT) containing LbL nanocomposites using weak intermolecular interactions and investigates the factors affecting the multilayer growth and the pH-stability of resulting films. The central idea is to noncovalently stabilize CNTs in assembly solutions of H-bonded multilayer (*hb*-multilayer) films in which polyvinylpyrrolidone (PVPon) is H-bonding acceptor and tannic acid (TA) is H-bonding donor. Single-wall CNTs (SWCNT) were first dispersed in aqueous TA solutions (resulting in TA-SWCNT) taking advantage of pi-pi stackings between aromatic moieties of TAs and pi-conjugated surfaces of CNTs. Buffering agents were not used in assembly solutions/dispersions because pristine CNTs aggregate in the presence of cations. Also, the usage of branched polyethyleneimine (BPEI) as an anchoring layer was avoided considering potential bioapplications. We used spin-assisted LbL (spin-LbL) for assembling *hb*-multilayers because it is faster compared to dip-assisted LbL (dip-LbL) and also requires less solutions/dispersions. In spin-LbL of BPEI-free multilayers, the multilayer growth profiles showed exponential-like initial phase followed by linear growth in the presence and absence of SWCNTs. We further examined this observation by studying dip- and spin-LbL of CNT-free PVPon/TA multilayers. Control experiments using dip-LbL showed zigzag-like exponential growth independent of the factors of BPEI, pH, and ionic strength. These observations differ from previously reported growth profiles of dip-LbL of (BPEI)(PVPon/TA)$_n$ which showed zigzag-like linear growth. Both the growth profiles and pH-stabilities of (PVPon/TA)$_n$ spin-multilayers showed significant dependence on the timescale of film deposition and pH-dependent disintegration processes. The differences were discussed in terms of kinetic trap of molecules in less favorable conformations in spin-assembled multilayers. Then, we prepared PVPon-functionalized SWCNT dispersions (resulting in PVPon-SWCNT) which are thought to be governed by a combination of charge-

transfer interactions, hydrophobic effects, and weak H-bondings. As a next step of our previous efforts, various combinations of SWCNT-doped *hb*-multilayers were prepared and characterized: $(PVPon\text{-}SWCNT/TA)_n$, $(PVPon/TA\text{-}SWCNT)_n$, and $(PVPon\text{-}SWCNT/TA\text{-}SWCNT)_n$. We successfully incorporated SWCNTs in *hb*-multilayers without sacrificing film stability using a combination of two different noncovalent functionalization routes and LbL technique. When the contact times of assembly fluids and growing films are minimized, growth profiles of SWCNT-doped *hb*-multilayers all showed perfectly linear growth. This suggests that well-defined bilayers having uniform thickness, less surface roughness, and reduced interdigitation between layers are obtained as a result of spin-LbL. The higher pH-stability observed for $(PVPon\text{-}SWCNT/TA\text{-}SWCNT)_n$ multilayers was mainly attributed to the hydrophobic stabilization of multilayers by CNT-CNT interactions. PVPon/TA pair is important for biomedical applications and SWCNTs are promising pharmaceutical excipients. The SWCNT-doped *hb*-multilayers introduced in this thesis have great application potential as novel biomaterials.

ÖZET

Birçok inorganik malzeme elektrostatik-temelli katmer nanoteknolojisi kullanılarak organik çokkatmanlıların yapısına katılmıştır. Ancak, H-bağları, pi-pi istiflenmeleri ve hidrofobik etkiler gibi zayıf etkileşimler katmerli melez (organik-inorganik) yapılarda elektrostatik bağlar kadar yoğun kullanılmamıştır. Bu tez bozulmamış karbon nanotüpler (KNT) içeren katmerli nanokompozitlerin hazırlanması için yeni yönergeler sunmakta ve ortaya çıkan filmlerin çokkatmanlı büyümesine ve pH-kararlılığına etkiyen etmenleri araştırmaktadır. Yararlanılan esas fikir, PVPon'un H-bağı alıcısı ve TA'nın H-bağı vericisi olduğu H-bağlı çokkatmanlıların (*hb*-çokkatmanlı) yapılanma çözeltilerinde KNT'lerin kararlı hale getirilmesidir. KNT'ler öncelikle, TA'ların aromatik kısımları ile tek katmanlı KNT'lerin (TKKNT) pi-eşlenik yüzeyleri arasında kurulan pi-pi istiflenmelerinden yararlanılarak, sulu TA çözeltilerinde (TA-TKKNT elde edilmek üzere) dağıtılmıştır. Katyonların varlığında bozulmamış KNT'lerin topaklaşması sebebiyle, tamponlama tuzları yapılanma çözeltilerinde/dispersiyonlarında kullanılmamıştır. Aynı zamanda, olası biyolojik uygulamaları göz önüne alarak, yapışma katmanı olarak dallı polietilenimin (DPEI) kullanılmasından kaçılmıştır. Daldırmalı katmer yöntemine göre daha hızlı olması ve daha az çözelti/dispersiyon gerektirmesi sebebiyle, döndürmeli katmer yöntemi *hb*-çokkatmanlıların oluşturulmasında kullanılmıştır. Hem TKKNT'lerin mevcut olduğu, hem de olmadığı durumda; DPEI içermeyen çokkatmanlılar üstelimsi başlayan ve doğrusal devam eden bir büyüme davranışı sergilemiştir. Sonraki aşamada, KNT'siz PVPon/TA çokkatmanlılarının daldırmalı ve döndürmeli büyümesini çalışarak bu gözlem incelemeye tabi tutulmuştur. Daldırmalı katmer yöntemi kullanılan kontrol deneyleri; DPEI, pH ve iyonik kuvvetleri etkenlerinden bağımsız bir şekilde zigzag-benzeri üstel büyüme göstermiştir. Bu gözlemler, daldırma ile büyütülmüş (DPEI)$(PVPon/TA)_n$ örtülerinin zigzag-benzeri doğrusal büyüdüğünü gösteren önceki kayıtlardan farklılaşmaktadır. Döndürme ile büyütülen $(PVPon/TA)_n$ çokkatmanlılarının hem büyüme, hem de pH'ye bağlı bozunma süreçleri kaydadeğer bir şekilde süre bağlılığı göstermiştir. Döndürme ile kurulan çokkatmanlı örtülerde moleküllerin elverişsiz biçimlerde kinetik tuzağa yakalanması üzerinden kaydedilen farklar tartışılmıştır. Ardından, TKKNT'ler PVPon ile (PVPon-TKKNT elde edilmek üzere),

yük-aktarımı etkileşimleri, hidrofobik etkiler ve zayıf H-bağlarının bir muhtemel bir bileşimi sayesinde işlevleştirilmiştir. Önceki uğraşının bir ileri adımı olarak, TKKNT ile yüklenmiş $(PVPon\text{-}TKKNT/TA)_n$, $(PVPon/TA\text{-}TKKNT)_n$ ve $(PVPon\text{-}TKKNT/TA\text{-}TKKNT)_n$ *hb*-çokkatmanlı biçimleri hazırlanmış ve nitelendirilmiştir. Bu çalışmada, iki farklı kovalent olmayan işlevselleştirme tarzı ve katmer yöntemi kullanılarak, TKKNT'ler *hb*-çokkatmanlılara film kararlılığından taviz vermeden ve başarılı bir şekilde katılmıştır. Yapılanma sıvıları ile büyüyen örtüler arasındaki temas süreleri azaltıldığında, TKKNT yüklenmiş *hb*-çokkatmanlılar mükemmel derecede doğrusal büyüme göstermiştir. Bu durum, döndürmeli katmer yönteminin bir sonucu olarak birörnek kalınlığa, düşük yüzey pürüzlülüğüne ve azalmış kenetlenmeye sahip sınırları iyi belirli çiftkatmanlıların elde edildiğini düşündürmektedir. $(PVPon\text{-}TKKNT/TA\text{-}TKKNT)_n$ çokkatmanlısının yüksek pH-kararlılığı KNT-KNT etkileşimleri sayesinde gerçekleşen hidrofobik kararlılaşmaya bağlanmıştır. PVPon/TA biyomedikal uygulamalar açısından önemli bir katmer çiftidir ve TKKNT'ler gelecek vaadeden ilaç katkılarıdır. Bu tezde ortaya konan TKKNT yüklenmiş *hb*-çokkatmanlılar özgün biyomalzemeler olarak büyük bir uygulama potansiyeline sahiptir.

ACKNOWLEDGEMENTS

At the end of a couple years, one came up with a bunch of ideas and findings which build up a thesis. In normal circumstances, it is for sure a matter of intellectual property of the owner of the thesis. But in reality, this is not so simple and inevitably many people directly or indirectly contribute to the work. So, to thank is not only an emotional, but also a professional obligation of the scientists and engineers. Also, it is not easy and fair to be concise in such a serious responsibility.

I met Dr. DEMİREL in "cyber world" to ask for a couple of papers of him and his colleagues when I was working in a private company. He was abroad and busy but immediately responded my e-mail with nice explanations and attachments. His generosity and kindness attracted me and I became a fun of his papers. After two years, I moved to Koç University and got the chance to work with him. He well-analyzed me and individually introduced most of the techniques by himself. He then inspired and supported me to grow not only as a researcher, but also as a self-sufficient and independent thinker. He was always in his office (or in laboratory) when I need him. Moreover, he always let me to develop new ideas, design experiments and commit them in my own way. He always gave credit to me when I do right, and shouldered the responsibility when I fail. Also, he refined the "physical" taste in my studies which is a once-in-a-lifetime opportunity. Last, he created an intellectually satisfying scientific environment with highly potent and nice team members which I benefited and hopefully contributed.

First, I would like to mention two special courses to me which were given by Dr. Levent DEMİREL and Dr. Mehmet SAYAR in Koç University as "Surface and Interface Properties of Materials" and "Intermolecular and Surface Forces" respectively. I have been deeply impressed from the content and style of those courses, and I have found the answers of many questions in my mind following the path showed in those courses. Somehow, these two courses complimented my past learning efforts towards the understanding of life and matter.

I learned the fundamentals of layer-by-layer technology from Dr. İrem EREL when she was working in our laboratory. She let me observe experimental tricks and allowed me to contribute her research. She was also very instructive in our discussions about supramolecular

chemistry. Pınar TATAR was always generous to fill up my gaps of knowledge in chemistry. I learned much of her about the experimental routines of our laboratory. Moreover, I enjoyed her scientific discussions which we frequently made. The contribution of Dr. Annamaria MIKO was also crucial. When my attention to carbonaceous materials had rekindled, she provided me her own carbon nanotube samples and she always encouraged me to try. Also, when I was her assistant in undergraduate chemistry laboratories, I learned several things which were critical for me as a nonchemist in the world of chemistry. I would also like to express my gratitude to Dr. Sanjay LATTHE for his good questions, limitless kindness and friendship. The rest of our laboratory members also indirectly helped me; at least they were always kind and participative in laboratory works. And, our smart students Yonca YAKUT, Eda İdil ÇOKER, Lütfiye EYÜBOĞLU (a.k.a. Çekirge), and Deniz KIYILAR (a.k.a. HalleDeniz)... Eda&Yonca (intentionally adjacent) accepted to try our fancy ideas and we gained valuable insights about layer-by-layer technique thanks to them. Contributions of Lütfiye and Deniz deserve a special mention. They were brilliant whilst helping me for many time-consuming and laborious experiments. They devoted themselves to our study taking our job serious as a fellow. Much more importantly, they asked questions worth to think about and some “mysteries” were ultimately solved. Moreover, without them, third chapter of this work was almost unthinkable.

Out of our laboratory was also quite helpful. I should first specially acknowledge Dr. Özgür BİRER. He was extremely helpful and open-hearted. He allowed us to use their facilities (e.g. ultrasonic horn setup) without hesitation, and I learned much of him. I also got assistance from his outstanding team (Recep KAŞ and Cansu YILDIRIM) throughout wonderful discussions (“Could you please explain me the cavitation phenomena one more time?!.”). Dr. Uğur ÜNAL and his student Ceren YILMAZ were also helpful; they made me feel at home in their laboratory. Dr. Mehmet SOMER wide opened his knowledge and facilities, and Selçuk ACAR was always helpful whenever I need him. Dr. Murat SÖZER and Bekir YENİLMEZ caused us to learn more about the dispersion of carbon nanomaterials (we made macrocomposites of sonolyzed graphite with them). Bekir also carefully prepared an apparatus for sonic bath to hold dispersion vessels. In characterization parts, I have also benefited from the infrastructure and human resources of KUYTAM. Dr. ÜNAL, Dr. BİRER and Dr. Barış YAĞCI helped me much throughout the operation of several devices or they meticulously performed the measurements. Also, Muharrem GÜLER (The Usta) made several nice glass works which made life easier and he solved our many technical problems.

Experimental results and scientific words are generally too dry to get attraction in the absence of high quality graphical representations. Analysis of huge data sets is also impossible without useful softwares. So, I like to acknowledge technical teams of MATLAB and Octave. In parallel, I am indebted to many anonymous people of open-code (mainly ".m") community all around the world and to Anders Brun for "Myaa" plugin which is available in official webpage of MatWorks, Inc. I have also exploited various softwares and tools for graphical illustrations. I want to acknowledge the developers of those nice projects: CoNTub, Nano-Tube Modeler, Inkscape, ImageBot, SVG-edit, GIMP, and EasyCapture. Finally, Mendeley Desktop, Wikipedia, and Google (not the Scholar one), I love you so much!

Special thanks go to my family and friends (particularly to Ahmet Can BERKYÜREK, Bekir, Bilge ERCAN, Caner NAZLI, Cansu, Ceren, Deniz, Gonca BAYRAKTAR, Hande ÖZTÜRK, Hasan SİNİR, Koral ÖZGÜL, Kurtuluş ÖZTÜRK, Lütfiye, Pınar, Recep, and Selçuk in alphabetic order) for their helps and constant encouragement. Lastly, I am sincerely indebted to my committee members who kindly provided valuable feedbacks to refine this manuscript. Particularly, I am grateful to Dr. F. Seniha GÜNER and to Dr. Fevzi Çakmak CEBECİ because they kindly accepted our invitation as committee members.

TABLE of CONTENTS

LIST of TABLES

LIST of FIGURES

LIST of EQUATIONS

NOMENCLATURE

AFM:	Atomic force microscopy
(B)PEI:	(Branched) poly(ethylene imine)
CAM:	Contact angle measurement
CFS:	Carbon few-sheet
CNB:	Carbon nanoball
CNP:	Carbon nanoparticle
CNS:	Carbon nanosheet
CNT:	Carbon nanotube
DLS:	Dynamic light scattering
DLVO:	Derjaguin, Landau, Verwey, and Overbeek
DW:	Double-wall(ed)
EMM:	Ellipsometry (measurement)
es-:	Electrostatic
(FE-)SEM:	(Field emission) scanning electron microscopy
FTIR:	Fourier-transform infrared
hb-:	Hydrogen-bonded
IS:	Ionic strength
L-B/S:	Langmuir-Blodgett/Schaefer
LbL:	Layer-by-layer
MW:	Multi(ple)-wall(ed)
OAS:	Optical absorption spectroscopy
OLM:	Optical light microscopy
PVPon:	Poly(*N*-vinyl-2-pyrrolidone) or polypropylene glycol
PLU:	Pluronics®
QCM:	Quartz crystal microbalance
RSM:	Raman scattering microscopy
RSS:	Raman spectroscopy
SAM:	Self-assembled monolayer
SEM:	Scanning electron microscopy
SW:	Single-wall(ed)
TA:	Tannic acid
TGA:	Thermogravimetric analysis
UV-vis:	Ultraviolet-visible
vdW:	van der Waals
vHS:	van Hove singularity
XPS:	X-ray photoelectron spectroscopy
ZPA:	Zeta potential (analysis)

GENERAL INTRODUCTION and OVERVIEW

Supramolecular chemistry brings molecular units having different functions together via intermolecular interactions to form/assemble “supramolecule”s which have multifunctional properties [1-5]. As an interdisciplinary subfield of contemporary physical science, supramolecular chemistry unifies basic themes such as macromolecules (polymers), particles, colloids, and surfaces in smaller dimensions [6-10]. Supramolecular approaches offer novel opportunities to manufacture nanofeatured and/or nano-ordered assemblies which makes is an emerging tool of nanochemistry [3,8,11-13]. Supramolecular chemistry also provides valuable insights for understanding cellular processes [11,14-18] and molecular/genetic evolution of life [19-24]. Molecules (and molecular or multiatomic clusters) substitute the role of atoms of conventional chemistry [2,7,25]. Differences between conventional and supramolecular chemistries are not limited to the selection of building blocks; the nature of interactions differs too. Conventional chemistry is principally established on covalent linkages, whereas the basic driving force of supramolecular systems is molecular self-assembly [2,26-27]. Broadly speaking; self-assembly denotes the interplay of spontaneous, complex and somehow intrinsically directed interactions between molecular entities through relatively weak intermolecular forces [28-30]. Just as Nature achieved in biological assemblies through self-assembly [3,31-33], supramolecular approach combines chemical and/or biological building blocks to generate functional and ordered materials. In addition, as counterparts of bioassemblies, supramolecular assemblies usually reveal a dynamic or at least environmentally responsive behavior [13,32,34-35]. Therefore, the common tendency to place supramolecular chemistry under the boundaries of chemistry,

physics, and biology [34,36] can be justified in the heart of self-assembly phenomena. So it is not a surprise, “supramolecular science” term has found increasingly popularized usage in the current literature.

There are two main strategies of fabricating nanomaterials: Top-down and bottom-up. Philosophical routes of top-down miniaturization were clearly manifested in the renown 1959 talk [37] of Feynman. The core concept of Feynman’s miniaturization notion is controlling and manipulating matter in atomic scales. Feynman’s foresight of miniaturization has been practiced through carving materials via nanolithography. However, top-down approach is virtually limited to hard materials and is not feasible for fabricating complex and dynamic nanoarchictectures [38-40]. Instead, as one of the fundamental tools of bottom-up nanofabrication, self-assembly is flexible and practical enough to create complex and responsive (e.g. pH-responsiveness) materials. In today’s nanotechnology, a wide range of materials (e.g. organic molecules, inorganic nanoparticles) can be used in many ways to buildup nanoassemblies based on self-assembly. Probably the first and frequently unintentional usages of self-assembly in nanotechnology are phase-separation in bulk polymeric blends as nanoclusters and nanodomain formation in (block)-co-polymers [41-44]. Another self-assembly related and conventional technique is the preparation of filled composites using nanoparticles [45-46]. One major extension of self- and/or guided-assembly in nanotechnology is the fabrication of multilayer ultrathin films or capsules using LbL assembly technology (see Chapter 1.1) [47-50]. This thesis on the other hand, focuses on assembly of nanotube-doped multilayers as a combination of last two approaches. Indeed, this is a hot topic of current LbL technology (see Chapter 1 below for further information).

Current nanotechnology is dominated by materials studies [35,51-55]. In the last couple of decades, scientific and industrial communities have paid increasing attention [24,52,54-58] to nanotechnology and to nanomaterial research accordingly. Many types of chemically or biologically synthesized nanoparticles have been introduced, developed and patented for different applications. As a general rule, remarkable performance of nanoparticles in those systems are favored by their geometrical (dimensionality, size and shape) and surface-related properties which are also interconnected. Predictions and experimental work on quantum confinement phenomena [59-62] explained some of peculiar optical and electrical properties of nanoparticles. In accordance, for many nanoparticulate systems, a direct correlation between geometrical and surface properties with thermal, mechanical, and biological characteristics were revealed [59,61,63-69]. Thus, nanoparticles

are generally acknowledged with their geometrical features[1] (e.g. nanodots, nanotubes, nanosheets) [68-70] and surface characteristics (i.e. functionalized/unfunctionalized, coated/uncoated see Chapter 1). Up to some extent, geometrical and surface properties of nanoparticles are controlled in the synthesis stage [62,71-72], but post-synthesis routines are also crucial for applications. For instance, solvent processability of some nanoparticles (e.g. CNT, boron nitride few-layers) is low to obtain stable colloidal dispersions[2] and this gives rise to the need of surface functionalization. Surface functionalization of nanoparticles can be maintained covalently and/or noncovalently. Added chemical functionalities through covalent modifications may hinder intrinsic properties of nanoparticles (see Chapter 1.2). On the contrary, noncovalent routes preserve nanoparticles close to their pristine state (see Chapter 1.2.6 below for details). This golden rule emphasizes the benefits of supramolecular chemistry and self-assembly in nanotechnology. As a result, especially for nanocomposite material applications, there is a tendency to put noncovalent chemistry to work.

Following "General Introduction and Overview" which clarifies the main concepts, this thesis is divided into five chapters starting with the literature background (Chapter 1). We introduce comprehensive surveys on LbL (self-)assembly (including nanoparticle-doped multilayer films) and CNT science. LbL and CNT fields have highly active literatures with hundreds of publications per year (see Appendix-A), where citation errors are so common indeed. So, in addition to an emphasis on the basics and technical aspects, we tried to provide historical perspectives on the development of these fields as well. However, experimental chapters also contain their specific introductory subsections. Hence, given literature background is not compulsory to follow the thesis, but highly recommended in case of need and also it helps reader to comprehend our contributions to the field. Starting from Chapter 2, we introduce our original contributions. Chapter 2 shows the incorporation of SWCNTs in spin-assisted multilayer films of PVPon and TA using TA as a mediator and additionally discusses the exponential growth in PVPon/TA multilayers. In the following chapter (Chapter 3), we further investigate the spin-LbL of PVPon/TA multilayers and discuss the nature and conditions of film stability. Chapter 4 advances our efforts on the incorporation of SWCNTs into PVPon/TA multilayer films by using PVPon as an additional mediator. This chapter provides information on possible hydrophobic stabilization of multilayers by SWCNT-

[1] For certain applications differently shaped nanoparticles might be preferred.

[2] Selection of appropriate solvents can make nanoparticles readily dispersible just after the synthesis, but solvent selection is frequently restricted.

SWCNT interactions. In the last chapter (Chapter 5) we first highlight the conclusive remarks of this study. Then we introduce our future outlook emphasizing our parallel works (i.e. incorporation of copper-based fine crystals in PVPon/TA multilayers, employment of PLU-stabilized SWCNT dispersions in PLU/TA multilayers) about the topic. As future directions we also specifically point out some aspects which are beyond the scope of our activities, which deserve to be investigated on their own account.

Chapter 1: LITERATURE BACKGROUND

Molecularly organized multilayer films are promising tools of nanotechnology for realistic applications [13,47,73-76]. Depending on the application of interest, one can design the final structure of multilayer film in detail. Main step of multilayer design is the proper selection of a mutually interacting couple as building blocks of assembly. Then, a suitable growing method such as L-B/S, SAM, or LbL is employed to fabricate multilayer nanocoatings. Even though, it is younger than L-B/S, this field is already dominated by LbL technique. Underlying reasons of the success of LbL are its versatility in selection of building blocks (e.g. polymers, particles) and its simplicity in operation. Detailed comparison of L-B/S, SAM, and LbL is beyond the aim of this literature survey, but a small comparison is available in Appendix-B and further information can be found elsewhere [13,39,77-78]. Instead, historical, theoretical, and technical aspects of LbL field are covered including nanoparticle-loaded applications. Subsequently, CNTs were introduced in a detailed manner to justify its selection and to create a basis before introducing our experimental works.

1.1. LAYER-by-LAYER SURFACE DEPOSITION

LbL deposition technology is a bottom-up surface modification technique that can incorporate a wide range of materials into nanocomposite molecular architectures [13,79]. Attracting building blocks are assembled (see Figure 1-1 below) on substrates via intermolecular interactions using different methods. In this technique, molecularly stacked multilayer films are formed on surfaces via performing the deposition process a couple of times in an alternating fashion. Conceptual origins of this technique were established in the era of Langmuir of General Electric Corporation [48,80]. Langmuir and his colleagues Blodgett and Schaffer studied deposition of monolayer and multilayer films on solid substrates in a systematic manner [81-87]. L-B/S (a.k.a. L-B-K giving credit to Kuhn for his noteworthy contributions [88-89]) technology is based on the formation and transfer of Langmuir monolayers (see [48] for an historical timeline on monolayer films as a pivotal step in the development of LbL self-assembly). Briefly, surface active molecules (surfactant) migrate to liquid-gas interface from dilute solutions. Disoriented molecules are condensed as Langmuir

monolayers on the liquid surfaces by mechanical force applied in Langmuir troughs. Then, monomolecularly packed layers are transferred on substrates and successive depositions lead to multilayer structures. This technique is still in great use but requires sophisticated devices (Langmuir troughs) and generally restricted with surfactant molecules. Fortunately, it is possible to simplify the technique and also to widen the arsenal of building blocks. This was first simultaneously achieved by Kirkland [90] and Iler [91] of DuPont Company in mid-1960s. In both reports, a simple way of surface adsorption-induced multilayer film formation of particles was introduced. Kirkland described the multilayer formation of inorganic particles concisely, but he clearly explained the advantages and success of applied coating technique. Iler provided a more detailed description of multilayer formation. His work was established on his previous effort [92] on the adsorption of charged inorganic particles as monolayers onto oppositely charged surfaces. Indeed, he extended his own technique to buildup multilayer films through alternating deposition of charged colloidal particles onto each other in a sequential manner. He also speculated on the possible adaptation of his technique to molecularly small building blocks and also studied some polymers in particulate form (i.e. gelatin, cationic polymers, cationic surfactant, and anionic dye). Then, his efforts remained fairly untouched before Decher. In early 1990s, Decher and his colleagues extended the technique to the purely organic molecular materials. Decher team announced LbL surface deposition of polyelectrolytes on planar surfaces [93-95], and they established the field in a couple of following years [96-99].

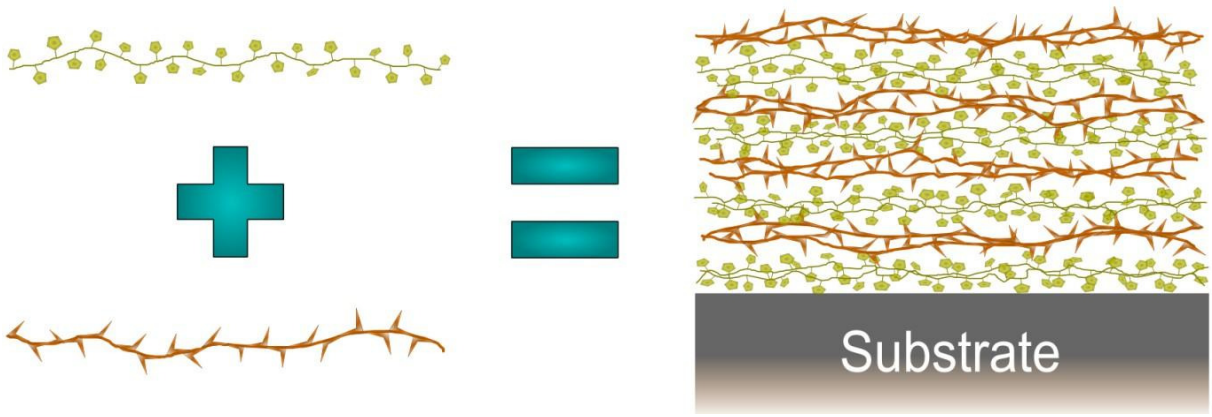

Figure 1-1. Representative formation of multilayer polymeric films.

Conventionally, LbL deposition is maintained via dipping substrates into dilute solutions of polyelectrolytes (see Figure 1-3 and Subsection 1.1.1.1). Upon immersion of a substrate in assembly solutions, material adsorption takes place onto the surface. Then, loosely bound chains are thoroughly rinsed in the following step. In third step, the charge of

polyelectrolyte-modified surface is reversed (viz. from "+" to "–" or vice versa) using an oppositely charged component. Rinsing step is repeated again and a bilayer (smallest unit of LbL nanoarchitectures) is obtained. When this cycle is performed more than once; a nanoscale thin, multilayer film is fabricated.

After seminal works of Decher's Team, LbL technique became popular and a vast of literature has been evolved. Hence, LbL film deposition is a highly flexible supramolecular platform (see Figure 1-2) nowadays. Many studies were devoted to improve LbL technique, to widen its applications, and to elucidate the mechanism behind. Synthetic/natural polyelectrolytes, nonionic polymers, micelles, nanoparticles, and even drugs can be assembled as multilayers using LbL. Different intermolecular interactions can be exploited and fine-tune of deposition conditions (control space) allows tailoring properties of LbL structures. According to their properties, resulting multilayers can suit for certain applications.

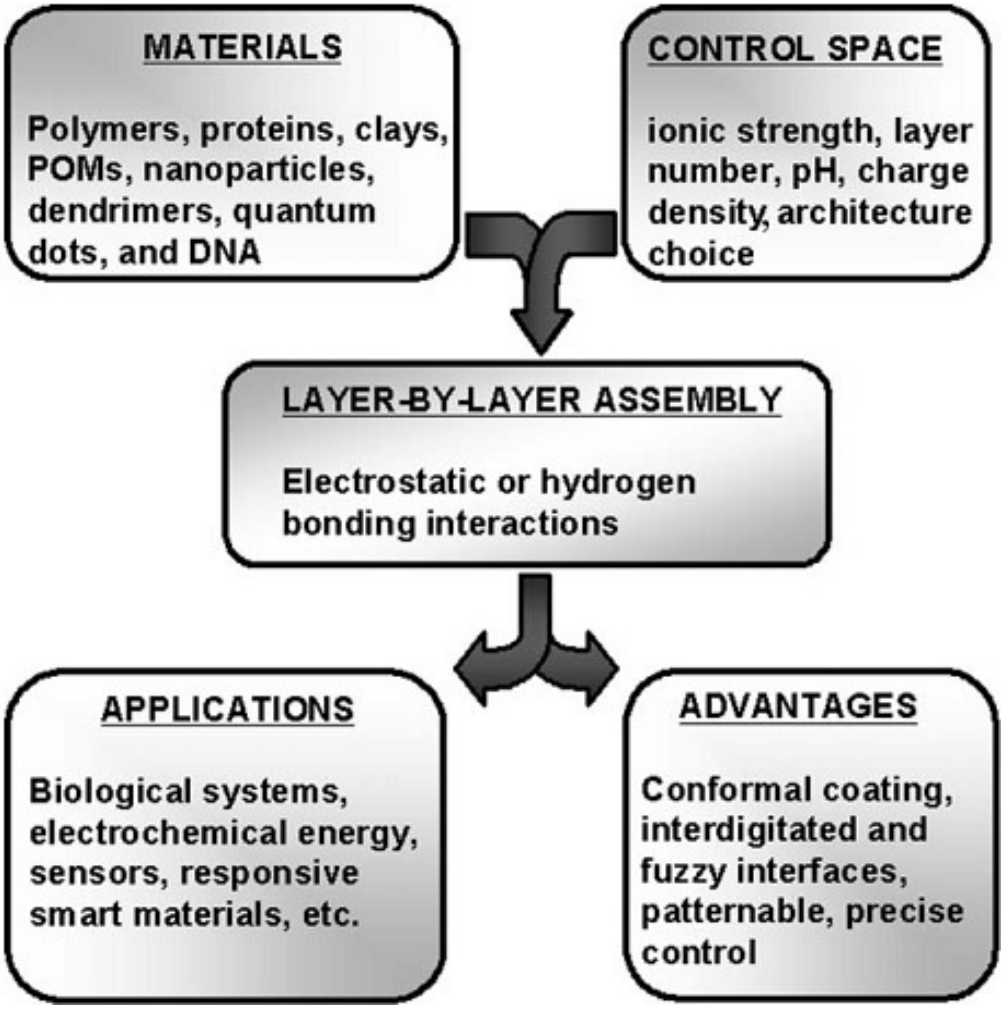

Figure 1-2. Flexibility and interconnection of layer-by-layer design parameters [100] (also see [101]).

1.1.1. Driving Forces of Layer-by-Layer (Self-)Assembly

There is a great flexibility of driving force selection in LbL self-assembly. Driving force of assembly may include one or more among electrostatical attractions, H-bondings, hydrophobic effects, pi-pi interactions, vdW forces, and even covalent linkages. We will mainly concentrate on *es*- and *hb*-LbL. *es*-LbL will be introduced first due to historical reasons. Then, *hb*-multilayers will be given briefly (more information on *hb*-LbL is available in experimental chapters). It is now well known, secondary interactions are also very essential for film stability and film growth. Therefore, hydrophobic stabilization of LbL systems will be given. We will keep the discussions on pi-pi interactions to the forthcoming sections. Pure vdW [102-103] and pure charge-transfer [104-106] bound films have secondary importance for our concern. Also, covalent bonding stabilized LbL films are beyond the scope of our current interest, but can be found elsewhere [107-109].

1.1.1.1. Layer-by-layer electrostatic assembly

es-LbL simply takes place between negatively and positively charged building blocks through oppositely charged. Electrostatical interactions are the conventional and also most common driving forces for LbL film growth. Both in Iler's and Decher's works on LbL film formation, the mechanism of *es*-LbL has been originally explained via multiple electrostatic interactions between building blocks of assembly. Simply, oppositely charged species attract each other and the thickness of the deposited material is controlled with charge repulsions. Key point of this process is again originally given as the "charge reversal" of bare or film evolving substrates in Iler's text [91]. One step forward of this explanation is then appeared as "charge overcompensation". After Iler's interpretations, theoretical and experimental evidences of other researchers [110-112] approved this mechanism. Today, reversal and overcompensation of surface charges at each step is accepted to be the fundamental mechanism of *es*-LbL process. According to this coupled phenomena, each assembly step is governed by surface charge reversal and overcompensation accordingly. Indeed, we believe, this basic concept is also applicable to the non-*es*-LbL systems in terms of interaction tendencies of building blocks (i.e. saturation of H-bonding acceptor/donor sites). In common, overcompensated surfaces become favorable for further deposition of complementary building blocks. So, after a thorough rinsing process, a "regenerated surface" reveals to keep the film growable (to see the depiction of the evolution of charge compensation process see Figure 1-3).

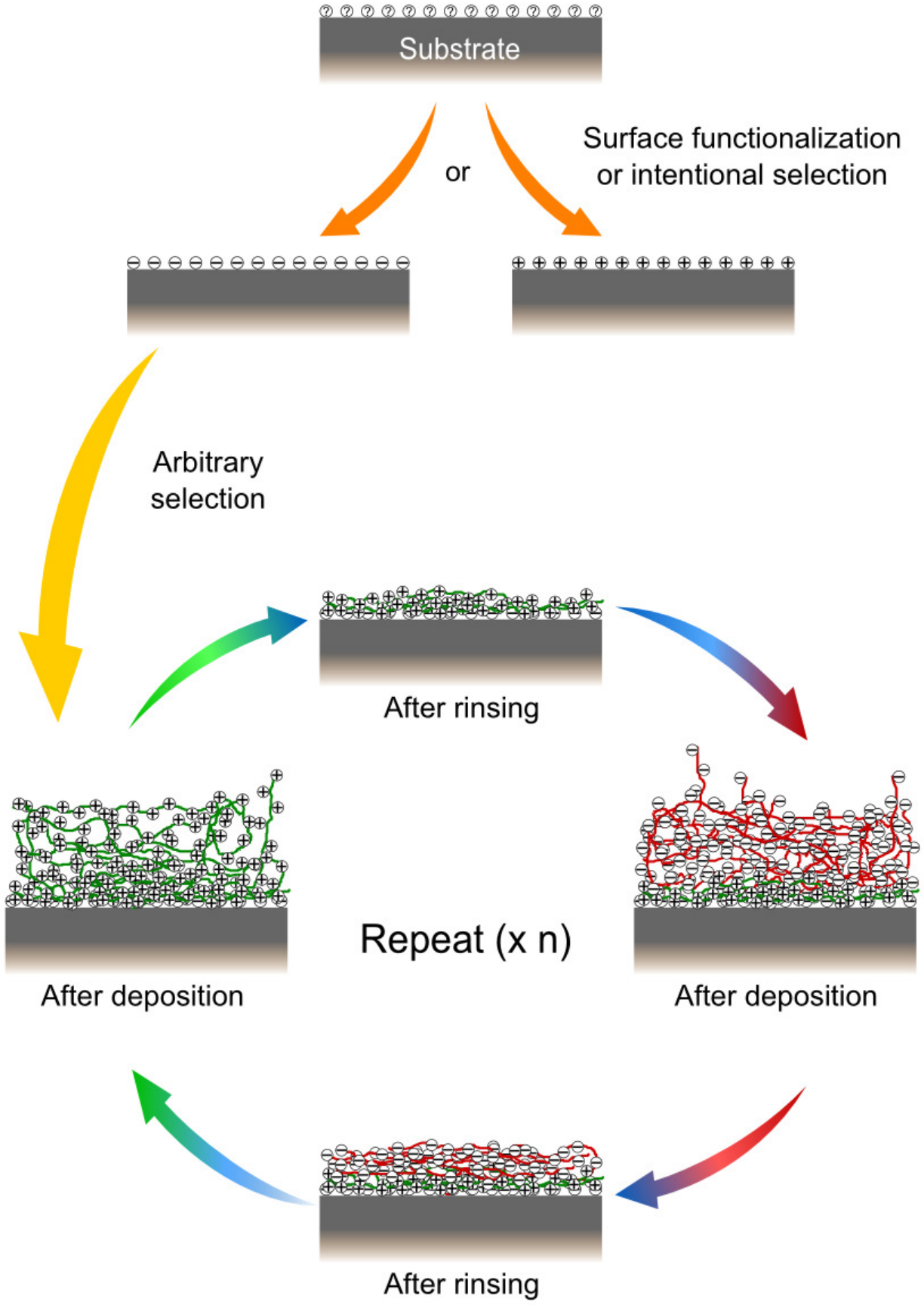

Figure 1-3. Depiction of the basic mechanism of electrostatically-driven layer-by-layer film growth: Charge reversal, charge overcompensation and desorption of loosely-bound chains (For one bilayer).

1.1.1.2. Layer-by-layer H-bonded assembly

LbL technique uses the advantage of multiple available interaction sites (a.k.a. binding points) of polymer molecules and/or particles [50]. Therefore, even weak interactions between binding sites can lead to a strongly-bound film formation. As explained above, LbL technique is originally based on electrostatic forces but non-electrostatic interactions also contribute to or directly drive LbL self-assembly. Among non-electrostatical interactions can favor LbL assembly, H-bonding interactions are the most convenient driving forces for LbL self-assembly. This advancement was almost simultaneously introduced in 1997 by Rubner's [113] and Zhang's [114] Groups. The role of H-bonding interactions in LbL assembly was well-studied and *hb*-LbL films are now achievable as robust as *es*-multilayers [115]. Hence, many H-bonding pairs (viz. H-bonding donors and acceptors) can successfully be used for LbL deposition. More importantly, *hb*-LbL made many uncharged materials available for LbL design and now H-bonded multilayer deposition (*hb*-LbL) is acknowledged as the next era of LbL surface engineering [115]. Detailed information is available about the technique in Chapter 3.

1.1.1.3. Hydrophobic contributions to film stability

Another essential contribution to the LbL self-assembly was proposed by Kotov. At the end of a thermodynamic analysis, Kotov concluded with the positive effect of hydrophobic interactions as a driving force of LbL assembly [116]. First experimental evidence on the contribution of hydrophobic interactions to film assembly has subsequently been reported by Clark and Hammond [117]. Then, Serizawa and associates have shown multilayer assembly of polymers in different solvophobicity (a hydrophilic and a hydrophobic) [118]. Finally, hydrophobic interactions has been satisfactorily approved to stabilize *es*-LbL films [119]. Even some researchers do not specifically emphasize, hydrophobic contribution to film stability is widely accepted for many polymer-based multilayer structures. Further insights about the topic are available in Chapter 4.

1.1.2. Technical Aspects of Layer-by-Layer Assembly

Iler studied most of the technical aspects of current LbL technology in his original text. He investigated the effect of types of building blocks, concentration of solutions (or dispersions), and effect of solution chemistry (pH and IS). He also commented on the substrate selection, and hence covered most of the technical aspects of LbL field. Then, starting from Decher, especially effect of pH and IS was deeply studied, and optimized conditions were elucidated

for numerous LbL systems. Below we will introduce major technical aspects of LbL technology in a concise manner.

1.1.2.1. Component selection for deposition

LbL technology is highly versatile in terms of the selection of building blocks. If a favorable interacting pair is available, virtually any building block can be assembled in multilayer form tailoring molecular/particular size and solution chemistry. Up to now, synthetic polymers, natural peptides, nucleic acids, small molecules, and nanoparticles were assembled in LbL nanostructures to name a few. Traditionally, polystyrene sulfonate, polyallylamine hydrochloride, and PEI are among the most used polyelectrolytes for es-LbL formulations. To name a few popular building blocks for designing *hb*-LbL multilayers; PEG, polyvinylpyridine, PVPon, polyacrylic acid, and polyvinyl alcohol can be listed.

1.1.2.2. Substrate selection and/or functionalization

Substrate selection criteria for LbL have been discussed elsewhere [48,120-121]. There is a vast flexibility of substrate selection. Practically any solid substrate (e.g. silicon, quartz, glass, mica, steel, gold, titanium, polyester, and Teflon) can be engineered with LbL technology obeying surface chemistry. Depending on the chemical nature of selected LbL system, a favorable surface is needed. Similar to the intermolecular interactions between LbL couples, substrates should specifically or nonspecifically interact with first layer of multilayer film. For *es*-LbL this may be maintained with surface charging through functionalization. Similarly, *hb*-LbL may be favored with H-bonding acceptor or donor surfaces. In any case, the first layer acts as a foundation of the multilayer architecture. Better adhesion encourages more robust growth or it may directly be crucial for the fate of assembly. Since, surfaces are not passive players in LbL self-assembly.

Covalent functionalization of substrates may not suffice or may be undesired due to practical or technical reasons. In this case, an “anchoring layer” (a.k.a. precursor layer) is used between substrate and multilayer film. The idea of “anchoring” in LbL field first appears in Iler as adhesion of a cationic surfactant to facilitate a subsequent adsorption of an anionic colloid [91]. Then, researchers used different anchoring materials but mostly PEI derivatives (linear, branched, highly/lowly charged, chemical functionalized etc.) are preferred. Typically, a monolayer of BPEI [122] or BPEI involved bilayers [123-124] are used. Recently, the effect of anchoring layer on film properties has also been systematically studied by different groups [125-130]. Especially, adverse bioeffects of PEI used in LbL films (as

film component or anchoring layer) is important for design [128-130]. Besides, PEI can be replaced by some other polymers or simply excluded is possible.

Another aspect of substrate selection flexibility comes from the geometry substrate. By using a suitable chemistry, even arbitrarily shaped substrates can be coated; LbL is not limited with flat surfaces. This flexibility also made possible LbL coated colloidal particles and even hollow LbL capsules (for comprehensive reviews about the topic see [49-50]).

1.1.2.3. Effect of solution chemistry

In LbL self-assembly, solution chemistry is not strictly definitive in the fate of assembly process in normal circumstances. However, it has a profound influence on the properties of resulting films. For instance, addition of salts to the assembly solutions generally yields thicker bilayers and film stability might be higher or lower. Effect of pH might be more dramatic for both *es*-LbL and *hb*-LbL of weak polyelectrolytes. Since, intermolecular interaction potency of weak polyelectrolytes is switchable from one regime to another (say H-bonding to electrostatic) via pH-dependent dissociation of molecules. Importance of pH and IS for uncharged polymers is also non-negligible, but significantly more complex. Some comments and discussions will be provided in the experimental parts (see Chapters 4) of this study (also see Subsection 1.2.6.1). Below, we will limit ourselves with the discussions on polyelectrolytes with an emphasis on weak polyelectrolytes to create a basis for TA. Curious readers are suggested to commit further readings [101,131-133] on the effect of salts and solution pH on neutral polymers.

1.1.2.3.1. Fundamental considerations

Final properties and performance of multilayers are greatly influenced by solution chemistry. Therefore, a crucial requirement of LbL technology is to tailor effective solution chemistry (mainly[3] pH and IS). Different LbL components can reveal different responses upon alterations of solution chemistry. Highly complex nature of the problem makes the generalizations rather unsafe, but fundamental physical chemistry of polymers still works (see [134-135]). Effect of pH and IS on surface adsorption and polymer conformation can be found elsewhere [110,136-137] in detail. Below, we will confine the content with linear weak polyelectrolytes and try to correlate solution behaviors with LbL technology.

For strong polyelectrolytes, pH alterations do not have a dramatic role comparing

[3] Here we intentionally disregard solvent quality aspects, since we all use water-based systems in this study.

weak polyelectrolytes. Since, pH alterations directly affect the ionization state of weak polyelectrolyte chains. So, in case ionized weak polyelectrolyte molecules are needed, pH of solution is shifted in required side of the acid-base phase equilibria of polyelectrolyte (negatively or positively charged polyelectrolyte is obtained then). This may be favorable for assembly or may be used to disintegrate assembled architecture and film components may be erased and released from the surface ("erasable film" concept) [138-139]. At that point, type of LbL film matters: *es*-LbL or *hb*-LbL. Charge evolution in weak polyelectrolyte chains normally favour *es*-LbL, whereas ionization may break H-bondings and disintegrate *hb*-multilayers. Such behaviors are not straightforward; pH perturbations may influence the system more dramatically.

Salts act as counterions for macroions (a.k.a. polyions and polyelectrolytes). Through condensation in the vicinity of the oppositely charged polymer chains, charge of polyelectrolytes can be screened (a.k.a. Manning's counterion condensation [140-142]). In dilute regime, non-charged-like polyelectrolyte chains may evolve due to charge screening of added salts and conformations of polyelectrolyte chains dramatically change accordingly. Also, there is interplay between effects of salts and pH levels of solutions (recall "activity factor" concept). Moreover, effect of salts on polymer behavior in not always colligative, type of salt is also effective (recall Hoffmeister series [143]). In accordance, effects of specific ions on LbL films have been shown [144-146]. But, NaCl and buffering agents (i.e. phosphate buffer[4]) are generally employed as "salts" in LbL designs and their effects are sometimes ignored.

1.1.2.3.2. pH and ionic strength as variable of assembly conditions

Naturally, properties of molecules in solution reflect to their behavior in deposited state. So, IS and pH "games" are widely played in LbL studies. An obvious effect of IS [95,112,147-151] and pH [152-156] variations on polyelectrolyte multilayers (a.k.a. PEM) is known to be on bilayer (or final) thickness. Effect of pH is generally more system specific. But generally, higher the IS, higher the film thickness. To formulate this outcome, different researchers came up with different relationships between the thickness of adsorption and the concentration of salts. For different LbL pairs, linear [157], linear-like [112], exponential [149], and parabolic [151] relationships have been reported for the dependence of deposited amount to the concentration of salt. Conformational change of polymers upon pH shifts and salt

[4] In the experimental chapters, we will frequently abbreviate the "phosphate buffer" as "buffer".

concentration variations is well known fact [158-160] which reflects to LbL films at least as topographical alterations (roughness change). Another important and also controversial issue is the presence of counterions in the film structure upon deposition. Counterions are sometimes assumed to release from the film and oppositely charged polyelectrolyte segments neutralize each other. But in fact, a portion of salts can remain in the structure ("extrinsic charge", see Equation 1-1) which might influence the properties of films drastically [161-164]. Especially, Schlenoff's Group has systematically studied the effect of salts in hydration and dissolution of *es*-multilayers in series of reports [165-168]. According to these studies, dissolved ionic species can shield charges (see Equation 1-1) of charged building blocks and contribute assembly process (a.k.a. intrinsic compensation) which is in accordance with counterion condensation (recall upper subsection). To us, it is clear whether due to the presence of salts in film structure or the effect of salts on polymer chains in solution reflects to the complexation event. But salts are reported to increase [139,161] or decrease [131,169] film stability. So, each system might require special attention to understand the effect of salts on assembly and disassembly.

Equation 1-1. Inclusion of salt counterions in polyelectrolyte multilayer complexes [162-163].

$$(\mathrm{Pol^+Pol^-})_m + n\mathrm{X^+_{aq}} + n\mathrm{Y^-_{aq}} \rightarrow (1-n)(\mathrm{Pol^+Pol^-})_m + n(\mathrm{Pol^+Y^-})_m + n(\mathrm{Pol^-X^+})_m$$

1.1.2.4. Selection of method for film deposition

LbL surface deposition is traditionally performed by dipping (immersing) the substrates in building blocks solutions/dispersions. However, LbL technique is not limited to dipping; there are other alternative techniques as well. Dip-LbL is still the most widely studied technique, but there is a growing tendency towards its novel counterparts. Below, we will focus on dip-, spray-, and spin-LbL giving an emphasis on the latter. Advantages/disadvantages of available techniques will be briefed. In addition to film composition comes from the selection of components; characteristics of end-products are also influenced by process parameters in LbL technology. Thus, we will also briefly emphasize the effect of method selection on film quality (Chapter 2 is referred for further information). Indeed, possible effects of film deposition technique on the properties of multilayer films have long been known. For instance, in late 1930s, Bikerman reported water wettability alterations of L-B/S films of different structures (X, Y, and Z) assembled using same materials [170]. Today, similar observations are being done for LbL films and such variations are of importance not only from technical, but also from scientific point of views (see Chapter 3).

1.1.2.4.1. Dipping-assisted film deposition

LbL surface deposition is traditionally performed by dipping (immersing) the substrates into dilute solutions/dispersions of oppositely charged building blocks in a sequential manner [50,93] (see Figure 1-4). LbL dip-adsorption of polymer chains is considered to be a "self-diffusion process" where diffusion of weakly-attached chains needs a considerable time [13,171]. Prolonged solution contact cause/increase rearrangements of adsorbed materials on the surface and also in the inner structure of film [13,171]. So, adsorbed layer become interpenetrated and multilayers of "fuzzy" [161] layers form. Also, as a result, surface roughness of dip-assembled multilayers are usually high [13]. On the other, hand some other dipping-like methods such as dewetting [172] and electric-field [173] due to their relatively less usage.

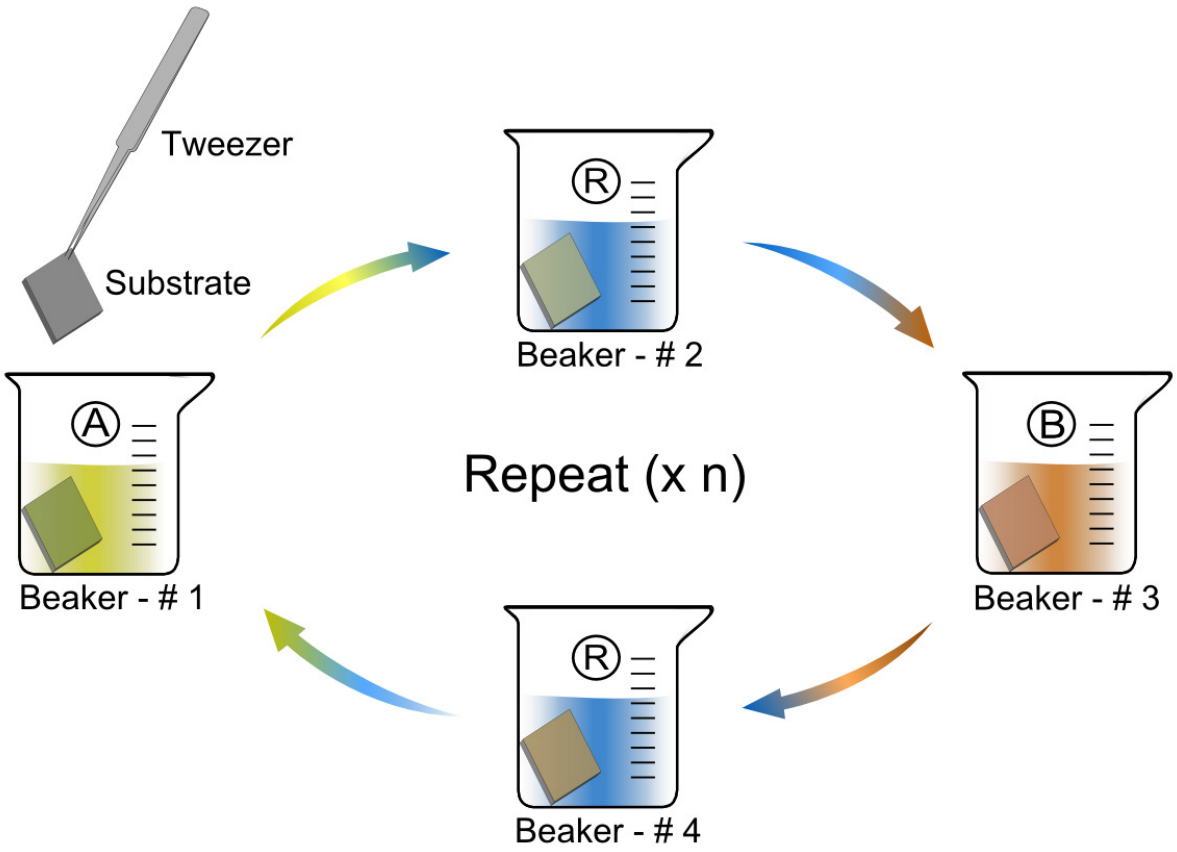

Figure 1-4. Dipping-assisted layer-by-layer film assembly: Tweezer and beaker deposition (A: Component A, B: Component B, R: Rinsing).

1.1.2.4.2. Spraying-assisted film deposition

In dip-LbL, each deposition step approximately takes 10-30 minutes depending on the system. When considering a moderate multilayer films consist of 10 to 20 layers, a day-long effort is

required. So, initially for practical reasons, alternative timesaving methods have been introduced. As first alternative of dipping, spraying (spray-LbL, see Figure 1-5) was reported [174]. Then, the versatility of technique was examined, deposition parameters were investigated, and additional advantages of spray-LbL were discussed by Decher Group [175]. Spraying reduces the time required for the deposition of a bilayer to the order of seconds from minutes (rinsing time is also reduced from 3-5 minutes to tens of seconds, and rinsing can also be eliminated). Also, substrate size limitations are eliminated; the size of coating area is not an impediment for spraying and this makes it convenient for scale-up.

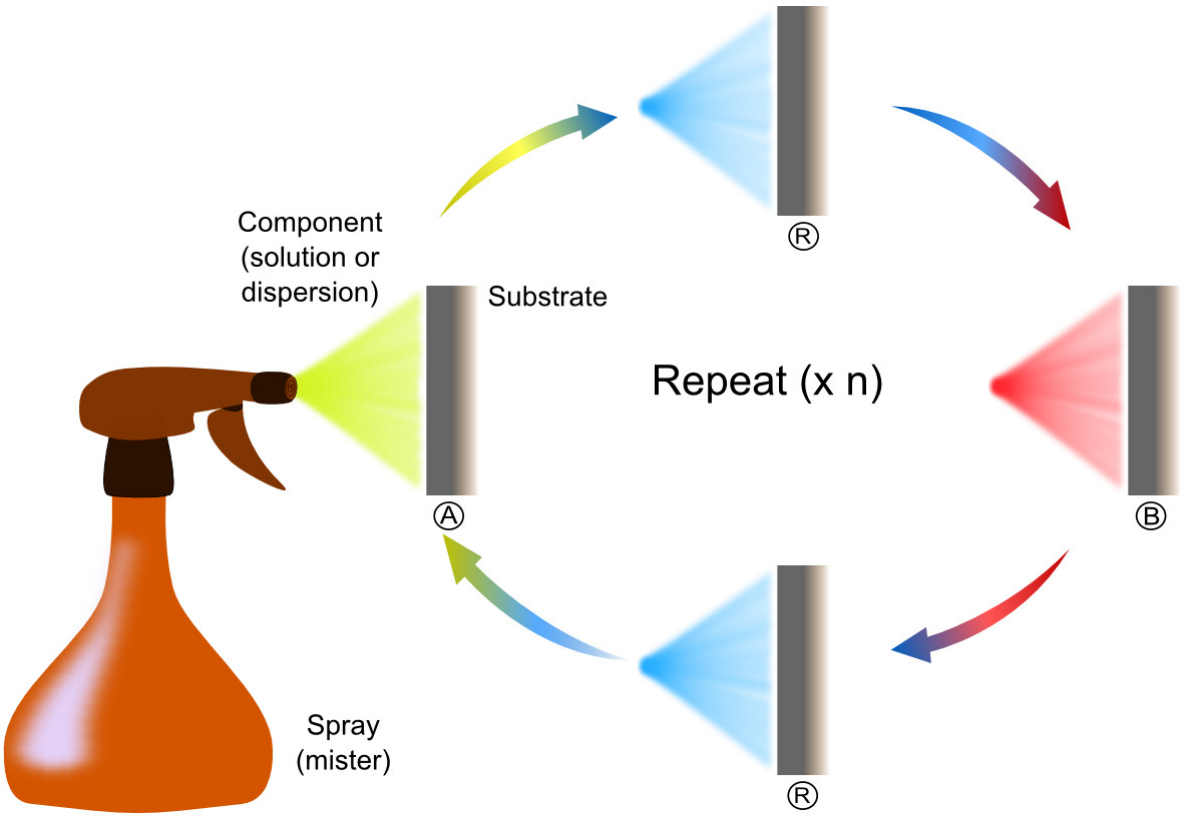

Figure 1-5. Schematic representation of spray-assisted layer-by-layer deposition technique (Note that the rinsing steps, "R"s, between depositions of A and B are shown, but can also be skipped).

In addition to practical aspects, spray-LbL also differs in terms of film properties [13]. First, in case all of mist get in touch with substrate during application, two different zones (see Figure 1-6) appear: Homogeneous inner and inhomogeneous outer zones [175]. On the other hand, surface roughness control seems better in spray-LbL comparing dip-LbL, but level of stratification is similar [176].

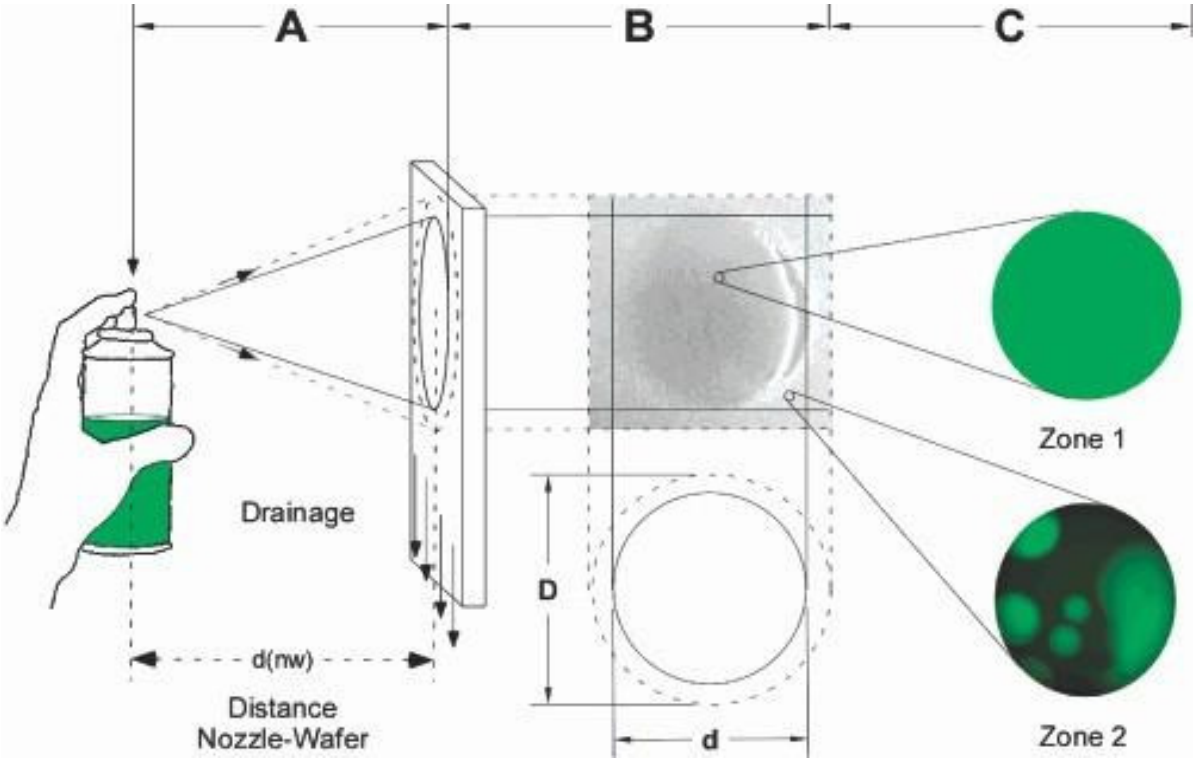

Figure 1-6. Formation of different zones in spray-assisted layer-by-layer films [175].

1.1.2.4.3. Spinning-assisted film deposition

Just after spray-LbL, spin-LbL [177-178] has been simultaneously introduced by two groups as a new alternative of dip-LbL (see Figure 1-7). The technique is nothing but alternating utilization of conventional [179-180] spin-coating (a.k.a. spin-casting) procedure. Rinsing step differentiates the spin-LbL technique from conventional spin coating, but fundamental theory of spin coating [181-186] are still valid for spin-LbL. That means fundamental process parameters of spin coating such as spin rate (rotation velocity), concentration and volume of applied liquid, size and shape of application area, ambient temperature, and environmental humidity affects the spin-LbL process as well. Among those parameters, spinning rate is probably the most crucial one and can be used to tailor bilayer thickness of LbL films [178,187]. Indeed, spinning rate adjustment has also commonly been used in regular spin-casting of polymer films for controlling final film thickness [184,186]. Here it is also beneficial to say some words on the basic mechanism behind this phenomenon (see Chapter 3 below for further details). Generally a decreasing asymptotic relation between spinning rate and film thickness (or bilayer thickness) is observed with increasing rates.

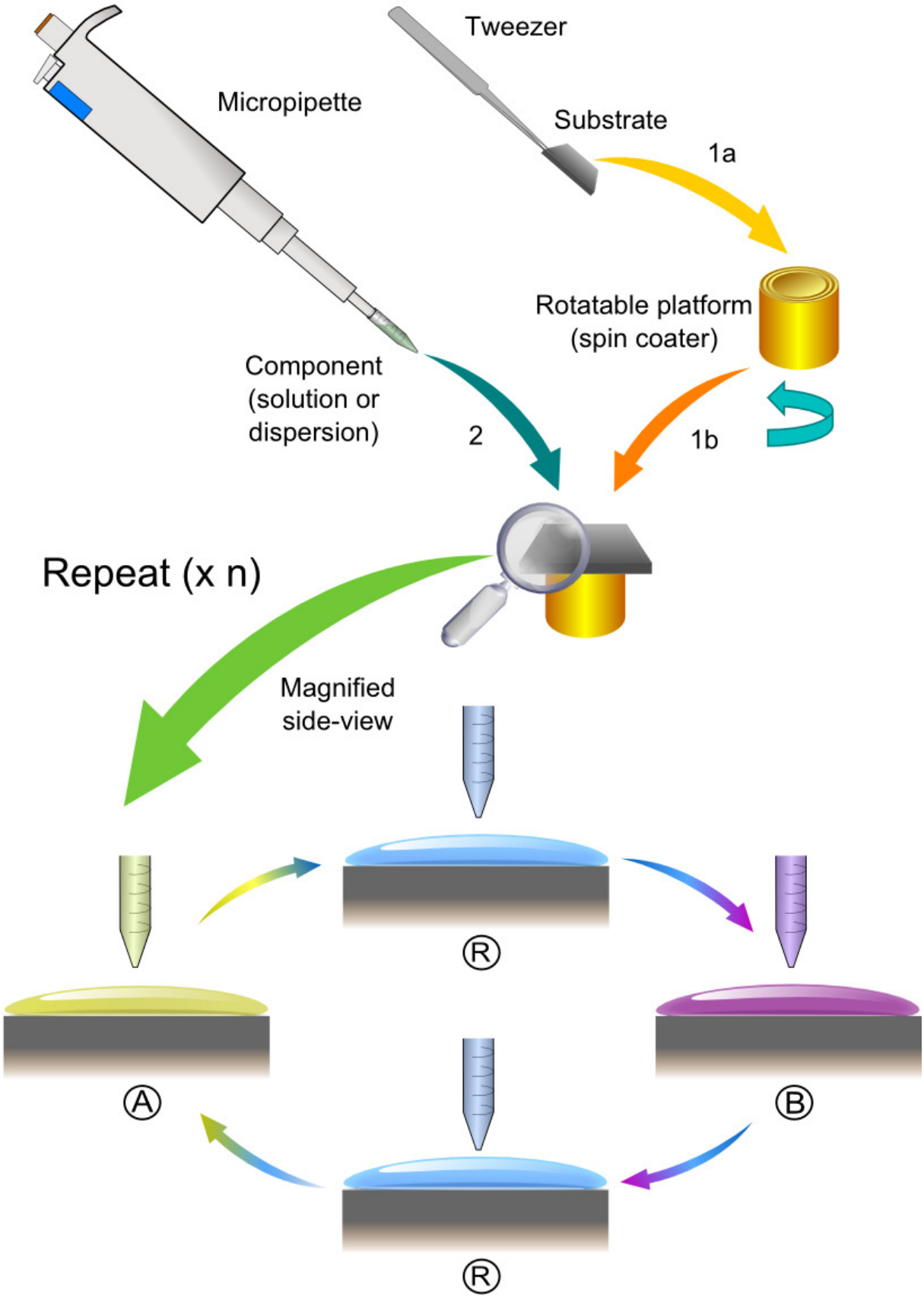

Figure 1-7. Spinning-assisted layer-by-layer assembly (A: Component A, B: Component B, R: Rinsing).

The decrease in the film bilayer thickness with increasing spinning rate is mainly due to larger centrifugal forces applied. With larger centrifugal forces, the solution applied is spread into thinner liquid films (see Figure 1-8). Then, solvent evaporation takes place and leaves a solid film behind (see Figure 1-9). Normally, thinner the liquid film, thinner the resulting solid film. Hence, film thickness in spin-LbL applications is spinning rate dependent (in addition to other factors above). Also, one major importance of spin-LbL is its impact on film thickness comparing other techniques. There are a number of studies [177,188-189] reporting on larger bilayer thicknesses obtained by spin-LbL comparing dip-grown multilayers. Fundamental models of spin-coating [180-183] can be employed to explain this important observation. In this framework; the centrifugal and inertial forces act in the same way and remove loosely-bound polymer chains, but at the same time fast removal of water thickens the solution and a thicker film is obtained. At the same time, an exceptional case is also reported [190] which we will discuss in detail later on (see Chapter 3). In spin-LbL, each spinning step is followed with rinsing and only well-adhered portion of spin-deposited material stays on the surface. Similar to spray-LbL, spin-LbL is highly time-efficient. Furthermore, physical properties (i.e. homogeneity, smoothness) of the spin-LbL films are generally better than dip- and spray-LbL films. Underlying reason of this quality improvement is believed to be short-term fluid contact during spin-LbL. In accordance, spin-LbL films are well-stratified due to decreased water contact duration [191] (for further information see Chapter 3).

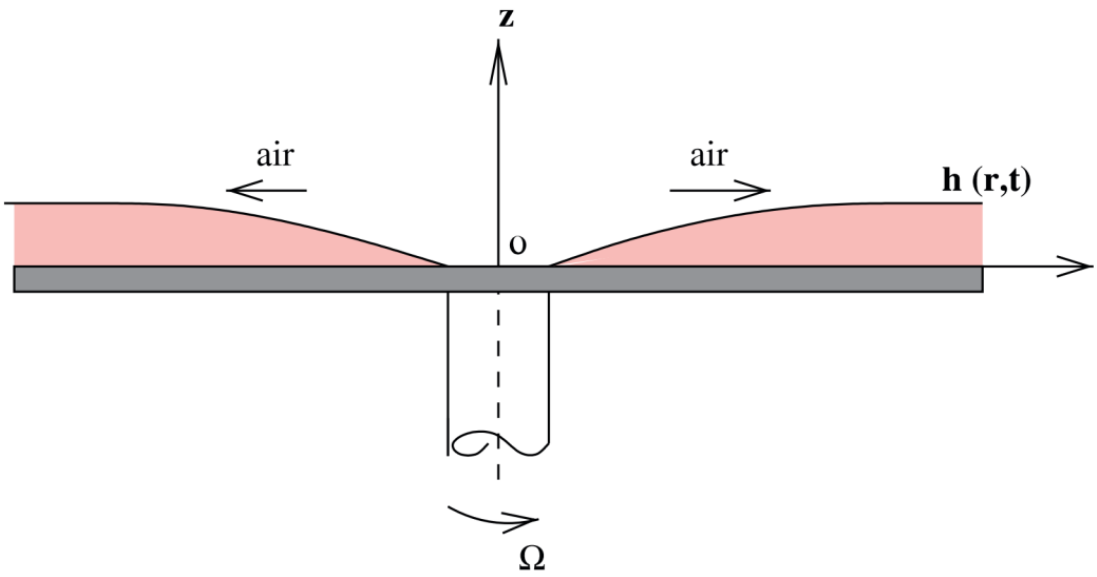

Figure 1-8. Schematic representation of air and fluid flow in spin-coating [192].

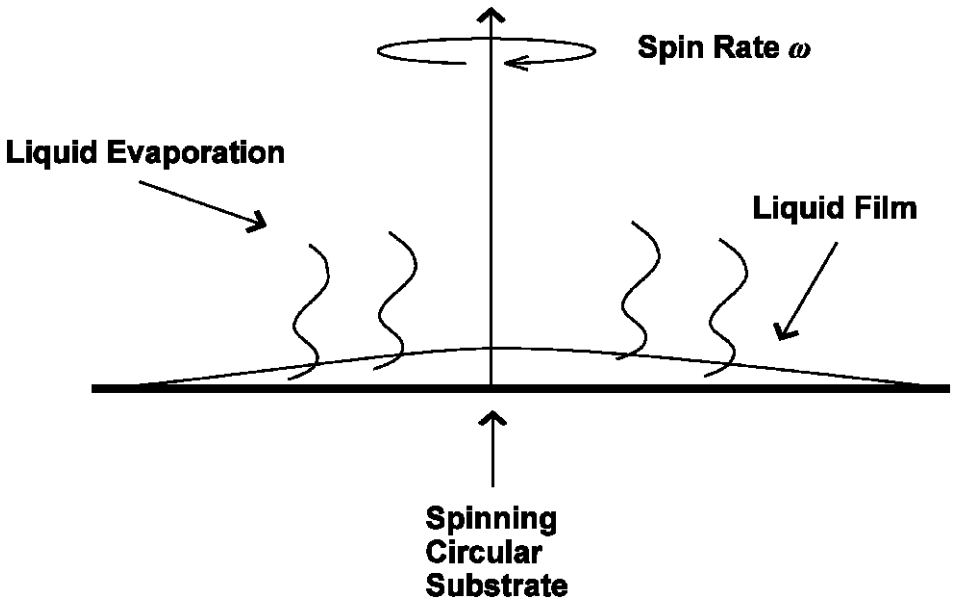

Figure 1-9. Schematic representation of spin-coating technique [193].

Spin-LbL offers an efficient platform for fundamental research on LbL technology but limited with smaller and plain substrates. As a recent advancement in LbL method, Merrill and coworkers introduced an interesting hybrid route for "directed self-assembly" of multilayer films: spin-spray-LbL [194]. In our sense, this technique is an extension of spin-LbL and we recognize the technique as "spraying-coupled spin-LbL" which combines the advantages of both spinning and spraying. So, we believe spin-spray-LbL is highly promising for large-scale applications as a scalable method. Especially, spin-spray-LbL reduces the assembly fluid amount needed for deposition and saves high-price materials such as nanoparticles [194].

1.1.3. Characterization of Multilayer Films

Some excellent reviews previously outlined the basis and current advancements [48,195] on characterization of LbL multilayers. Therefore, this section is not meant to present a full picture of the topic. Rather here we will provide an easy outline of the characterization aspects emphasizing the techniques we employed in our study. We will also try to explain why and where characterization is crucial for LbL technology. Also, we intentionally will exclude application-based characterization aspects such as biological characterizations.

1.1.3.1. Growth regime and film thickness

LbL technology is established on film deposition phenomena and material deposition takes place in step-wise manner. Character of film growth (a.k.a. growth regime/mode) may change

from system to system and depending on deposition conditions the amount and/or density of adsorbed components alter on the surface. In following two subtitles, growth models and analysis will be given.

1.1.3.1.1. Linear versus exponential growth

In terms of growing regimes, multilayer films are divided into two major types: Linear and exponential growing. Generally, thickness of LbL films linearly increase with increasing number of deposited layers. Linear growth is easily justified with basic adsorption knowledge; in each step an equal amount of material is deposited on the surface. However, exponential growth is rather complicated. It is believed, LbL adsorption occurs in two kinetic steps: i) Diffusion-induced adsorption of polyelectrolytes onto the surface (fast), ii) Rearrangements of the adsorbed species (slow). First step is driven by intermolecular forces and the diffusion of polymer segments to the adjacent layers takes place due to slow chain rearrangements [171,196]. In exponential growth, aforementioned mechanism is not so straightforward. A great effort has been devoted to explain the details of growth mechanism duality. Proposed models are still disputed and the complexity of problem is widely accepted.

Exponential growth regime was generally attributed to the "in" and "out" diffusion[5] (a.k.a. interlayer diffusion) [197-199] of at least one of the assembled building blocks which is rather free in the material reservoir (viz. LbL film) [199-200]. This explanation is quite important, but there are still open questions and current roughness[6] models (see Figure 1-10) [200] may explain the experimental observations better in some occasions. Recent findings on exponential growth of polyoxazoline/TA films [123] and block copolymer micelle based *hb*-multilayers [124] observed by our group might maximize the reputation of roughness-mediated nonlinear growth observations [153,201-202] and models [200]. Here, we would like to stress that, there is no need to choose one of those models. We believe there might be some systems which are equally explainable with both models or not explainable with any of those. LbL pairs we see in current literature is negligible comparing the possibilities, hence composition design in LbL is virtually unlimited. The interplay of various parameters involved (i.e. solution chemistry [203-204], Mw of polymer [205], number of layers [206]) overcomplicates the picture. On the other hand, those models might be presupposing each other in a complex manner. Currently, experiment and theory are in action to elucidate the

[5] From now on, we will call this term as "in&out" diffusion.

[6] Note that, dendritic and island models also indirectly suggest rougher surface topologies.

underlying mechanism of LbL growth [207-209]. A holistic understanding towards the underlying mechanism can be gathered in near future and a unified explanation might be proposed.

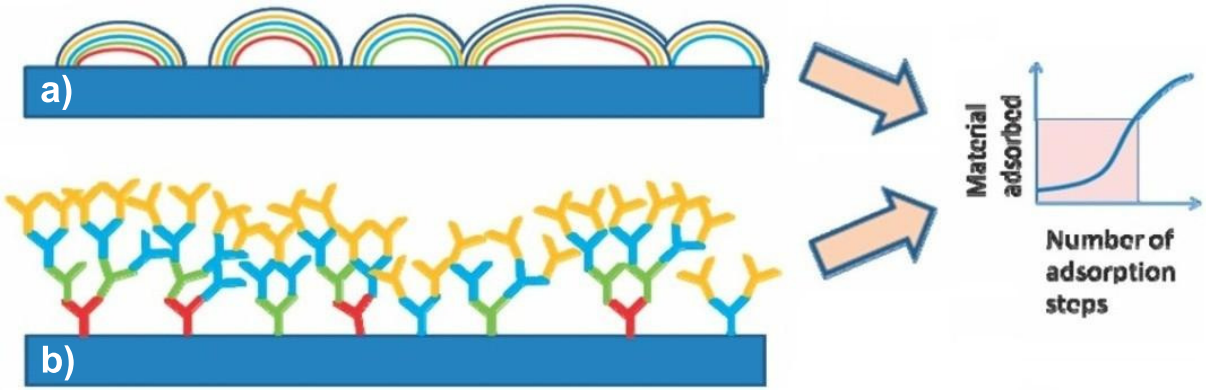

Figure 1-10. Roughness-trigger like explanations of exponential growth in layer-by-layer film deposition: a) Island, and b) dendritic models [200].

In addition to linear and exponential regimes, there are many studies [122,210-217] reporting a deviation from linear/exponential growth behavior namely "zigzag" growth. Actually, "zigzag" growth is an indirect indication of the destabilization of complex and has been both observed in *es*- and *hb*-multilayers. In case desorption takes place in a significant ratio whilst adsorption proceeds, surface reversal (i.e. plus to minus or donor to acceptor) delays and a portion of already adsorbed material migrate to solution. If rinsing step is successfully performed, zigzag growth also suggests thermodynamic instability of resulting complex (see Chapter 2 and 3 for further discussions).

1.1.3.1.2. Monitoring film growth and thickness

OAS and EMM are widely employed for film growth monitoring as conventional routes. OAS provides a useful way to study film growth monitoring of light absorbing materials, but do not directly give film thickness information. Instead, EMM directly gives film thickness information whilst film growth is being monitored. EMM [218] is a well-established optical technique for thin film characterization (see [219-220] for historical aspects). A non-destructive laser of known polarization hits the surface as a collimated beam. Polarization state of reflected light becomes different than incoming light and this difference is analyzed (see Figure 1-11). Normally, linearly (plane) polarized light is sent (photon-in) and elliptically polarized light is obtained (photon-out) [221]. Raw data is generally produced in terms of two angle information: Amplitude ratio (ψ) and phase shift/difference (Δ) of both p- (parallel) and s-polarized (perpendicular, from German word "*senkrecht*") light waves [222-224]. These

values appear in complex reflectivity ratio (a consequence of Fresnel equations, see Equation 1-2). For a certain incoming light (angle of incidence and wavelength are set), in case refractive indice of surrounding environment (typically air) and substrate are known (N_0 and N_2), thickness or refractive indice of thin films can be extracted (see Figure 1-12). Mathematical inversion (from ψ and Δ to calculated values) is performed through algorithmic fitting to the models [225]. These operations are quite heavy but currently held by softwares of commercial ellipsometers. Therefore, EMM is widely used to monitor LbL film growth as a practical and precise way.

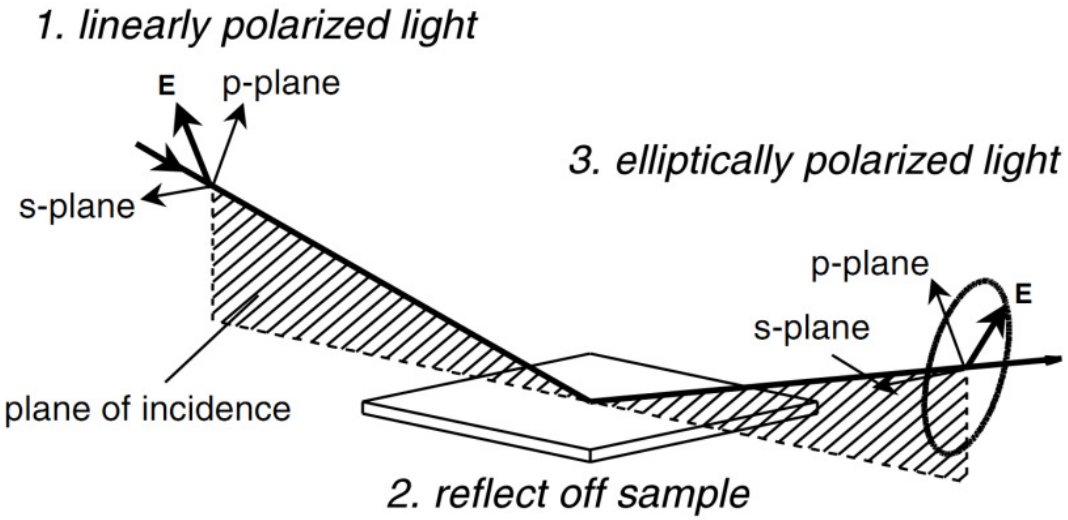

Figure 1-11. Geometry of ellipsometric measurement [221].

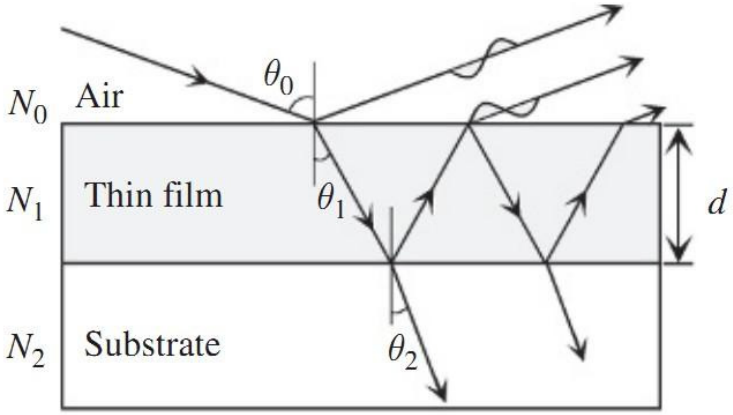

Figure 1-12. Basic optical model for ellipsometry measurement consisting three different mediums [225].

Equation 1-2. Basic mathematical representation of the theory of ellipsometry [221,225].

$$\frac{R_p}{R_s} = \tan(\psi) \times e^{i\Delta} = \rho\left(N_0, N_1, N_{2,} d, \theta_0\right)$$

There are some other complementary techniques to monitor multilayer growth and film thickness. QCM and surface plasmon resonance techniques are also preferred to probe

film growth by some researchers.[7] However, these techniques cannot be easily used to estimate film thickness. AFM can also be utilized to measure film thickness via scratching the film in contact mode [226]. But it is quite painstaking, error-prone, and also invasive. So, AFM is not suitable to monitor continuous applications such as multilayer growth monitoring. X-ray reflectometry is also potent to study thin film thickness [227-228], but it is not practical enough for the monitoring of LbL film growth. SEM is also used as a complementary technique for high thickness multilayer films [229], which seems as a misleading technique to us for thickness measurement purposes (not useful for few nanometer samples and not accurate enough).

1.1.3.2. Film morphology

Film morphology of LbL films are mainly studied by electron or probe microscopies. Surface topography resolutions of force microscopes are finer than electron microscopies in normal circumstances and sample preparation is also easier [230]. So, (scanning) probe microscopy is widely utilized to investigate surface morphology of LbL films. At least 25 different scanning probe microscopy techniques are available and AFM [231-232] is the one of the most powerful one surface characterization [233-234]. AFM gives surface topology information about materials in nanometer resolution. Resolution limit of the technique is highly dependent to the quality and dimensions of probes [235-237]. A sharp[8] tip mounted on flexible cantilever tracks the morphology of surface line-by-line as a probing stick of blind man (see Figure 1-13). Progress of scanning is sensitively maintained by piezoelectric material equipped process control elements and four-quadrant photodiode detectors [234,237-238]. In the rest condition, laser reflecting from cantilever is located to the photo-detector [234-238]. Throughout surface scanning, probe (tip) and surface atoms/molecules interact (tip-surface interaction) in a Lennard-Jones potential like manner which cause cantilever deflection [237-238]. According to mode of study, a mode (and a suitable feedback strategy) is selected and deflections are compensated with piezo actuator responses [234-238]. Among the modes available, most widely used one is semi-contact (a.k.a. intermittent and tapping) mode which surface topography is scanned in a dynamic manner. Semi-contact mode provides additional information other than surface morphology [233]. Local mechanical properties of surfaces can

[7] In Appendix-J, we show our preliminary results on the utilization of QCM for monitoring pH-dependent disintegration of multilayer films.

[8] Normally, radiuses of tips are in the order of tens of nanometers.

be mapped in phase contrast imaging option of semi-contact mode [237]. Stiffness differences in different localities within a sample cause different energy dissipations and cause different phase mismatches. Mapping of phase shift between given (natural resonation) and detected oscillations of cantilever give phase imaging.

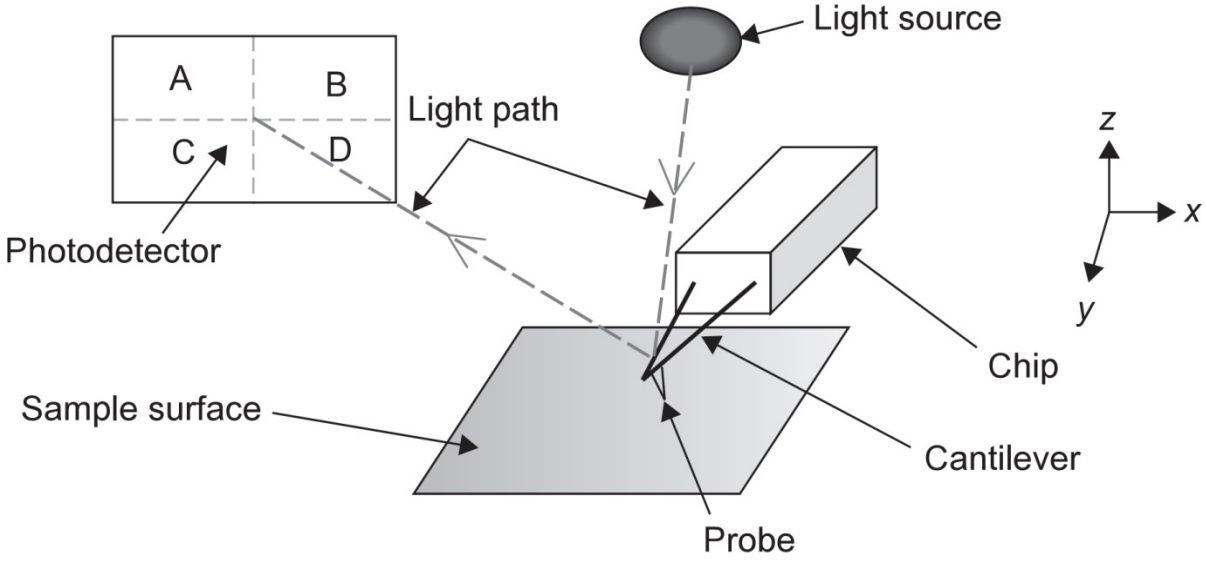

Figure 1-13. Representative set-up of atomic force microscopes [237].

Surfaces get in touch with surroundings solids/liquids and promote to be interfaces. Interfacial properties of materials influence biological, mechanical, electrical, and thermal responses of materials. Especially, interfacial characteristics of materials have a profound impact on biological properties of materials (see following reviews [239-240]). Biological properties of interfaces (biointerface) are linked to physical texture and mechanical properties of material surfaces or coatings [241-242] (also see following reviews [243-244]). So, nanomechanical properties of surfaces are also important from application point of view. When LbL films are doped with inorganic materials (see section 1.1.5), nanomechanical properties of resulting might differ significantly. However, determination of mechanical properties in nanoscale requires advance equipments and elaborate experimentation [245]. Indeed, AFM can provide information about nanomechanical properties of LbL films by force spectroscopy [246]. However, production and interpretation of nanomechanical data are not straightforward [247-250]. Thus, we did not focus on these aspects and curious readers are suggested to read following studies [241-242,251-253].

1.1.3.3. Internal structure

Internal arrangement and of LbL films is of interest from both fundamental and application points of view. Spatial arrangement of building blocks in multilayer is a consequence of

internal arrangements and directly affects material characteristics of films. Internal structure analysis of LbL films requires sophisticated reflectometry (X-ray or neutron) studies. Most of early studies on this topic were performed by Decher and associates [94-95,99,161,254-255] using dip-LbL films. Stacked but still interpenetrated but nature of dip-LbL films has been demonstrated. Interdigitation of subsequent layers in multilayer structure was explained via distributions polymer segment along the surface normal. To depict interpenetrating behavior, this phenomenon has been coined as "fuzzy" structure [161,256]. Then, spray-LbL (recall Subsection 1.1.2.4.2 above) and spin-LbL were analyzed similarly and (recall Subsection 1.1.2.4.3 above) and the effect of growth method on internal structure is established.

1.1.4. Applications of Layer-by-Layer Surface Deposition

When it is needed to improve the surface characteristics of materials without sacrificing any bulk property, coating applications can be highly effective. LbL is surely the most versatile soft coating method and can be designed for almost any bulk substrates. LbL is also highly successful in functionalization nanosized materials and can also be considered as a nanoparticle fabrication technique. Therefore, applications of LbL are extremely vast. Different application areas of LbL technology have been reviewed by top researchers in the field [48-49,77,100,257-261]. To name a few applications; biomedical, pharmaceutical, antimicrobial, antireflection, separation, sensing, and electronics can be listed. One reason behind extreme versatility of LbL technology is its compatibility with nanoparticles. Nanoparticles serve as useful agents to tailor LbL films for certain applications through using them as functional additives. Below, we introduce nanoparticle-loaded multilayer films.

1.1.5. Nanoparticle-Loaded Multilayer Films

Mother Nature combines a vast type of organic and inorganic materials which seem incompatible at first glance. Multilayer assembly offers a useful tool to mimic this life-sustaining ability of Nature. Nanoparticle-incorporated multilayers have been the subject of several studies. Particularly LbL platform is highly rich in terms of nanoparticle-doped systems (for nanoparticle-doped L-B/S systems see following research [262-263] and review [65,264] papers). Many inorganic nanoparticles have been doped in LbL architectures such as metal (oxide) nanoparticles, natural clays, and CNTs to name a few groups. The first appearance of inorganic/organic hybrid LbL films can be taken as boehmite/protein and silica/polymer films of Iler. In his monumental work, Iler gives one of his future look as "Another possibility involves building up heterogeneous films of different inorganic

substances or alternating organic and inorganic components" [91]. Iler's foresight is a fruitful research topic of current nanotechnology.

After a series pioneering works [265-274], nanoparticle-filled LbL field has been dominated by Kotov Group. Kotov Group has systematically studied incorporation of several nanoparticles in LbL systems and characterized various properties of those. Especially, nanoclay and CNT based studies of Kotov Group and their collaborators deserve to be highlighted. They demonstrated high performance LbL nanocomposites using nanoclay [275-278] and CNTs [279-280] each of which were mostly *es*-multilayers. They also covered the field with excellent reviews which are full of their studies [281-283].

es-LbL has been used as a paradigmatic system to study nanoparticle/LbL nanocomposites. Hundreds of papers appeared dealing incorporation of nanoparticles in *es*-multilayers, but a handful of publications report nanoparticle-doped *hb*-systems (i.e. semiconductor quantum dot: [284], gold nanoparticle: [285], polymer nanoparticle: [286], polymer-linked silica nanoparticles [287], modified SWCNT: [217,288], pristine SWCNT: [289-291]). In these studies, generally one of the interacting components is doped with dopant nanoparticle; and then, multilayer assembly is held. Among SWCNT-doped designs, (poly(allylamine hydrochloride)/poly(vinyl sulphate))$_3$(polyguanine-SWCNT/polycytosine-SWCNT)$_n$ of Nakashima's Group [291] is the unique example of double-loading (see Figure 1-14). For further literature details on CNT-doped *hb*-LbL designs please refer Chapter 2 and 4.

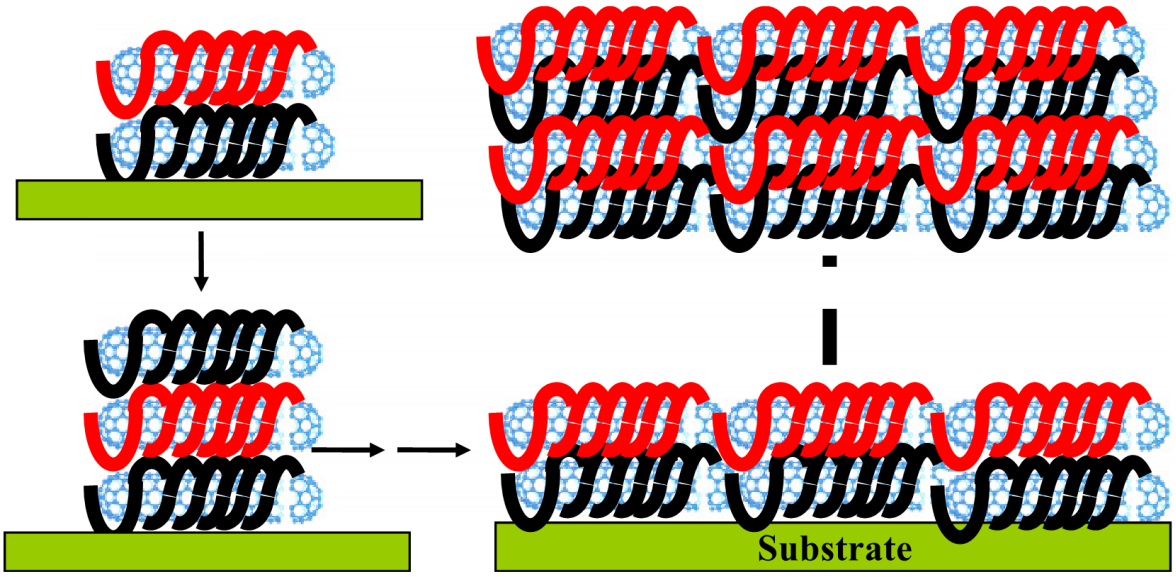

Figure 1-14. Model of Nakashima for single-wall carbon nanotube doped layer-by-layer films [292].

1.2. CARBON NANOTUBES

C is one of the most abundant chemical elements in universe [293] and among the six essential elements of known life [294]. C is considered to be among main constituents of prebiotic molecules [293,295] and uniquely rich chemistry of C is responsible for molecular diversity. Today, above 90% of both natural and synthetic chemical substances are C-based [296]. Not surprisingly, organic chemistry was established around C in the past two centuries. And in the last couples of decades, C has dominated inorganic chemistry via its novel nanoforms. Today, we particularly witness an exciting competition between these CNPs. Indeed, CNTs reached their majority over their progenitors (CNBs). Realization of CNS [297] is rather new and the field is not well-grounded yet. However, since rediscovered in 1991 by Iijima of NEC Corporation [298], CNTs are the most studied players of current nanotechnology. So, scientific literature of CNTs is voluminous and a complete historical survey should either be excessively long or arbitrarily selective. Below, we will try to cover up the essential aspects of CNTs for our particular study.

1.2.1. Fundamentals of Carbon Chemistry

C owes its critical role in chemistry mainly through catenation and hybridization [295-296]. In a simplest way, catenation can be explained as the property of same elements to form either linear or ring type chains [296]. This property gives rise to organic polymers and surely makes life possible. C also serves as structural building blocks of multifarious inorganic polymers thanks to catenation. But, catenation is not enough to justify immensely diversified molecular compounds of C. The rest of the problem is solved by another chemical behavior: Hybridization. Depending on the hybridization state, C can take different coordination numbers from 2 to 4 to satisfy well known octet requirements.[9] C has three hybridization states: sp, sp^2, and sp^3 which cause a ternary phase behavior [299]. Naturally, geometry of bonding (atomic arrangement) and hence global geometry of molecules is also hybridization-dependent. Linear acetylenic forms of C are driven by sp hybridized double or triple bonded C atoms. Linearly catenized C is restricted with small structures such as carbyne[10] molecules in pure hybridization state [296]. On the contrary, sp^3 state is rather compatible with three-

[9] Here, we do not consider intermediate forms of C.

[10] In IUPAC Recommendations, “carbyne” term appears as “organic radicals of C”. Indeed, a variety of terms such as “polyyne”, “poliyne”, and “alkynes” can be seen elsewhere. However, scientific community has widely been adhered to the usage that we also prefer.

dimensional networks. Pure sp^3 networks of C gives two natural forms: Diamond (cubic) and lonsdaleite (hexagonal). Minor inclusion of sp^3 in sp^2 or sp also cause three-dimensional C networks (i.e. amorphous C, C black, C nanofoam, glassy C, diamond-like C, C fibers) [296,299-300]. In sp^2 hybridization state of C, one s orbital (2s) and two p orbitals ($2p_x$ and $2p_y$) involve hybridization. Newly formed sp^2 orbitals contribute stable sigma bonds which mainly maintain the atomic arrangements around C. Also, nonhybridized p orbital (viz. $2p_z$) electron(s) forms pi bonds. pi bonds can either be double bond which is localized or contribute to resonance which is delocalized [295]. Pure sp^2 is probably the most productive state of C and is symbolized with graphite of three different lattices (turbostratic, rhombohedral, and hexagonal) [299]. Next to natural graphite, graphitic (sp^2) nanoforms of C (viz. CNPs) are also available. sp^2 hybridized CNPs are mainly CNBs,[11] CNTs, and CNSs which are widely considered as low-dimensional allotropes. Some believes hybridization state of C should be the basis of allotropy in C [299] and tend to exclude low-dimensional forms. Whereas, hybridization states of these forms are distorted (sp^3-like or quasi-sp^2) [296,301] mainly due to geometrical effects [302]. Curved geometries (of nanoballs and nanotubes) act as constraints for the realization of pure sp^2 and also influence aromaticity level [302]. Also, inclusion of pentagonal rings in the structures further alters the behavior of sp^2 state (see following review [296] for the citation information original studies).

1.2.2. Carbon Nanotubes: A History of Effort

CNTs (see Figure 1-15) are skinny and long cylinders of C atoms. A single CNT tubule[12] practically consists of two compartments: Hemi-spherical CNB caps[13] and a tubular side-wall. This formalism is given for SWCNTs, but also covers MWCNTs since nested (viz. not scroll-type) MWCNTs are concentric SWCNTs (3 or more[14]) of varied diameters (see Figure 1-16). Similarly, CNBs have MW forms which are known as C-onions [303]. So, both SW and

[11] There is a plenty of variations for the terminology of CNBs. In the original paper, Kroto and coworkers reported the discovery of first member of CNBs and provided a simple nomenclature. They coined the structure with two terms as "C60" because it has 60 atoms and "Buckminsterfullerene" due to the resemblance of the C60 to geodesic domes (see Appendix-B). They also, visualized the structure with football whilst suggesting truncated icosahedral structure. Then, many researchers preferred to use related terminologies including buckyball, fullerene, and NB. In case we want to emphasize the number of atoms in the structure we will use numbered style and otherwise will prefer to use "NB" term.

[12] From this point on, we use the term "tubule" to indicate an individual nanotube.

[13] CNB caps can be absent due to processing induced truncation and premature CNTs may form during synthesis.

[14] DWCNTs are also available but unless stated they can also be taken as MWCNTs.

MWCNTs can be considered as extended forms of CNBs (see Figure 1-17 and Figure 1-18) [304-305].

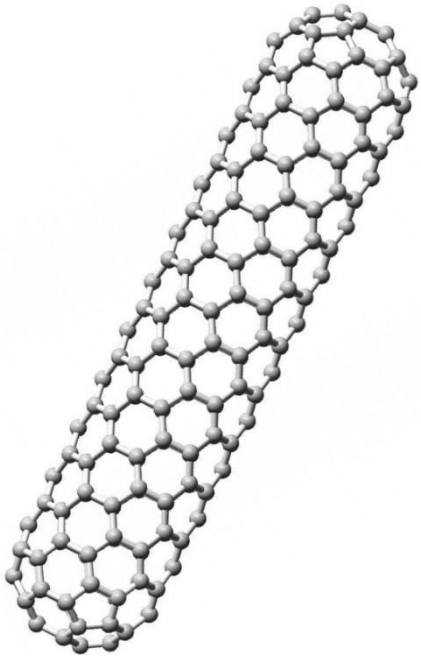

Figure 1-15. A short single-wall carbon nanotube [306].

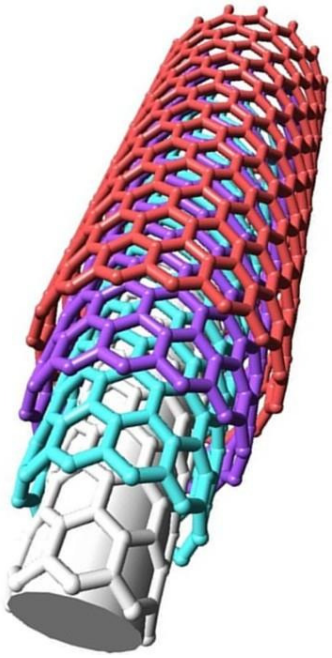

Figure 1-16. An arbitrary type multiple-wall carbon nanotube [306].

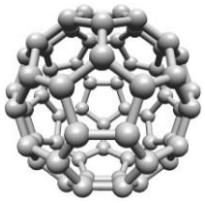

Figure 1-17. Truncated icosahedral carbon nanoball: C60 [307].

Figure 1-18. C70 as a very short single-wall carbon nanotube [307].

CNTs are outcomes of a world-wide effort from different scientific and technologic interests on C species. Naturally, CNTs seems as a continuation in the history of CNBs. In reality, CNTs have been synthesized before groundbreaking works of Iijima, but did not gain attention (see Table 1-1). CNTs have first unconsciously been formed centuries ago by Damascus steel makers [308] and have been serving as *in situ* reinforcer as a result of high temperature processing (forging and annealing) of C in the presence of metal impurities (viz. catalysts) [308-310]. This was as an example of optimized C-steels and appearance of real CNTs waited a long time. Then, in the early 1950s, CNTs have been synthesized and also C was studied in fiber form (recall Table 1-1). Age of nanotechnology experienced the rediscovery of MWCNTs and revelation of SWCNTs by Iijima and a systematic research on CNTs has been triggered accordingly. Today, CNTs are surely the most studied nanoparticles and offers a flourishing plethora of applications. Indeed, the term “CNT” comprises nearly limitless types of tubular CNPs. These materials offer a variety of fundamental research and practical application opportunities. From application point of view, synthesis, characterization, purification, sorting, and dispersion are prerequisites for successful applications. Today, every single aspect of CNTs reveal a fruitful literature with hundreds (or even thousands) of papers and patents.

Table 1-1. Essential milestones in carbon nanotube science and technology (note that applications are excluded).

Year	Summary of breakthroughs and main contributions	Reference(s)
1917	Demonstration of puckered layers in preheated graphite samples	[311-312]
1930	Estimation of curved layers in natural mineral materials	[313]
1952	Discovery of MWCNTs: Electron micrographs of hollow carbon fibers (about 50 nm in diameter) of decomposed CO	[314-315]
1953	Discovery of MWCNTs: Vermicular growth of C probed by SEM	[316-318]
1960	Fabrication of arc technology produced rolled graphite fibers (*whiskers*)	[319-320]
1960	Clear electron micrographs of MWCNTs	[321]
1970	Scientific prediction of the possibility of fullerene (CNB) structures	[322-323]
1976	Transmission electron micrographs of chemical vapor deposited carbon fibers that contain SW/DW-like portions	[315,324]
1984	Laser vaporized C clusters of 1-190 atoms	[325]
1985	Discovery of C60: Artificial synthesis of first CNB and proposition of its molecular structure	[326]
1990	Isolation, non-aqeous dispersion (in benzene), and purification of C60 solid (fullerite) in macroscopic amounts and experimental confirmation of its icosahedral molecular structure	[327-328]
1991	Observation of coalesced CNBs as elongated CNBs	[329]
1991	Rediscovery of MWCNTs: Arc-discharge based synthesis	[298]
1992	Evidence of concentric (MW)CNBs (a.k.a. C-onion)	[303]
1992	Aqueous dispersion of CNBs: Guest@host stabilization	[330]
1993	Simultaneous discovery of SWCNTs by two groups	[331-332]
1996	Demonstration of the roped (bundled) state of SWCNTs	[333-334]
1997	Aqueous dispersion and purification of CNTs via surfactant molecules	[335]
1999	Non-aqueous dispersion of CNTs: Polymer wrapping concept	[336]
2001	Aqueous dispersion of CNTs via linear polymer wrapping	[337]
2001	Separation of SWCNTs according their electronic properties	[338]
2001	Protein-assisted aqueous dispersion of pi-stacking agent modified CNTs	[339]
2002	One-step aqueous dispersion of CNTs via pi-pi stacking interactions	[340]

It should also be emphasized that rediscovery of (MW)CNTs [298] initiated a new field sometimes called as "nanotube science". The first non-C nanotube [341], tungsten disulphide in MWNT form, was demonstrated by Tenne and co-workers in 1992. Then, boron nitride nanotubes [342] were reported as new pi-conjugated nanotubes. Today, literatures of boron nitride nanotubes and CNTs are particularly intertwined, but due to space concerns we do not concentrate on boron nitride nanotubes.

1.2.3. Synthesis, Purification, Sorting, and Characterization

1.2.3.1. Synthesis and purification

Synthesis and growth of CNTs is out of interest of this study, but a fundamental understanding is helpful to understand extreme diversity of CNT molecules and the importance of noncovalent functionalization. Today, there are three main routes for CNT synthesis [343-344]: Pioneering works at NEC Corporation on CNTs[15] [298-331] were performed via electric-arc discharge evaporation (in short, arc discharge) using catalysts. This process yielded with detectable amount of CNTs, but it was not enough for real-life applications. Since then, one of the most challenging goal of researchers was to obtain CNTs in high amount [345-346]. Large-scale (gram and above) synthesis of CNTs (MWCNTs: [347], SWCNTs: [348]) first achieved by metal catalyzed arc discharge synthesis. In the meantime, pulsed laser ablation (vaporization) was exploited to achieve large amount SWCNTs in the presence of transition metals [333-334]. One major advantage of this technique was to obtain purer products [349]. Then, conventional technique (through pyrolysis of C-based species) was applied to SWCNT production [350] and became today's most common commercial manufacturing routine [343] due to its economic benefits (i.e. low temperature and moderate pressure synthesis) [331] (particularly see HiPCO [346] and CoMoCAT [351] processes). Interestingly, the properties of CNTs considerable change depending on the synthesis route applied. Purity level and homogeneity are the most prominent factors affecting synthesis-property relationship of CNPs. Purification is a pre-requisite to prevent interference of impurities before many applications [352-353] and sorting is especially required to benefit geometry-depended properties of nanoparticles [354-355]. Thus, synthesis, purification and sorting should be considered as a whole for CNT applications.

[15] Here, we intentionally exclude the initial –but fairly unnoticed– studies of pre-Iijima era of the field (see Table 1-1 for significant breakthroughs of this period).

Large scale synthesis of CNTs paved the road towards applications. But, industrial CNTs cannot be safely and successfully used as they are. As-produced (raw) products contain catalyst residues, amorphous C, and different types of C-based nanoparticles [352,354]. Catalysts and amorphous C may impede applications. So, purification is a necessary step for CNT processing. Purification of CNTs is a multistep combination of different chemical and physical treatments (see following original articles [356-357] and reviews [358-359] for details). Chemical treatments are generally performed in two steps: i) oxidation and removal of amorphous C (in gas or liquid phase), ii) catalyst dissolution via acid treatment. Chemical treatments are normally performed via manufacturers. As a regular stage of production, filtration [352,357] is also done. Further physically treated CNTs are also available in the market as ultrafine materials. These physical treatments need well dispersed CNTs. Hence, covalent modification, organic solvent dispersion or noncovalent functionalization accompany [360]. Here it should also be noted that, some manufacturers commercialized extremely pure and extremely unfunctionalized CNTs which is available in the market. However, the prices of samples are astronomic; also, surfactants are used during the purification and sorting routines. For a typical example, you are recommended to visit webpage of NanoIntegris Inc. (www.nanointegris.com).

1.2.3.2. Sorting

CNTs are cylindrical polymers of C [361] having different lengths, diameters, and chirality (see following subsection) which have unique properties. For some coarse applications, it is not highly required to reach single-species enriched monodisperse CNT samples [362]. On the contrary, purification is not enough for some applications and sorting might be compulsory due to polydispersity. Some electronic and biomedical applications might require monodisperse materials to achieve high performance (refer following reviews to reach original studies [363-364]). Although there is a great effort [351,365-368], there is no perfectly optimized synthesis recipe to manufacture monodisperse SWCNTs. So, length [369-372], diameter [372-374], and chirality[16] [375-379] based sorting of CNTs are well studied in the literature. Chromatography [369-370,372], electrophoresis [337,380-381], and ultracentrifugation [371,379,382] based procedures are applied for such advanced separation applications (also see following reviews [363-364,383-384]). In addition the effect of

[16] Note that especially diameter and chirality sorted samples are automatically sorted according to electronic structure (see the following subsection).

methods, some noncovalent stabilizers (e.g. deoxyribonucleic acid) *per se* contribute to sort CNTs owing to selective intermolecular interactions [378,385-387].

1.2.4. Structure-Property Relationship

1.2.4.1. Structural basis

Current synthesis strategies do not allow producing mono-type CNT samples. Instead, as-produced samples contain different members containing different numbers of walls, size (diameters and length), chirality and impurity level (catalyst residues and amorphous materials). And, there is an evident structure-property relationship for CNPs, particularly for CNTs. CNT ensembles exhibit different properties which arise from peculiar electronic band structures of individual members [302].

CNBs –ancestor of (SW)CNTs– exhibit five and six membered faces which favor curving into ball-like closed geometries [326]. Defect-free C60 is made up of 20 hexagons and 12 pentagons and exhibits icosahedra symmetry (see Figure 1-17 below and recall Euler rule of pentagon-mediated closure in hexagonal arrays). CNBs are widely known as fullerene (see Appendix-C for etymological route of the term) and generally named with their number of atoms in the structure (e.g. C60, C70 etc.). Considering their chirality, a sophisticated classification can be done for CNBs using molecular symmetry approaches [388-389]. But in practice, simple "C#" convention is practically sufficient to distinguish CNBs from each other. Once it was believed [334] CNTs can be mono-molecularly pure in terms of structure [390]. Whereas, there are infinitely high possibilities to form CNTs each of which having distinct physical properties. At a first glance, the reason behind this enormous molecular diversity seems to be mainly originated from length variations (as it is in organic polymers). Indeed, CNTs can be short as CNBs, and can even reach to the order of centimeters in length. However, underlying reason is not limited tube length, rather related to tube diameter and mostly a result of cylinder chirality. Tube chirality is a geometrical property and explained via chiral vector (C_h, see Equation 1-3) [391]. As a geometrical origin of variation, chirality (mirror symmetry) makes it possible to form a bunch of tubes. So, to identify any type of (SW)CNT, a simple vector formalism based on chirality can be used as an indicator of tube identity (unless stated the rest of the paragraph is written based on the original works [304,392-393] which provided the foundation of notation). In this notation, SWCNTs are

considered as seamless cylinders of rolled graphene sheets (see Figure 1-19).[17] An arbitrary lattice point of graphene sheet (viz. (n,m)) is superimposed to another lattice point which is denoted as origin (O(0,0)). Imaginary superimposition cause Graphene sheet to roll and the roll-up direction is determined by the chiral angle (see Equation 1-4) between tube axis and zigzag direction of hexagons. When "n ≠ m ≠ 0", chiral symmetry occurs and achiral tubes reveal when "m = 0" or "n = m" (see Figure 1-20). Achiral tubes can be in two different forms namely "zigzag/sawtooth" (n,0) and "armchair/serpentine" (n,n). Using geometrical relationships, tube diameters can hence be calculated from chiral indices (see Equation 1-5). Therefore, chiral indices are fingerprint of SWCNTs as molecular materials. Even isomerism can be defined using chiral indices [364,394] for three different types of SWCNTs: (n,m) and (m,n) are isomeric forms (right- and left-handed) where "n" or "m" can also be "0".

Equation 1-3. Representation of the lattice vector and unit cell of graphene sheet (a_1 and a_2 are unit vectors; m and n are chirality indices/integers) [393].

$$\boldsymbol{C_h} = (a_1, a_2) = (m \times \vec{a}_1) + (n \times \vec{a}_2)$$

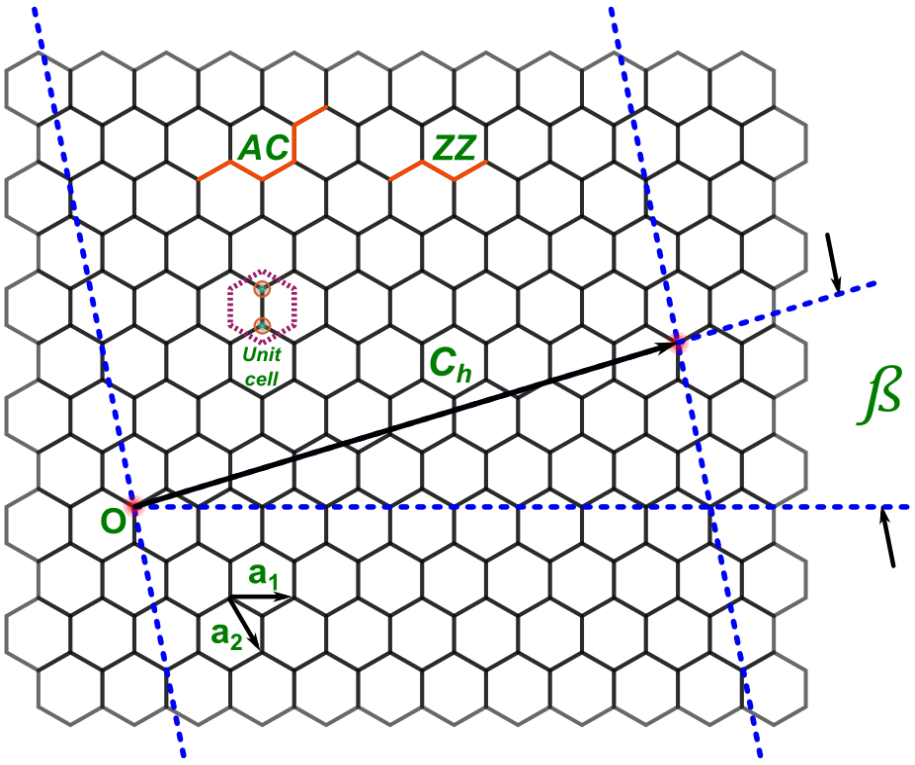

Figure 1-19. Representation of the notation to identify nanotubes using graphene lattice (O: origin, ß: chiral angle, AC: armchair, ZZ: zigzag) (Drawn based on [393,395-396]).

[17] This notation is also valid for MWCNTs, because coaxial arraying of different diameter SWCNTs yield MWCNTs, but not so pronounced.

Equation 1-4. Chiral inclination angle [393].

$$\beta = arctan\left[-\frac{n \times \sqrt{3}}{n + (2 \times m)}\right]$$

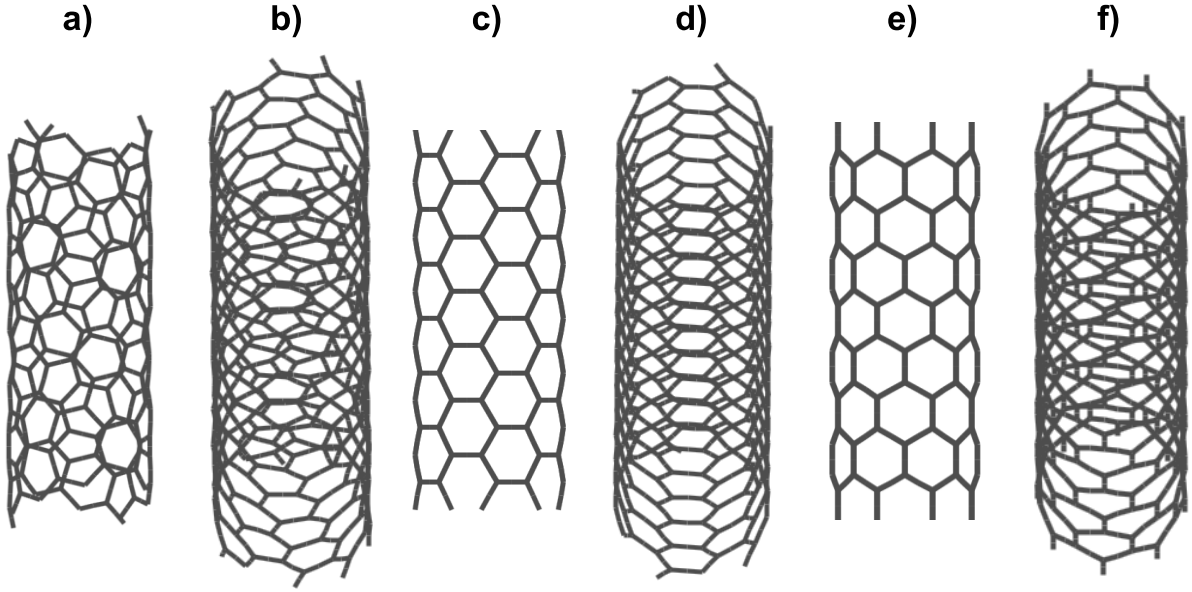

Figure 1-20. Side views and three dimensional like representations of specific single-wall carbon nanotubes: (a-b) chiral (7,3), (c-d) armchair (5,5), and (e-f) zigzag (8,0) (created using CoNTub Version 1.0 [397]).

Equation 1-5. Estimation of the diameter of perfectly cylindrical single-wall carbon nanotubes [393].

$$d = \frac{a \times \sqrt{m^2 + (m \times n) + n^2}}{\pi}, \{\text{where } a = 1.42 \times \sqrt{3}\,[\text{Å}]\}$$

1.2.4.2. Property variations: Origin of the phenomena and its consequences

From both scientific and application point of view, property variations in CNTs are of importance. Geometrical origin of property variations for CNTs has two main dimensions.[18] First, wall number (viz. MW, DW or SW) maintains the properties of CNTs significantly. Especially for biological applications, it is well-known that, wall number (and also length) variations influence the performance and we believe these variations linked to the alteration transport properties in different SWCNTs. Second, as fine geometrical features, helicity variations profoundly influence the characteristics of CNT samples. Above, we indirectly emphasized the role of chiral indice on the properties of CNTs, physical insights behind mostly remained untouched.

[18] Here, we consider purified catalyst and amorphous carbon free CNT samples.

Property variations of CNTs fundamentally arise from electronic structure variations. In the first sense, as graphite [398-400], CNTs might be expected to be low carrier density (viz. semiconducting or semimetallic) materials. Indeed, as-produced SWCNT samples are normally enriched in terms of semiconducting species and approximately two third of possible SWCNTs are semiconductor (see Figure 1-21) [376,401-402]. Conductor tubes are either directly conducting/metallic (armchair tubes) or semimetalic with very small band-gap (so a.k.a. small gap semiconducting) where "n – m" values are evenly divisible by "3" [392,403]. Clearly, electronic type variations are important for electronic applications. However, electronic properties molecular materials are correlated with intermolecular interaction potency [404] and semiconducting SWCNTs are known to be more aromatic than conducting ones [405]. Here, also note that, MWCNTs are conducting regardless of the chiralities of concentric tubules [406-407].

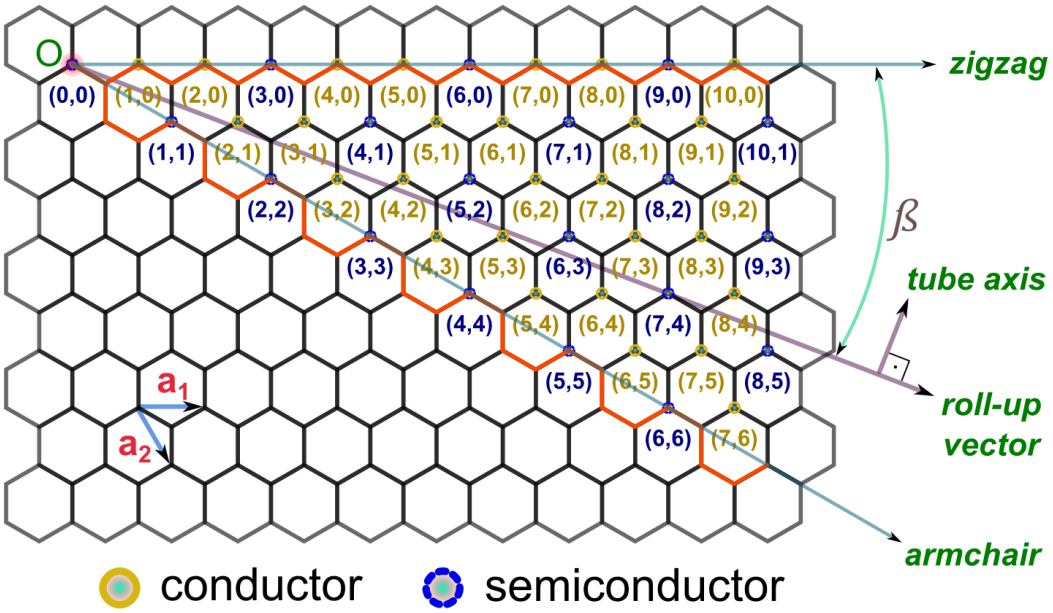

Figure 1-21. Chirality dependent electronic structure variations of single-wall carbon nanotubes: Conductor (metal and semimetal) or semiconductor (drawn based on [393,402]). Note that, some exceptions (small diameter tubules etc.) were ignored for the sake of clarity.

Chirality/diameter dependent band-gap energy variations of SWCNTs are the origin of their peculiar electronic duality [401,408-410]. When band gap energy profiles of different SWCNTs are plotted as a function of tubule diameter, allowed electronic transitions reveal in a group fashion (see Figure 1-22). This behavior is widely explained by electronic transitions between the sharp kinks (spikes) of opposite sides in the density of states of SWCNTs near the Fermi level (theoretical: [392-393,399,411-414], experimental: [401,414-419]). These spikes correspond to vHSs [420] arising from one-dimensional (see Figure 1-23) quantum-

confinement of electrons [421-422]. Aforementioned electronic transitions between electrons (E) and holes (H) (see Figure 1-24) are abbreviated using different notations, but commonly following information is given: Path of transition (from i^{th} to j^{th} for absorption and inverse for emission), electronic type of CNT.[19] This notation is also widely used in the jargon of spectroscopy (i.e. optical absorption, photoluminescence, Raman) since optical properties a direct consequence of their electronic properties. Therefore, successful spectroscopic characterizations of CNTs also rely on a proper knowledge on electronic properties of them.

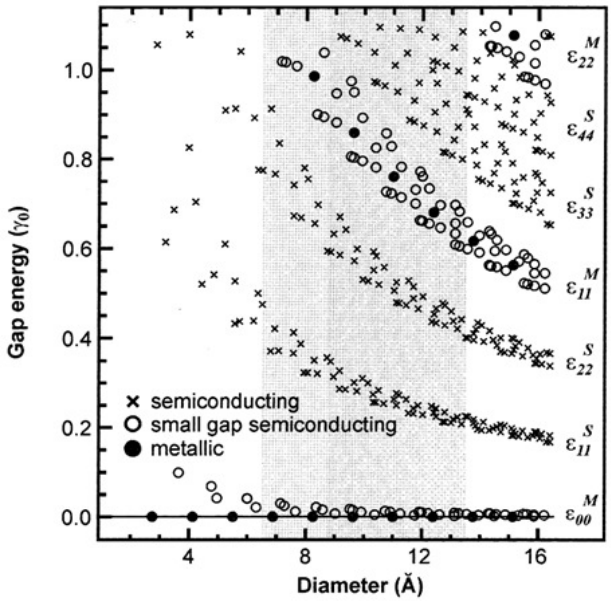

Figure 1-22. Electronic types of single-wall carbon nanotubes as Kataura plot: Tubule diameter dependent band-gap energies (grey shaded area emphasizes dominant tubule types in a regular tubule ensemble) [409]. Note that conduction behaviours of small gap semiconducting ones might be considerably close to the conduction behaviour of metallic ones (look to the bottom of the graph).

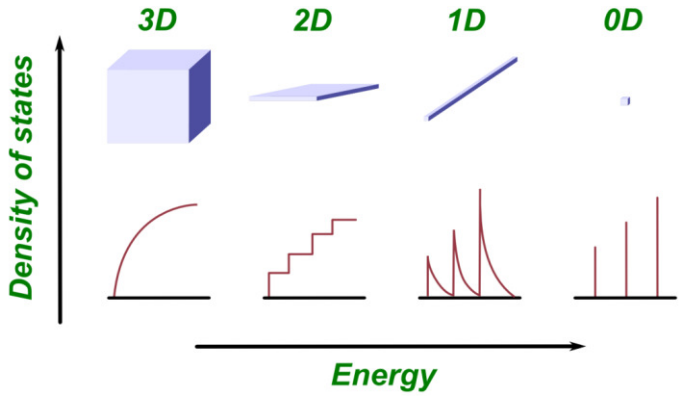

Figure 1-23. Dimensionality based variation of density of states profiles of materials (Redrawn from [59]).

[19] For instance, "$\mathcal{E}_{11}^{M}$" can be seen elsewhere as "E_{11}^{M}", "M_{11}"; or without denoting electronic type, directly "E_{11}" is preferred by some researchers.

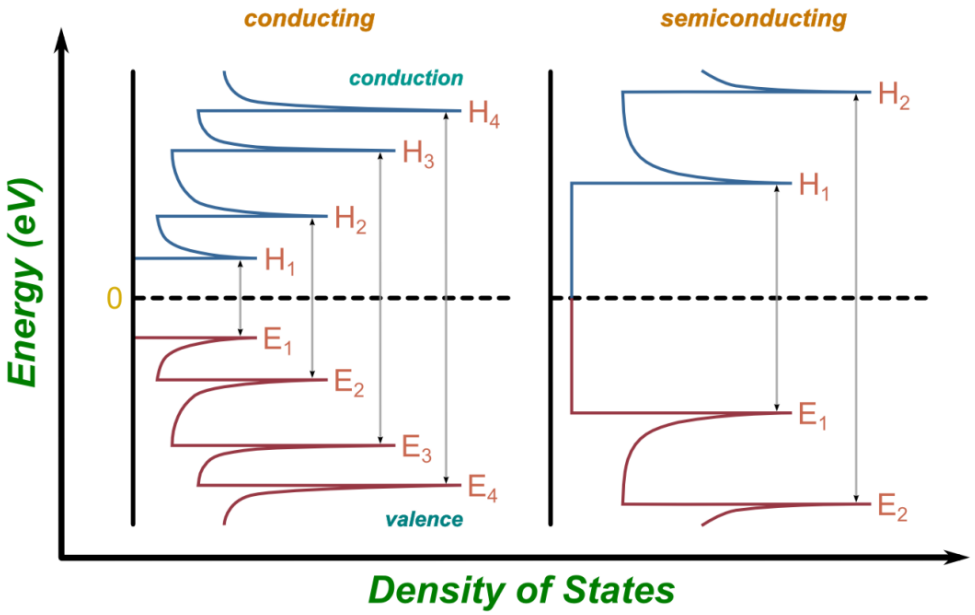

Figure 1-24. Idealized representation of allowed interband transitions for semiconducting and conducting single-wall carbon nanotubes (Drawn for ~1.5 nm diameter arbitrary tubules based on [403,409,423]).

In concept, CNTs are considered as perfectly rolled tubules of CNSs. In reality, geometrical variations of CNTs are beyond wall number and chirality/helicity differences. There are point defects and major geometrical distortions like junctions, helicoids, and rings [424-425]. Also environmental distortions are highly possible due their elasticity [426]. The presence of non-NT carbonaceous nanoparticles (i.e. nanoring, nanojunctions) influences the properties of CNT samples. Wall number and helicity variations readily make the applications and characterizations tricky and imperfections overcomplicate the picture.

1.2.5. Applications and Challenges

Superior physical properties and interesting biological activities of SWCNTs triggered a worldwide attention towards applications. Potential and realized applications of CNTs span of fields including electronics, optics, sensing, imaging, membrane fabrication, filled composites, energy storage, catalysis, pharmaceuticals and biomedical to name a few (see following reviews [427-431]). For different applications, acceptable levels of CNT quality (mainly purity, polydispersity) differ. Some applications such as filled macrocomposites might require lower quality materials comparing advanced bioapplications such as bioimaging. Whatever the needed level of quality, good solvent processability is a common requirement for almost any application of CNTs. Below; applications of filled nanocomposites will be covered emphasizing biological aspects. Then, main challenges against CNT applications will be addressed.

1.2.5.1. Nanocomposite applications

Composite materials are composed of matrix and additive elements. There are three main classes of composites as macro, micro and nanocomposites. Macro and microcomposite applications are generally devoted to mechanical improvements. The additives (such as reinforcer fibers) are responsible for mechanical durability. Mechanical durability of reinforcers is important for successful applications, but interactions (interfacial bonding) between matrix and additive elements are more important in terms of performance issues. In nanocomposite case, interfacial area between matrix and additive is considerably higher due to high surface-to-volume ratio of nanoparticles [46,432-433]. The importance of 1D nanoparticles such as CNTs reveals at this point: Higher surface area and fiber-like geometry of CNTs make them advance counterparts of carbon fibers and graphite whiskers [428,434]. Today, CNT-reinforced polymer nanocomposite products such as tennis/badminton rackets, ice hockey sticks, and bike frames are available in the consumer market [434-435]. CNT-doped nanocomposites are useful beyond mechanical considerations. CNTs can also successfully serve as building blocks of inherently nanoscale (not bulk) materials such as nanocomposites films (viz. nanofilms) and nanoparticle containing nanocarriers. So, any interesting properties of these nanoparticles become exploitable. FE displays and touch screens are already commercialized electronic applications of thin CNT films [428,436-437]. Biological (i.e. biomedical, antimicrobial) applications of CNTs nanocomposites are also vastly available in the scientific literature, but real commercial applications of CNTs require more attention due to direct human interface of those applications (see following subsection).

1.2.5.2. Biological applications

Nanoparticles, especially nanotubes, can directly and easily interact with biological systems mainly due to length scale match and remarkable molecular mobility [17,438]. CNTs are internalized through cellular membranes probably without the need of biosignal molecules [439-442]. So, biological importance of CNTs is manifold. pi-networked surface of CNTs serve a multifunctional delivery vehicle for delivery of some highly toxic and/or poorly water-soluble drugs [443-448]. Further, CNT-based bioconjugates are possible for specific targeting [445,449-452]. CNTs are also bioactive surface modifiers in LbL film design. Stimulation of neural cells for growth [453-454], triggering of stem cell for differentiation [280,455] have been reported for SWCNT involved LbL formulations. Surely, both the nature and assessment of interactions between cells and nanoparticles, particularly CNTs, are quite complex [456-459]. As earlier reported by many groups, physicochemical properties of CNTs

drastically influence their bioactivity. For properly purified (catalyst-free) CNT samples; size (diameter [438,460] and length [461-462]) and electronic structure [463] are main determinants of bioactivity. CNTs might cause structural (and hence functional) changes on adsorbed proteins [464-465]. Moreover, CNTs, as any other nanoparticles, are potentially more harmful for human health in aggregated form because aggregates exceed engulfment-mediated clearance capacity of macrophages [441,466-469]. Properly individualized and biopassivated CNTs (i.e. PEG-based encapsulation [470-471]) are still promising for biomedical applications. low water dispersibility of CNTs is the major barrier against bioapplications [472]. CNTs (especially SWCNTs) are well known antibacterial agents in solutions [462,473]. Inhibition of biofilm formation using CNTs of importance especially against antibiotic resistant bacterial strains [474-475]. SWCNT-doped *es*-LbL formulations were already proposed for biofilm inhibition purposes [476] and we believe SWCNT-doped *hb*-LbL designs are good candidates for the same purpose.

1.2.5.3. Main challenges against applications

High polydispersity and low purity of as-produced CNT samples is the first barrier against some advance applications. Current purification and sorting techniques are capable to refine raw CNT samples. But, insolubility is an inherent property of CNTs and arises as major current challenge. In order to increase vdW contact and to reduce surface free energy, individual tubules are well-packed hexagonally. CNTs are also flexible and long aspect ratio materials, so their crystals (bundles) are highly entangled (see Figure 1-25). As a result, multipoint bound and entangled CNT crystals (bundles) tend to stay intact solvent media, especially in polar (i.e. water, ethanol) solvents. Fortunately, dispersant materials (i.e. surfactants, wrappers, pi-stackers) can provide thermodynamically more favorable surfaces in solvent environment and kinetically stabilize the particles in dispersions.

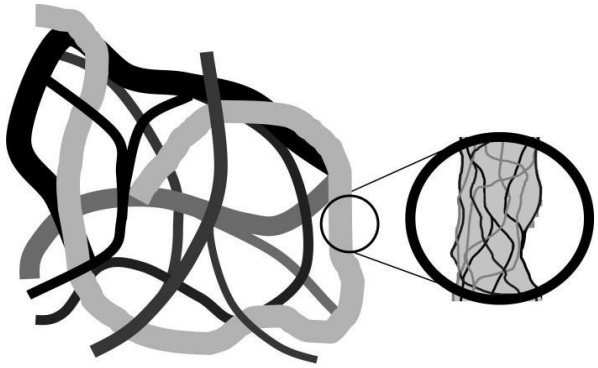

Figure 1-25. Different length scales of bundling in carbon nanotube dispersions:
Bundles in liquid environment (left) and individual tubules in swollen bundles (right) [477].

There are two main approaches to "solubilize" CNTs: Covalent and noncovalent chemistry. In both covalent and noncovalent chemistry of CNTs, pi-network of CNT surfaces is the main concern. Covalent modifications might proceed through regions where pi-networked system is broken (weaker) rather than highly stable sidewalls [478-480]. Topological (i.e. pentagon-heptagon pair) and point (i.e. hole) defects are less stable than hexagons and susceptible to reactions [479]. Similarly, capless (open end/tip) CNTs and even caps themselves are prone to chemical derivatization [479,481]. Chemical derivatization can be done via attachment of small functional groups [482-483] or polymers [484-485]. In any case, molecular properties of CNTs alter due to the disruption of pi-conjugation [339,486] which is sometimes avoided to preserve pi-networks. Here we should also emphasize that, when "pristine" (virtually unfunctionalized and highly pure) CNTs are under question, a minute level of covalent functionalization present is ignored. Since, there is a tradeoff in between purity and pristinity. As already mentioned, purification routines functionalize CNTs depending on the stringency of purification. But still, even researchers (naturally also the manufacturers) consider those particles as "pristine". In accordance, those unwanted but inevitable functionalities are not enough to disperse CNTs in aqueous environments. So, further covalent and/or noncovalent treatments are performed.

1.2.6. Noncovalent Functionalization

Simplest way to noncovalently disperse CNPs is to exploit suitable organic solvents. Some common solvents such as 1,2-dichlorobenzene, chloroform, *N*-methyl-2-pyrrolidone and dimethylformamide effectively "solubilize" CNTs [487-488]. The yields or stability stay below expectations and compatibilizer molecules (dispersing agents) are used as surface modifier agents. Indeed, it is inevitable to make use of those agents to disperse pristine CNTs in water. In the literature, there are numerous studies reporting noncovalent functionalization of CNTs in dispersing agents containing organic solvents. Below, we concentrate on water-based system mainly due to two obvious reasons. First, biological applications normally enforce water-based systems. Second, water is the most environmentally benign solvent.

The idea behind all noncovalent stabilization routes is to modify and shield tubule surfaces via creating supramolecular complexes of molecules and CNTs. A plethora of natural, synthetic, and custom designed molecules are available in the literature for this purpose. Below, we will concentrate on the literature of specific polymer wrappers (e.g. PVPon) and sidewall pi-stackers (e.g. TA). We will intentionally do not emphasize non-polymeric surfactants and will directly exclude inorganic nanoparticle decoration assisted

solubilization. Lucid accounts of past developments and current interests were reviewed elsewhere [360,489] and strongly recommended.

The adsorption of dispersing agents onto CNT surfaces is influenced by a series of parameters (see Chapter 2 and 3). Some major variables are as follows: i) Types of dispersing agents, solvent media, and CNTs, ii) absolute and relative concentrations of dispersing agents and CNTs, iii) the charge nature (pH) and the charge level (IS) of dispersion environment, and last but not least iv) method of dispersion process. Regardless of the dispersing agent used, surface adsorption on particles is regulated by the intermolecular interactions; so, favorable interactions are needed. Up to now, electron-donor acceptor, charge-transfer, pi-pi stacking and CH-pi weak H-bondings interactions were suggested for different systems.

1.2.6.1. Polymer wrapping

Polymer wrapping is an in demand noncovalent functionalization strategy as a nondestructive route to overcome processability problem of CNTs. Adsorbed polymer chains isolate the adsorbents (tubule surfaces) from solvent media as a barrier layer. PVPon is an amorphous vinyl polymer first synthesized by Reppe in 1930s. Its name comes from its pendant lactam ring of five C atoms which is called as pyrrolidone. PVPon is a traditional stabilization agent for hydrophobic particles [490-491], is also reported by O'Connell et al. as the first nonionic homopolymeric wrapper for CNTs [337,419]. They provided a thermodynamic basis to explain the success of PVPon. Indeed, although PVPon is highly soluble aqueous environments, water is not considered as a good solvent for PVPon [492-494]. Intermolecular interactions between PVPon and pi-surfaces of CNPs were commonly explained based on molecular structure of PVPon in a number of ways. Charge-transfer (electron donor-acceptor) mechanisms were discussed to explain the formation of PVPon-CNB[20] complexes [495-498]. Based on electron spin resonance or nuclear magnetic resonance investigations, majority of the papers [495-497] proposed charge-transfer interactions between carbonyl groups of PVPon chains and CNB surfaces. Charge-transfer interactions between positive tertiary amine and negative pi-surface of CNBs is also proposed [498]. Negative oxygen and positive nitrogen of pyrrolidone group cause a strong permanent dipole (3.53 D) [492,499-500]. Induction forces between amide group (pyrrolidone) and negative pi-surface have long been considered to be important for the interactions of PVPon and aromatic molecules (see [501-

[20] Even it is widely ignored in CNT dispersion literature, requirements for aqueous dispersion of CNBs is almost the same. Naturally, useful dispersing agents are also common and PVPon is one of those.

505] for notable discussions about the problem). Backbone of PVPon contains hydrophobic methylene groups and hydrophobic interactions between hydrophobic aromatic groups and PVPon is highly likely [505]. Also, as some other synthetic polymers do [506-507], backbone of PVPon might interact with aromatic tubule surfaces through “CH-pi” type weak H-bonds [508-510]. So, we believe, charge-transfer mechanisms, hydrophobic interactions, and weak H-bondings would cooperatively be responsible for PVPon-aided dispersion of CNPs. Indeed, the solubility of the resulting PVPon-CNT complexes (see Figure 1-26) should be ensured as well. Amide carbonyl functionalities and unbound parts (loops and tails, see following pragraph) of PVPon chains can presumably maintain water-dispersability.

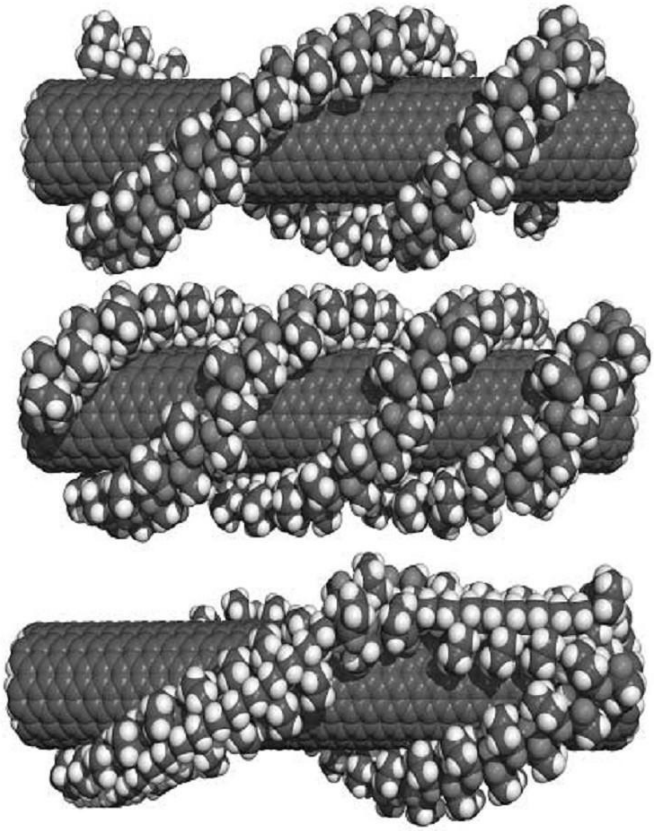

Figure 1-26. Some possible arrangements of poly(N-vinyl-2-pyrrolidone) chains wrapping around an individual single-wall carbon nanotube: Double helix, triple helix, and switchback (top to bottom) [337].

Another ambiguity on PVPon-SWCNT dispersions arise about the arrangement of polymer chains. Even there are limited cases that conformations of polymers on CNTs are well-defined (i.e. helical arrangement of polymers on CNTs [386,511-513]), general scenario fits to Scheutjens-Fleer theory [514-515]. In Scheutjens-Fleer theory (a.k.a. “train-loop-tail” model, see Figure 1-27), adsorbed polymers are considered to partially sit on particles if the concentration of polymer chains is enough for high surface coverage [514-516]. PVPon adsorption of particles is generally considered to arrange on particle surfaces according to

"train-loop-tail" model [499,517-518]. But, O'Connell et al. originally proposed helical arrangement of PVPon chains on SWCNTs (recall Figure 1-26). We believe, recent demonstration of the hollow fiber assembly of PVPon in water [519] also indirectly suggest the possibility of helical arrangement. But, PVPon is a nonionic homopolymer with varying helicity according to its tacticity. And commercial PVPon samples possess mixed tacticity which might break perfect helical arrangement. So, both of the models (train-loop-trail and helical wrapping) would likely coexist in PVPon-CNT dispersions.

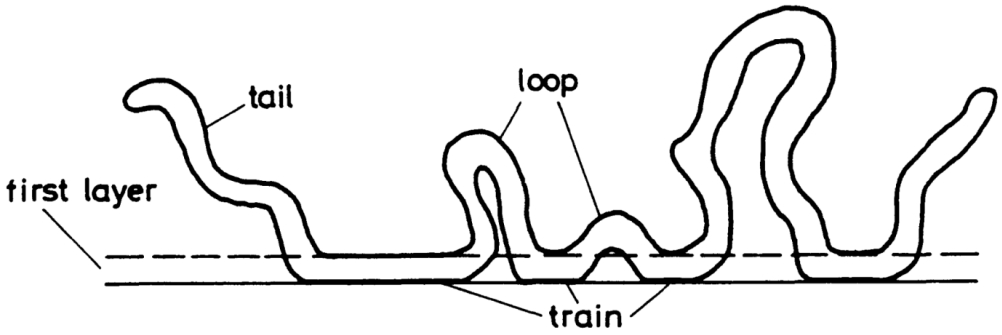

Figure 1-27. Depiction of train-loop-tail model of polymer adsorption on surfaces [516].

On the other hand, PVPon is a strong-bonding acceptor [601] and among the most studied nonionic polymers used in *hb*-LbL architectures [110,201,599,602]. Therefore, PVPon is a potential agent as a mediator for the incorporation of CNTs in *hb*-multilayers.

1.2.6.2. Sidewall functionalization via pi-stacker molecules[21]

CNTs are pi-networked aromatic systems and are naturally prone to aromatic-aromatic (a.k.a. arene-arene, pi-pi) interactions. There are many pi-interacting polymers such as PSS and deoxyribonucleic acid [386,520] that can effectively disperse CNT in solvent media mainly through pi-pi interactions. Even weaker interactions between CNT surfaces and polymers might be enough to achieve stable complexes as multipoint binding of polymers might resist against thermal barrier [158]. In the opposite, small molecules might suffer if relatively strong interactions are absent. Aromatic interactions are strong enough and so even small aromatic molecules can disperse CNTs. First, aromatic macrocyclic molecules belonging porphyrin and phthalocyanine families were employed to disperse CNTs in organic solvents [521-522]. Then, plant polyphenols (both condensed and hydrolysable forms) are suggested as dispersing

[21] The term "sidewall functionalization" is also in use to express functional group attachment to the sidewalls of CNTs through covalent chemistry. So, we would like to emphasize pi-stacking interactions between small pi-stacking molecules and pi-networked CNT surfaces (in abbreviated form as "sidewall pi-stacking").

agents for CNTs. So far, catechins (green tea extract) [523-524], humic acids [525-526], fulvic acids [525,527], and TAs [525,528-529]) were confirmed as effective agents for the stabilization of CNTs in water. In fact, first ultrasonic comminution of graphitic C was reported by Matuyama in mid-1960s. In his fairly unnoticed but highly splendid study [530], some surfactants and TA were reported as effective stabilizing agents. Among the pi-stacking agents available, TA not only stands out as a successful dispersing (stabilizing) agent, but also draws attention due to its popularity in LbL field [122-123,213,531].

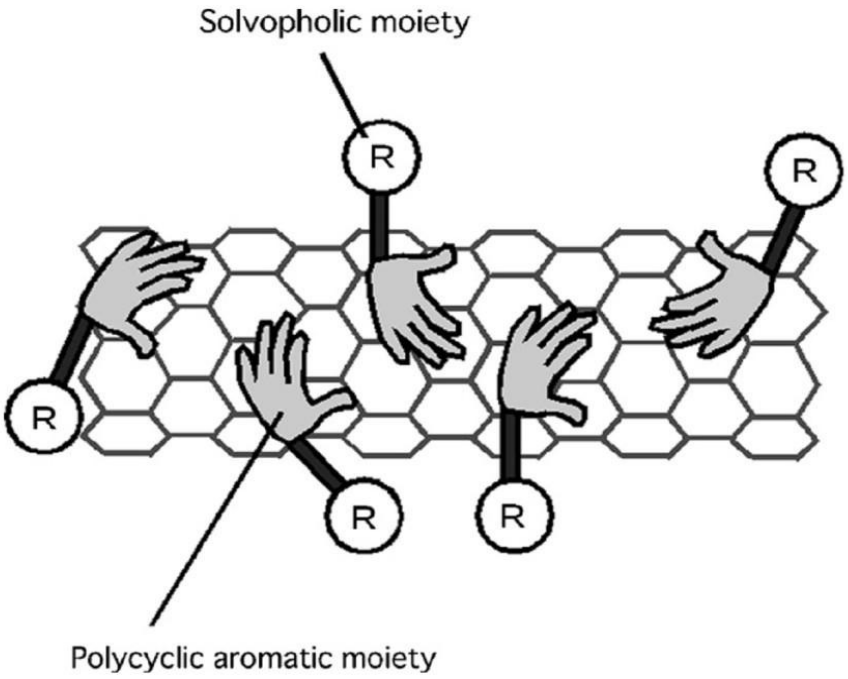

Figure 1-28. Depiction of the functionalization of carbon nanotubes using small aromatic molecules [532].

In addition to relatively high binding energy of pi-pi interactions, geometrical properties and bendability of TA [533-534] likely contribute to the effectiveness of interactions. Since, geometrical distortion of adsorbed aromatic molecules might increase intermolecular interactions and favor surface adsorption. This has previously been shown for benzene adsorption on platinum surfaces [535] using density functional theory through computation. Then, this principle was also suggested [536] to be important on the interactions of aromatic polymers and CNTs. It is logical to expect a similar contribution to interaction tendency via distortion of aromatic polyphenols on CNTs. So, not only the abundance of aromatic groups but also the spatial arrangements of those are important for the fate of intermolecular interactions between CNTs and polyphenols. Natural polyphenols are typical weak polyelectrolytes and effect of solution chemistry might be drastic on weak

polyelectrolyte aided CNT dispersions [528,537]. So, ionization degrees, conformational properties, and solubility of polyelectrolytes are pH-, and IS-dependent. Indeed, researchers are aware of pH-dependence of small polyelectrolyte adsorption on C surfaces for decades [538-539] and sorption tendency (coefficients) of polyphenols on CNTs exhibit pH dependence [528]. In fact, this is probably not only a consequence of the behavior of polyphenols; also intermolecular tendencies of CNTs are influenced by solution chemistry.

1.2.6.3. Ultrasound-aided Debundling of Carbon Nanotubes

CNT bundles, as many other layered/stacked nanoparticle sources, might be exfoliated in two ways: i) Spontaneous dissolution via appropriate solvents, ii) mechanical energy mediated disruption of particle-particle interactions. Spontaneous dissolution of CNTs is achievable using superacid [540-541] or organic [542-543] solvents.[22] On the contrary, pristine (or slightly functionalized) CNT bundles require mechanical energy to disperse in solvent media. There are two main energy source to exfoliate CNT bundles namely shear and cavitation forces. Pure shear force mediated exfoliation suit to viscous fluids[23] and can be applied in many ways including calendering (a.k.a. three roll milling) and high shear mixing [544-546]. Whereas ultrasonic cavitation (see [547-548] for a historical account of the technology) assisted exfoliation rather suits dilute to semi-dilute systems.

Cavitation phenomenon is originated from the formation of vapor filled bubbles (cavities, voids) in liquid due to the oscillating pressure changes of surrounding acoustic waves [547,549-551]. Formation of cavitation bubble (nucleation) proceeds with growth and collapse stages (see Figure 1-29) in multiple locations of the transfer media [547,549-551]. Collapse of cavitation bubbles near solid surfaces causes formation of “liquid (micro)jets” (see Figure 1-30 and Figure 1-31) [551-553] which is accompanied by the evolution of violent energy (see Figure 1-32) in “hot spots” [549,550,554-555]. Liquid jets not only apply shockwaves to surfaces; but also induce microscopic vortices (a.k.a. microturbulence, microstreaming and microeddy) [556-560]. Microturbulence cause intense mechanical agitation and friction (viz. shear forces) between medium and solids [561-563] which is probably the fundamental mechanism of CNT exfoliation using sonication. In addition, velocity of microjets are transferred to the particles and particle-particle collisions take place at a high speed [544,552,554] which might grind CNT bundles and facilitate exfoliation.

---

[22] Superacids not only serve as solvent, but also functionalize CNTs.

[23] So, generally preferred for high volume nanocomposite applications (i.e. resin transfer molding).

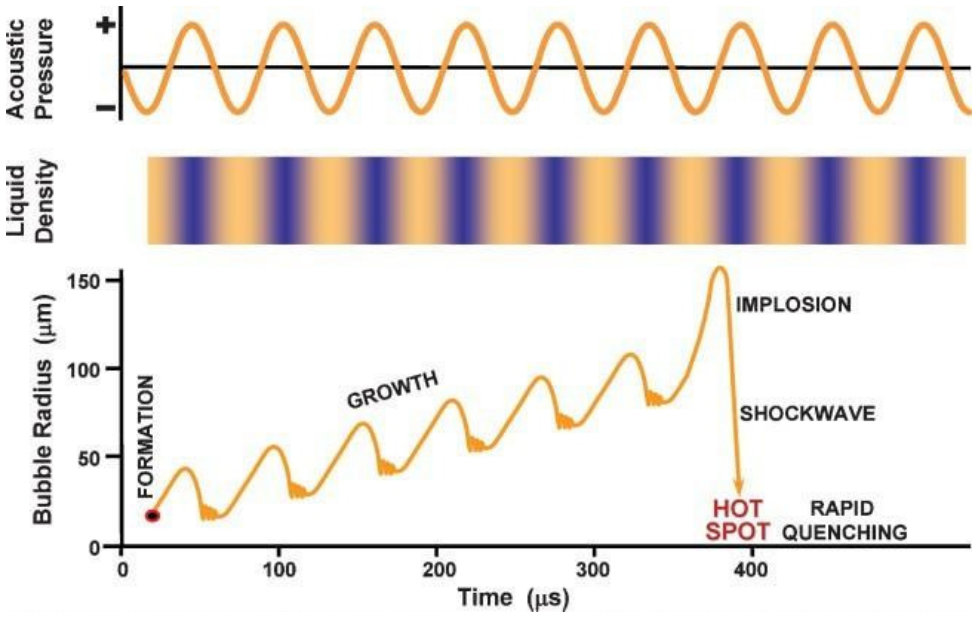

Figure 1-29. Scheme of oscillation in transient life of a single acoustic cavitation event [553].

Figure 1-30. Scheme of the stages of a cavity implosion near a surface and the formation of the liquid jet [551].

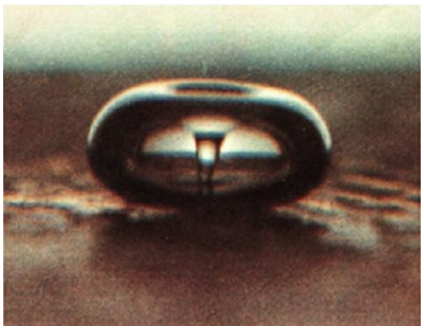

Figure 1-31. Photomicrograph of a liquid jet (size of the bubble is ~150 μm) [551].

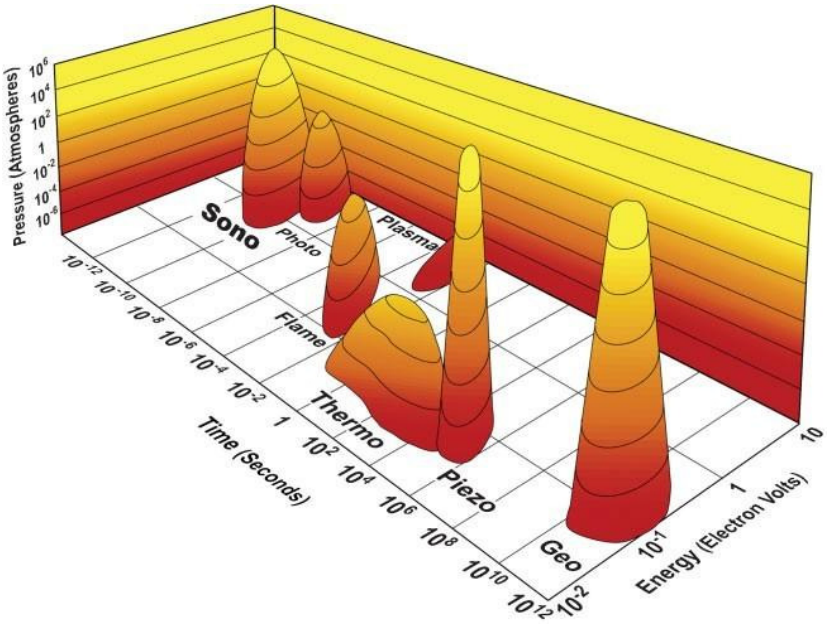

Figure 1-32. Extreme energy and time space of sonochemistry comparing some other chemistries [553].

CNT dispersion problem is a complex process optimization task [563-565]. Due to great variety of CNT samples and dispersing agents, each couple requires specific conditions for better results. In the literature, one can reach hundreds of procedures to debundle CNTs via ultrasonication. Most researchers arbitrarily select and modify a predefined procedure and the details of the modifications are vague or completely lacking. Cavitation phenomenon is sensitive to many coupled variables and reproducibility is only achievable via decreasing uncertainties. Intensity of acoustic power, ultrasonic frequency and duration of agitation are the main parameters of sonication experiments [563,566-567] and hence commonly reported. Other fundamental parameters such as solvent viscosity, surface tension, vapor pressure and gas solubility [548,563,568] can be estimated using solvent and solute compositions (types and concentrations). However, cavitation-induced increase of heat perturbs the system and a strict control is frequently needed on global (bulk) temperature. In addition to a strict control on the temperature, geometrical parameters should also be reproducible for process optimization. Flow patterns in ultrasonic baths and vessels are inhomogeneous and cavitational yield of different zones might vary significantly due to continuous attenuation of sonication energy by surrounding media and constructive/destructive interference of sonic waves [569-575]. In accordance, i) position and number of transducers [576-577], ii) material [578] and dimensions [572] of vessels, and iii) volume and position of sample [579-580] (and also transfer media in ultrasonic baths) are also important. Unfortunately, the complexity of the problem is not limited to the cavitational yield and energy transfer efficacy aspects. Since, high power and/or prolonged ultrasonication possess adverse chemical/physical effects on graphitic surfaces of CNT [581-582], and organic molecules (i.e. phenolic materials and polymers, see Chapter 3). Therefore, dispersion recipe preparation is also a matter of balance and less harsh conditions are searched. Prior wetting (and swelling) of CNT bundles with dispersion solvent might increase the efficacy of sonication and decrease required duration. So, CNT powders are incubated in solution of dispersing agent under low speed shaking to maintain complete wetting. Prior wetting facilitate debundling of CNT ropes but a portion of well-packed bundles inevitably don not disperse. Specific gravities of individual CNTs are normally smaller than bundled CNTs and bundled particles precipitate in time [335,419,583]. To accelerate sedimentation and collect stable dispersions, dispersions are subjected to centrifugation. As a result, main element of dispersion procedures is ultrasonication but quality of end product is not only determined by sonication parameters as well.

1.2.7. Characterization of Carbon Nanotubes

To maintain reproducibility, characterization of used CNT is crucial and is held basically in different states solid and dispersed state. Solid state characterizations are mainly held to assess impurity and pristinity levels (the rest of this paragraph is collaged from following reviews [584-585]). For instance, FT-IR and XPS are used to assess the presence of (un)wanted functional groups on CNT surfaces; XPS, SEM, and TGA[24] are employed to detect presence of residual catalysts. However, dispersed state is much more fruitful in terms of characterization opportunities and requires a solid knowledge of structure-property relationship in CNTs. Below; we will discuss the characterization colloidal SWCNT dispersions briefly.

1.2.7.1. Dynamic light scattering

Thermal energy driven motion of dispersed particles can be exploited for the estimation of size distribution. In the dispersed form, particles undergo Brownian motion [586-587] and behave as though they were spinning. In case, dispersions are exposed to light, the intensity of scattered light is influenced by the motion of particles in the dispersion (see Figure 1-33). DLS (a.k.a. Quasielastic Light Scattering, and Photon Correlation Spectroscopy) records particle size dependent scattered light intensity variations in solvent media and intensity of light fluctuates in time is correlated with the diffusion coefficient using Stokes-Einstein relation (see Equation 1-6). Correlation data is analyzed using Laplace inversion based fitting algorithms[25] and particle size distribution is obtained. Hence, the technique does not give direct information of individual particles; a particle size distribution is obtained for ensemble of particles. The theory behind is devoted to spherical particles and so, spherical equivalent of solvodynamic (a.k.a. hydrodynamic size for water-based systems) diameters are obtained in case no correction treatment [588-589] is applied.[26]

Equation 1-6. Stokes-Einstein relation of diffusion constant (D: diffusion constant; k_b: Boltzmann constant, T: the absolute temperature, η: solvent viscosity, r: hydrodynamic radius of the particle) [590].

$$D = \frac{k_b \times T}{6 \times \pi \times \eta \times r}$$

[24] TGA is also used for thermal stability and dispersion efficiency assessments (see Appendix Q).

[25] Stringency of applied algorithm might influence resulting data.

[26] Hence, actual size of the particles might differ.

CNTs are evidently cylindrical, but DLS is widely used to characterize CNTs with or without geometry correction [591-593]. There are several reasons of wide use of DLS in CNT characterization such as noninvasive measurement, fast data collection, and *in situ* measurement capability. However, the technique is vulnerable to large aggregates [587,594]. In fact, DLS can handle large aggregates up to a certain limit (several micrometers) and this limit is high enough to judge aggregation state of CNT samples.

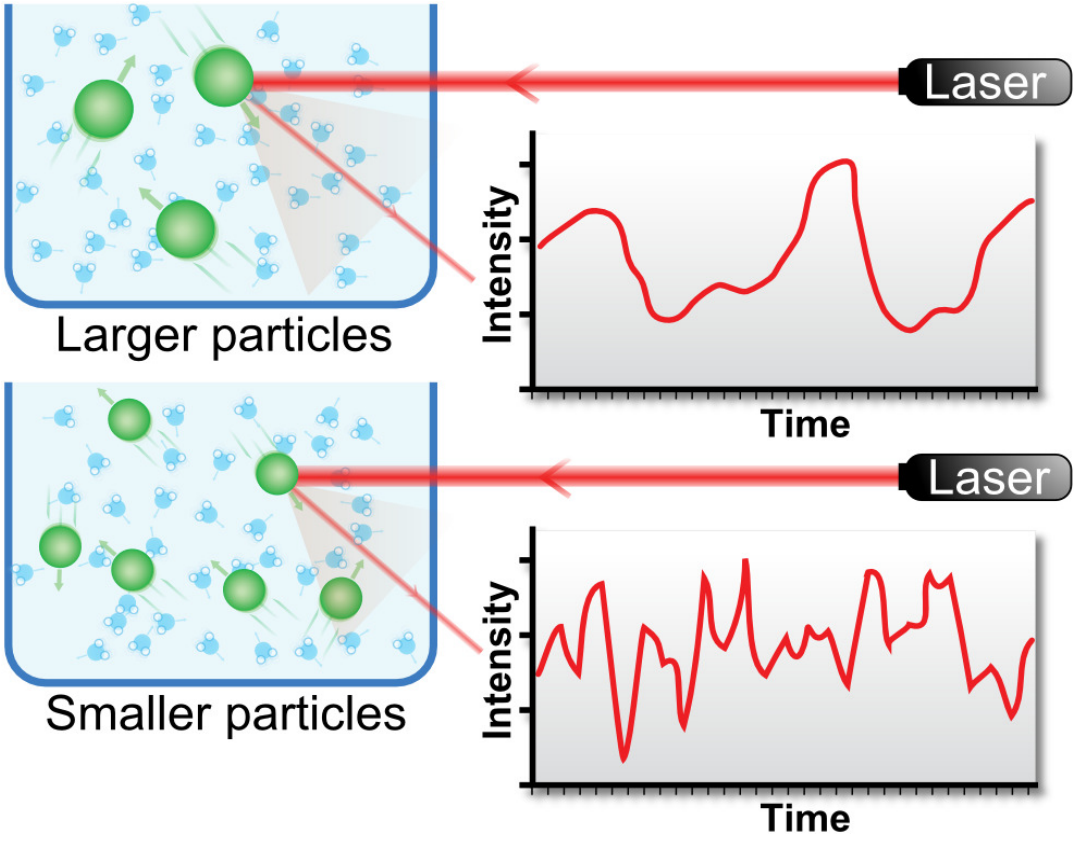

Figure 1-33. Dynamic light scattering of two samples have larger and smaller particles (Obtained from "http://en.wikipedia.org/wiki/Dynamic_light_scattering" and slightly modified).

1.2.7.2. Zeta potential analysis

Stability of particles in dispersions is maintained via two fundamental mechanisms called steric and repulsive stabilizations. Steric stabilization describes the isolation of particles from each other using molecular barrier which are typically adsorbed polymers [595]. The other mechanism is repulsive stabilization and explained via surface charges. There is no direct way to measure surface charge of dispersed particles, but ZPA (a.k.a. Laser Doppler Velocimetry) provides an elegant way to converge surface charge values [596]. The basic phenomenon of ZPA can be described using diffuse double layer model. In this model, each charged particle is considered to be surrounded by a double layer of electrostatic charges in solvent media (see

Figure 1-34). The first layer is assumed to involve as dense layer of counterions within a small distance around the surface to neutralize surface charges. Around the first layer, a second layer forms which is rich in counterions (a.k.a. diffuse layer). Then, the bulk solution comes which is charges evenly represented. Such a formation of charges causes an electrokinetic potential between the surface and bulk liquid. When a voltage is applied to the surface charge carrying particles containing liquid, particles move having a fixed velocity which is called as electrophoresis. Mobility of particles is correlated to two main factors: i) electrical potential in the outer surface of double layer (a.k.a. slip(ping) or shear plane), and ii) physicochemical properties of suspending liquid such as dielectric constant and viscosity (see Equation 1-7).

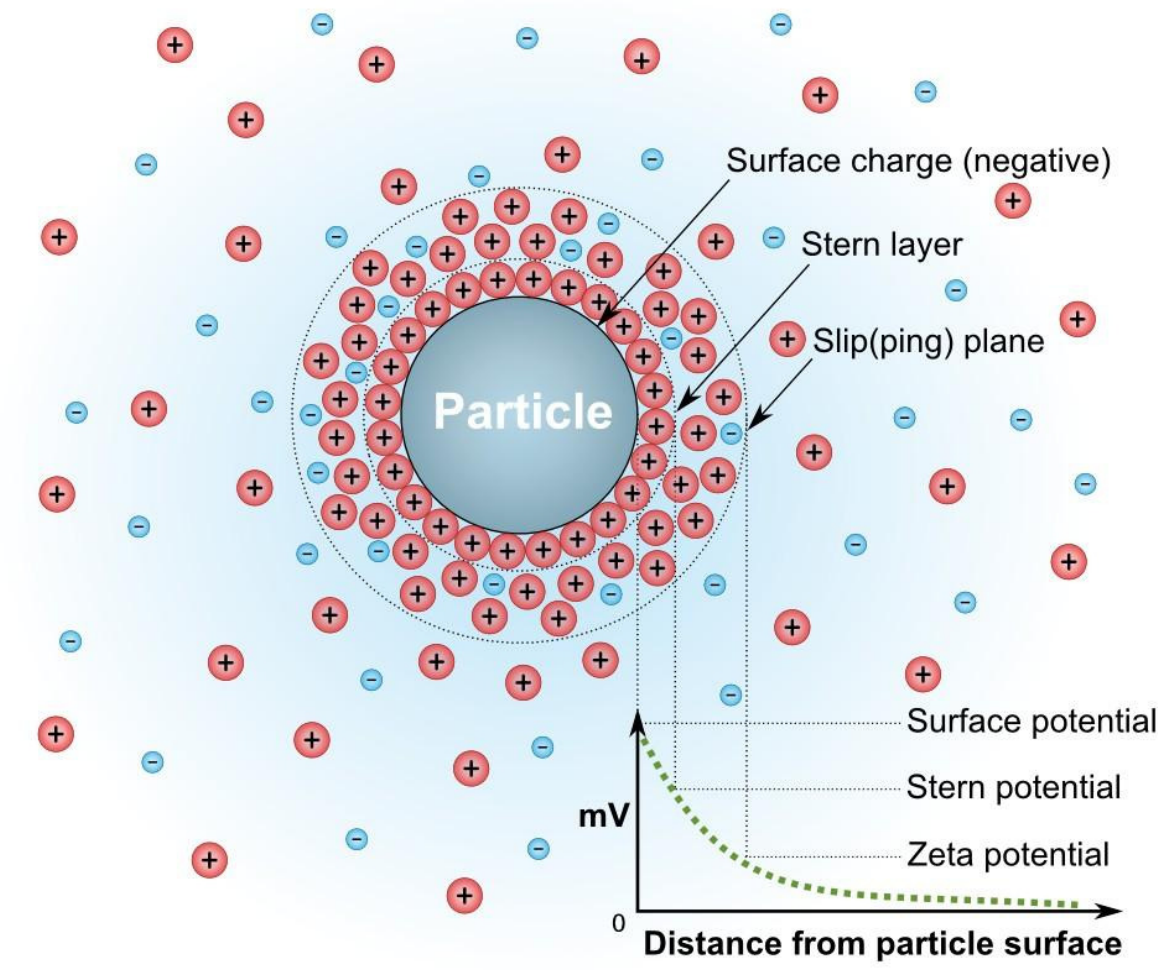

Figure 1-34. The electrical double layer formed around a spherical particle and zeta potential occurred in slipping plane (Obtained from "http://en.wikipedia.org/wiki/Zeta_potential" and slightly modified).

Equation 1-7. Henry's equation of electrophoretic mobility (μ: electrophoretic mobility, ζ: zeta potential, ε: dielectric permittivity constant, η: viscosity, κ: Debye length, a: radius of a spherical equivalent particle, f(κ×a): Henry's function which is taken as "1.5" in Smoluchowski's approximation for polar media such as water and is taken as "1.0" for nonpolar media in Hückel's approximation) [597].

$$\mu = \frac{2 \times \zeta \times \varepsilon}{3 \times \eta} \times f(\kappa \times a)$$

Similar to DLS, theory of ZPA is established on the assumption of perfectly spherical particles and shape irregularities increase deviations. But regular ZPA is still used as a routine for CNTs [598-601] without complicated correction treatments [602-603] to assess dispersion efficacy of dispersing agents and applied protocols. Also, there are a number of studies on the analysis of CNT-salt interactions using the framework of DLVO theory. It is believed that counterions (here cations) screens surface charges of SWCNTs and aggregation is favored. According to DLVO theory, stability of colloidal dispersion is a function of attractive (i.e. vdW interactions) and repulsive (i.e. charge-charge interactions of like-charges) forces [592]. Higher the repulsive forces, higher the stability and increased surface charge (higher absolute zeta potential) means enhanced stability. But, total repulsive force is also directly influenced by type and concentration of counterions surrounding charged particles [604]. In fact, role of counterions in DLVO theory directly explains the observations of Schulze and Hardy on salt-induced precipitation of particles [605-606]. Salt-induced coagulation of CNTs (see Chapter 2) also follows Schulze-Hardy rule, and hence obey DLVO theory [595,607]. But, DLVO is incapable to fully explain the stability of noncovalently stabilized CNT dispersions, as steric effects and solvation forces are non-DLVO in nature. So, CNT dispersion is not explainable using DLVO framework alone.

1.2.7.3. Optical absorption spectroscopy

OAS is conventionally used to monitor concentration of molecules/clusters[27] in solvent media or on solid substrates. The technique is generally held in UV (190-380 nm), visible (380-750 nm), and shortwave near-IR (750-1100 nm) regions [608]. In optical experiments, incoming light basically experience three phenomena: Scattering, transmission, and absorption. Among these, absorption (absorbed light) provides extra energy input to the molecules. When the energy of incoming photons matches with the energy difference between an occupied valence and an empty conduction states, transition of the valence electrons takes place. Excitations

[27] From this point on, for the sake of clarity we will just emphasize "molecules", but atoms of "clusters" can also be used via OAS.

promote ground state (minimum energy) electrons to the higher energy levels.[28] This photonic absorption is experimentally characterized using Beer-Lambert-Bouguer (or in brief, Beer's) principle (see Equation 1-8). For known molecular extinction values at a specific wavelength,[29] concentration of dissolved/dispersed molecules can be estimated.

Equation 1-8. Beer-Lambert-Bouguer principle of light absorption
(T: transmittance, c: concentration, l: path length, A: absorbance) [609].

$$T(\lambda) = \frac{I}{I_o} = 10^{-\varepsilon(\lambda) \times c \times l} \text{ and}$$

$$A(\lambda) = colog\big(T(\lambda)\big) = \varepsilon(\lambda) \times c \times l$$

Molecular extinction (a.k.a. and absorption) coefficient ("ε") acts as an indication of light absorption-induced electronic transitions and is a direct consequence of molecular orbitals [609-610]. Conventionally, electronic transitions are explained via real-space molecular orbitals and multiplicity aspects are widely considered [302,611]. However, for large clusters, mainly due to high electron correlations, discrete energy levels do not exist [60,612]. Hopefully, in many-atom systems, atomic energy levels divide into bands and "electron energy density of states" becomes a useful tool to explain the origin of observed transitions [612-613]. (SW)CNTs are molecular ensembles in which different members of the group can be differentiated in optical properties (see Figure 1-35) which is attributed to vHSs (recall Subsection 1.2.4.2 and see Figure 1-36). Depending on the variation of nanotube diameter/chirality, required interband transition (band gap) energy also varies [402,414]. Therefore, OAS is traditionally exploited to probe (n,m) structures and hence electronic properties of SWCNTs [401,614-615].

[28] Usually, transition from "highest occupied" to "lowest unoccupied" molecular orbital (a.k.a. HOMO-LUMO transition).

[29] Note that, any environmental parameter (i.e. pH, IS, temperature) may influence the value of "ε".

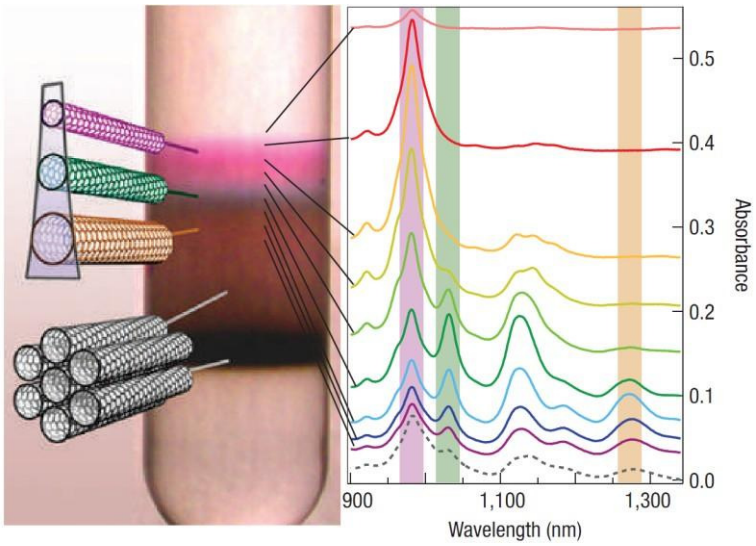

Figure 1-35. Optical behavior variations of density gradient sorted single-wall carbon nanotubes (note that spectra of bundle is dashed curve and is featureless comparing other curves) [377].

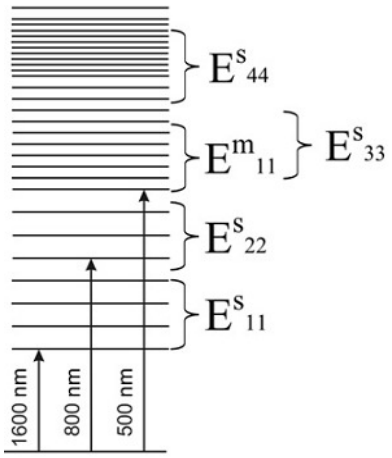

Figure 1-36. Light absorption of single-wall carbon nanotubes in ultraviolet to near-infrared region and corresponding van Hove singularities [616].

In stabilization procedures of CNTs, a significant portion of starting material is normally discarded via ultracentrifugation(s) (recall Subsection 1.2.3.1). So, concentration of CNTs in resulting dispersions is an important parameter to evaluate the efficiency of applied procedures. Especially for noncovalently stabilized systems, OAS serves as a practical route to estimate CNT concentration in liquid media. In the literature, there are a number of studies reporting extinction coefficients of SWCNTs (see Table 1-2) and researchers pick up one of these coefficients. Here we would also like to emphasize that, OAS is not only technique to estimate concentrations of CNTs in dispersions. Some researchers prefer TGA and a recent report showed that RSS also can be employed for semi-quantitative analysis of SWCNT concentration in dispersions [617].

Table 1-2. Available molecular extinction coefficients for carbon nanotubes.

SWCNT Type	Dispersion Technique, Solvent, and Stabilizing Agent (if any)	ε and Wavelength (or Energy)	Reference(s)
HiPco	Ultrasonication, organic solvent (dichlorobenzene), no stabilizer	2.86×10^4 cm^2/g [3.43×10^2 L/mol/cm][30] @ 500 nm	[488,618]
HiPco	Ultrasonication, organic solvent (dimethylformamide), no stabilizer	4.20×10^2 L/mol/cm @ 500 nm	[619]
Laser vaporization	Ultrasonication, organic solvent (dimethylacetamide), no stabilizer	30.0 L/g/cm @ 1.65 eV = ~751.5 nm	[620]
Arc discharge	Ultrasonication, organic solvent (dimethylacetamide), no stabilizer	40.0 L/g/cm @ 1.78 eV = ~696.6 nm	[620]
Arc discharge	Ultrasonication, D_2O (pH 10), sodium dodecyl sulfate	30.3 L/g/cm @ 1035.3 nm	[621]
CoMoCAT	Ultrasonication, H_2O, labeled deoxyribonucleic acid oligomer	4.40×10^2 L/mol/cm @ 991 nm	[622]

1.2.7.4. Vibrational spectroscopy

OAS is the principle spectroscopic method for the characterization of CNT samples. But, in case detailed structural information is needed for examined sample, photoluminescence and vibrational spectroscopies might provide deeper insights. In our study, we studied vibrational spectroscopy of modified SWCNTs and SWCNT-doped multilayer films. Thus, we give brief information below, for vibrational spectroscopy with an emphasis on RSS of CNTs. Because RSS provides deeper molecular insights and can serve fingerprint information of CNTs.

Molecular vibration is the second large portion of energy storage mechanism for molecules after electronic energy [611]. FT-IR and RSS together constitute vibrational spectroscopy and vibrational modes of molecules generally become either Raman- or IR-active (either IR- and Raman-active or inactive modes are also possible). As complementary techniques, vibrational spectroscopy is quite useful for molecular materials and widely used to characterize CNTs. FT-IR spectroscopy of CNTs is tricky and less informative because CNTs absorb IR light highly (dark absorbing property). But, it is still used to verify pristinity of raw CNTs or is used to probe surface functionalities upon covalent/noncovalent modifications. Unlike IR spectroscopy which is based on the measurement of absorbed light,

[30] Concentration is taken as mg/L for transformation.

RSS measures a specific type of emission called inelastic scattering. When the light (photon) and matter collides each other, a portion of light is scattered. The large part of scattered light preserves its energy (in other words wavelength) and this type of scattering is known as Rayleigh scattering which is also called as “elastic” scattering by a mechanical analogy. Conversely, “Raman Effect” can take place which is the exchange of energy between light and matter during light scattering which (a.k.a. “Smekal-Raman Effect” in German and “combination scattering” in Russian literatures). Raman Effect can be in two ways: Either the incoming photon loses some of its energy and a lower energy photon is emitted (Stokes scattering) or the matter transfers a portion of its energy to emitted photon (anti-Stokes scattering). In light-matter interaction rarely both Stokes and anti-Stokes events occur, but anti-Stokes scattering is less likely. Thus, Stokes lines are usually measured which are dowbshifted in wavelength (corresponds to lower wavenumbers). To maintain consistency among different studies performed using different laser sources (different wavelengths), Raman spectra is generally recorded as wavenumber shift (or Raman shift) relative to Rayleigh line. However, CNTs also greatly affected the irradiation wavelength [623].

CNTs exhibit three different important modes, namely radial breathing mode, and disorder (or defect-induced) and graphitic (or tangential) bands [375,624-625]. The most specific feature in the Raman spectra of CNTs is the radial breathing and observed between 75 and 300 cm^{-1}. Radial breathing mode is originated from vHSs, hence can be used probe electronic properties CNT ensembles [375,624]. On the other hand, isolated SWCNTs exhibit an interesting dependence between radial breathing mode and inverse diameter of tubules [375,624]. However, for unsorted samples and complex environments, information of radial breathing mode might be complex to decipher. Instead, disorder (D) and graphitic (G) band are more straightforward. D-band is located around 1330-1360 cm^{-1} and originates from structural defects in graphitic materials. G-mode corresponds to the tangential movements (stretching) of C atoms in their graphitic planes and located around 1580 cm^{-1}. G-mode is the most intense feature of CNTs in their Raman spectra and D/G ratio is conventionally regarded as the level of defects [626-627]. All of those modes can be studied in (aqueous) dispersed form and powder form. Here we should also mention that as useful extension of RSS, Raman microscopy, enables screening of the materials for specific Raman signal and provides spatial information as maps [628]. Particularly, RSM is widely used to probe CNTs in nanocomposite and living cells [623,629].

Chapter 2: TANNIC ACID MEDIATED DEBUNLING and SPIN-ASSISTED LAYER-by-LAYER DEPOSITION of SINGLE-WALL CARBON NANOTUBE DISPERSIONS[31]

LbL assembly is a successful technology for fabricating composite nanomaterials. Here, we show a simple route for incorporating SWCNTs in *hb*-multilayers using TA as a mediator. We selected PVPon/TA pair considering its potential towards bioapplications. We first studied the dispersion of SWCNTs in salt-added TA solutions for preparing stable TA-SWCNT colloids to further follow the study of Erel and Sukhisvhili [122] which reports salt-added multilayer dip-assembly of PVPon and TA. We ultrasonically debundled SWCNTs in pH-adjusted TA solutions and characterized resulting colloids using DLS, ZPA, and OAS. In agreement with earlier reports, we observed the adverse effect of electrolytes on colloidal stability. At low pH values (below pH 6.00), only a trace amount of SWCNTs were dispersed. Then, we employed electrolyte-free TA solutions for dispersing SWCNTs and obtained highly stable and more concentrated colloids. We also checked adding buffering salt in buffer-free stable colloids, but again fast aggregation was observed. So, we preferred using buffer-free solutions and dispersions for multilayer assembly to work in ion-free conditions. At this stage, we switched from dipping to spinning as well, since spin-LbL is a faster and material-efficient process. We observed exponential-like starting and linearly proceeding growth for both electrolyte-free and pH-adjusted solutions at bilayer thicknesses around 3.0 and 6.5 nm respectively. In addition to spin-LbL, we also studied dip-assembly of PVPon/TA multilayers and we observed zigzag-like exponential growth regardless of the conditions applied. Then, we prepared (PVPon/TA-SWCNT) multilayers using spin-LbL. We characterized resulting films with SEM, RSM, AFM, and CAM. There are three main outcomes of this study. First, we verified that TA can effectively disperse SWCNTs (in the absence of buffer salts). Second, we identified exponential character in both spin- and dip-assembly of PVPon/TA multilayers for the first time. Last, we showed that TA can serve as a mediator for the incorporation of SWCNTs in *hb*-multilayer. This study is the first demonstration of the incorporation of small pi-stacker molecule functionalized SWCNTs in *hb*-multilayers. Prepared nanocomposites might find use as antimicrobial coatings and drug delivery platforms.

---

[31] Partially presented in "Karahan, H. E., Erel, I., & Demirel, A. L. (2010, September). Incorporation of side-wall functionalized single-walled carbon nanotubes into H-bonded layer-by-layer nanofilms. Poster in *Workshop and School of Synthesis, Characterization and Applications of Nanomaterials (S.C.A.N 2010)*, Bilkent University, Ankara, Turkey."

2.1. INTRODUCTION

Fullerene research [326-327] led to the rediscovery of MWCNTs [298], SWCNTs were discovered subsequently [331-332]. Since then, the nanotechnology race became intense and both the research on and applications of nanoparticles increased exponentially. Especially, nanocomposites of CNTs are of interest for fabricating biomaterial [630] and delivering hydrophobic therapeutic agents which contain aromatic moieties [429,443-444,631]. *hb*-LbL films might serve as an appropriate host for the design of CNT-doped nanocomposites for drug loading applications. But, low water dispersibility of CNTs arose as a big challenge. Indeed, covalent chemistry is convenient to produce "soluble" CNTs, but the disruption of pi-conjugated networks is observed [339,486]. On the contrary, noncovalent approaches (i.e. surfactant stabilization [335], polymer-wrapping [335,337], and sidewall pi-stacking [339,486,521,532]) successfully unzip bundles in aqueous environment whilst preserving the intrinsic properties of CNTs. Many studies were devoted to the incorporation of covalently or noncovalently functionalized SWCNTs in *es*-multilayers [279,283,454,632-633]. But, only a few studies [289-291] were reported on CNT-loaded *hb*-LbL films.

Here we propose the use of TA as a mediator for the incorporation of pristine SWCNTs in PVPon/TA multilayer films. PVPon-TA pair is a promising LbL system for biological applications. Tannic compounds (a.k.a. tannins) [634-635] have a variety of biologically important properties (antimicrobial [636-638], antitumor [639-641], antiprionic/amyloidogenic [642-644], anti-inflammatory [635,640,645], antioxidant [635,646], antidiabetic [641-647], antitoxin [648] activities). On the other hand, PVPon is considered to be nontoxic and widely used in cosmetic, pharmaceutical, food applications [649-652]. In addition, a recent study [653] reported high biocompatibility of (BPEI)(PVPon-TA)$_n$ capsules towards yeast cells.

TA-aided dispersion of CNTs was previously reported by different groups. Liu and coworkers claimed to have stable SWCNT dispersions using TA as a dispersant without clearly providing the details of solution chemistry and dispersion characteristics [525]. Lin and Xing systematically studied TA-facilitated dispersions of SWCNTs and MWCNTs [528-529]. They first studied ultrasound-free solubilization of CNTs [528] and revealed that solubility of SWCNTs is low compared to MWCNTs. Lin and coworkers also studied the effects of pH and IS on ultrasonically debundled TA-MWCNT dispersions. They claimed achieving stable TA-MWCNT dispersions above pH 4.80 when concentration of cations is

low (i.e. 0.007 M Na^+).

In this study, we first ultrasonically dispersed SWCNTs in pH adjusted (pH 5.00) or native (a.k.a. natural) pH (pH-Nat) solutions of TA. Then, we characterized the resulting colloids and checked the effect of pH on dispersion stability qualitatively. Then, we studied the effect of pH adjustment on dispersion efficiency. Although TA-SWCNT dispersions were obtained at pH 6.00, buffer-free (pH-Nat) solutions provided better stability over time. So, we preferred to use electrolyte-free (or ion-free) solutions for film growth and we employed spin-assisted assembly as a fast process. We exploited TA-SWCNTs colloids in spin-LbL and fabricated SWCNT-doped *hb*-multilayers. Resulting nanofilms were characterized in detail using different techniques. As opposed to available literature knowledge on dip-assembled PVPon/TA multilayers [122], we observed a sign of exponential character in spin-assembled multilayers with or without SWCNTs in the structure. Thus, we also studied dip-assembly of ion-free solutions for the sake of comparison and verified the exponential behavior of PVPon/TA system.

2.2. EXPERIMENTAL DETAILS

2.2.1. Chemicals

PVPon of Mw 360 kDa (see Figure 2-1) was obtained from Scientific Polymer Products, Inc. TA (M_w ~1.7 kDa) (see Figure 2-2), HCl, NaOH, and $NaH_2PO_4{\cdot}H_2O$ (phosphate buffer) were purchased from Merck Chemicals (US). Unfunctionalized Elicarb™ SW (high purity, diameter < 2 nm) SWCNTs was procured from Thomas Swan & Corporation Ltd. (England). All chemicals were used as received without further purification. Pure ~18.2 MΩ water (DI-H_2O) was produced using Milli-Q filtration system (Millipore Corporation, USA). Prime quality silicon (100) wafers were purchased from Ultrasil Corporation (USA).

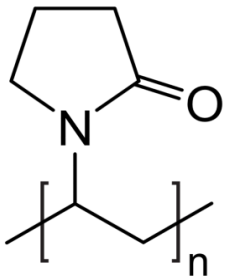

Figure 2-1. Repeating unit of poly(*N*-vinyl-2-pyrrolidone).

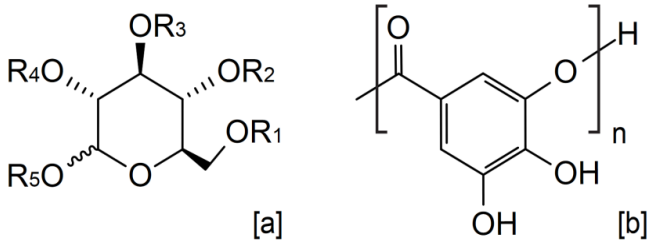

Figure 2-2. Generic molecular structure of tannic acid(s) in uncharged form ([a] is R-attached core structure in compact representation, and [b] is side R groups, n: 1-5).

2.2.2. Instrumentation and Analysis[32]

All pH adjustments were performed using EcoScan pH 6 (Eutech Instruments Pte. Ltd., USA). Samples were weighed using a digital balance with a sensitivity of 0.001 g (SPB31, Scaltec Instruments GMbH, Germany). Low speed sample shaking was done by an analogue orbital shaker (3005, GFL, Germany). Sonication experiments were held using two different setups (see Appendix-D for detailed information and representative images of device): i) Bath-sonicator equipped with three resonators (Ultrasons-H Code: 3000838, J.P. SELECTA, S.A., Spain), ii) Horn-sonicator (SONOPULS HD 3100, Bandelin Electronic, Germany) equipped with titanium-based tips of the same manufacturer. Centrifugations were performed using a classical bench top centrifuge (MIKRO 220R, Hettich GmbH & Co.KG, Germany). OAS experiments were performed using a double-beam spectrophotometer (T80+ UV/VIS Spectrometer, PG Instruments Limited, UK) operated with manufacturer's own software package (UVWin 5.0.5). Particles sizes were studied via DLS using Nano-S Zetasizer (Malvern Instruments Ltd., UK) equipped with a fixed wavelength (633 nm) monochromatic coherent He-Ne as laser source (4.0 mW). The intensity of the scattered light was detected by "non-invasive back scatter" technology at a detection angle (173°) and diffusion coefficients were calculated by the software (DTS Version 5.00). Collected diffusion coefficients were transformed to particle size distributions using built-in Non-Negative Least Squares algorithm of manufacturer's software in Multiple Narrow Mode. ZPA investigations of the dispersions were performed using ZetaPALS Zeta Potential Analyzer (Brookhaven Instruments Corp., USA) which is equipped with a 675 nm laser source. Transformation of electrophoretic mobility data to zeta potential values were done by the software of the instrument (palsw32, Version 3.38) based on Smoluchowski equation. Spin-assisted film depositions were performed using a manual spin coater (Model P6708D, Speciality Coating Systems, Inc., USA). Dip-assembly studies were either performed by hand or using an automatic dipping machine (KSV-NIMA, Biolin Scientific AB (Sweden) operated with 1000 mm/min. Both film growth and dissolution profiles were monitored using a single-wavelength (632 nm HeNe laser) ellipsometer (EL X-01R Rotating Analyzer Ellipsometer, Dr. Riss Ellipsometerbau GmbH, Germany) operated at 70° angle. Multilayer films were characterized with FE-SEM (ULTRA PLUS, Carl Zeiss AG, Germany), RSM (inVia™ Raman microscope, Renishaw plc, England), AFM (Solver P47, NT-MDT, Russia), and CAM (a home-built setup equipped with

[32] Unless stated, these instruments and setups are also used for other chapters of this study.

a Kodak Digital Science MDS 100 camera equipped with a Leica 10x lens). FE-SEM images were performed at 1 kV and the images provided by device were used as they are. AFM studies were performed using gold-coated silicon tips of ~10 nm curvature radius (HA_NC Etalon, NT-MDT, Russia) and data is analyzed using NOVA SPM Control Program (NT-MDT, Russia). CAM images were analyzed using MB-Ruler software. RSM images were collected using a 633 nm laser at full power and image outputs of the manufacturer's own software (WiRE™ 3) were used. Raw data of DLS, ZPA, OAS, EMM, AFM, and CAM studies were processed in MATLAB (R2010b) using our own custom-made scripts. In experimental figures, statistical error bars are used show standard deviations.

2.2.3. Methods

2.2.3.1. Noncovalent dispersion of nanotubes

PVPon or TA solutions of 0.50 g/L were prepared in DI-H_2O or in 0.01 M (0.01 M) aqueous phosphate buffer using regular glass containers. Native (natural) pH values of fresh and dilute (0.50 g/L) TA solutions in DI-H_2O measured as pH ~4.30 in room temperature. Similarly, 0.5 g/L TA solution in 0.01 M buffer (pH-Nat ~4.70) has a pH value ~4.35. In order to exceed reported value (pH 4.80) for stable TA-MWCNT dispersions, we set the pH of buffered solution to pH 5.0. Conical macrocentrifuge (50 mL) tubes made of polypropylene (ISOLAB Laborgeräte GmbH, Germany) were used for sample preparations, ultrasonic treatments and centrifugations. To prevent any interference of impurities, tubes were first thoroughly rinsed with DI-H_2O, were completely filled with DI-H_2O, and were subjected to bath sonication (~10 minutes). SWCNT powders were directly weighed to be 0.50 g/L in dried tubes. Fresh solutions were transferred into SWCNT-added or –free tubes. Ultrasonic dispersion is performed based early reports on TA-aided CNT dispersion [525,528-529], we combined and modified reported procedures. Followed multistep strategy can be summarized as follows: i) Bath-sonication – 2 hours, ii) shaking – 5 days, 300 rpm; iii) horn-sonication – 50% amplitude, 10 min, continuous mode, 0 °C; iv) centrifugation – 6000 rpm, 1 hour; v) decantation – 60% of total volume. Dispersion studies were performed using 25 mL filled 50 mL macrocentrifuge tubes. Prepared dispersions and control groups were kept in regular glass containers. TA solutions and TA-SWCNTs dispersions were covered with aluminum foils to avoid decomposition due to light exposure.

2.2.3.2. Characterization of nanotube colloids

Mean particle size (Z-ave) data was preferred as particle size to probe level of aggregation practically. Fifty data points were collected for both particle size and particle stability studies and no data filtration was applied. In order to minimize scattering, dispersions and control solutions were diluted to 5% of their original concentration. Unlike pH 5.00 and pH-Nat dispersions; pH 2.00, 6.00, and 10.00 dispersions were inspected qualitatively.

2.2.3.3. Fabrication of undoped and doped multilayers

Silicon (100) substrates were cleaned and oxidized before film deposition by using an acid-base treatment similar to previous reports [122-124] (see Chapter 4 below for details) and cut into ~1×1 cm^2 pieces. PVPon/TA and PVPon/TA-SWCNT composition were assembled using spin-LbL at 2000 rpm using 70 μL of assembly solution and rinsing liquid was used for rinsing (rinsing was performed once). Approximately 10-20 s film-fluid contact times were allowed without a strict control. Dip-LbL studies were performed either by hand or using automatic dipping machine. In manual dipping intermediate drying is performed using N_2 flow, but no drying is applied in automated dipping. 20 mL liquids were used in manual dip-LbL and 40 mL liquids were used in automated dip-LbL.

2.2.3.4. Characterization of films

Film growth studies were performed by collecting one data point from five different locations of the films (one point from the center and four points in total from ~1-2 mm inside of each edge). We operated FE-SEM without coating the samples. Also, due to burning of multilayers at high energy, low voltage was applied. In RSM studies, an arbitrary point was studied near the centre of substrate and consistency of collected data checked by shifting focus to different positions. Based on the information given by manufacturer and our OAS studies, we employed a polydisperse CNTs sample in our study. So, we did not focus on radial breathing mode region, rather we studied in the region cover D- and G-bands which are informative on defect concentration and nanotube metallicity (tangential vibrations of carbon atoms are geometry dependent). Particularly, G-band is the most intense Raman feature of CNTs, so we selected D-band for mapping. We studied RSM of this sample by line and are mappings. In AFM studies, two different roughness analyses were performed. In the first analysis, rms roughness values of 0.5×0.5 μm^2 particle-free squares in the images provided in the text were averaged to have an idea about the background roughness. In the second analysis, three different 2.0×2.0 μm^2 images were used for each sample to calculate global roughness of

samples. In this analysis, the effect of large aggregates and SWCNTs (if any) were not examined. CAM studies were performed using ~5 μL DI-H_2O transferred with a sensitive syringe under the ambient conditions.

2.3. RESULTS and DISCUSSION

2.3.1. Preparation of and Characterization of Dispersions

In the literature, there are many reports claiming the effective dispersion of CNTs in electrolyte containing dispersant solutions [520,654-656]. But, there are also others reporting the adverse effect of cations [321,510-511,578,600,605-606,657]. We studied SWCNT dispersion efficiency of buffered (0.01 M buffer) and unbuffered (DI-H_2O) TA solutions (see Figure 2-3). We employed a multistep procedure that includes shaking, sonication, and ultracentrifugation steps. Horn-sonicated fresh dispersions of both buffer-free and pH-adjusted (0.01 M phosphate buffer and required amount of 0.25 NaOH, pH 5.00) dispersions were almost indiscernible to the naked eye. But, in a couple of minutes (around 5 minutes), coagulates became visible in salt-added dispersion. Upon ultracentrifugation, a dramatic sedimentation was observed for buffer containing sample. To quantify this observation, size and surface charge of particles within dispersions were studied using DLS and ZPA.

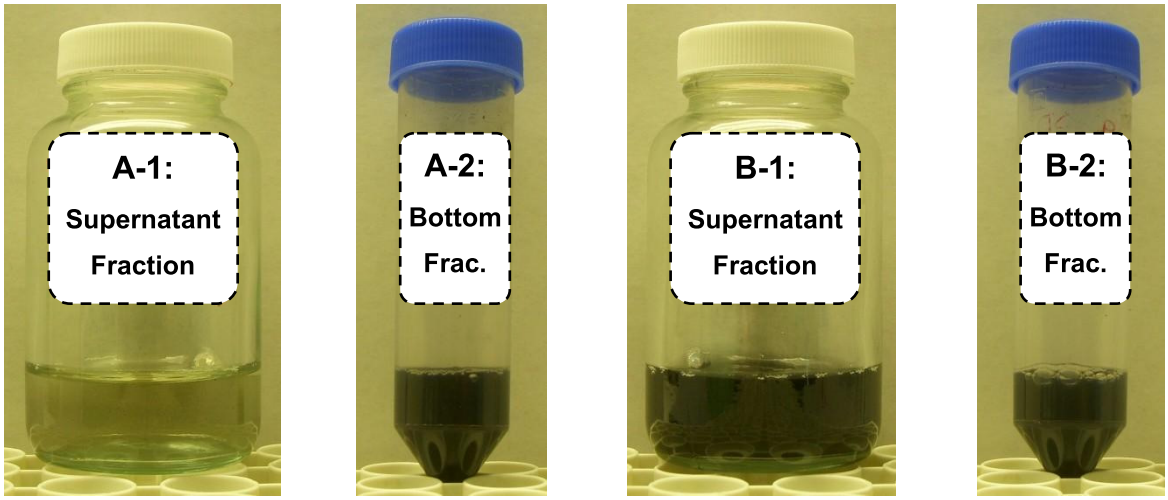

Figure 2-3. Effect of pH adjustment on the dispersion efficiency of single-wall carbon nanotubes (Sample A: TA-SWCNT in 0.01 M buffer at pH 5.00; Sample B: TA-SWCNT in DI-H_2O at its native pH ~4.30).

Table 2-1 shows size and zeta potential values of particles present in both supernatant and bottom phases of TA-SWCNT dispersions. Bottom fractions of each system are normally enriched by bundles and have bigger aggregate sizes. Although particle concentration of supernatant of salt-added dispersion (A-1) is considerably low compared to buffer-free case

(B-1), its particle size is higher. This is a clear indication of adverse influence of added salt (buffering agent) on dispersion efficiency. Zeta potential results are less straightforward. Slight increase in the surface charge of salt-added sample comparing buffer-free one is probably related to the slight pH difference (TA is slightly more charged at pH 5.00). But interestingly, bottom fraction of buffer-free dispersion also exhibits higher surface charge which normally suggests higher dispersion stability. This peculiar behavior might be originated from low concentration of individual particles in the system.

Table 2-1. Effect of buffering agent on the particle size and charge of tannic acid stabilized single-wall carbon nanotube dispersions.

Sample / *Measurement*	**In buffer (pH 5.00): A-1 / A-2**		**In DI-H_2O (~pH 4.30): B-1 / B-2**	
	Supernatant	**Bottom**	**Supernatant**	**Bottom**
Particle Size (nm)	297.10 ± 26.62	1123.0 ± 0.56	128.70 ± 8.17	317.30 ± 6.39
Zeta Potential (mV)	–41.67 ± 1.09	–14.41 ± 4.52	–39.04 ± 0.88	–3.15 ± 4.21

OAS is widely used to compare or estimate concentration of (SW)CNTs in dispersed state. Different extinction coefficients are available in the literature for SWCNTs [488,620-622]. It is believed [658-659] that the region below 600 nm gives more reliable data. To stay above the high absorption cross-section region of TA (below 400 nm) and suggested upper limit (600 nm), we selected 500 nm for single-wavelength photometric investigations. We characterized both stable supernatant and bottom phases of dispersions. As expected, buffer-free dispersion (B-1) contains more than ten times SWCNTs comparing salt-added dispersion (A-1). Using the extinction coefficient "2.86×10^4 cm^2/g" reported by Bahr et al. [488], concentration of SWCNTs in buffer-free TA-SWCNT dispersion roughly calculated as ~0.034 g/L. This means SWCNT recovery is below 10% which is quite low. We believe that defects present on SWCNT surfaces might be causing an underestimation of particle concentration.

Table 2-2. A simple photometric evaluation of particle concentration of dispersions (Note that samples were diluted to their 5% with DI-H_2O and aggregates did not considerably sink down during measurements).

Sample		$OD_{(500\ nm)}$	Interpretation
pH-adjusted (pH 5.00)	A-1 (bottom)	0.228	High amount of bundles (*scattering*).
	A-2 (supernatant)	0.003	Dilute dispersion.
	Sonicated TA solution	0.002	Slight absorption.
Native pH (~4.30)	B-1 (bottom)	0.162	High amount of bundles (*scattering*).
	B-2 (supernatant)	0.048	Concentrated dispersion.
	Sonicated TA solution	0.005	Slight absorption.

Colloidal stability of polyelectrolyte-SWCNT dispersions is mainly IS-dependent, but pH-sensitivity is also highly important especially for weak polyelectrolytes. To further understand the role of solution chemistry, we studied the effect of pH using a small set of samples. TA-SWCNT dispersions of pH 2.00, 6.00, and 10.00 (see Figure 2-4) were compared. pH 2.00 batch of TA-SWCNT was almost water-clear in the transparency. At low pH, TA is expected to be virtually uncharged and considered to be less hydrophilic [213]. In this case, adsorption of TAs on pi-surfaces of SWCNTs cannot result in dispersion. When pH is adjusted to 6.00, TA can dissolve SWCNTs better which suggests an acidic dissociation between pH 5.00 to pH 6.00. There is a conflict in the literature on pK_a value(s) of TA [122,213,529]. Our findings are in good agreement with recent report of Lin and Xing [529]. They reported a dibasic pK_a profile for TA as "4.90 ± 0.50" and "7.40 ± 0.60" [529]. A similar dibasic profile is also known for gallic acid as ionization of carboxyl groups (pK_{a1} 4.20) and phenolic hydroxyls (pK_{a2} 8.78) [660]. Indeed, idealized penta-digalloyl form of TA does not contain carboxyl functionalities, but TA is a natural mixture of polyphenolic compounds (thus we sometimes call this molecule family as TAs). Some molecules in TA samples might be containing carboxyl functionalities [661-663] and these individuals might be responsible for the dispersion of SWCNTs at pH 6.00. Also, TA can hydrolyze into gallic acid by heat and/or alkaline treatments [664-665]. Therefore, a portion of ionized molecules at pH 6.00 are probably dispersing CNTs thanks to charge-charge repulsions. Uncharged molecules will also inevitably interact with SWCNT surfaces and will sterically limit reaggregation. In this scenario, incomplete deprotonation of TA seems to be enough for achieving CNT dispersions.

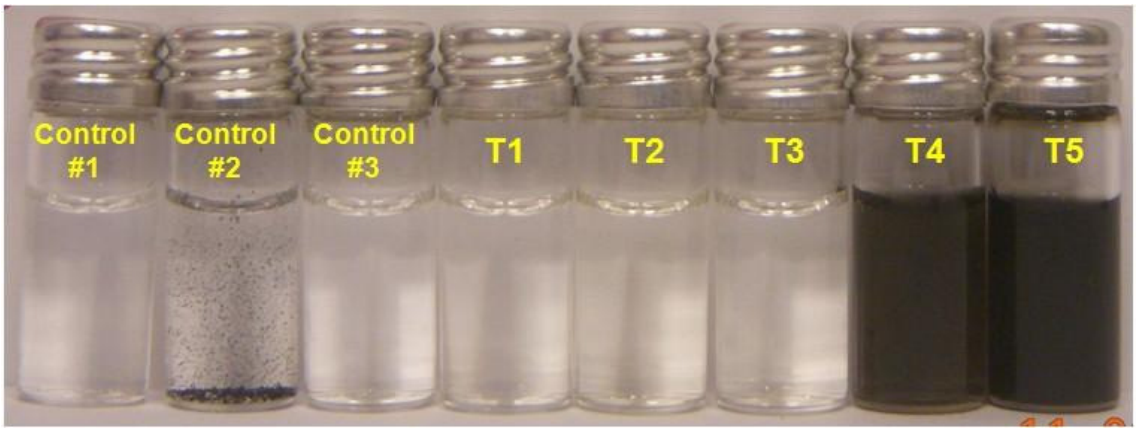

Figure 2-4. Effect of pH adjustment on tannic acid aided dispersion of single-wall carbon nanotubes (Control#1: DI-H_2O; Control#2: Sonicated SWCNTs in DI-H_2O; Control#3: Fresh TA; T1: Sonicated TA, T2: Aged TA; T3 to T5 are pH 2.00, 6.00, and 10.00 dispersions respectively).

Erel and Sukhishvili showed that PVPon/TA multilayers can be assembled at pH 4.00 and 7.50 other than pH 2.00. Thus, at first glance, there is no obstacle in the way of assembling SWCNT-doped PVPon/TA multilayers at pH 6.00. Indeed, pH-stability issues may come out as a problem due to possible weaker complexation between PVPon and TA at pH 6.00. But on the other hand, (TA-chitosan)$_n$ LbL films were previously assembled at pH 4.00, 6.00, and 9.00 [213]. So, TA-SWCNT dispersion at pH 6.00 can be employed in *es*-multilayers. However, a sign of faster aggregation was observed even at pH 10.00 (TA is fully ionized) comparing with pH-Nat TA-SWCNT dispersion. Thus, pH-Nat solutions/dispersions were preferred for multilayer assembly in this study. In fact, if a strict control is needed over pH of assembly solutions/dispersions, zwitterionic buffers can be used. Those agents are more compatible with SWCNTs (i.e. 3-(*N*-morpholino) propane sulfonic acid [527]). But, they potentially bind [666] both tubule surfaces through tertiary amines and interact with dispersing agents (PVPon and TA) via H-bondings which will normally cause contamination in resulting films. As a result, the usage of pH-Nat solutions/dispersions seems as a practical way to prepare pristine CNT-doped[33] *hb*-LbL assemblies using noncovalent chemistry.

2.3.2. Fabrication and Characterization of Multilayers

LbL (self-)assembly of pH-sensitive components such as weak polyelectrolytes is conventionally performed using pH controlled solutions/dispersions. In (PVPon/TA)$_n$ *hb*-LbL

[33] We intentionally generalized our claims here, because these experiments were also repeated using MWCNTs and considerable more concentrated dispersions were obtained (data not shown).

system, TA is the pH-sensitive component due to acidic dissociation of phenolic hydroxyl groups. In previous reports [122,653,667-670] on dip-assembly of PVPon-TA pair, buffer solutions (typically 0.01 M of phosphate buffer with or without NaCl addition) were used and pH of assembly solutions was adjusted between acidic to neutral conditions. Nevertheless, solution chemistry requirements for achieving stable CNT dispersions directed us to employ electrolyte-free solutions/dispersions for film assembly.[34]

Dip-LbL is a time consuming (disadvantageous for the stability of CNT dispersions) process which requires larger amounts of fluids comparing spin-LbL. So, we preferred spinning as the method of assembly for preparing SWCNT-doped nanocomposites. In Figure 2.5, growth profiles of spin-grown multilayers are seen. Although there are many recent reports on dip-assembly of PVPon/TA pair, the only study reporting the growth profile of multilayers is the original paper reported by Erel and Sukhishvili [122]. They observed zigzag-like linear growth with a bilayer thickness around 4.5 nm for twelve bilayer films. We rather observed a linear growth with a hardly indistinguishable exponential phase in the first 4-5 bilayers. Indeed, a closer look shows that the growth profile of dip-assembled PVPon/TA multilayers exhibited an initial exponential-like behavior in the report of Erel and Sukhisvhili as well. Initial exponential-like behavior was followed by a zigzag-like linear growth again starting from tenth layer. Thus, they considered overall deposition profile as a linear growth and zigzag character of this system was attributed to desorption of self-associated TA molecules from the surface by subsequent PVPon deposition steps in their report. We will try to show, based on our observation of exponential growth in dip-assemby of PVPon/TA films (see Appendix-E), that PVPon/TA pair tends to grow exponentially and zigzag character is a consequence of this tendency. We first observed this growth profile duality with manual deposition of multilayers. Then, we repeated the experiments using an automatic dipping machine as performed by Erel and Sukhishvili and exponential was again observed.[35] So, observed growth profiles for spin-assisted multilayers can be taken as "exponentially-starting linear growth". On the other hand, as seen in Figure 2-5 below, the presence of buffer

[34] Buffering activity of humic substances is well known in the literature and we expect TA to have a similar behavior due to the structural similarities between humic acids and TAs. Therefore, although no external buffering agents were added, TA might be working as an internal buffer in the system.

[35] Exponential behavior was obvious in dip-LbL of PVPon/TA multilayers regardless of the deposition conditions (e.g. substrate selection, presence/absence of precursor layer, pH/IS of solution) applied (see Appendix-D). On the other hand, we tried dip-assembly of BPEI-free PVPon/TA multilayers at pH 5.00 and erratic growth behavior was observed (see Figure App-3).

(electrolytes) in assembly solutions slightly favors this exponential character.[36] Also, the addition of electrolytes yields approximately two times more bilayer thickness as expected.[37]

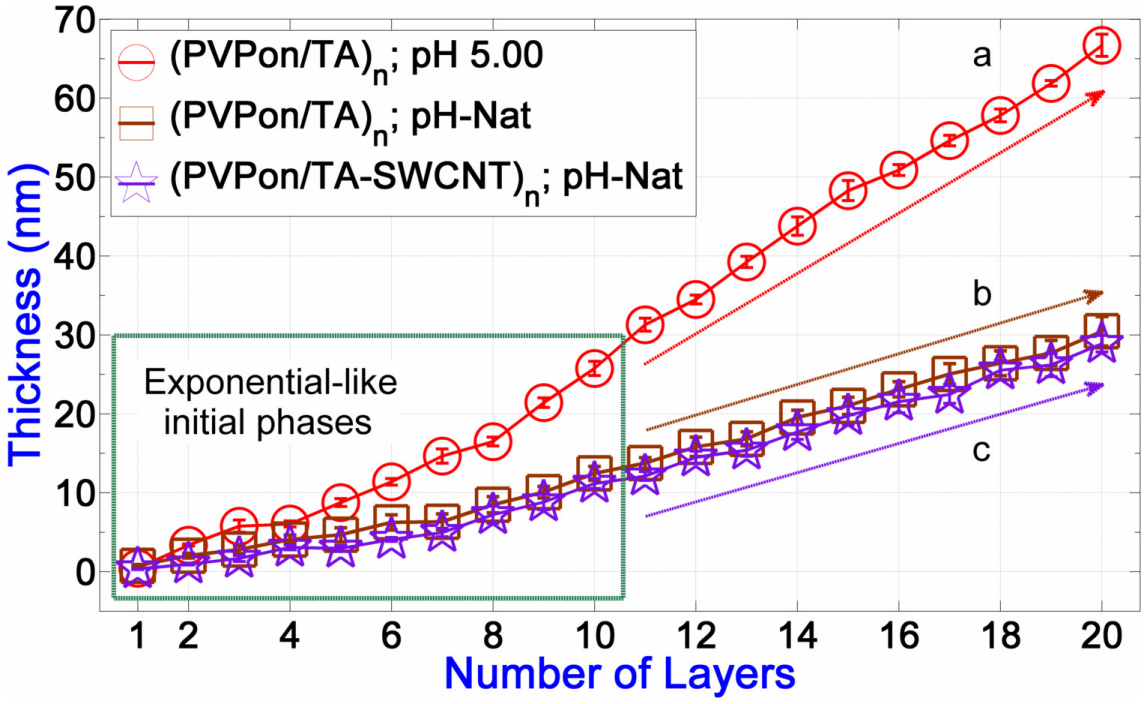

Figure 2-5. Multilayer growth profiles of a) pH-adjusted, b) buffer-free, and c) buffer-free and particle-doped multilayers (Note that arrows are put for guiding the eye, no scale or fitting was meant).

We simply justify the suppression of zigzag character of PVPon/TA pair in spin-LbL considering the force applied (we also observed zigzag-like character particularly in the initial growth phases of dip-assembled multilayers, see Appendix-E). However, the reason why we observe exponential growth but Erel and Sukhishvili observed linear growth (see Appendix-F) is not clear. When we ignore the difference in the M_w of BPEI used in some of our studies, which is not a serious concern, we can claim to have performed almost the same experiment with Erel and Sukhishvili. Besides, PVPon is a commercial[38] synthetic polymer, but TA is a natural substance and some chemical changes might be the point in question for different products. On the other hand, it seems external mechanical effects might influence the growth characteristics in multilayer assembly of PVPon/TA system. In spin-LbL, mechanical force applied is easily controlled by spinning rate. In dip-assembly, entrance and withdrawal (exit)

[36] Selection of pH 5.00 is not on purpose for this manner. This experiment was linked to our TA-SWCNT dispersion studies at pH 5.00.

[37] For exponentially growing multilayers, bilayer thickness considerations is not directly meaningful. But here, we do not concern initial exponential-like phase, because overall character is much more linear-like.

[38] We use the same M_w PVPon with Erel and Sukhishvili which is procured from the same manufacturer.

speed of substrates possess a similar role, but we believe it is not safe to ascribe observed difference to such a vague mechanical effect.

Here, we should also mention the report of Schmidt and Hammond [667] which provides important clues about the exponential nature of PVPon/TA pair. In that report, Schmidt and Hammond dip-assembled (BPEI)(PVPon/TA)$_n$ multilayers and dissolved those electrochemically. In the supplemental information of this study [671], they provided the details of film growth and reported a bilayer thickness of around 8 nm. Such a large bilayer thickness can be inferred as an exponential growth. Indeed, they performed the film growth using an automated dipping machine and only used resulting films for further investigations. On the other hand, they attributed observed bilayer thickness change to several changes[39] they made in assembly conditions. The mechanism of exponential growth in this system also deserves discussion. Basically there are two main frameworks explaining exponential growth which are roughness-trigger [153,200-202] and in&out diffusion [197-199]. It is well-known that the presence of salts (electrolytes) in assembly solutions usually increases surface roughness of LbL films. We assembled buffer-added and buffer-free multilayers and exponential-like character was relatively predominant in salt-added case as already mentioned (recall Figure 2-5).

Last but not least, based on our experience, we supposedly decided that duration of film-fluid contact is important on the dominancy of exponential character as well. In spin-LbL, assembly fluid and growing film are practically kept in contact for couple of seconds before spinning. Then, liquid thin film forms and solidifies in time.[40] In this study, timescale of contact was typically around 10 to 20 seconds, but we also observed a dramatic influence of longer fluid-film contact times in growth profiles of spin-deposited multilayers (see Appendix-G). Indeed, in&out diffusion is an extremely fast process [206,672] and there is no certain correlation between fluid-film contact time and in&out diffusion. But, kinetic nature of observed exponential character suggested us the possible importance of in&out diffusion

[39] Those changes are as follows: i) Rinsing the multilayers thrice for 1 min instead of 2×5 min, ii) switching from phosphate buffer (0.01 M) to phosphoric acid (0.01 M) as supporting electrolyte, iii) using higher M_w PVPon (1300 K instead of 360 K), and iv) employing gold-coated silicon substrates in lieu of oxidized silicon wafers. On the other hand, they grew 20 bilayer multilayers which we believe ensures exponential growth in PVPon/TA system. Besides, we could not grow dip-assembled multilayers beyond approximately twelve bilayers without stagnation and destruction of film growth. They might be staying in a possible stagnation phase in their conditions or stagnation might be delayed mainly due to the usage of high M_w PVPon. In addition, we also grew dip-assembled PVPon/TA multilayers on gold-coated substrates and observed delayed exponential behavior and smaller final thicknesses.

[40] Solvent evaporation and hence solidification rates are correlated to spinning rate.

process in this system. We will be focusing on this topic in Chapter 3 below.

Up to this point, we concentrated on the observation of zigzag-free and exponentially-starting linear growth in spin-LbL of PVPon/TA multilayers. From now on, we will focus on SWCNT doping in multilayers. We will compare particle-free and -doped compositions. Also we will try correlating the dispersed and deposited states of TA-SWCNT particles. First, we observed no significant growth behavior change between particle-free and SWCNT-doped multilayers. In our measurements, we ignored the possible refractive indice change upon incorporation of SWCNTs in film structure. Clayton et al. [673] and Nadler et al. [544] reported refractive indice values around "1.4"; so we assumed a refractive indice of "1.5000" for both particle-free and -doped multilayers at the beginning. Then, using measured thickness values to estimate the refractive indice of multilayer films using inbuilt the software of device. Calculated refractive indice of undoped PVPon/TA film was "1.4872" and final thickness of film increased by ~0.41 nm after remodeling (from "30.4575 ± 1.8653" to "30.8687 ± 1.8559" nm). For SWCNT-doped multilayer, again refractive indice change was slightly above the refractive indice of undoped multilayer (1.4919) which corresponds to an increase in thickness as ~0.27 nm (from "28.8690 ± 1.0458" to "29.1370 ± 1.1560" nm). These results either correspond to a low level of SWCNT-doping or refractive indice of SWCNTs is close to the refractive indice of multilayers. Below, we will evaluate filling and homogeneity issues based on RSM and SEM investigations.

We studied the surface morphology of particle-free and -doped spin-grown films using FE-SEM (see Figure 2-6). From the FE-SEM images, it can be seen that, SWCNTs were incorporated in multilayers and hence TA can serve as a mediator to incorporate SWCNTs in *hb*-multilayers. (SW)CNTs are usually depicted in perfect geometries, however they are flexible particles which can be distorted by their surroundings [426]. Also, different types of geometrical defects and features are present in regular (SW)CNT samples as we employed in this study. So, we observe bended and broken tubules in the image. In the panel, upper right and lower left images belong to center and edge locations respectively. As it is clearly seen, SWCNT bundles were accumulated along the edges; center zone of the film is less occupied by SWCNTs. Centrifugal forces acting on SWCNT bundles might to carrying them towards the edges. Also, there are particles other than SWCNTs. We studied XPS of employed SWCNT powder and no catalyst-related signal was observed (see Appendix-H). In this study, we used commercially available pristine SWCNT samples. When the manufacturers mean unfunctionalized and highly pure (or in brief "pristine") CNTs, they generally mean that no

chemical functionalities were introduced on purpose. No promise is given for complete removal of non-CNT CNPs in the samples, because this is related to level of sorting. Approximately 10% non-CNT materials (other CNP, ashes, catalyst residues etc.) are expected to be in the samples based on the claims of manufacturer. We employed a milder routine comparing the routines available in the literature, but still CNTs can transform into non-CNT CNPs during ultrasound irradiation. Erosion of titanium-based ultrasonic horn during debundling process might also be another source of contamination although ultracentrifugation potentially removes most of titanium impurities. Dispersions used for LbL deposition were more than one month old (consider preparation of dispersions and assembly of films). In this period of time, no apparent coagulation was observed, but reaggregation of SWCNTs and aging-induced structural changes (SA of polyphenols, and PVPon) of polymers likely to take place. Therefore, it is reasonable to observe nonfiber-like objects in the films. In our FE-SEM studies, we could not focus to the samples very well. PVPon/TA multilayers were undergoing extremely fast burning under electron irradiation (see lower right figure in the panel) and when we tried to focus, much more severe burning was observed. So, we worked in low energy (1 kV) and hesitated to focus to monitor individual tubules.

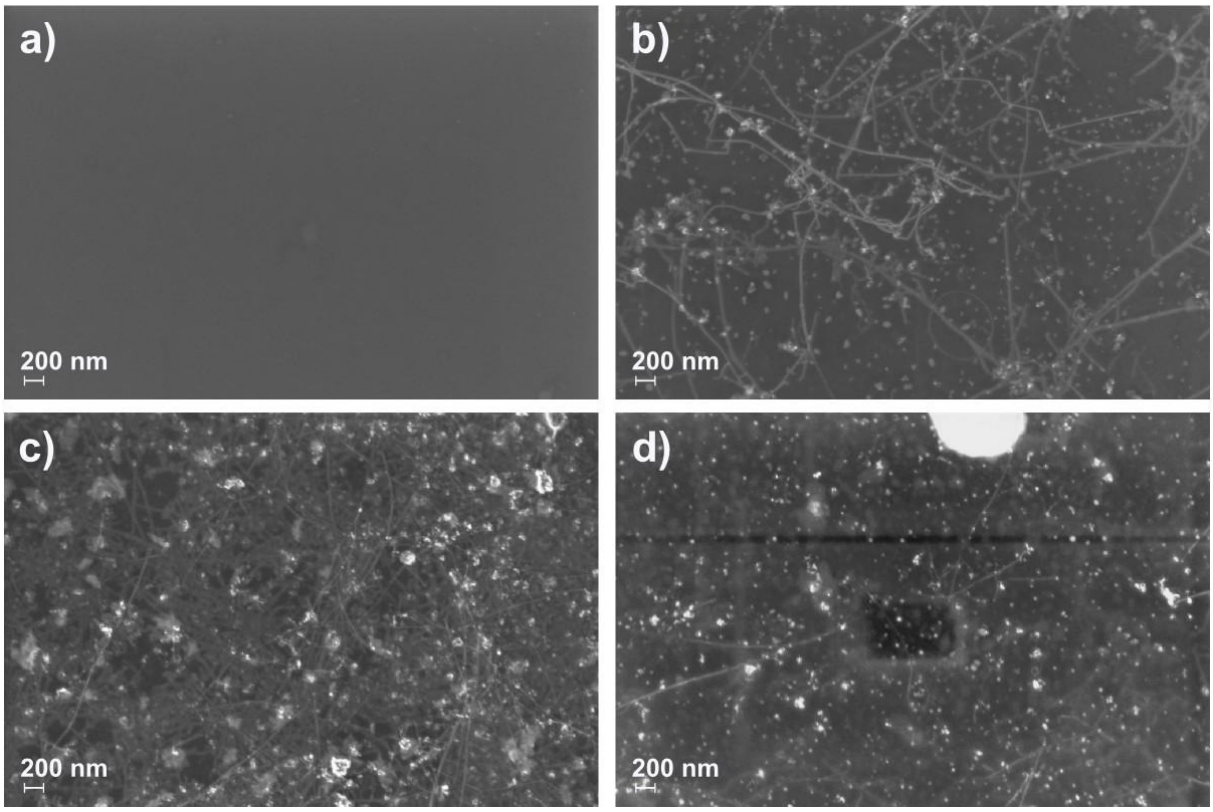

Figure 2-6. Field-emission electron micrographs of ten bilayer films: a) SWCNT-free multilayer, b) center of SWCNT-doped films, c) edge of SWCNT-doped films, d) fast burning of multilayers (an arbitrary location).

In FE-SEM studies, we obtained information mainly about the outermost layers and homogeneity of particles in film remained unanswered. RSM offers the possibility to provide more information about the homogeneity of SWCNTs within the multilayer matrix because Raman signal can be collected within the multilayer as well. SWCNTs possess different Raman features such as radial breathing mode, D-band, and G-band. In this study, we are interested in fine geometrical properties of SWCNTs, so we did not study on radial breathing region. Instead, we focused on D- and G-bands which corresponds to disorder level and metallicity of (SW)CNTs respectively. In Figure 2-7, we show line and area mappings of SWCNT-doped multilayers. In line mapping (above in the figure), we have investigated the disorder level, location of G-band, and doping uniformity of SWCNTs. D-band intensity of SWCNTs were quite low comparing G-band (D/G ratio) which means we did not harm SWCNTs much during ultrasonication process. Line map suggests a uniform dispersion of SWCNTs and also shows the location of D-band which will be used for area mapping. Area mapping (below in the figure) supported the information obtained from line mapping and also confirmed the polydispersity of sample used.

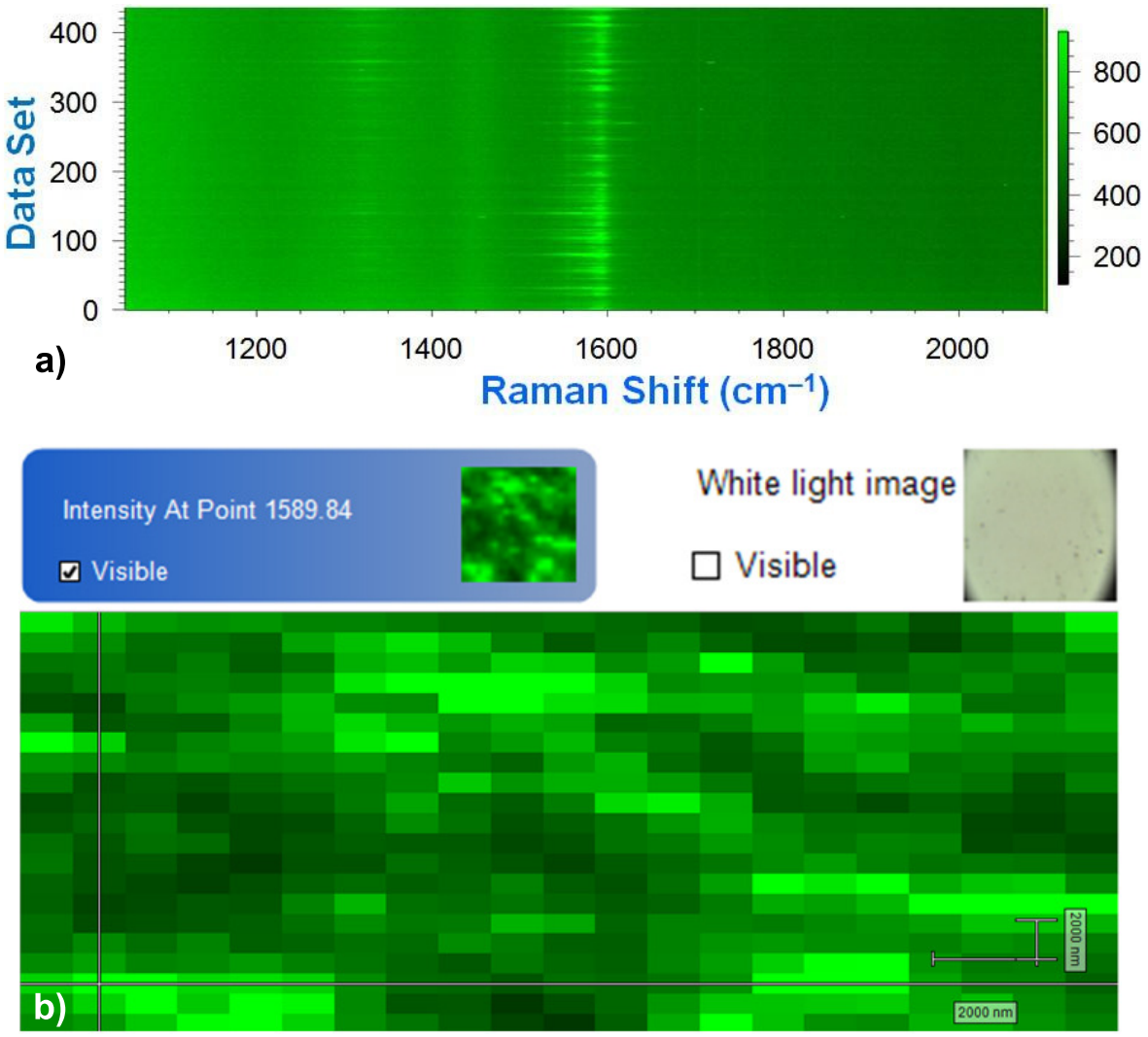

Figure 2-7. Raman microscopy mapping of nanotube-doped multilayers: a) Line mapping of the region covers D- and G-bands, b) area mapping of an arbitrary wavenumber in the G-band region.

FE-SEM investigations showed that SWCNTs were incorporated in multilayers and RSM studies confirmed the uniformity of doping. In fact, RSS can also be used to learn about level of individualization in SWCNTs, but AFM can provide related information more directly and practically. We have performed tapping mode AFM measurements of undoped and SWCNT-doped multilayers. We have collected some representative images of AFM results in Figure 2.8. As expected, no features were observed in undoped multilayers other than some irregular particles and individualized SWCNTs were captured in SWCNT-doped sample (two tubules are assigned in the figure). From line profile analysis, ~3-4 and ~2-3 nm (data not shown) diameters were estimated for "i" and "ii" respectively. Both undoped and doped multilayers exhibited smooth backgrounds with rms roughness values around 1.5-2.0 nm unlike rougher salt-added multilayers (rms: ~6.2 nm). However, "1.87 ± 0.20", "4.69 ± 1.23" and "7.06 ± 0.84" nm rms values were calculated in overall analysis. This indicates that

SWCNTs (and other objects present in doped-multilayers) increase the roughness significantly, but still their effect is less than salts' effect (Note that pH-adjusted sample is prepared using relatively fresh solutions and no aggregate-like particles are present on their surface).

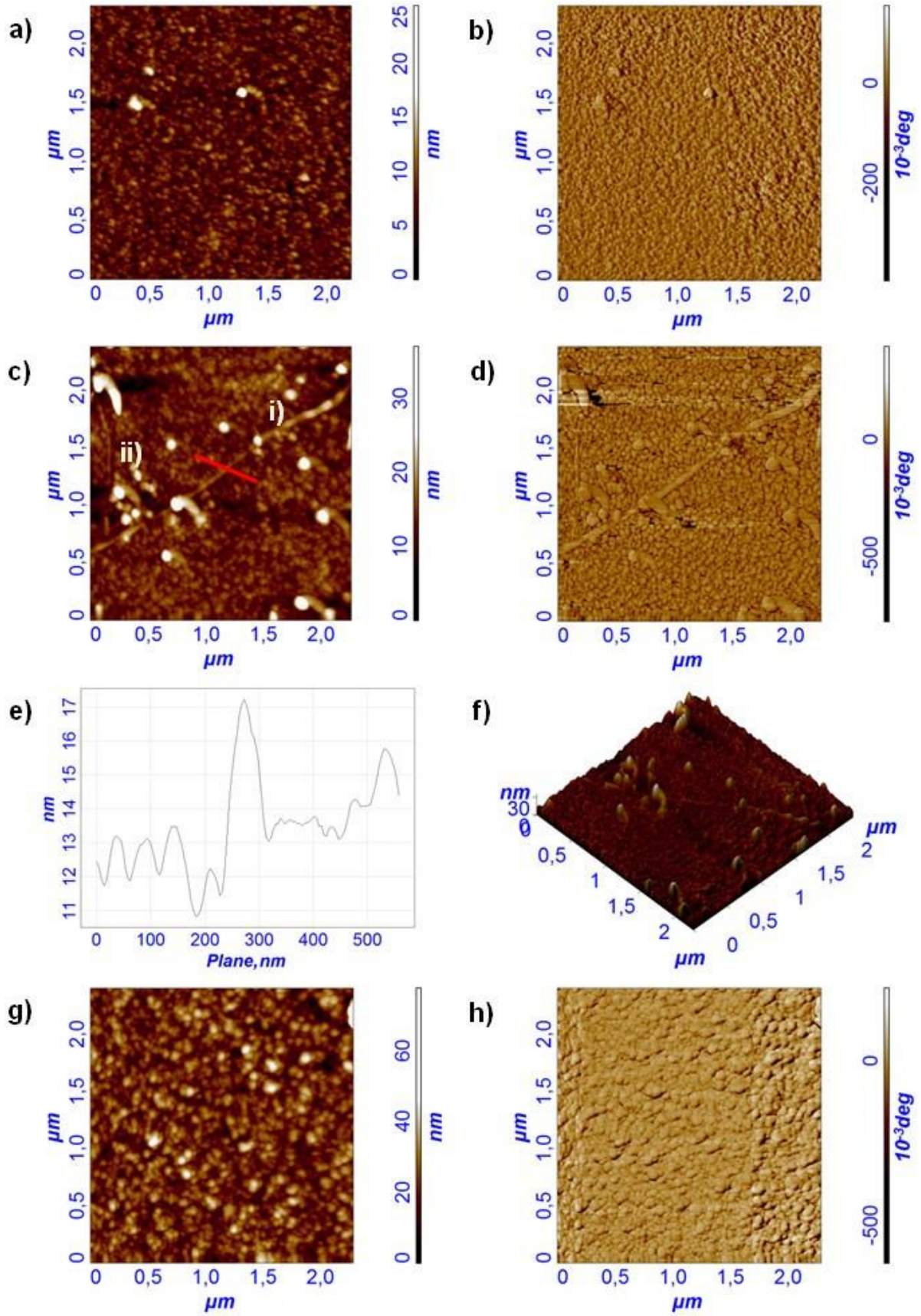

Figure 2-8. Atomic force microscopy images of undoped/buffer-free, particle-doped, and undoped/buffer-added multilayers: a) height, and b) phase images of undoped/buffer-free; c) height and d) phase images, e) height line profile, and f) 3-D height plot of SWCNT-doped; g) height and h) phase images of undoped/buffer-added films.

FE-SEM and AFM studies confirmed the presence of SWCNTs on the outer layer (and RSM verified the embedding of SWCNTs in matrix). As already mentioned, CNTs are hydrophobic materials and we dispersed them with the help of TA which is amphiphilic by its nature. For good colloidal stability, we expect virtually full coverage of SWCNTs with TA molecules. In this case, multilayers should be presenting SWCNT directly in their surface. CAM can be employed to evaluate the level of uncoated SWCNT fragments presented on the surface. As can be seen in Figure 2-9, no significant contact angle variation is observed between undoped and SWCNT-doped multilayers although rms roughness of SWCNT-doped surface is slightly high. We regarded this observation as high level nanocoating of SWCNTs with TA molecules during dispersion process.

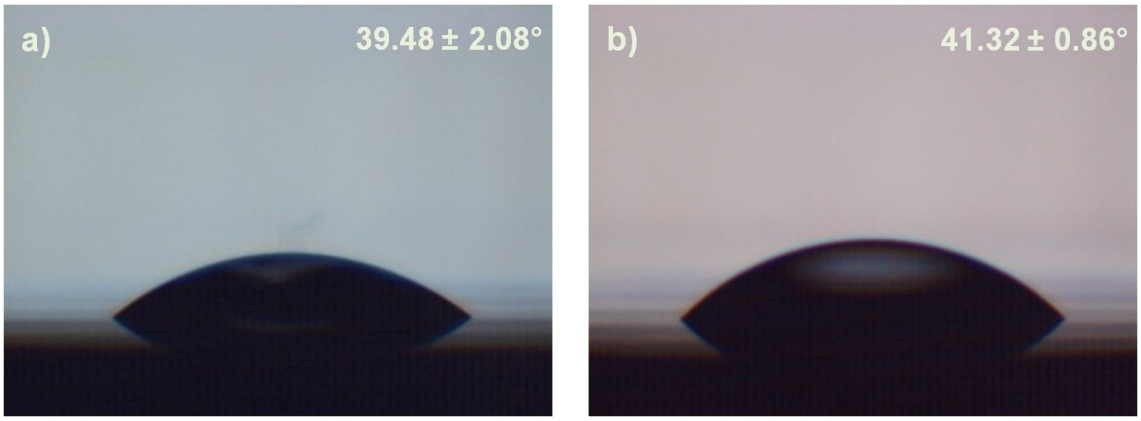

Figure 2-9. Representative contact angle images of multilayers: a) Undoped (PVPon/TA), and b) SWCNT-doped (PVPon/TA-SWCNT) multilayers (note that droplets are manually put by a syringe around ~5 μL).

2.4. CONCLUSIONS and OUTLOOK

Depending on the application of interest, virtually any material can be employed in LbL in case suitable assembly conditions are satisfied. One major success of LbL strategy is the usage of water as processing media. But, the usage of water makes the incorporation of hydrophobic nanoparticles (e.g. carbon nanotubes) in LbL nanocomposites challenging. Here we showed a simple method for incorporating SWCNTs in *hb*-multilayer nanocomposites. We noncovalently functionalized pi-conjugated sidewalls of SWCNTs with a natural polyphenol to compatibilize SWCNTs and water. We confirmed the adverse effect of buffering media on successful dispersion of (SW)CNTs and modified deposition conditions accordingly. For the first time, we employed PVPon/TA in spin-LbL. We showed the inherent exponential behavior of those multilayers as opposed to current literature. We also showed the exploitation of PVPon/TA pair for the incorporation of nanoparticles in multilayer films. Both

PVPon/TA pair and SWCNTs are biologically important, thus we anticipate a growing interest in *hb*-LbL for the design of organic-inorganic nanocomposites.

Deposited components might not have chance to assemble in their thermodynamically favored conformations in spin-LbL due to kinetic hindrance (a.k.a. kinetic trap). However, dip-assembled multilayers are less kinetically trapped and potentially behave different. Also, we did not focus on spray-LbL of TA-SWCNT colloids for practical reasons (e.g. high volume requirements). It might be worthwhile to study dip- and spray-LbL of this system in subsequent investigations. In addition, here we employed TA as the mediator of SWCNT incorporation in PVPon/TA multilayer films. Nevertheless, PVPon is likely the best available homopolymer to disperse pi-conjugated nanoparticles (CNB: [498,674-677], CNT: [337,678-681], CFS: [682], boron nitride nanotube: [683]). As a continuation of this study, PVPon-functionalized SWCNTs (see Chapter 4) and other pi-conjugated nanoparticles can be incorporated in *hb*-multilayers.

Chapter 3: FACTORS AFFECTING SPIN-ASSEMBLY of POLYVINYLPYRROLIDONE and TANNIC ACID[41]

Dip-assisted layer-by-layer assembly of PVPon and TA pair was intensively studied in the last couple of years. Here we report on spin-assisted assembly and pH-triggered disintegration of PVPon/TA multilayers. We first demonstrate the effect of spinning rate on bilayer thickness and pH-stability in the range of 1000 to 3000 rpm. Bilayer thickness of multilayers declined and leveled by increasing spinning rates in agreement with theoretical models and experimental findings of other researchers. pH-stability of grown multilayers showed a significant variation in case pH-disintegration study was continuously held in a short period of time (fast) or was perfoemed with intermediate time intervals given between each step (slow). We found that, when the experiment is fast, there is no dramatic dependence between pH-stability and spinning rate. However, when the experiment is held slowly, critical dissolution pH values of films vary significantly which we consider as a sort of "annealing". Annealed samples (slow pH exposure) exhibited a general trend of pH-stability increase with increasing spinning rate. We attributed this behavior to the spinning rate dependent variation of contact time between assembly solutions and growing films. We supported this interpretation by studying the effect of solution-film contact time on growth of multilayers at 2000 rpm. At low contact times (from ~4 to 30 s), no significant pH-stability variation was observed. As the contact time increases exponential character of film dominated the system and even complete destruction of multilayers was observed. We also observed the importance of time given during assembly process in parallel to the importance of time given in dissolution experiments. It seems, when more time is given during assembly, multilayers tend to reach their equilibrium state which is manifested as an exponential growth. We also studied the effect of contact time on pH-stability. Again, pH-stability of those multilayers showed a nonmonotonic and complex nature when pH-disintegration study was held fast. However, when the experiment was performed slowly, films were again likely annealed to their equilibrium states during the experiment. In this case, we observed that lower the contact time, higher the stability. We attributed observed anomalies in growth and dissolution of spin-assembled multilayers to their kinetically trapped nature. This study provides valuable insights on pH-stability of electrolyte-free PVPon/TA films and shows an evidence of "kinetic trap" in H-bonded multilayers.

[41] To be submitted as "Karahan, H. E., Eyüboğlu, L., Kıyılar, D., and Demirel, A. L. Spin-assisted layer-by-layer assembly of PVPon/TA multilayer films: Growth and pH-triggered dissolution."

3.1. INTRODUCTION

LbL assembly is a versatile bottom-up surface modification nanotechnology based on molecular assembly [13,684]. The technique is originally established on alternated deposition of electrostatically attracting building blocks using sequential dipping method [91,93-95]. Then, H-bonding interactions were reported to be feasible driving forces for LbL assembly [113-114]. *hb*-LbL introduced many uncharged and stimuli-responsive biomedical materials into the toolbox of LbL design [115,685]. In time, *hb*-LbL especially grew in importance as a novel agent delivery platform [124,138-139,686-688] and now acknowledged for pharmaceutical applications [689-690].

Subsequent to the expansion of driving forces, spraying [174] appeared as the first alternative of conventional [91,93-95,113-114] dipping method. Then, just after the utilization of spinning for film drying [691] and realization of dip-LbL on rotating substrates [112], spin-LbL was reported as an individual method [177-178,692]. Major advantage of new methods over dip-LbL first revealed as time efficiency. But, structural influences of method selection on film properties have also been recognized. Uniformity [174,177-178], bilayer thickness[42] [174,177], internal structure (i.e. interpenetration vs. stratification) [177,692], and surface roughness [177,692] variations were pronounced in the early studies. Then, further investigations verified the validity of early findings for both spraying [175-176,693] and spinning [187-188,190-191,694-697] methods. Observed structural variations among the techniques commonly explained by fluid[43]-film contact time differences.

LbL deposition is a kinetically controlled surface adsorption process [112,161,211,698-701]. In conventional dip-LbL, solution-film contact time is generally adjusted between 10 to 60 minutes to assemble a bilayer. Longer solution-film contact generally favors interpenetration of layers in dip-assembled multilayers [161,163,702]. In contrast, solution-film contact times of spraying and spinning techniques are considerably short (typically below 1 min.). Therefore, spray- [176] and spin-LbL [191] multilayers are better stratified than dip-LbL films. On the other hand, incomplete surface coverage [174] and liquid drainage [175] problems may cause inhomogeneities in spray-grown LbL films. So,

[42] For a two-component multilayer architecture, a bilayer can be considered as the simplest unit of film structure.

[43] Colloidal dispersions can be used as assembly solutions rather than solutions. So we preferred to use "fluid" term to generalize. On the other hand, spin-LbL is a fluid mechanics problem in a manner and this term fits better although the "liquid" or "solutions" terms are generally preferred in LbL literature.

spin-LbL not only offers a better control over timescale of solution-film contact, but also ensures better uniformity in multilayer formation. Nevertheless, in relation to the spinning rate selection, solution-film contact time is still considered an effective parameter on bilayer thickness of spin-grown multilayers [121,189].

Dip-assembled versions of PVPon/TA multilayers were well-studied by other researchers. (BPEI)(PVPon/TA)$_n$ films were originally reported by Erel and Sukhishvili [122]. They studied the effect of pH on film growth and dissolution of those multilayers. Then, Schmidt and Hammond studied electrochemical disintegration of (BPEI)(PVPon/TA)$_n$ [667]. Finally, Tsukruk's Group modified this system to fabricate flat films, microcapsules, and living cell encapsulates of (BPEI)(TA/PVPon)$_n$ and (TA/PVPon)$_n$ architectures [653,668-670]. Our group is also studying on precursor-free PVPon/TA multilayers to fabricate nanoparticle-loaded nanocomposites. We optimized the assembly conditions for carbon nanotubes based on electrolyte-free solutions/dispersions using spin-LbL (recall Chapter 2). Also, we are currently focusing on the effect of carbon nanotubes on pH-stability of PVPon/TA multilayers.

In this study, we report on the effect of spinning parameters on pH-stability of PVPon/TA multilayers. To our knowledge, there is no report on spin-assisted assembly of PVPon/TA system. Also, pH-stability of precursor- and electrolyte-free PVPon/TA multilayers is not yet studied. Here, we first investigated the effect of spinning rate on pH stability of PVPon/TA multilayers. We checked the validity of power law relation between spinning rate and bilayer thickness of multilayers [187] for PVPon/TA system. Then, we investigated the link between spinning rate, bilayer thickness, and pH-stability of spinning rate varied multilayers. We observed a sign of the influence of kinetic trap/lock/pin/freeze (local minimum in free energy) on pH-stability of spin-LbL assembled *hb*-multilayers. Finally, we tested our interpretation by increasing solution-film contact time up to typical solution-film contact times of dip-assembly. This set of experiment supported our interpretations on the thermodynamic nature of resulting complexes.

3.2. EXPERIMENTAL

3.2.1. Chemicals

PVPon (see Figure 3-1) of M_w ~360 kDa was obtained from Scientific Polymer Products, Inc. TA (M_w ~1.7 kDa) (see Figure 3-2), HCl, NaOH, and $NaH_2PO_4 \cdot H_2O$ (phosphate buffer) were purchased from Merck Chemicals (US). Silicon wafers were procured from Ultrasil

Corporation (USA). Pure ~18.2 MΩ water (DI-H_2O) was produced using Milli-Q filtration system (Millipore Corporation, USA).

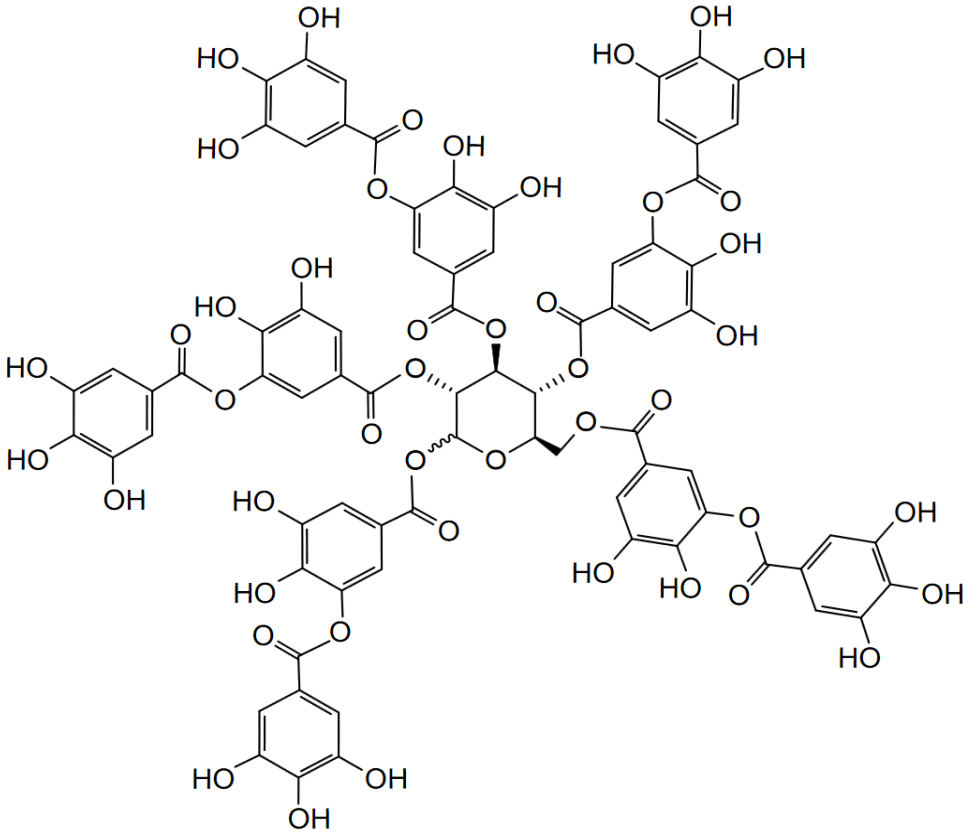

Figure 3-1. Idealized molecular structure of neutral tannic acids: 1,2,3,4,6-penta-O-digalloyl-ß-D-glucose.

3.2.2. Substrate preparation

Silicon wafers were used as substrates and acid-base cleaning was performed prior to film deposition following a procedure derived from previous reports [122-124]. First, silicon wafers were cut into ~(1×1) $in.^2$ pieces and were kept in UV-Ozone Cleaner (Model 42-220, Jelight Company, Inc., USA) for 3 h. Ozone-treated wafers were rinsed with DI-H_2O and dried under N_2 flow. Acid-base treatments were performed just after ozone cleaning. Four liquid bathes of 15 mL liquid were prepared in glass containers as follows: a) concentrated sulfuric acid, b) acid wash (DI-H_2O), c) 0.25 M aqueous NaOH, and d) base wash (DI-H_2O). Wafers were dipped into each bath (including rinse bathes) for ten minutes respectively. After each washing step, excess amount of DI-H_2O was used to rinse away any acid or base residue. Prepared substrates were kept (1 to 3 days) in closed Petri dishes and were thoroughly rinsed with DI-H_2O and dried under N_2 before usage.

3.2.3. Solution preparation

PVPon and TA solutions (0.5 g/L) were prepared using DI-H_2O and no pH adjustment is performed (for this concentration native-pH of PVPon and TA are ~4.5 and ~4.2 respectively). Solutions were prepared in glass tubes less than half an hour before film deposition and were homogenized by shaking at 250 rpm for fifteen min.s (3005, GFL, Germany).

3.2.4. Spin-assisted multilayer deposition

Spin-LbL was performed at different rpm values (from 1000 to 3000 rpm) for 1 min (2-3 s acceleration, 54-55 s plateau, 2-3 s deceleration) using a spin coater (Model P6708D, Speciality Coating Systems, Inc., USA). In each deposition, 100 µL[44] of solution was used for assembly. 60 s elapse time was given before the spinning process for self-adsorption of first layer (this routine was also followed for contact time varied set). 150 µL DI-H_2O was used for rinsing, and static contact of water and film for 30 s was allowed before each rinsing step. Solution-film contact time (static) was adjusted from least possible (~4 sec) to 5 min. using a regular chronometer. Contact time of ~4 s is a typical time for a continuous spin coating process, the time between dropping the solution on the substrate and the start of spinning. For larger contact times, the solution was dropped on the substrate and waited during which adsorption of molecules on to the underlying layer took place. The maximum contact time of 300 s was chosen to follow the dipping time used in previous reports [122,667] which is also typical for dip-assisted LbL films. Multilayer growth was monitored with a single-wavelength (632 nm HeNe laser) ellipsometer (EL X-01R Rotating Analyzer Ellipsometer, Dr. Riss Ellipsometerbau GmbH, Germany) which is operated at 70° angle. Data was taken from five different zones (one point from the center and four points from ~1-2 mm inside of four edges) of the films and five data points were collected for each point.

3.2.5. pH-triggered film disintegration

pH-triggered disintegration studies were performed in buffer solutions (0.01 M phosphate buffer) and pH-adjustment is done using dilute NaOH solutions (0.25 and 0.10 M) in 0.01 M buffer solution (Note: this base-buffer solution always used fresh to prevent precipitation). In each step, samples were dipped in 20 mL of solution and kept for 20 min. To inhibit

[44] 100 µL is an optimized volume for good surface coverage on 1×1 in.^{2} substrates.

contaminations all buffer solutions were used freshly and refreshed after every exposure step. For both spinning rate and contact time varied sets dissolution experiment is repeated twice. In the first experiment, the onset of dissolution was reached in less than 24 hours and the experiment was continued after the onset of dissolution (whole experiment is performed approximately in two days). In the second experiment, after film when the onset of dissolution was reached in the first day, the experiment was slowed down and finished in approximately one week. All samples used were at most two weeks aged. Dissolution of films monitored using ellipsometry after gentle drying the films under N_2 flow.

3.3. RESULTS and DISCUSSION

Spin-assisted LbL assembly briefly consists of the following steps: (i) Transferring a certain amount of building block (here PVPon or TA) solution on the bare or film coated solid substrate, (ii) keeping the solution in static contact with the substrate for a certain time, (iii) spinning the substrate with liquid on top at a specified rate, (iv) putting a certain amount of rinsing liquid (here water) to wash away the weakly bound materials, (v) repeating the steps ii and iii, vi) repeating the steps i to v for the other component of LbL pair, (vi) repeating the steps i to v to assemble consecutive bilayers. The spinning rate (step iii) and the contact time of assembly solution with the substrate (solution-film contact time) before spinning (step ii) are the two important factors affecting the characteristics of resulting films. First, effect of spinning rate was investigated in detail both in terms of growth profiles (number of layers vs. film thickness) and in terms of pH stability (pH of solution vs. remaining film thickness). Then, effect of solution-film contact time was studied to obtain a further understanding about the kinetic nature of system.

3.3.1. The Effect of Spinning Rate

3.3.1.1. Multilayer growth

Spin-assisted PVPon/TA LbL films were grown at spinning rates varying between 1000 rpm to 3000 rpm with 500 rpm increments. Figure 3-2 shows the film thickness as a function of number of layers at different spinning rates. At all spinning rates, a fairly linear growth profile was observed. No report is available on spin-LbL of PVPon/TA, but Erel and Sukhishvili studied dip-LbL of (BPEI)(PVPon/TA)$_n$ system at pH 2.00, 4.00 and 7.50 (precursor layer deposited at pH 7.50) [122]. They observed linear growth profiles regardless of deposition pH. At pH 4.00 and 7.50, they tracked growth profile of this system at each bilayer and the

details of film growth remained unclear if any. But, a clear zigzag-like growth profile was shown for pH 2.00. Deviation from linearity was explained by desorption of TA aggregates from the surface which leaves a strongly-bound monolayer at following deposition step. Similar explanations were originally done for the zigzag growth behavior of polyphenol/polyelectrolyte multilayers by Ariga et al. for aromatic dyes [210] and Shutava et al. for TA [213]. If proposed explanations are true, it is reasonable to assume that a certain time is needed for desorption of self-associated TA aggregates from the surface. Unlike referred dip-LbL studies, we grew multilayer films by spin-LbL in which the static contact time of assembly solutions and underlying film was kept constant at ~4 s. The contact of thin liquid film and growing multilayer in the dynamic stage of spin-LbL is on the order or seconds (typically around 10 to 20 s) due to evaporation of water. Under these conditions, the time given for the interaction of PVPon solution with top layer TA film might not be enough to dissociate TA aggregates. Electrolyte-free and fresh TA solutions are expected to contain less phenolic aggregates and desorption of aggregates is not a concern throughout the process. In our previous studies, we observed exponential growth in dip-assembly and exponentially-starting linearly-proceeding growth in spin-assembly PVPon/TA system in a variety of conditions (see Chapter 2 below for related discussions). However, a clear linear character of spin-LbL films is obvious in Figure 3-2. One major difference of current conditions and the conditions showed in Chapter 2 is the control over fluid-film contact time. Also, film-fluid contact time is considerably higher in dip-LbL. Indeed, Lee et al. also observed a similar growth mode change variation between dip- and spin-deposited weak polyelectrolytes [703]. In their system, although spin-LbL showed a sign of exponential growth, dip-grown films were apparently exponential. We believe the underlying reason this observation is contact time variation among the techniques. Indeed, we also checked the film growth of the same system using spray-LbL and again linear growth was observed (see Appendix-I) which supports short contact time argument. Further discussions on growth mode variations among techniques are available in Subsection 3.2. Below, we will concentrate on the evaluation of spinning rate originated changes in growth and dissolution behavior of multilayers.

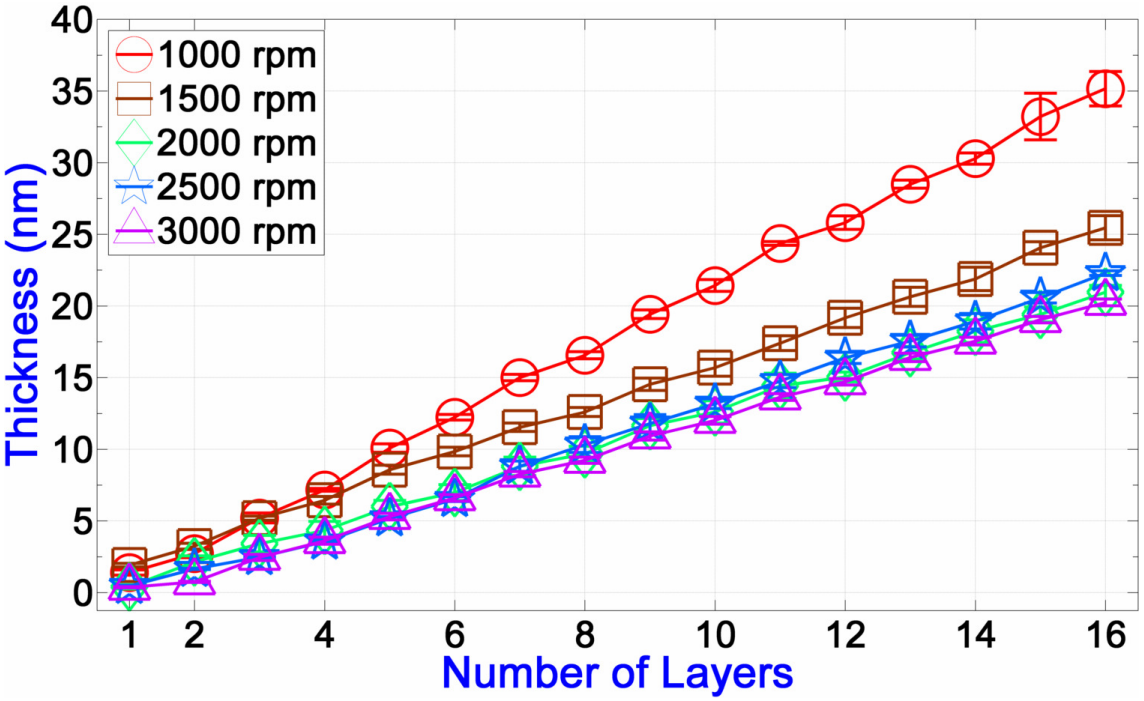

Figure 3-2. The growth profiles of spin-assisted multilayers assembled at different spinning rates.

In Figure 3-2, the slope of the growth profiles decreased with increasing spin rate from approximately 2.2 nm at 1000 rpm (corresponds to bilayer thickness of 4.4 nm) and leveled at around 1.3 nm for 2000 rpm (corresponds to bilayer thickness of 2.6 nm). Slopes of film growth profiles can be used to determine bilayer thickness of linearly growing multilayers. But, to gain a statistical understanding, we also studied the bilayer thickness of films as a function of the spinning rate using multiple ten bilayer samples (each data point is an average of at least three different samples, see Figure 3-3).[45] This cross check supported the bilayer thickness obtained from growth profiles.[46] An asymptotic power law relation was observed as the general trend similar to the findings of previous works [178,187,692] on spin-LbL of polyelectrolytes. Common explanation of this observation was the compaction of layers at higher rates due to increased mechanical forces and lowered adsorption due to shorter film-fluid contact. Indeed, this explanation is in parallel to fundamental models and experimental results [180,182,184,704-705] on spin-coating of polymers. Thus, our results are another example of this inverse power law relation. In addition, by increasing spinning rate, film-fluid contact time also decreases and this might be causing a decrease in the amount of deposited

[45] Bilayer thickness 3500 rpm sample is "2.81 ± 0.02 nm" for ten bilayers which is an average of a single sample.

[46] Bilayer thicknesses of 20 bilayer samples also follow a similar trend for different spinning rates.

material in each step. Moreover, both in Figure 3-2 and 3-3, we observed slightly higher bilayer thickness in 2500 rpm compared to 3000 rpm. Errorbar of 3000 rpm is high to safely compare 2500 and 3000 rpm samples. But, when we compare 2000 and 2500 rpm, it is clear that 2000 rpm samples are slightly thinner than 2500 rpm. This might be originated from the slight change in film-fluid contact time change in those samples. Because 2500 rpm films are expected to be thinner than 2000 rpm samples if there is no other effective parameter.

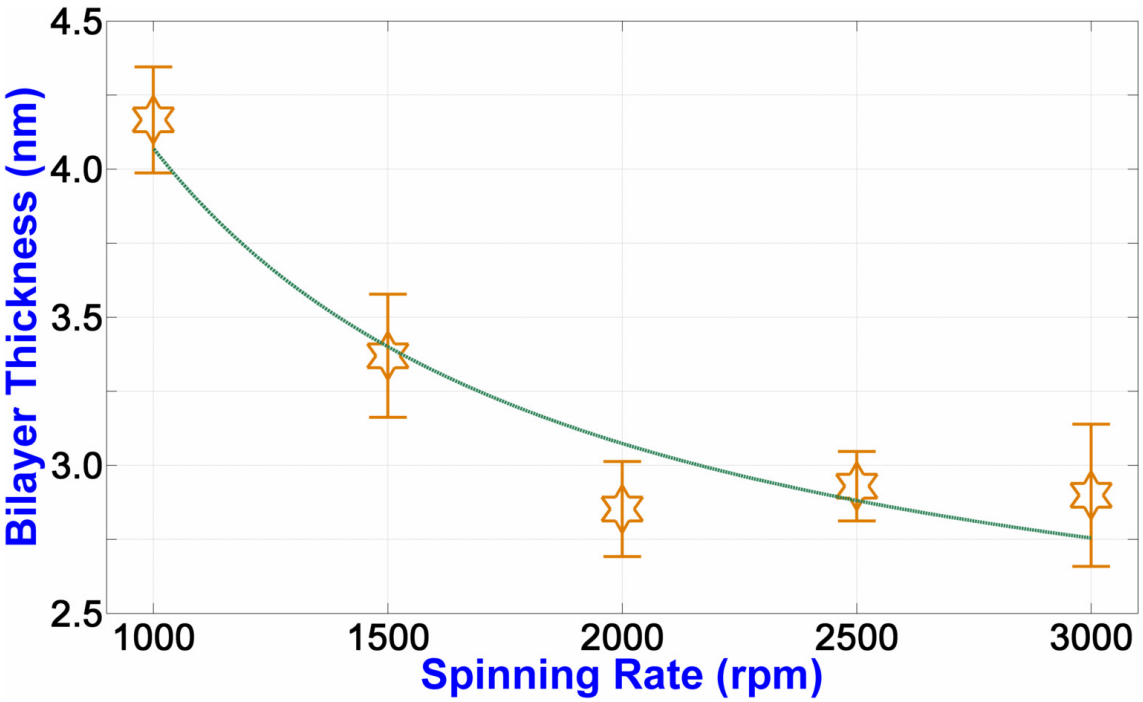

Figure 3-3. Bilayer thickness of multilayers as a function of spinning rates
(each data point is averaged from total thickness of at least two different ten bilayer samples).

The scenario explained above is easily understandable for large molecules such as polymer chains. But, if we consider small molecules as more rigid bodies, the level of compaction should be different. In fact, a slight zigzag-like but not up/down behavior is observable in growth behavior of PVPon/TA films assembled at 1000 and 1500 rpm due to this difference. In Figure 3-4, we plotted the individual contribution of PVPon and TA to bilayer thickness. It seems spinning-induced thinning of PVPon chains by increasing rpm values is slightly greater than that of TA layers. This can be justified considering shear-induced conformational changes of PVPon chains and the structure of TA molecules. LbL spin-assembly of polyelectrolytes was previously modeled by Dobrynin's Group [189-697]. In their Flory-(Huggins)-type models, the effect of ionic strength and spinning rate were formulated and the effect of shear flow on conformational changes of polymer chains (or

blobs [706-708]) was revealed. In brief, at low spinning rates shear force is less distorting and hence adsorbed chains are less compact. This behavior is clearly seen for PVPon, but TA layers also became more compact at higher spinning rate. In solution, galloyl groups of TA bend molecule fits to a globule-like shape [534]. When TA is adsorbed on surfaces its globule-like shape can flatten up to the thickness of an individual molecule (theoretical dimensions of TA in penta-monogalloyl form is 1.85 × 1.65 × 1.01 nm [709]) and we reach this limit in 3000 rpm. Here, it should also be noted that, at 2500 rpm contribution of TA to the bilayer thickness increases which drops again at 3000 rpm. This shows that more TA molecules s adsorp on PVPon layers at 2500 rpm, but the reason behind is unclear to us other than our interpretations presented in the previous paragraph.

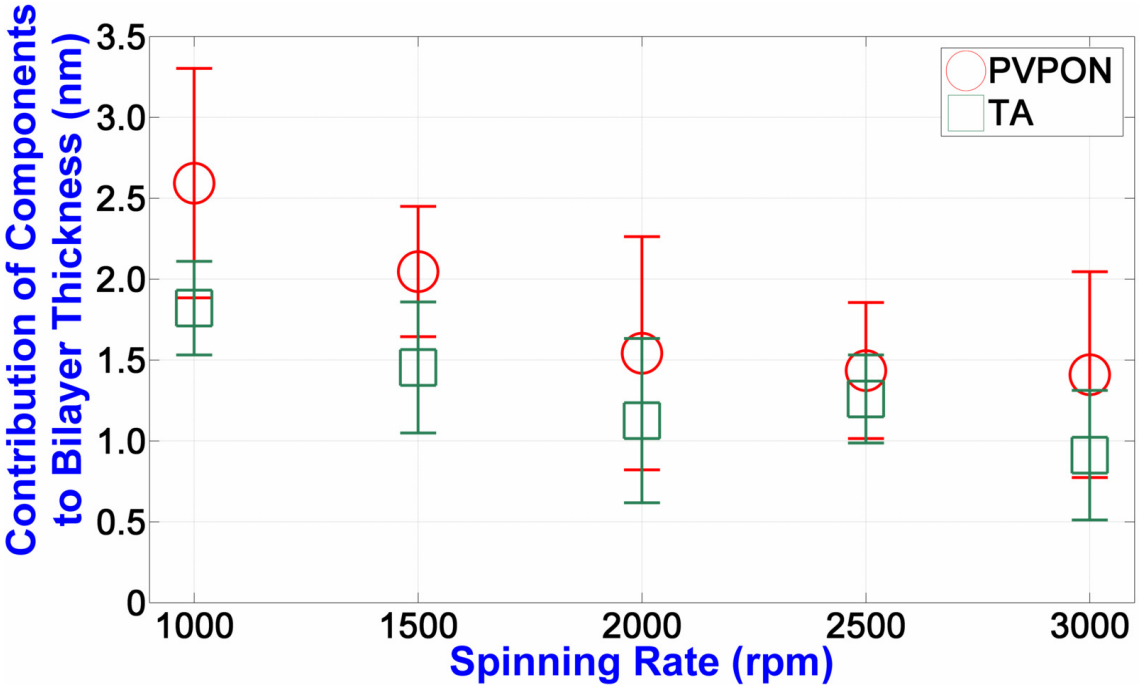

Figure 3-4. Bilayer thickness of multilayers as a function of spinning rates
(each data point is averaged from growth profiles of at least two different eight bilayer samples).

In spin-coating, solid film evolves in two main stages as spinning-induced liquid thin film formation and solidification of liquid thin film via solvent evaporation. The thickness of evolved liquid film and the time required for solvent evaporation are correlated to spinning rate. As a result, spinning rate is not only linked to liquid film thickness, but also effective on the solution-film contact time. Various researchers highlighted the effect of film-fluid contact time change on thickness of spin-LbL films by changing spinning rates [121,178,692,694,710]. Those researchers also discussed mechanical aspects which we extensively discussed. The effect of solution-film contact time on film growth will be

discussed in the next section.

3.3.1.2. pH-stability

Figure 3-5 shows the normalized dissolution profiles of spin-assisted $(PVPon/TA)_{10}$ films prepared at different spinning rates whose growth profiles are shown in Figure 3-2 for discontinuous growth. Independent of the spinning rate, the onset of dissolution was observed at pH 8.50 for all films. This is similar to the onset of dissolution observed in zigzag-grown dip-coated PVPon/TA LbL films prepared at pH 2.00 [687]. In our case, better pH-stability was observed for exponentially-growing dip-coated PVPon/TA LbL films prepared at pH 2.00 (films are stable at pH 9.00, see Appendix-J). In addition to identical pH dissolution onset values at different spinning rates, critical dissolution pH values (pH at 50% dissolution) stacked between pH 8.75 and 9.00. This was surprising for us because we were expecting to see more evident distinctions. We also expected to achieve better pH stabilities comparing dip-LbL films assuming spin-LbL films are more hierarchic than dip-LbL ones. At first step, we took into consideration the differences in bilayer thicknesses. The bilayer thickness changes either with the number of the molecules in each layer or with their conformations. In either case, we assumed larger bilayer thickness corresponds to less H-bond per molecule with the underlying layer and decreasing the average number of H-bonds per layer. So, we expected low pH-stability for 1000 rpm and so on. Indeed, Figure 3-5 does not conflict with this prediction, but does not support either. To be certain on this observation we repeated the experiment. In the second trial, we unintentionally performed the experiment slower and observed a completely different picture which fulfills the missing parts of the puzzle. It seems, when the dissolution experiment is performed discontinuously (slower[47]), pH-stability of multilayers dramatically increase (see Figure 3-7). We considered this observation as a sort of “annealing” effect. We could not find any significant difference between two sets other than the timescale of experiments. So, we see no harm to attribute this peculiar observation to the kinetically trapped nature of spin-LbL multilayers.

[47] Those experiments are extremely laborious and when three people works together ten pH steps takes more than one day.

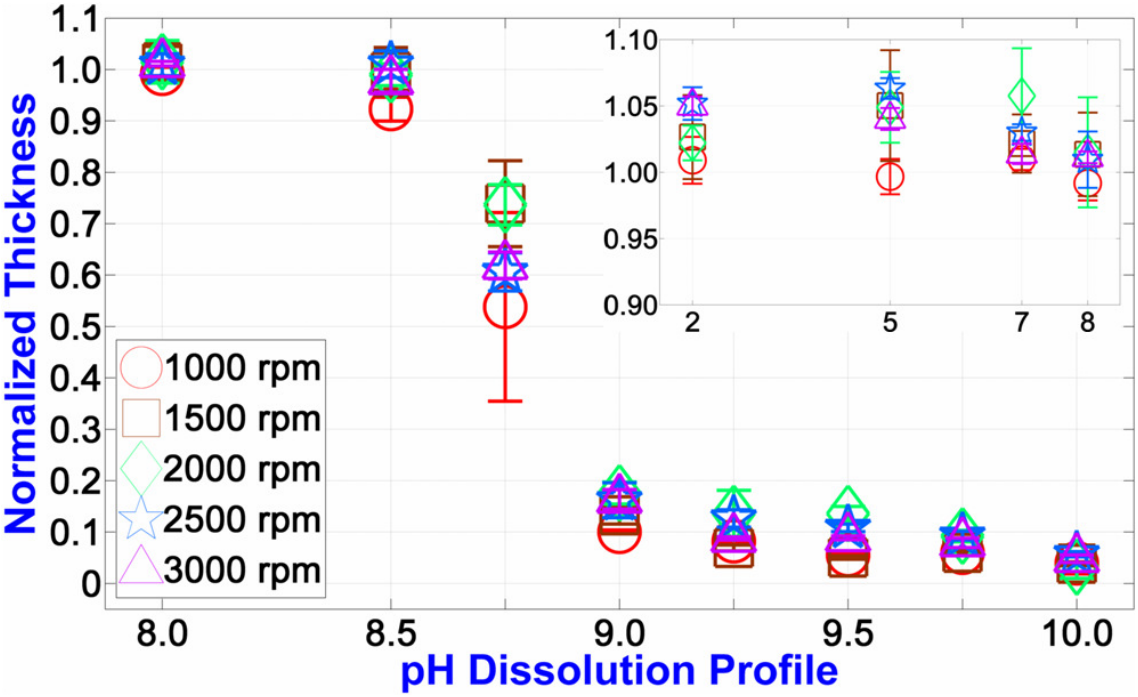

Figure 3-5. The dissolution profiles of spin-assisted films prepared at different spinning rates: Continuous (fast) experiments (inset shows the dissolution profile from pH 2.00 to 8.00).

Figure 3-6 (below) shows dissolution profiles of spin-assisted films prepared at different spinning rates when the dissolution experiment was performed discontinuously. Those results fit our previous predictions better and expected distinctions are observed clearly. The films prepared at 1000 rpm showed the least stability such that only 30% of the initial film retained on the substrate at pH 9.00. The films prepared at higher spin rates all showed better and similar stability. More than 50% of initial film thicknesses retained on the substrates at pH 9.50. Although no dramatic stability differences were recorded for 1500 rpm and above, a trend is seen apparent except 3000 rpm: The lower the spinning rate, the lower the stability. On the other hand, the deviation from this tendency at 3000 rpm can be justified considering deposition mechanism in spin-LbL. It has long been known that, adsorption mechanism of spin-deposition and self-adsorption (dipping) is different [711]. Based on theoretical models and experimental evidences [189,692,694,712], many researchers concluded that the adsorption of chains in spin-LbL is mechanically-controlled. According to this view, deposited chains are entangled with underlying film during spinning. When a certain spinning rate is exceeded entanglements might be also mechanically disrupted which might induce slightly less pH-stability. On the other hand, the time required for initial adsorption of polyelectrolyte chains in dip-LbL is known to be on the order of a few seconds ([188] and references therein) and this is likely to be similar in *hb*-multilayers. So, molecules

might be adsorbed unspecifically in higher spinning rates due to less contact time (solution-film contact time in 3000 rpm is presumably around 10 s). This picture also underlines thermodynamically not equilibrated (kinetically trapped) nature of spin-LbL films and justifies lower pH stability of spin-LbL films (if no annealing effect occurs). In fact, kinetic trap of spin-coated molecules in nonequilibrium conformations is well-known for polymeric thin films [713-717]. More specifically, this phenomenon has also been speculated for spin-casted multilayers [718-719] and spin-grown LbL films [190-694]. But, to our knowledge, no report is comparing pH-stability of spin- and dip-assembled multilayers and the role of kinetic trap on pH-stability is untouched. As a continuation, we would also like to reinterpret the similarity of pH-stability between dip-assembled (BPEI)(PVPon/TA)n films at pH 2.00 and spin-grown pH-Nat (PVPon/TA)n films (recall Figure 3-6). We think that similarity might be due to cancellation of opposite effects. In the first hand, we expect better pH-stability from pH-Nat multilayers due to elimination of osmotic pressure effect (no salts are present in pH-Nat films). But, kinetically trapped nature of spin-grown multilayers likely weakened the films and two opposite factors cancelled out each other. However, time-annealing of those multilayers (recall Figure 3-6) revealed the potential of spin-grown films and better pH-stabilities were achieved.

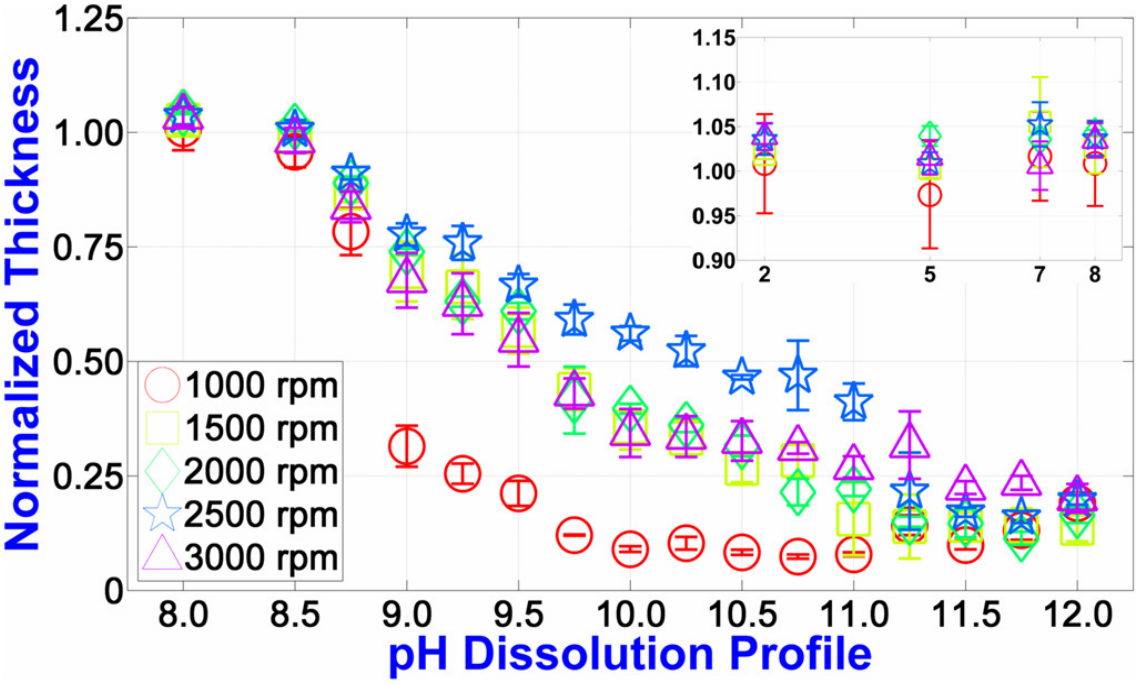

Figure 3-6. The dissolution profiles of spin-assisted films prepared at different spinning rates: Discontinuous (slow) experiments (inset shows the dissolution profile from pH 2.00 to 8.00).

The effect of rinsing in spin-LbL and its possible adverse effects on observed film stabilities should be discussed. The major difference between conventional spin-coating and spin-LbL is the intermediate rinsing step between the depositions of adjacent layers. Rinsing is a very important step of LbL technology and effective on stability of multilayers [281,720-721]. We believe, rinsing effect in spin-LbL is considerably more stringent than static rinsing of dip-LbL and we assume that no loosely-bound molecules stay on the surface in spin-LbL. On the other hand, according to McShane and Lvov [121], some researchers believe that air drag (shear force) applied during spin-LbL strengthens the intermolecular interactions between polyelectrolytes [177,188-189]. But, we preferred bilayer thickness framework as a simpler and easily understandable explanation. The way we consider the effect of bilayer thickness on film structure is also related to air drag explanation in a manner.

3.3.2. The Effect of Solution-Film Contact Time

3.3.2.1. Multilayer growth

Hybrid forms of dipping and spinning has been previously used by different researchers [112,691]. We also combined dipping and spinning methods in a different way. We varied static contact time of solutions with growing films and then spinning at a fixed rate was applied. Figure 3-7 shows film growth behavior of multilayers as a function of solution-film

contact time at 2000 rpm. As the solution gets in touch with the underlying substrate (or film), the PVPon (or TA) molecules start adsorbing on the surface by making H-bonds. If the adsorption process is faster than desorption, more molecules are expected to adsorb as contact time increases as it is for dip-LbL [112]. We observed a somehow different picture. First, there is no significant thickness change within 15 to 60 s which corresponds to a bilayer thickness of around 3 nm. If spinning rate dependent film-fluid contact time variation had a dominant effect on film thickness, bilayer thickness of 1000 rpm would be close to the bilayer thickness of 60 s (film-fluid contact time of 60 s sample is higher than 60 s).[48] Thus, spinning induced shear effect seems to have a more critical impact on film thickness at low contact times than solution-film contact variation. It is also important to compare contact time varied samples within themselves. As expected, growth characters of low contact (15 and 30 s) time samples are almost identical with growth profile given for 2000 rpm in previous part. Interestingly, an S-shaped buckling is seen for 60 s sample which is indicating the exponential character of the system when enough time is given for the restructuring of the film. This exponential tendency is more dominant for 120 s sample up to twelfth layer and film growth slows down afterwards. At the typical contact time for dip-LbL of PVPon/TA (300 s), a zigzag-like growth was observed and film was stripped as well. Keeping the solution in contact with surface for some time before spinning can be considered as a two-step process that involves dip-LbL like self-adsorption and spin casting. If the first stage is more dominant in film character, we can expect a slow exponential growth yielding around 10 nm for 8 bilayers as we observed in dip-LbL of electrolyte-free PVPon/TA system (see Appendix-E). In dip-LbL, stagnation of growth and destruction[49] of film structure is sometimes observed after a point. This can be justified by considering adsorption-desorption equilibrium of self-adsorption and surface reversal problems. In spin-LbL, adsorption is mechanically controlled [692,694,710], but surface reversal is still required. According to Shukla and Hammond [693], stagnation of growth is due to the rupture of charge reversal and interpenetration of layers during assembly is the main trigger. We apply the essence of this idea to our H-bonded system. If interlayer mixing takes place, outermost layer of growing film might become a mixture of H-bonding acceptors and donors. When a level is reached, there might be no available H-bonding sites expressed for the deposition of subsequent layers. In other words,

[48] Here we accept the difference between quiescent contact (dipping) and dynamic contact (spinning), but we would like to emphasize the general trend.

[49] Erel and Sukhishvili use the term “fouling” in their report to explain a similar behavior of another multilayer system.

virtually all sites are occupied by neighboring components in the mixture. This scenario explains the stagnation of film growth, but destruction of films requires further explanation. We have evidence on PVPon-induced destabilization of PVPon/TA films. We have exposed PVPon/TA multilayers into PVPon solutions and observed the destruction of film chains in time (Appendix-K). Electrostatic LbL deposition is known to be a self-limiting process in relation to charge reversal phenomena [165,174]. But, if diffusion of chains inside the film is possible, formation of outermost layer might not be limiting the interaction which might cause destabilization. We believe, this explanation also fits to zigzag-like linear growth profile in general.

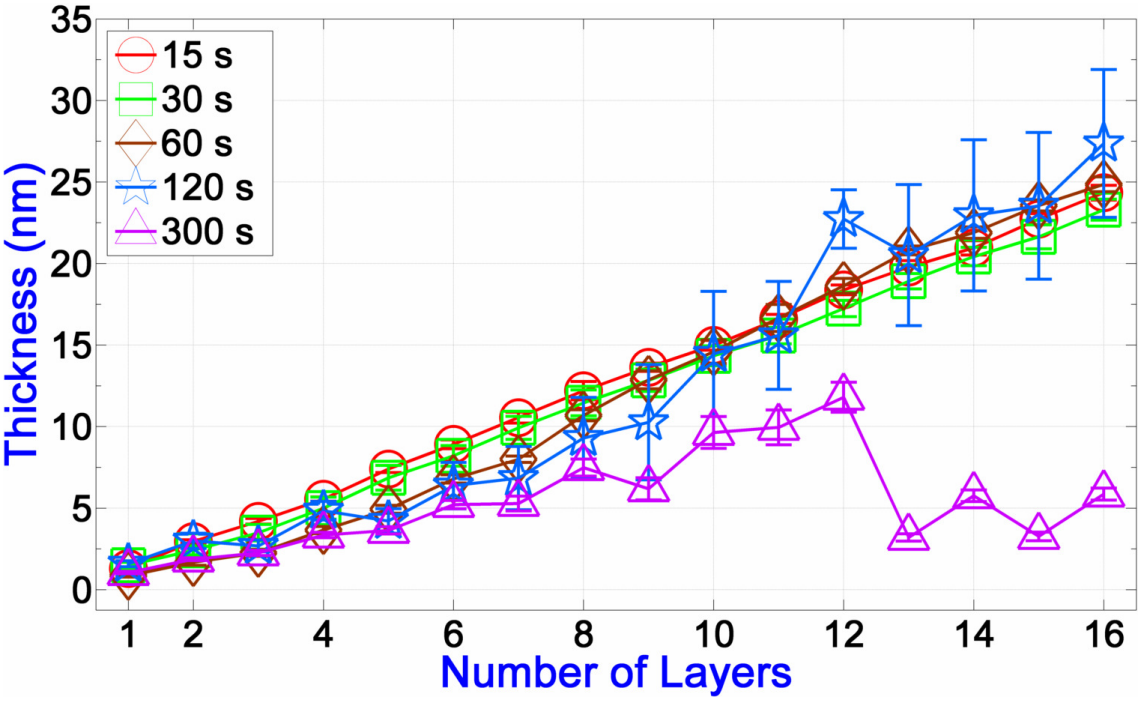

Figure 3-7. Effect of solution static contact time on growth profiles of multilayers at 2000 rpm.

As we did above for the determination of bilayer thickness of spinning rate varied samples, multiple films were grown to obtain information about statistical reproducibility about the system. Unlike film growth monitoring studies, no intermediate time intervals were given during film growth. The bilayer thicknesses of films were calculated using final thickness of films. Figure 3-8 shows that bilayer thickness depends logarithmically on contact time (bilayer thickness vs. log(time) curve is linear, plot is not shown). Similar behaviors were previously observed by others for dip-adsorption kinetics of polyelectrolyte films [112,698]. A similar behavior was also reported for spray-LbL by Schlenoff's Group [174]. They observed that, when a few more seconds spray is applied, bilayer thickness increases

50%. Here we would like to stress an important point. The trend shown in Figure 3-8 below is in agreement with the observations provided in literature. But, it looks like there is a conflict between 300 s samples of Figure 3-7 and Figure 3-8. Indeed, this difference highlights the influence of timescale on film growth. Data presented in Figure 3-7 and Figure 3-8 produced by discontinuous (viz. ellipsometry measurement at each step) and continuous (viz. neither ellipsometry measurement nor waiting until the end of multilayer assembly) growth respectively. As mentioned above, bilayer thickness of contact time varied films are around 3.1 nm in discontinuous growth except 300 s contact time for which an erratic growth was observed (recall Figure 3-7 above). When the deposition is performed continuously, films become thicker and bilayer thicknesses of films vary in power law form rather than stacking around a fixed value which was ~3.1 nm (recall Figure 3-8 above). Interestingly we did not observe the destruction of film at 300 s in this set of experiment. We attributed observed time-induced variation in film growth to the instable and kinetically trapped nature of PVPon/TA pair. To further support this view, we spin-grew another 300 s contact time sample and monitored the film thickness intermittently (see Appendix-G). The speed of film production was kept between two previous cases. In agreement with the rest of the picture we observed, we recorded exponential growth which reaches to “19.4 ± 2.1 nm” at 8 bilayers and “26.3 ± 2.0 nm” at ten bilayers. This result shows that the overall duration of film growth influences film growth profile, but the exact mechanism is not clear.

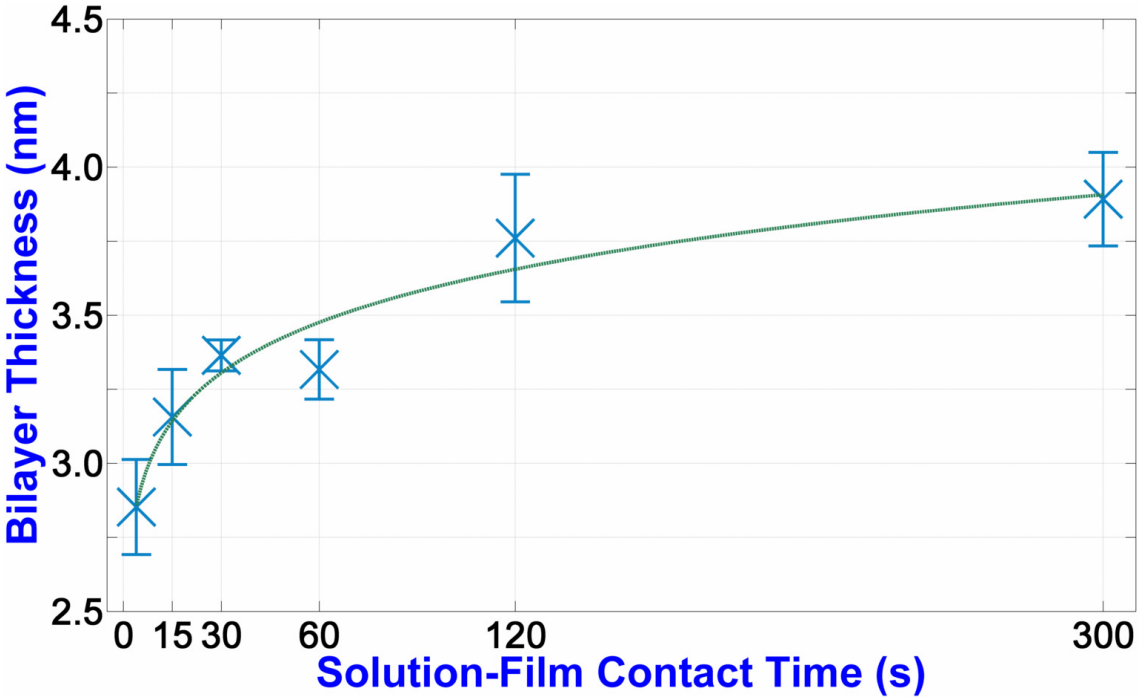

Figure 3-8. Bilayer thickness of as a function of static solution-film contact time before spinning at 2000 rpm (each data point is an average of at least two different ten bilayer samples).

In dip-coating, molecules find enough time to adsorb on surface in thermodynamically favorable conformations. This process takes place in two main steps which are anchoring of some segments of molecules to underlying material and relaxation of molecules to pack to the surface which are fast and slow respectively [196,698]. In dip-LbL the whole process is quiescent and external forces on molecules during assembly are minimal. In contact time varied spin-LbL, spin-casting takes place in addition to self-adsorption mechanism which is explained above. It is not easy to isolate the effect of these two processes on the character of final film. Moreover, the molecular picture might be more complex for exponentially growing films due to so-called in&out diffusion of molecules inside the film. For instance, some chains might be diffusing along the film while their tails sitting at the outermost layer. In this case, a single chain might experience force pulling it outwards during rotation.

Up to now, we generally emphasized the possible role of in&out diffusion which seemed to be important in our system. But, the exact mechanism behind exponential growth is still under debate [200]. There are two main views explaining exponential growth in LbL films which are i) roughness-trigger [153,201-202], ii) in&out diffusion [197-199]. Our group's previous observations [123-124] were in good agreement with the surface roughness model. Spin-LbL usually ends up with smoother surfaces comparing dip-LbL and spinning might be suppressing/delaying exponential character of PVPon/TA system. But, although a

correlation might exist, we believe roughness-trigger model [200] is not enough to explain our observations alone. Indeed, in&out diffusion model [197-199] is more widely accepted in the literature [207,672]. This model suggests a "reservoir" of freely movable materials present in the film structure. During the film growth (and rinsing), those materials migrate inward and outward which controls the amount of material adsorbed in each step (recall surface reversal and overcompensation mechanisms). This picture underlines the kinetic nature of LbL growth and seems match with our case considering its time-dependency. We might be observing a system which both models are equally relevant.

3.3.2.2. pH-stability

It is widely accepted that short contact times of spin-LbL reduces interpenetration of layers during assembly [191,691,696]. When contact time is increased, it is reasonable to expect an increase in the interpenetrations of layers similar to dip-LbL. Also, as mentioned above, exponential growth is associated with the interpenetrations of layers. We believe interpenetrated state is more thermodynamically stable than stratified but kinetically trapped state. pH-stability data on spinning rate varied experiments showed an example of interpretation towards the nature of the system. We also found that pH-stability of stratified films can be enhanced by a sort of annealing effect. If our interpretations are true, one would expect a significant pH-stability difference among stratified but annealed multilayers. It would also be justifiable to observe a complex pH-stability picture in kinetically trapped state. The experimental results were consistent with those expectations. Figure 1-9 (below) shows the dissolution behavior of multilayers subjected to fast dissolution experiment. The onset of dissolution observed at pH 8.00 for all samples, none of the samples retained its 50% of thickness at pH 9.00. A rapid dissolution was observed in all samples without expressing an order between contact time and pH-stability. However, dissolution behaviors of "annealed" films obey to the explanations above.

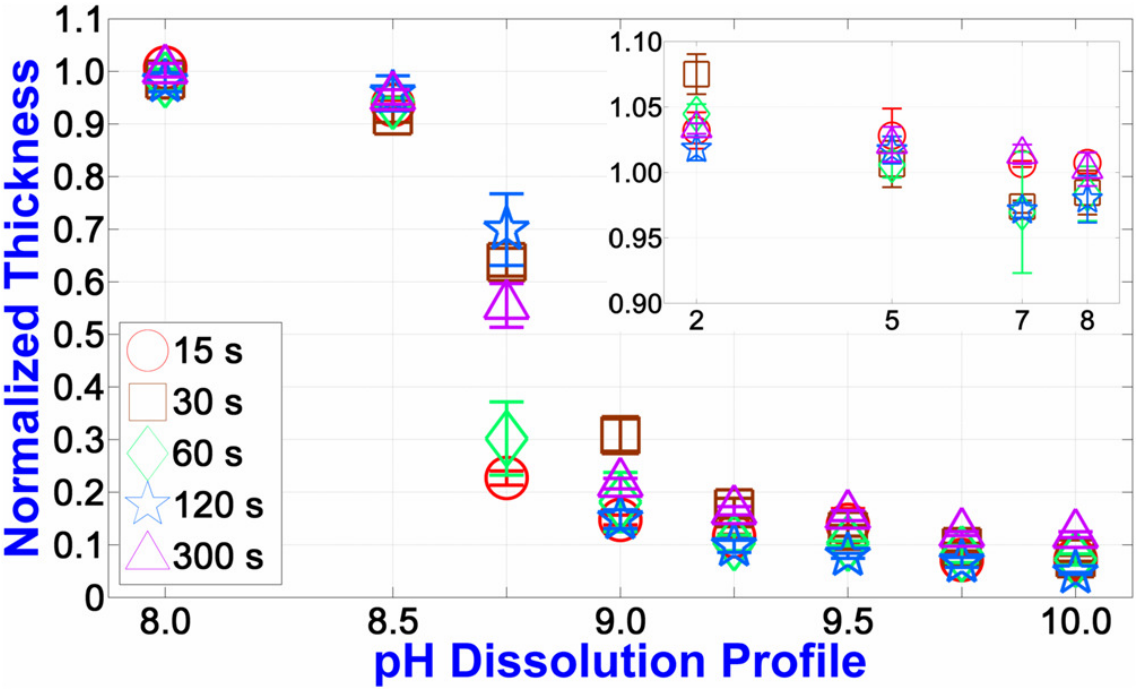

Figure 3-9. The dissolution profiles of spin-assisted multilayer films prepared at 2000 rpm by varying contact times: Continuous (fast) experiments (inset shows the dissolution profile from pH 2.00 to 8.00).

In Figure 3-10, the pH-stability of contact time varied multilayers subjected to slow dissolution experiment is seen. The onset of dissolution was at pH 8.50, similar to those prepared at different spinning rates. The dissolution profiles varied significantly beyond 8.50. The dissolution was slower as a function of pH change for films prepared at smaller contact times which are likely to be more hierarchical. The critical dissolution pH of varied nearly by 1 pH unit, from ~8.8 to ~9.7, as the contact time decreased from 300 s to 4 s (compare Figure 3-9 and Figure 3-10), respectively. The only deviation from the overall trends is observed in 120 s which might be due to the swelling of this film (please pay attention to the inset in Figure 3-10). We believe the swelling of this film before dissolution gave the structure enough freedom to equilibrate itself against pH as a perturbator. Here it should also be addressed why such a swelling (>10%) was only seen at 120 s. We believe this is a consequence of the exponential character of this film (recall Figure 3-7). Moreover, complexation at 120 s might be more favorable than 60 s, but it might be still hierarchical enough which seems to be important for pH-stability of annealed spin-grown multilayers.

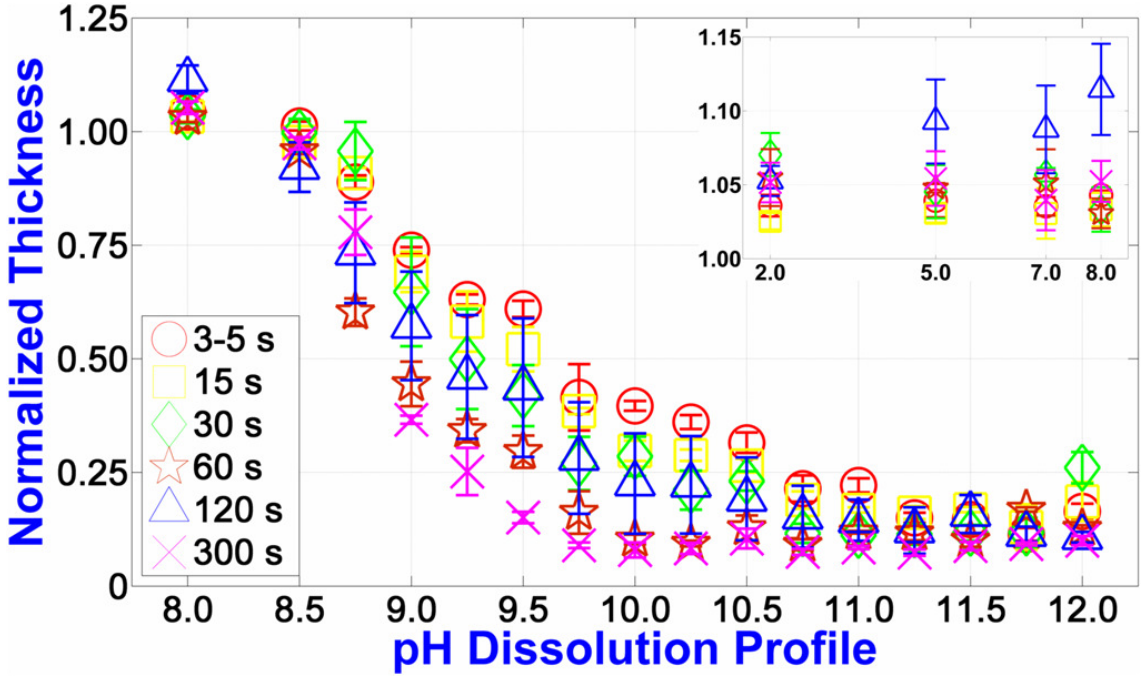

Figure 3-10 The dissolution profiles of spin-assisted multilayer films prepared at 2000 rpm by varying contact times: Discontinuous (slow) experiments (inset shows the dissolution profile from pH 2.00 to 8.00).

Kinetically trapped nature of spin-assembled PVPon/TA multilayers was evident in pH-depedent dissolution experiments. We also showed the implications of kinetic trap on film growth. However, we do not claim that spin-LbL films are kinetically trapped, but dip-LbL films are not. Dip-assembled films are more likely to be in thermodynamic equilibrium, but kinetic trap is still a concern. As a matter of fact, Hammond's Group showed [699] the rearrangement of kinetically trapped components into more ordered arrangements in dip-assembled electrostatic multilayers [701]. Also, we should admit that the complete mechanism behind enhanced pH stability is not clear yet. We believe, when the experiment is performed slowly and we gave pauses to dissolution experiment, molecules find enough time to realign themselves into more favorable conformations. This might be due to enhanced orientational mobility of building blocks at pH values that the film is not dissolved by small movements of building blocks are allowed. We know from the literature and our own experiments that TA has a pK_a below 6. We performed the dissolution experiments starting from pH 2.00 and we exposed the multilayers to pH 5.00, 7.00 and 8.00 before the onset on dissolution is observed. Therefore, before film dissolution becomes observable, some H-bonds inside the film might be broken and corresponding molecules might gain flexibility. However, acidic dissociation is not a permanent process at pH values close to pK_a values (remember that those multilayers inevitably contain a small amount of water in their

structure). Hence, broken H-bonds might reestablish in more favorable conformations. This process might be time taking so we might be observing the effect a time effect. But, we might also be observing a new type of annealing effect which we call “pH-annealing”. In nature, there are a number of pH-dependent biological processes accompanies with conformational changes of molecules. For instance, it is well-known that, even small pH variations might induce proteins to switch from one conformation to another one. Starting from pH 5.00, partially charged TA molecules might be evolving inside the film in opposite to the mechanism suggested above. Besides, PVPon molecules carry partially positively charged lactam rings in their side chains [501,503-504]. An electrostatic interaction might be taking place between dissociated hydroxyls of TAs and tertiary amines of PVPon. Finally, at high pH, TA molecules become slightly more hydrophobic. Slightly more hydrophobic TA molecules might be interacting with main chains of PVPon which might be contributing to the pH stability. In future, we will be investigating the origin of our observations.

3.4. CONCLUSIONS

Self-adsorption of molecules typically requires more time compared to to time given in spin-LbL applications. Spinning rate controls the thickness of thin liquid film and the time required for solvent removal and the air shear force applied to the growing film is dictated by spinning rate. As a result, film growth is mechanically controlled by spinning rate selection and molecules are kinetically trapped as multilayers instead of reaching a true thermodynamic equilibrium. In fact, those aspects of spin-LbL were already known, but experimental evidences were limited and the complications of this picture on growth and pH-stability of *hb*-multilayers was lacking. This study elucidated factors controlling the growth and pH-stability of spin-grown PVPon/TA multilayers. We observed linear growth profiles for different spinning rates unlike dip-LbL versions of PVPon/TA pair. The relation between spinning rates and bilayer thicknesses were found to follow a power law. We checked the effect of solution-film contact time on film growth observed linear-to-exponential transition by increasing contact time. We, for the first time, observed the dependence of pH stability on spinning rate and solution-film contact time. Comparing pH-stability of dip-LbL films, we observed weaker stability and we attributed this observation to kinetically trapped nature of spin-LbL multilayers. But at the same time, here we show that time (and presumably pH) annealing of spin-LbL multilayers reveal their potential towards high stability. When pH dissolution experiments were performed slower remarkable pH-stabilities were recorded. We

consider this observation as an evidence of kinetically trapped molecules. To the best of our knowledge, our results give the first evidence on kinetic trap effect on pH stability of H-bonded multilayers. The main trigger of annealing (i.e. pH, time) effect is not clear yet. But, our results might be indicating the first evidence on annealing effect by "pH-annealing" phenomena. Further studies should be undertaken to fully elucidate the factor affecting pH-stability of those multilayers.

Chapter 4: INCORPORATION of NONCOVALENTLY FUNCTIONALIZED SINGLE-WALL CARBON NANOTUBES in H-BONDED MULTILAYERS[50,51]

In this study, we extend our previous efforts on the preparation of SWCNT-doped PVPon/TA multilayers which was based on the usage of sidewall pi-stacking. Here we show that polymer-wrapped SWCNTs can also be employed to fabricate LbL nanocomposites. We exploited PVPon as polymeric wrapper and TA as sidewall pi-stacker for the stabilization of SWCNTs in water. Resulting supramolecular complexes (PVPon-SWCNT and TA-SWCNT) were characterized with DLS, ZPA and OAS. Dispersed complexes and bare (undoped) solutions were employed as building blocks of LbL film fabrication. We took advantage of self-assembling nature of dispersing agents to construct $(PVPon/TA)_n$-based multilayer architectures. H-bonding interaction driven $(PVPon/TA)_n$, $(PVPon-SWCNT/TA)_n$, $(PVPon/TA-SWCNT)_n$, and $(PVPon-SWCNT/TA-SWCNT)_n$ multilayers were built via spin coating. Film growth and pH-dependent disintegration profiles were tracked using EMM. Similar to our previous studies, we observed linear growth profiles via spin-LbL. Increased pH resistance (~2 unit) is observed for $(PVPon-SWCNT/TA-SWCNT)_n$ composition. This observation was attributed to the hydrophobic stabilization by SWVNT-SWNCT interactions and diminished ultrasonic degradation of stabilizing agents in the presence of SWCNTs. Film wettability was studied with CAM and no significant variations were observed which is a sign of good coverage dispersing agents on SWCNTs. FE-SEM studies were performed to monitor the presence of SWCNTs in film structure and RSM investigations confirmed the uniformity of SWCNTs within the matrix. Surface roughness variations were probed with AFM and considerable increments were recorded in case SWCNTs are present in film structure. To our knowledge, PVPon-functionalized CNT dispersions have not been yet reported for the assembly of *hb*-multilayers. Hence, here we advance our previous design for the incorporation of (SW)CNTs in *hb*-multilayer films. Considering pharmaceutical relevance of used building blocks, we claim to have been developed promising nanomaterials for biomedical applications.

---

[50] Partially presented as "Karahan, H. E., Erel, I. & Demirel, A. L. (2011, June). Incorporation of polymer-wrapped and side-wall functionalized single-wall carbon nanotubes into layer-by-layer self-assembled nanocoatings. Poster and abstract in *ICMAT 2011*, *Symposium B: Synthesis and Architecture of Nanomaterials*, Singapore."

[51] To be submitted as "Karahan, H. E., and Demirel, A.L. Incorporation of SWCNTs in H-bonded multilayers of a surfactant-like polymer and a natural molecule."

4.1. INTRODUCTION

In the past three decades, LbL surface deposition has received considerable attention as a versatile, easy and low-cost multilayer fabrication method. The technique was first utilized by Kirkland [90] and Iler [91] for alternate deposition of oppositely charged micron-sized colloidal particles. Then, Decher and his colleagues extended the technique switching from hard materials to soft molecules [93-95]. Just after the demonstration of SAM-based *hb*-multilayer stackings [722], *hb*-LbL assembled film compositions [113-114] were reported. Exploitation of H-bonding interactions introduced a great flexibility to LbL field. So, a variety of nonionic polymers were appended to component spectrum of LbL. In the meantime, colloidal particles (viz. nanoparticle dispersions) were again popularized as advanced dopants or structural components [268-274,279].

Nanoparticle-doping in LbL architectures is mostly achieved via electrostatical interactions and relatively few studies have been devoted to nanoparticle-filled *hb*-multilayers. If we further constrain the type of nanoparticles with unfunctionalized CNTs, as far as we are aware, only two studies are available in the literature: (poly(styrene sulfonate)-SWCNT/poly(vinyl alcohol))$_n$ [289-290] of Kotov's Group and (poly(allylamine hydrochloride)/poly(vinyl sulfate))$_3$(polyguanine-SWCNT/polycytosine-SWCNT)$_n$ of Nakashima's Group [291]. In both architectures, polymer-wrapped CNTs have been utilized for dip-assisted LbL self-assembly. In their design, one of the components of LbL pair was carrying CNTs and main concern was the exploitation of resulting multilayers for a specific application. Nakashima's Group provided more fundamental insight about the physicochemical properties of their system and evidence of H-bonding interactions was presented using urea as a chaotropic agent. Still, detailed microscopy investigations and pH-dependent film stability studies were lacking. Several properties of nanoparticle-loaded multilayers have been investigated by other researchers, but no report is available on the effect of nanoparticles on pH stability of LbL films. The LbL pair we used is rather different than the reported systems. Previously, an ionic pyrene derivative coated CNTs have been used as templates for *es*-LbL capsule deposition [723]. Similarly, Paloniemi et al. have used ionic polyaromatic molecules to functionalize SWCNTs in water [724] and have utilized resulting dispersions to build up dip-assembled *es*-multilayer [725]. We believe our effort is the first demonstration of sidewall pi-stacking functionalized CNTs in *hb*-LbL nanofilms. Also to the best of our knowledge, PVPon, one of the most successful polymeric wrappers and

biomedical polymers, has not yet been reported in SWCNT-incorporated LbL formulations.

In this study, a linear polymer (PVPon) and a natural macrocyclic polyphenol (TA) are used as stabilizing agents to disperse SWCNTs in water. Resulting SWCNTs dispersions were employed as building blocks of LbL nanocomposites (see Figure 4-1 below for the schematic representation of our strategy). Using spin coating, we assembled SWCNT-doped *hb*-LbL films. Effects of SWCNT incorporation on the properties (i.e. pH-stability, surface roughness and surface wettability) of multilayer films have been investigated. High pH-resistance of $(PVPon\text{-}SWCNT/TA\text{-}SWCNT)_n$ films have been observed.

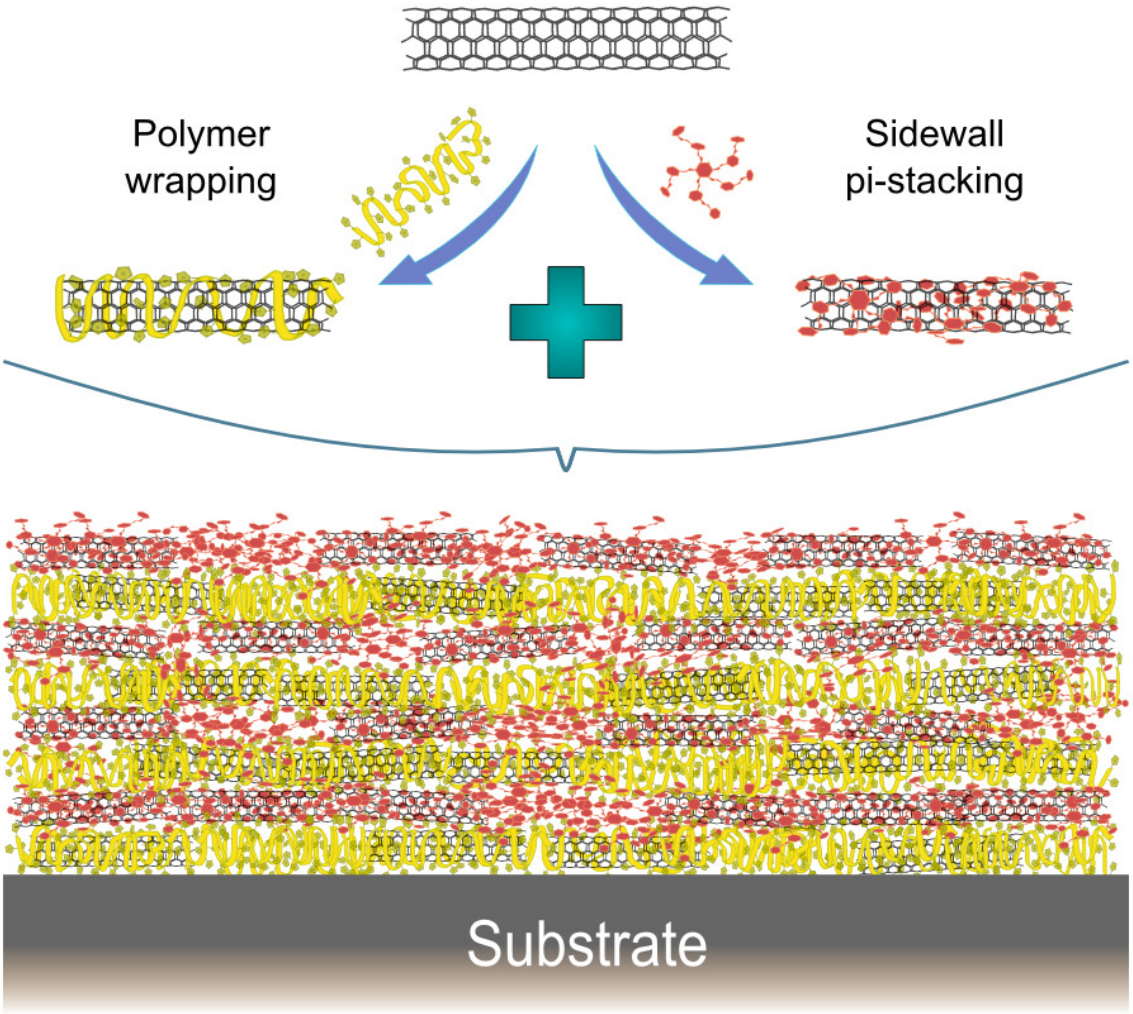

Figure 4-1. Depiction of employed strategy to fabricate carbon nanotube doped H-bonded multilayer films.

4.2. EXPERIMENTAL

4.2.1. Chemicals

See Section 2.4.1 for the origins of PVPon, TA, HCl, NaOH, phosphate buffer, SWCNT, and silicon wafers.

4.2.2. Methods

4.2.2.1. Dispersion of single-wall carbon nanotubes

We modified our previous procedure for dispersing SWCNTs. Main aim of new modifications to our previous routine (recall Chapter 2 above) was to increase dispersion efficiency by applying more energy to the samples. Considering violent heat evolution by prolonged sonication, ultrasound medium always kept cold (~0 °C) as earlier did by other researchers [520,654,726]. Aqueous solutions of dispersing agents (PVPon or TA) were prepared in fixed concentration (0.50 g/L). Varying amounts of dry SWCNT powders (0.50, 0.25, 0.10 g/L) were directly weighted in 50 mL macrocentrifuge tubes using a 5 digit semi-micro balance (XR205 SM DR, Precisa Instruments AG, Switzerland). 25 mL of dispersant solutions were transferred on SWCNT powders. All vessels were covered with aluminum foil and were shaken at 250 rpm for ten days in room temperature. Swollen SWCNT powders first sonicated for 30 minutes in ice-cooled sonic bath. At each round, four tubes were located at a fixed position to maintain equal distance from three resonators (see Appendix-D). Liquid level of ultrasonic bath was adjusted to be in the same level with liquid level of samples and bottom of vessels were approximately 1.5 cm apart from basement. Bath-sonication was followed by horn-sonication using titanium tips of the same manufacturer. High power sonic irradiations were performed in pulse mode (on: 3 s, off: 3s) for 30 minutes at around 0 °C (~55-65 kJ were applied). Resulting stable dispersions and control groups (PVPon and TA solutions) were kept under room temperature (1-2 hours) and subjected to centrifugation at 9000 rpm. 20 mL of supernatants were gently collected from each tube and were transferred to aluminum foil covered glass containers (note that control solutions may contain titanium particles out of sonication tips). Samples were first kept in room temperature for approximately less than one week before solution-based characterizations. Then, samples were kept in a regular refrigerator (4 °C) [654] expecting a supression in hydrophobic interactions between CNTs. Before film assembly, samples were exposed to a final bath sonication (post-sonication) step using previously employed conditions.

4.2.2.2. Characterization of dispersions

4.2.2.2.1. Optical absorption spectroscopy

Initial concentrations of dispersing agents and (SW)CNTs somewhat influence the dispersion efficacy in a non-linear fashion [598,727-729]. So, in order to maximize both absolute and relative concentration of SWCNTs, we studied a small set of different stabilizer/SWCNT

ratios. Dispersed form of unsorted (SW)CNTs are normally blackish due to different molecular structures that reflects the combination of the colors of "rainbow" [379]. Level of the darkness of (SW)CNT dispersions still gives a qualitative idea about the concentration of particles in the dispersion. But, in order to quantify visual observations, we used OAS. Fresh dispersions (~10 days) were investigated between 200 nm and 1000 nm range using quartz cuvettes. We diluted samples to 5% of their original concentrations and diminished the influence light scattering. Then, we also checked the applicability of Beer's Law studying linear relationships of absorbance values with respect to different particle concentrations [609]. Concentrations of the dispersions were roughly estimated using an available extinction coefficient (2.86×10^4 cm^2/g, at 500 nm) [488,618]. Note that absorption backgrounds that come from PVPon and TA were negligible at used wavelength.

4.2.2.2.2. Particle size measurement

Dispersions were diluted to their 20% with DI-H_2O and 0.5 mL of sample was introduced into low volume polystyrene cuvettes. Fourteen data points were collected for each sample over fixed time spans. Data was accumulated for 55 s to produce auto-correlation function and 5 s elapse times were given between each data accumulation. All measurements were conducted at 25 °C after 6 min. pre-equilibration and General Purpose Mode was used for the calculation of intensity data. In order to compare aggregation tendencies, mean values of intensity averaged size distributions were further averaged. Outlier scores (if any) were eliminated using a MATLAB script operating a two step filtering algorithm as follows: i) Data points greater than ten-fold or smaller than one fifth of median were eliminated and mean values were taken, ii) Data points ten-fold standard deviations away from mean value were eliminated and mean values were taken. As a control experiment to assess self-assembly (i.e. self-stacking) of TA, hydrodynamic size of TA molecules in fresh solution was also studied. 10.0 g/L of aqueous TA solution was prepared and approximately one hour waited for dissolution. Then solution was filtered using 200 nm polymeric membrane and particle size measurements were performed without dilution.

4.2.2.2.3. Surface charge measurement

All dispersions and solutions were diluted to 20% of initial concentration and no pH adjustments were applied. Disposable acrylic cells were used as cuvettes. Each datapoints were averaged out from ten runs and ten data points were collected for each sample. No data elimination was applied and simple arithmetic means were taken.

4.2.2.3. Film fabrication and disintegration

4.2.2.3.1. Substrate preparation

Silicon (100) wafer surfaces were used as substrates and prior to film deposition acid-base cleaning was performed similar to previous reports [122-124]. 4 inch wafers were cut into ~(1×1) cm^2 pieces and were kept in UV-Ozone Cleaner (Model 42-220, Jelight Company, Inc., USA) for 3 h. Ozone treated wafers were rinsed with DI-H_2O and dried under N_2 flow. Acid-base treatments were performed just after ozone cleaning. Four liquid bathes of 15 mL liquid were prepared in glass containers as follows: a) concentrated sulfuric acid, b) DI-H_2O rinse, c) 0.25 M aqueous NaOH, and d) DI-H_2O rinse. Wafers were dipped into each bath for ten minutes respectively. After washing steps, excess amount of DI-H_2O was used to rinse away any acid or base residue. Prepared substrates were kept (1 to 3 days) in Petri dishes and were thoroughly rinsed with DI-H_2O before multilayer deposition. Mixed oxide layer thicknesses on Si wafer substrates were measured just before film assembly.

4.2.2.3.2. Spin-assisted multilayer assembly

Processed solutions (PVPon and TA) and stable dispersions (PVPon-SWCNT and TA-SWCNT) were exploited for film deposition. Dip-LbL of $(PVPon/TA)_n$ system has been previously shown by Erel-Unal and Sukhishvili using pH adjusted solutions and anchoring layer deposited silicon substrates. To improve the adhesion of multilayer to the substrate, BPEI was used as anchoring layer in their report, but we removed this step in our spin-LbL studies (recall Chapter 2 and 3 above). Also, increased IS of solvent media decreases the stability of SWCNTs in dispersions, hence buffering agents was kept out. In our previous studies, we observed that it is possible to spin-assemble $(PVPon/TA)_n$ and (PVPon/TA-SWCNT) films using pH-Nat solutions without deposition of anchoring layer. We repeated this strategy and spin-LbL was performed at 2000 rpm for 1 min (2-3 s acceleration, 54-55 s constant speed plateau, and 2-3 s deceleration) using manual spin coater. In each deposition, 70 μL of liquid was used for assembly and 105 μL DI-H_2O was used for rinsing. 60 s elapse time was given before the spinning process for self-adsorption of first layer. Then, film-fluid contact was kept as ~10-20 s (especially before PVPon and PVPon-SWCNT deposition steps). There different compositions (A: PVPon-SWCNT/TA, B: PVPon/TA-SWCNT, C: PVPon-SWCNT/TA-SWCNT) and a control group (PVPon/TA) were assembled. Each composition was assembled as “small” (2.5/3.0 bilayer), “medium” (9.5/10.0 bilayer), and “large” (24.5/25.0 bilayer) forms in terms of deposited bilayers. Film growth experiments

were performed by continuous tracking of film thickness and 8 bilayers of multilayers were grown. Other measurements were performed using small-, medium-, or large-form multilayers and those multilayers were grown without intermediate wait times to reduce time-induced aggregations (recall Chapter 2 above) and film behavior alterations (recall Chapter 3 above). pH-dependent disintegration studies were performed using medium-form multilayers which are prepared from freshly post-sonicated (one to two days) samples. Small- and large-form multilayers were built posterior to medium-form and final film thicknesses were checked with ellipsometry (data collected from five different zones of the films and five data points were taken for each point). Considering earlier reports on refractive indice[52] (~1.4) of SWCNTs [544,673] and practical reasons [224], refractive indice variations upon nanoparticle doping was first not taken into account and refractive indice was taken as "1.500". Then, effective refractive indice of small-, medium-, and large-form films were calculated using a built-in algorithm in the software of device. We exploited the algorithm in three steps. First, we iterated the data fitting algorithm between the refractive indice values of "1.2500" to 2.2500" with "0.01" stepping. In this step, we obtained a rough estimate for the real part of multilayers (particle-free or -doped) refractive indice. In second step, we defined a "0.2" unit wide (from start to finish) of refractive indice range around the rough estimate and rerun the algorithm with "0.001" stepping. In the last step, range was kept as "0.02" and stepping were "0.0001" unit (the rest is the same with second step). In each step, film thickness range was given from half (lower limit) to one and a half (upper limit) times of the raw thickness data in which refractive was taken as "1.500". This analysis was performed for large-form films. We took the "deviation" number provided by the software as the tolerance of iteration (we accepted maximum deviation of "0.1" at the third step of our analysis). Refractive indice obtained for large-form films were also used to remodel the multilayer growth data to check for possible deviations (data not shown). Based on the minute influence of assumed refractive indice on calculated film thicknesses, we did not remodel pH-dissolution data sets after refractive indice correction. Indeed, possible shifting in absolute thickness values becomes ignorable after normalization.

4.2.2.3.3. pH-dependent film disintegration

pH-dependent disintegration of LbL films is a critical indication of the intercomponent interactions. Also, growth mechanisms of LbL films somehow reflect to disintegration

[52] In ellipsometry, the modeling was performed using real part of the refractive indices.

profiles. At elevated pH values, polyacids become deprotonated and H-bonding interactions are broken, so *hb*-LbL films disintegrate [122,139]. We investigated the effect of SWCNTs on pH dissolution behavior of the films different compositions. Considering possible adverse effects of harsh processing conditions and aging on H-bonding capacity of dispersing agents; we prepared a control sample using fresh solutions of PVPon and TA. Immediately after growth of fresh control sample, disintegration studies were performed similar to the procedure explained in our previous work (recall Chapter 3 above). Briefly, pH adjusted 0.01 M solutions of buffer were used as dissolution media. Slightly acidic (pH-Nat 4.70 to 4.75 at around 25°C) of 0.01 M buffer solutions were adjusted with 5.00 M and 0.25 M of HCl and NaOH solutions via as small as possible volume addition. Medium-form films were exposed to 10 mL dissolution media for 20 minutes and film thicknesses were measured upon nitrogen gas assisted drying. As an addition to previous procedure, we applied a prior hydration step using DI-H_2O (denoted as t_1) before exposure to buffer solutions. As we did before, buffer solutions were refreshed at every exposure step to prevent contaminations.

4.2.2.4. Homogeneity of particles within matrix

In film dissolution studies, we considered SWCNTs as an active component of assembly. We assumed SWCNTs are homogeneously embedded inside the films (recall Chapter 2 above). Using RSM, we checked the reliability of our assumption. We selected medium-form film of most CNT-rich composition for this measurement, which is $(PVPon\text{-}SWCNT/TA\text{-}SWCNT)_{10}$. We first coated this sample with a thin layer (~2.7 nm) gold using Cressington Sputter Coater 108auto equipped with Cressington Thickness Monitor mtm 10 (Elektronen-Optik-Service GmbH, Germany). Then we performed area and line mappings.

4.2.2.5. Film morphology

We have investigated the surface morphology of different film architectures using FE-SEM and AFM. FE-SEM was used to verify the presence of SWCNTs in resulting nanocomposites. Small-form films were used to probe initial stages of SWCNT deposition and large-form films were studied to probe continuity of SWCNT deposition. FE-SEM investigations were performed via focusing on center regions of films to globally compare different architectures (note that abundance of tubules are normally less in center regions due to gravitational force applied by spin coating). Finer topography details were studied via AFM operated under tapping mode. The presence of individual SWCNTs was tracked using small-form films to better differentiate individual SWCNTs and surface roughness. Surface roughness properties

of different architectures were compared using 5 different arbitrary ~(2 × 2) μm^2 areas from the center regions of the films. Height count data of images were extracted from the software of the device was processed in MATLAB R2010b environment using our own frequency count script. In this script, contributions of non-SWCNT big particles (>50 nm) were suppressed to compare basement roughness of the films.

4.2.2.6. Film wettability

We expected a decrease in hydrophilicity of $(PVPon/TA)_n$ films upon SWCNTs incorporation. So, water wettability of the films was investigated using a video-based optical contact angle measurement device (Contact Angle System OCA20, DataPhysics Instruments GmbH, Germany). In order to compare any possible surface structure, we studied both 2.5 and 3.0 bilayer forms of each film composition. Three measurements were performed for each surface using 2 μL of DI-H_2O. At least 20 frames were collected per second and first sharp edged frames of each image were taken as zero time of liquid-surface contact. Then, fifth second of contact was selected to gather contact angles. SCA20 uEye 4.1.11 software of the manufacturer was used in its elliptic fitting mode.

4.3. RESULTS and DISCUSSION

4.3.1. Characterization of Dispersions

4.3.1.1. Particle concentration

Solution chemistry (pH and IS) [337,730] and relative concentrations of dispersing agents and (SW)CNTs [728-729] influence the success of dispersion procedures. In our previous studies (recall Chapter 2), we studied SWCNT dispersion in pH adjusted (also means higher IS) and in native pH (also means lower IS) solutions of PVPon and TA. We observed a remarkable improvement on dispersion efficiency using pH-Nat solutions (recall Chapter 2 above), but the effect of relative concentrations was lacking. Here, we studied the effect of SWCNT/dispersant ratio fixing PVPon-SWCNT and TA-SWCNT dispersions. The influence of initial nanotube powder concentration on final dispersion concentration found apparent to the naked eye (see Figure 4-2).

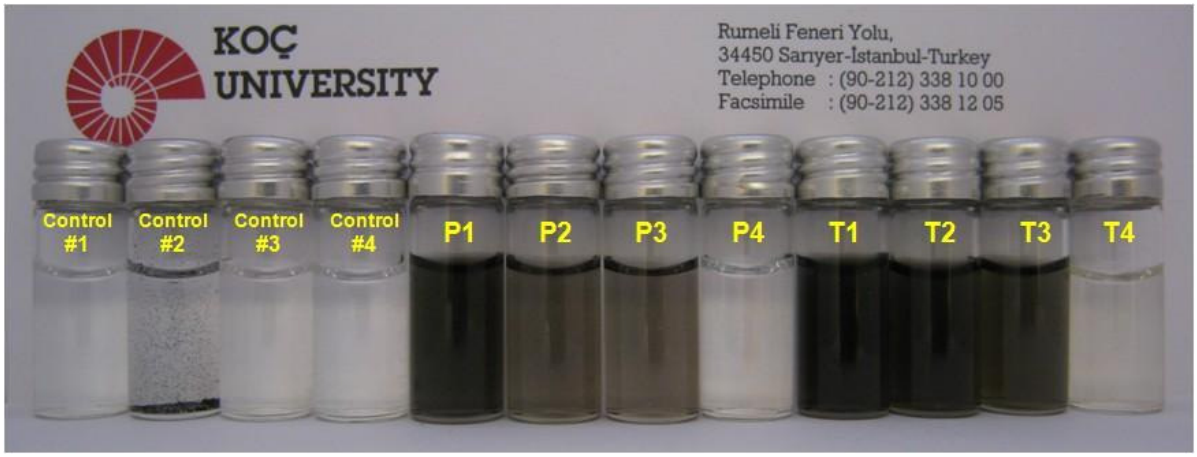

Figure 4-2. Visual observation of noncovalently functionalized single-wall carbon nanotube dispersions (Control #1: DI-H_2O, Control #2: Sonicated SWCNTs in DI-H_2O without dispersing agent, Control #3: Fresh PVPon solution, Control #4: Fresh TA solution, P1 to P3 and T1 to T3: PVPon-SWCNT and TA-SWCNT dispersions of 0.50, 0.25, 0.10 g/L initial SWCNT concentration, P4: Processed PVPon solution, T4: Processed TA solution).

Visual observations were quantified with OAS studies because such a comparison of the particle concentrations of dispersions would be crucial to maximize the abundance of nanotubes in resulting LbL films. We obtained featureless spectra (viz. no specific peaks) of SWCNT dispersions (see Figure 4-3 and 4-4) as previously obtained by numerous groups [482,487-488,731-732]. Featureless optical spectra of as-grown chemical vapor deposition produced SWCNTs are explained in different ways. First, coexistence of various types of SWCNTs (polydispersity) [732] decreases the abundance of specific nanotubes and superposition of individual spectra clear up expected characteristic peaks. Optical features of (SW)CNTs also become broadened, shifted and depleted (theoretical: [733-734], experimental: [419,735-736]) in bundled (or aggregated) form. PVPon-SWCNT dispersion might be slightly suffering from bundling (see following subsection). pi-pi stacking interactions are considered to make the optical spectra broader [616,737] and this would also be valid TA-SWCNT dispersions. Another physical reason behind broader spectra can be low tubule length [738] due to ultrasonic shortening of tubules. Extreme chemical functionalization, and high amorphous C content might be other typical causes [620,656]. Based on RSM investigations (see Subsection 4.3.4), increase of non-SWCNT species (other CNPs) in the system seems the main reason behind featureless spectra.

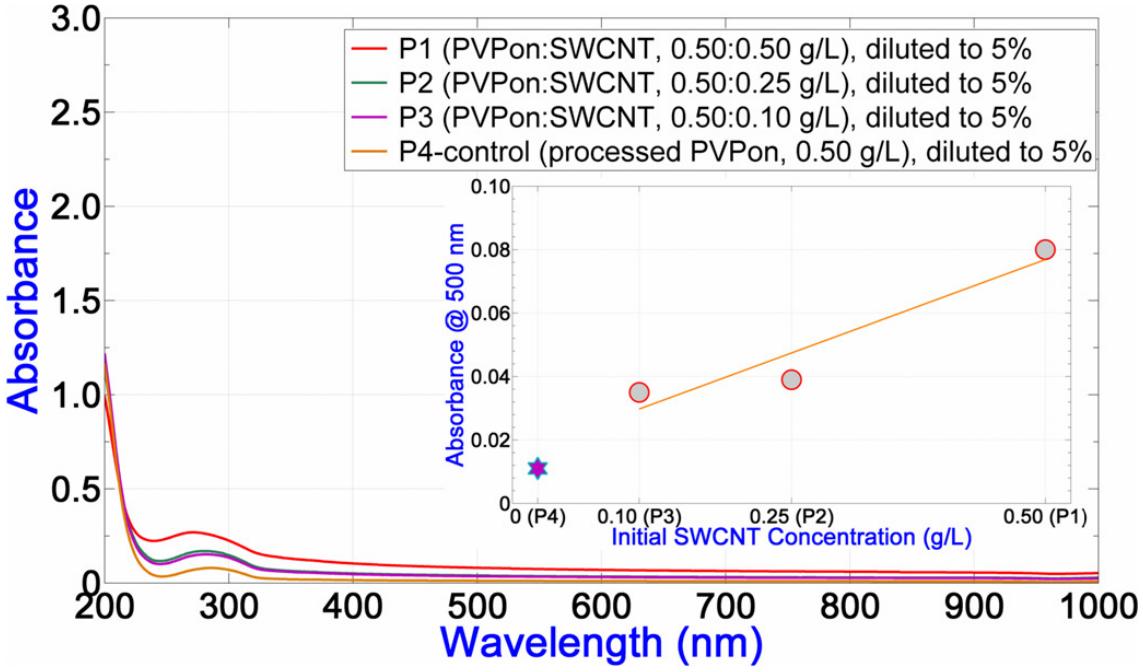

Figure 4-3. Optical absorption spectra of poly(*N*-vinyl-2-pyrrolidone) aided dispersions of single-wall carbon nanotubes at different initial concentrations (inset shows absorbance values at 500 nm for each samples).

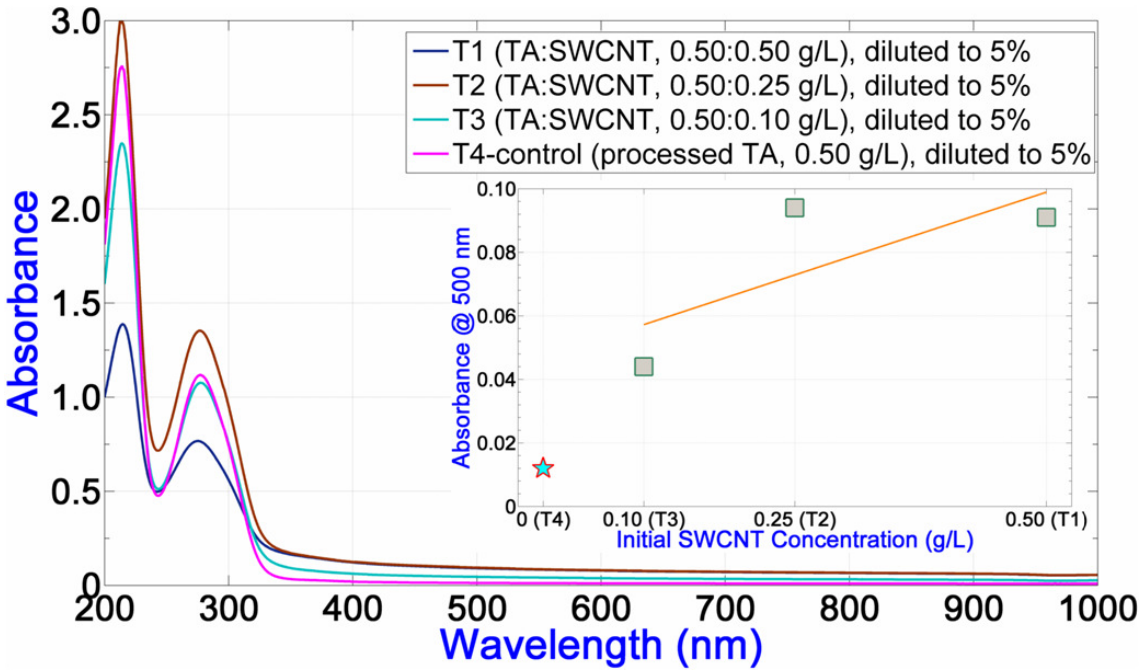

Figure 4-4. Optical absorption spectra of tannic acid aided dispersions of single-wall carbon nanotubes at different initial concentrations (inset shows absorbance values at 500 nm for each samples).

Using a widely preferred [525,618,739-740] extinction coefficient (2.86×10^4 cm^2/g) [488], concentration of SWCNTs in PVPon-SWCNT and TA-SWCNT dispersions are roughly estimated as ~0.056 g/L and ~0.064 g/L respectively (at least 10% of SWCNTs are recovered). Utilization of featureless spectra to estimate concentration of SWCNTs is

considered to be erroneous [659]. But, it is surely safe to compare different batches within themselves (see insets of Figure 4-3 and 4-4 above). In addition, it is desirable to select less dispersing agent containing dispersions to decrease free dispersant level in dispersion. Based on these considerations, P1 of PVPon-SWCNT and T1 of TA-SWCNT are selected for further LbL studies. P1 contains particles approximately twice that of P2. SWCNT concentration of T2 is more than T1, but TA concentration of T2 is also higher (see the characteristic peaks of TA below 300 nm). We also checked the applicability of Beer's Law, performing a concentration-dependent study (see Figure 4-5). Before this study, samples were approximately three weeks more aged in comparison to the age of the samples used in previous measurements. Hopefully, linear trends were observed, but optical absorption values of SWCNTs were suppressed due to aging. So, prolonged aging would cause underestimation of the particle concentration. In time, optical absorption of PVPon-SWCNT seems reduced from 0.080 to 0.062 (22.5% reduction). Similarly, concentration of TA-SWCNT dispersion was 0.091 and 0.074 (~18.7% reduction) which means the optical density of TA-SWCNT was less affected by aging in correlation its higher stability.

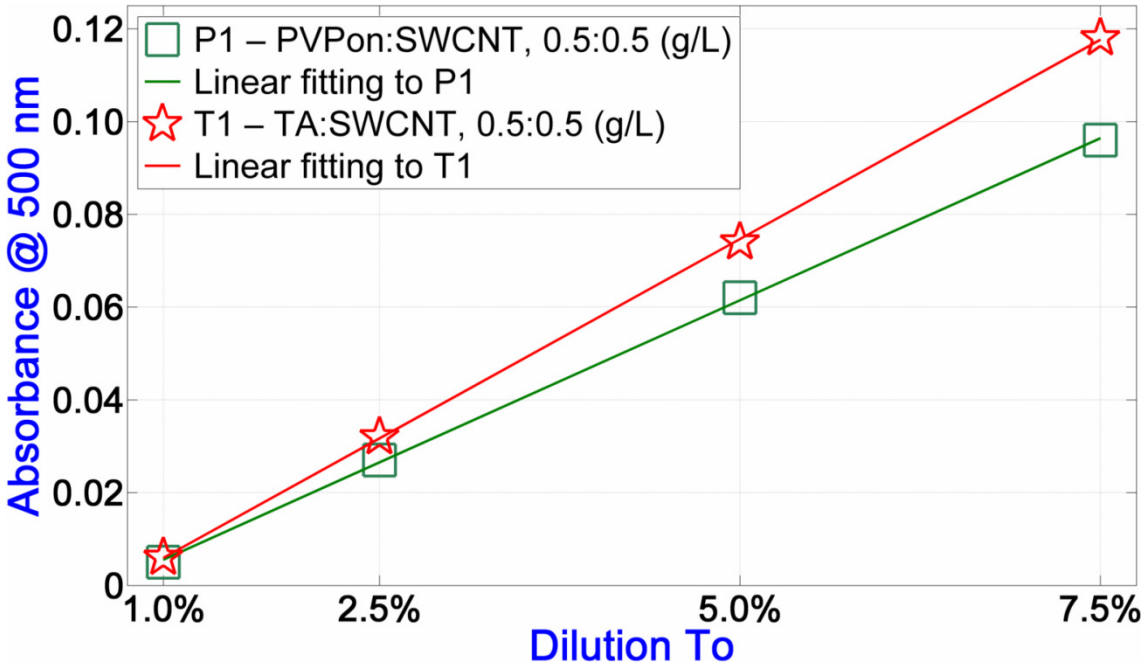

Figure 4-5. Verification of linear optical absorption behavior of single-wall carbon nanotube dispersions.

Oxidation of TAs to quinonic forms (see Appendix-L) can be tracked via color formation [122,213,741] and can be accelerated via ultrasonic irradiation [742]. pi-pi interactions between SWCNTs and TA might suppress or shift optical features. But, our TA-SWCNT dispersions exhibited almost no significant suppression or shift of absorption bands

in accordance with the claims of Liu et al. [525].[53] Chemical effects of ultrasonic irradiation on aromatic molecules are known to be time dependent and relatively minute in short time intervals [568,743-744]. So, our optimized procedure might be gentle enough to protect chemical nature of TA molecules. Sonochemical degradation of polycyclic aromatic hydrocarbons was previously reported to be reduced via addition of fulvic acid [745] and humic acid [746] to the systems. Similarly, SWCNTs and TA might be somehow protecting each other against ultrasonic degradation to a certain extent. We also checked the stability of TA (and PVPon) upon ultrasonication via FT-IR. FT-IR spectra of processed and raw TA were almost identical (see Appendix-M) which supports aforementioned scenario.

4.3.1.3. Particle size and stability of dispersions

DLS measurements provided valuable insights not only to compare PVPon- and TA-SWCNT dispersions, but also to interpret the effect of SWCNT concentrations on resulting complexes. First, hydrodynamic size of PVPon-SWCNT complexes is two or three times greater than that of TA-SWCNT complexes (see Figure 4-6). This result is probably a combination of the success of TA on dispersion efficacy and the state of PVPon chains on SWCNTs. Based on our previous results (recall Chapter 2 above), we believe TA-SWCNT dispersions are more stable than PVPon-SWCNT dispersions and the ratio of individualized SWCNTs are expected to be higher. Size distributions of PVPon- and TA-SWCNT dispersions (see Figure 4-7) support our previous interpretations. Approximately twenty times wider distributions were observed for PVPon-SWCNT comparing TA-SWCNT cases (ignoring P3 and T3). We would like to speculate on possible reasons. Conformation of PVPon chains on SWCNTs would be expected to obey train-loop-tail model [499,514-515,517-518]. Loops and trains of a chain would normally be revolving around the particle surfaces semi-freely while the rest of the chains (trains) would reside on the surfaces. Non-train parts (especially trains) are expected to contribute hydrodynamic radius of the particle as an additional factor. Also, exchange of PVPon chains might cause transient long-tail conformations and might increase measured particle size. So, swollen PVPon chains on SWCNT surface will normally increase actual and measured hydrodynamic diameter of the complexes. This effect was reported to be in the order to tens of nanometers [516,747]. Another interesting point of DLS results is the non-Gaussian size distribution observed in third samples of both systems (P3 and T3). This might

[53] We also recorded no apparent change in the optical spectra of T4-control comparing fresh TA solution (data not shown).

be attributed to the decreased cavitation efficiency by decreasing particle density in the system. It is well known that increasing amount of particles provide additional nuclei for cavitation and the number of cavitation events increases [568,748].

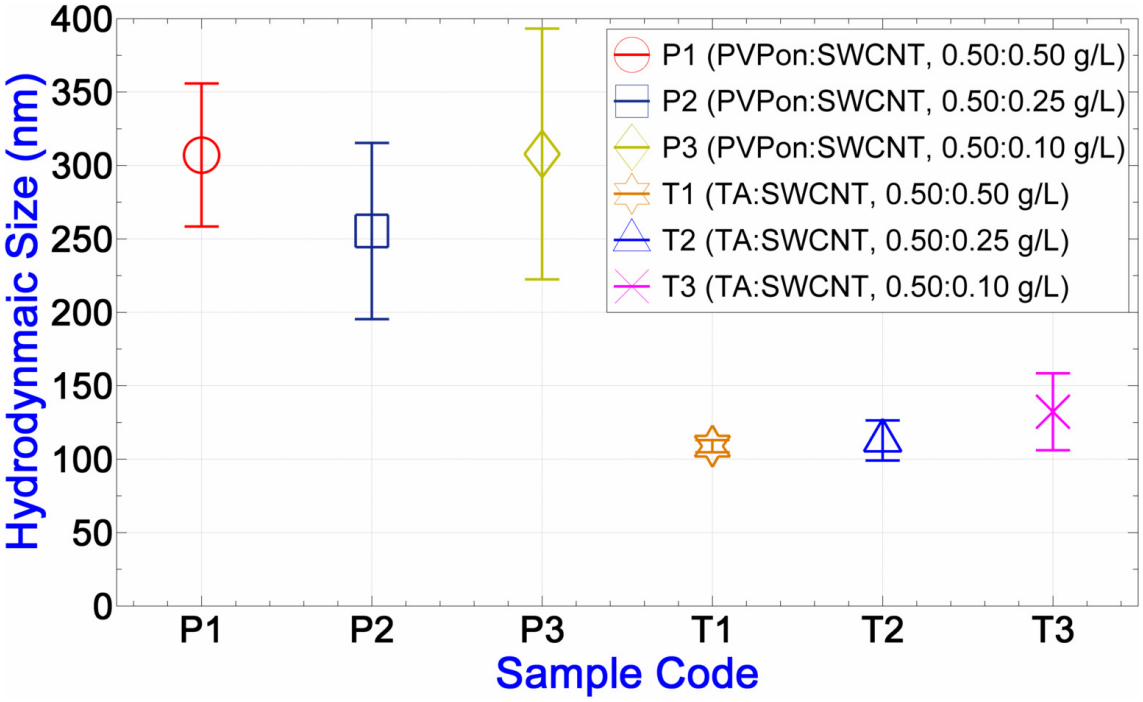

Figure 4-6. Intensity-weighted average particle size profile of poly(*N*-vinyl-2-pyrrolidone) and tannic acid aided dispersions of single-wall carbon nanotubes.

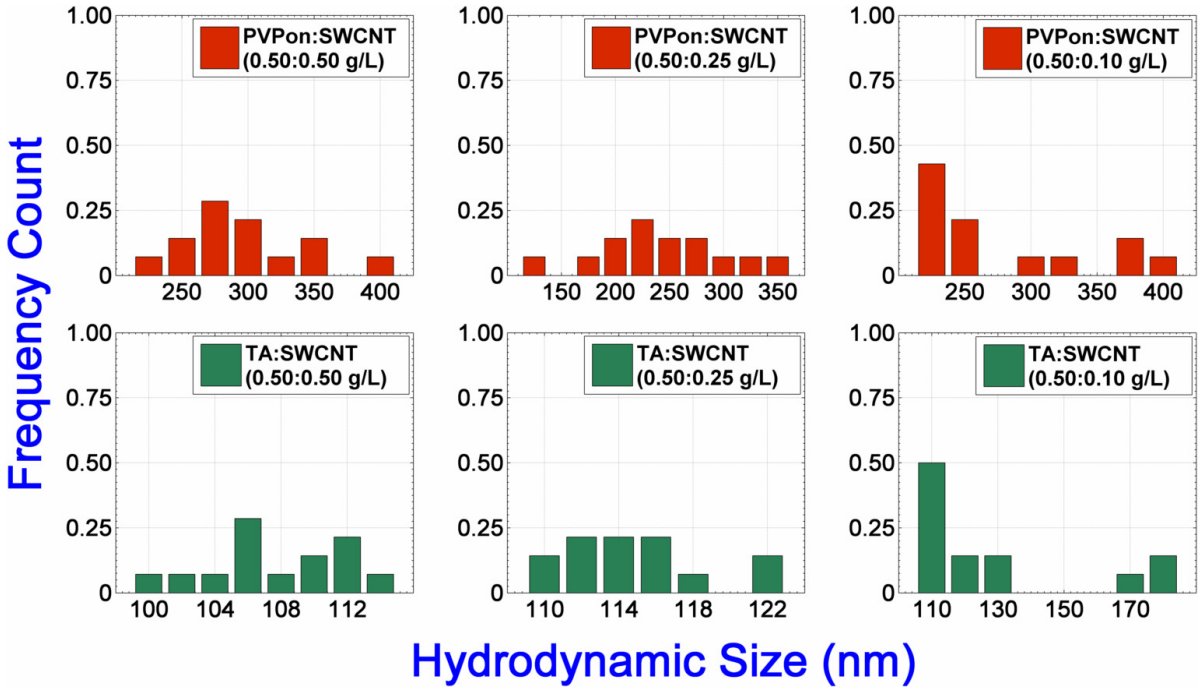

Figure 4-7. Intensity-weighted hydrodynamic size distributions of poly(*N*-vinyl-2-pyrrolidone) and tannic acid aided dispersions of single-wall carbon nanotubes.

Similar to DLS, ZPA results of dispersions were grouped according to the type of dispersing agents (see Figure 4-8). There is a direct relation between particle size and zeta potential values (compare the trends observed in Figure 4-6 above and Figure 4-8). Generally, absolute zeta potential values above 30 mV are considered to be stable. TA-SWCNT samples are above the limit and probably, steric stabilization effects contributed to the stability of PVPon-SWCNT complexes. As a result, both systems were stable to eye for several months (indeed PVPon-SWCNT complexes are less stable).

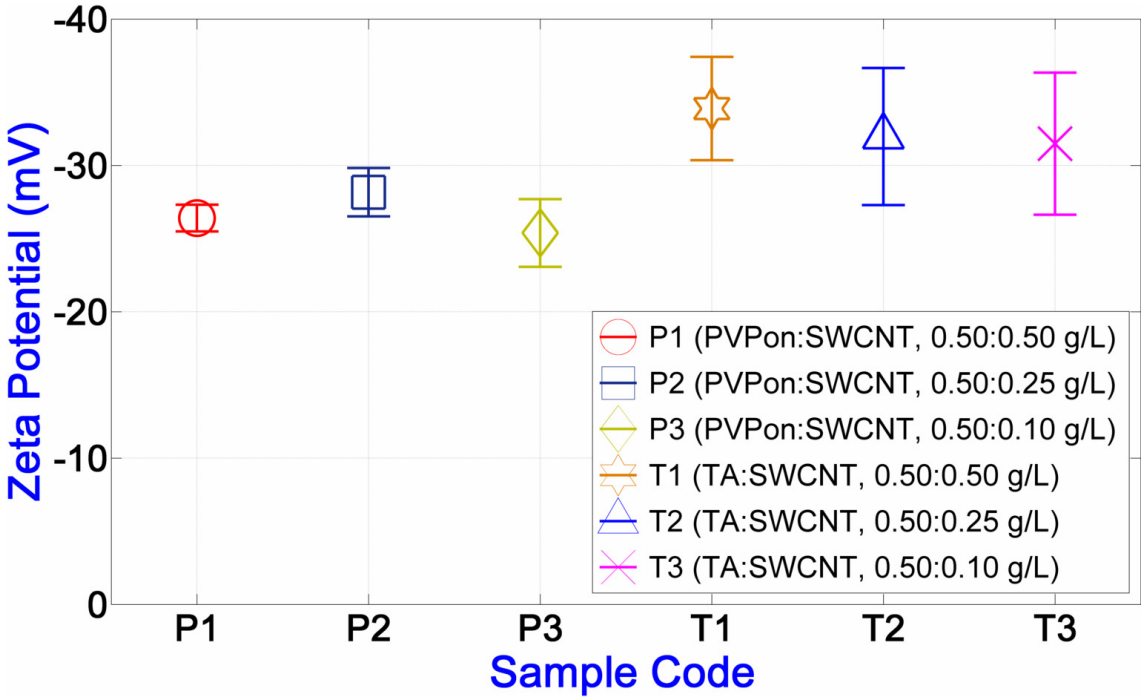

Figure 4-8. Average zeta potential profiles of poly(*N*-vinyl-2-pyrrolidone) and tannic acid aided dispersions of single-wall carbon nanotubes.

4.3.2. Film Growth

hb-LbL growth and pH-dependent stability of $(PVPon/TA)_n$ films have already been reported by Erel and Sukhishvili [122]. In this report, phosphate buffered (0.01 M, pH 2.0-4.0-7.5) dilute (0.5 g/L) solutions grew in a zigzag-like linear fashion by dip-LbL. Zigzag growth is an erratic growth profile compared to straight linear growth and also suggests disruption of hierarchical character. We observed straight linear growth profiles (see Figure 4-9) by spin-LbL. The first study on dip-LbL of PVPon/TA pair reported that assembly at pH 2.00 is better compared to higher pH values (4.00 and 7.50). We applied no pH adjustment and pH-Nat solutions and dispersions were applied in Chapter 2. This might be indicating that spin-LbL favors film deposition by forcing components to stack in multilayers.

Monogalloyl form of TA is reported to have approximately 1 nm height in the planar form [709] but freely (not forced by spinning) dip-adsorbed TA layer which gives ~3-4 nm thickness [122,213]. This suggests self-association of TA into multimeric assemblies in solution. Micelle-like self-complexation of polyphenols and the effect of solution chemistry on those have been validated by many groups [749-755]. It seems, low pH and high ionic strength trigger self-association of natural polyphenols. Effect of low pH is explained via the domination of hydrophobic interactions due to low degree of ionization. In addition, it is well-known that, multivalent cations clearly complex with polyphenols. We believe, monovalent cations at least serve interact with TAs through metal-pi interactions which favor self-complexation. In fact, long-term (months) aged TA solutions in DLS do not exhibit any signal in agreement with molecular dimensions of TA [661,709]. However, fresh solution of 10.0 g/L TA gives "3.21 ± 0.20 nm" hydrodynamic size which is in agreement with literature values (theoretical: [661,709], DLS: [756]). So, in dip-LbL of salt added solutions, PVPon (a surfactant-like polymer) might be breaking TA-TA interactions and hence a portion of TA might be desorbing from the surface as suggested earlier [122]. Then, the surface regenerates with a monolayer-like layer of TA which is mostly interacting with the underlying layer (PVPon). If this explanation is correct, adsorption of the PVPon chains take place after these initial steps. Indeed, this scenario is an extended version of previous explanations on TA-involved LbL films [122,213]. In parallel, spin-LbL might be enriching individual TAs on the surface rather than multimeric forms.[54] Or, applied shear forces [193,757] might be dissociating loosely-formed TA complexes on the surface upon anchoring to the PVPon layer. Multimeric forms of TA might also be more mobile upon centrifugal force due to higher size. Second, two major differences of our $(PVPon/TA)_n$ films from previous design are the exclusion of buffering agent and applied film growing method. Both the exclusion of salt ions from solutions [163] and switching from dip- to spin-LbL [191] are expected to reduce surface roughness and interlayer mixing (interdiffusion). In our previous studies (see Chapter 2 above), we checked the effect of salts on surface roughness of $(PVPon/TA)_n$ architecture and phosphate buffer [112,148] increased surface roughness of films. Reduced interlayer mixing normally enhance the ordering of layers and desorption problem of TA from the surface is restricted. Moreover, BPEI-free growth profiles of spin-LbL films are linear and robust, but on the contrary, dip-LbL films are relatively erratic. Kinetic nature of films is

[54] Note that, when the multilayer assembly is performed, TA molecules are aged in solution at least more than one month including the time required for the preparation phase of dispersions and film deposition.

directly effective on growth behaviors.

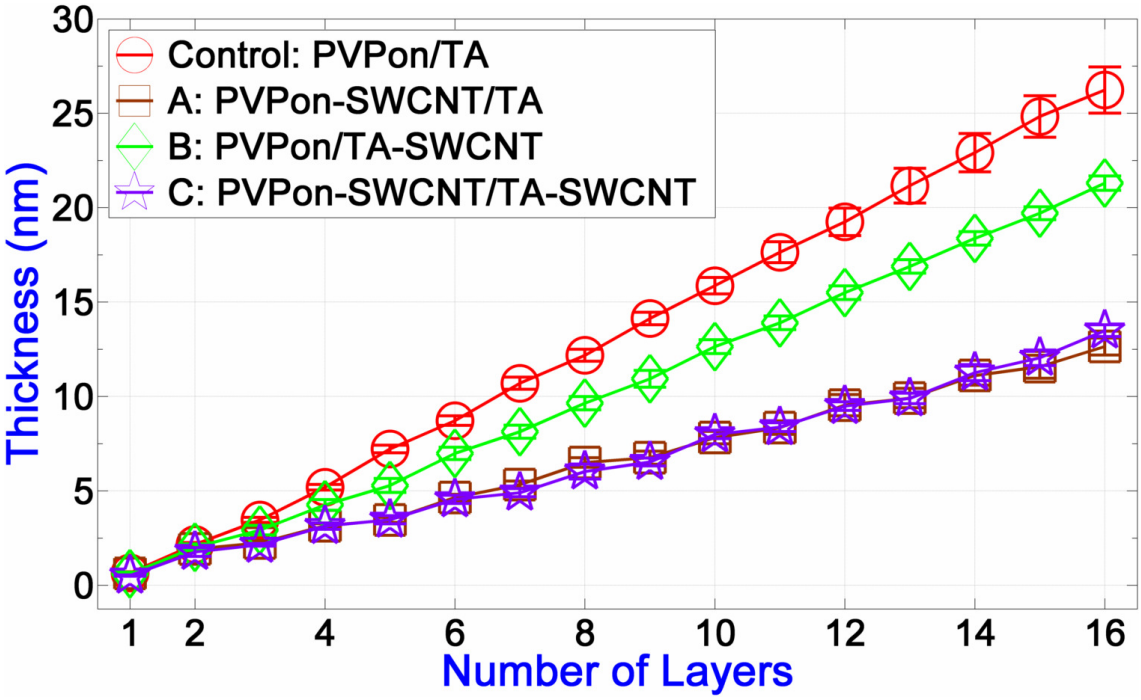

Figure 4-9. Multilayer growth profiles of single-wall carbon nanotube doped films of different compositions (with growth profile of control sample assembled using ultrasound-applied and aged solutions).

The bilayer thicknesses of control sample and different compositions significantly differed. Fresh (no aging and ultrasound exposure) solutions give final thickness slightly below 21 nm at eight bilayers (which corresponds to ~2.62 nm and bilayer thickness around 2.85 nm for ten bilayer films (recall Chapter 3). But, final thickness of control sample is ~26.23 nm (equals to bilayer thickness of ~3.28 nm). We attribute this difference to aging of TA particularly. Indeed, final thickness of control sample and composition-A are far apart TA-SWCNT dispersion involved compositions (B and C). In the presence of SWCNTs, TA molecules are naturally anchored on SWCNT surfaces and they are not as free as SWCNT-free case. So, as an added benefit, SWCNTs seem preventing the complexation (supramolecular aggregation) of TAs (i.e. dimers, trimers). On the other hand, ultrasound energy might potentially cause covalent oligomerization of TA molecules. Thus, TA solutions might be more susceptible to chemical reaction in the absence of SWCNTs (also the ultrasound energy is dissipated between SWCNTs and TA when SWCNTs are present). We have more quantitative aids to compare the bilayer thicknesses of different compositions within themselves. However, before discussing those issues, we should underline one of our important assumptions. In Figure 4-9 above, while modeling the ellipsometric data (which is the ellipsometric angles, see Literature Background for details), we assumed that refractive

indice of all compositions are the same as “1.500”. However, refractive indice of SWCNTs is not necessarily “1.500” and literature values of refractive indice for SWCNTs might be misleading. By its very nature, unsorted SWCNT samples are complex materials containing virtually infinite types of individuals exhibiting different physicochemical properties (recall Literature Background for details). We calculated the contribution of SWCNTs on the overall optical properties of films in terms of effective refractive indice considerations. Using large-form[55] multilayers, we calculated the effective refractive indices of control sample and different compositions of SWCNT-doped film. Indeed, we employed ellipsometry as an ensemble-average technique. Results of this analysis are tabulated below as Table 4-1. When we compare the refractive indices of SWCNT-doped multilayers relative to the refractive indice of control sample, the increases of different compositions are 0.0037, 0.105, and 0.277 units respectively. In theory, effective refractive indices of multi-component mediums can be calculated starting from the refractive indices of individual components using different appropriate models (i.e. Lorentz-Lorenz, Maxwell-Garnett, and Bruggemann). Backward operation is also presumably possible, but we are not certain about the particle filling ratio of multilayers. Still, there are two clear results of the analysis we performed. First, refractive indice of SWCNTs are probably higher than “1.5000”. Second, composition-C certainly contains more SWCNTs comparing other compositions. Here we should also admit that, in this part we totally ignore surface roughness which would be a significant factor if variations were considerable. Further investigations on this system might be valuable from a physicochemical point of view.

Table 4-1. Remodeling of ellipsometric thickness values of particle-doped multilayers considering refractive index variations due to the addition of single-wall carbon nanotubes in film structure.

Composition and Type	Real Part of Refractive Index		Calculated Thickness (nm)	
	Before Analysis	After Analysis	Before Analysis	After Analysis
Control / high	1.5000	1.5598	87.80 ± 2.66	81.90 ± 2.90
A / high	1.5000	1.5635	66.85 ± 3.60	61.00 ± 3.22
B / high	1.5000	1.5703	58.33 ± 1.95	53.26 ± 1.60
C / high	1.5000	1.5875	60.78 ± 1.80	53.94 ± 1.50

[55] Presumably, large-form multilayers provide better information for the estimation of refractive indice.

4.3.3. pH-Dependent Film Disintegration

Figure 4-10 shows pH-dependent film dissolution profiles of SWCNT-doped and undoped PVPon/TA multilayers. There are three main outcomes of observed dissolution behaviors. First, there is a clear improvement on pH stability of spin-LbL films over dip-LbL films. This is probably a combination of growth method selection and exclusion of salts. Spin-LbL films are more hierarchical and presumably their ordering provides better stability. Also, self-adsorbed polymer chains might be more compact comparing spin-adsorbed chains which might decrease H-bonding interactions per polymer chains. Effect of the exclusion of salts is also expected to be profound. The presence of salt ions in multilayer films restrict the ratio of physically crosslinked polymers (polymer-A/polymer-B) in film structure [167]. In accordance, LbL films are semipermeable membranes and entrapped salt ("extrinsic charge") in film structure increases osmotic pressure [131,169,758] and increase water pairing which weaken the film. Another reason behind better pH stability of no pH adjusted $(PVPon/TA)_n$ system might originate from TA-salt interactions. We observed the effect of buffering salt on coloring of TA qualitatively. Divalent and trivalent cations are known to form colored precipitates with tannate forms of TA [759-760]. Effects of monovalent cations are generally ignored. But in a couple of months, native pH (buffer-free) solutions of TA become slightly yellowish, even at low pH (i.e. pH 2). This suggests the formation of phenolates in solution which decrease H-bonding capacity of TA to an extent. The mechanism behind is not clear, but metal-pi interactions might be involved. Ultrasonication might also be triggering the dissociation of TA, but OH band was clearly observed in FT-IR spectra (see, Appendix-M). Comparison of the LbL films of sonicated (processed) and fresh solutions is also interesting. It is well known that ultrasonication breaks the linear polymer chains mostly from center points. To minimize ultrasonic scission of PVPon chains [761-765] we did not prolong horn-sonication. When, degree of polymerization decrease, critical disintegration pH of *hb*-multilayers are normally expected to downshift due to diminished branching points were chain. Disintegration profiles of processed (control-1) and fresh (control-2) films are considerably different from each other. This suggests the adverse effect of ultrasound on assembly solutions. The third, and probably the most essential, finding of this investigation is clarified at this point. This can be attributed to the effect of pi-pi stabilization on pH stability. Especially, two component (PVPon and TA) aided doping of SWCNTs results with robust $(PVPon\text{-}SWCNT/TA\text{-}SWCNT)_n$ composition without a significant loss on pH stability. This might be the first evidence of SWCNT percolation against pH perturbation (see [102,766-

768] for the properties percolated CNTs networks). If a percolated network of SWCNTs is responsible for observed stability, TA-SWCNT/SWCNT and SWCNT/SWCNT pairs might be interacting each other through pi-pi interactions in this network which causes hydrophobic stabilization. On the other hand, we also checked the pH-stability samples shown in Figure 4-10 after a couple of months beyond pH 10.00. Those results show that composition-C is significantly than control-2 (see Appendix-N). This shows that, SWCNT not only stabilize those multilayers against pH-perturbtion, it also stabilizes those multilayers against the adverse effects time. We believe, SWCNT protects TA from oxidation in TA-SWCNT complexes and preserve the pH-stability of those multilayers.

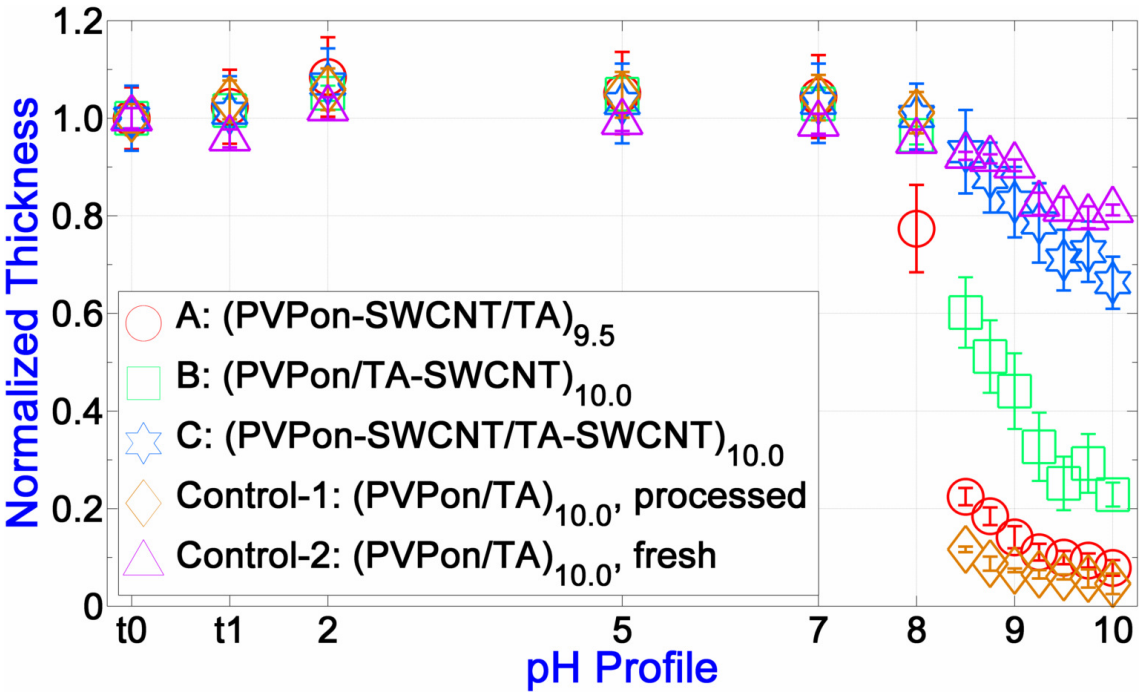

Figure 4-10. pH-dependent disintegration of undoped and nanotube-doped multilayer films.

Nature and classification of pi-stacking interactions were debated for a long time [769-771], but vital role of pi-pi interactions was well documented in supramolecular field and in LbL literature as well. Contribution of pi-pi interaction to stability of LbL films has been reported [772]. In a recent study, Kotov Group also observed [217] possible contribution of SWCNTs to LbL growth as an active component. Using dip-LbL, they grew (HOCS/SPEEK-SWCNT)$_n$[56] architecture and (HOCS/SPEEK-SWCNT)$_n$ as control group. For no-CNT case, they observed an "erratic" growth pattern which was a clear zigzag profile in our

[56] HOCS: Hydroxyethyl cellulose; SPEEK: Sulfonated poly(etheretherketone).

consideration. They interpreted their observation to the contribution of possible hydrophobic and vdW interactions between HOCS and SWCNTs. But, restriction of the mobility of SPEEK chains might also decrease desorption of already grown film. In any case, both ours and Kotov's evidences suggest the contribution of SWCNTs to film buildup process. Indeed, disintegration profile of composition-C (PVPon-SWCNT/TA-SWCNT) suggests hydrophobic stabilization by tube-tube interactions. We have also checked long-term stability of the films exactly the same employed in Figure 4-10 (above). We observed that, only SWCNT-doped films are stable beyond pH 10.0 when aged more than three months after the exposure of pH 10.0. Particularly, composition-C remained intact above pH 11.00 which is remarkable of H-bonded complexes and suggests hydrophobic stabilization. On the other hand, we presume that SWCNT-SWCNT interactions are stronger when structural defects are minimized. But, ratio of D-band/G-band, which is indicative on structural disorders, shows a high number of defects (see Subsection 4.3.4 for details). If defect ratio is minimized more dramatic pH-stability can be obtained.

Here we should also stress other issues which might be effective on observed pH-stabilities. Burke and Barrett have been reported [773-774] dissociation constant shifting of polyelectrolytes upon adsorption of weak polyelectrolytes to the surfaces. For polyacrylic acid shifting is upwards about 4 unit and added salts are also effective. In addition, according to theoretical estimations, H-bonding capacities of pi-pi stacked molecules vary significantly comparing their individual states [775-776]. Thus, H-bonding capacity of TA (and presumably PVPon) would differ in complexed form with SWCNTs. We believe that here we observed a combination of aforementioned influences at the same time which might cooperatively explain observed extreme pH-stabilities in addition to hydrophobic stabilization. On the other hand, local and bulk pH solution might differ [160,667]. Thus, probed pH of solutions does not exactly represent the level of pH that every single molecule experience. Lastly, we would like to mention our parallel work (recall Chapter 3) on the stability of undoped PVPon/TA multilayers which investigates the effect of timescale in growth and dissolution of spin-assembled PVPon/TA multilayers. In that study, we showed that, when the experiment is performed after a time period where spin-assembled could find enough time to reequilibriate themselves; better pH-stabilities are observed. In current study, we also performed the experiments in a discontinuous manner, time- (and/or pH-, refer Chapter 3 above for discussions) dependent "untrap" of multilayers might be favoring our observations.

4.3.4. Particle Homogeneity Analysis

RSS is in common use for probing structural characteristics of CNTs. On the other hand, RSM of CNTs is at the centre of current attention as CNTs require no label other than their own Raman-activity which is dependent on their geometrical/structural properties. In accordance, many researchers track the localization of CNTs in living cells and on surfaces using RSM. In a similar manner, we studied RSM of SWCNT-doped multilayers. In Figure 4-11 (below), area and line mapping graphs are seen for a medium-form composition-C multilayer ((PVPon-SWCNT/TA-SWCNT)$_{10}$) which contains more SWCNTs than other compositions. It is clearly seen that, D-band is considerably intense and G-band is broader than expected (see Chapter 2 above). In Chapter 2, we observed less disorder signature (D-band) in SWCNTs which is probably due to shorter ultrasound exposure and higher temperature of dispersion medium which decreases cavitation energy.

RSM observation also justifies observed featureless spectra in OAS studies (also see Appendix-M for FT-IR of raw SWCNT powder). One minor objective of this study was to preserve CNTs in their "perfect" form in addition to chemical pristinity. In this study we modified our CNT dispersion procedure to increase the particle concentration in the dispersions. Indeed, our modified procedure is more successful in terms of dispersion efficiency, but suffers from imperfections in pi-conjugated CNT surfaces likely due to longer ultrasonic irradiation durations and low temperature as mentioned above. Here we should also note that, D/G ratio might be misleading in the presence of high level of carbonaceous impurities [777]. Indeed, FE-SEM investigations suggest the presence of non-SWCNT particles in the films which are potentially other types of CNPs. In accordance, D-band signal might be enhanced primarily due to the increase of non-SWCNT CNPs in the system rather than high level imperfections of SWCNT. We are not clear about whether covalently functionalized or ultrasonically-harmed SWCNTs are potentially more successful in drug loading applications or non-SWCNT CNPs hinder the applications. If this level of disorder or non-SWCNT CNPs is an obstacle for possible applications, more optimization should be performed in SWCNT dispersion procedure. On the other hand, we anticipate that, disorders in SWCNTs might be helpful for their biological removal (for enzymatic degradation of CNTs see [778-780]).

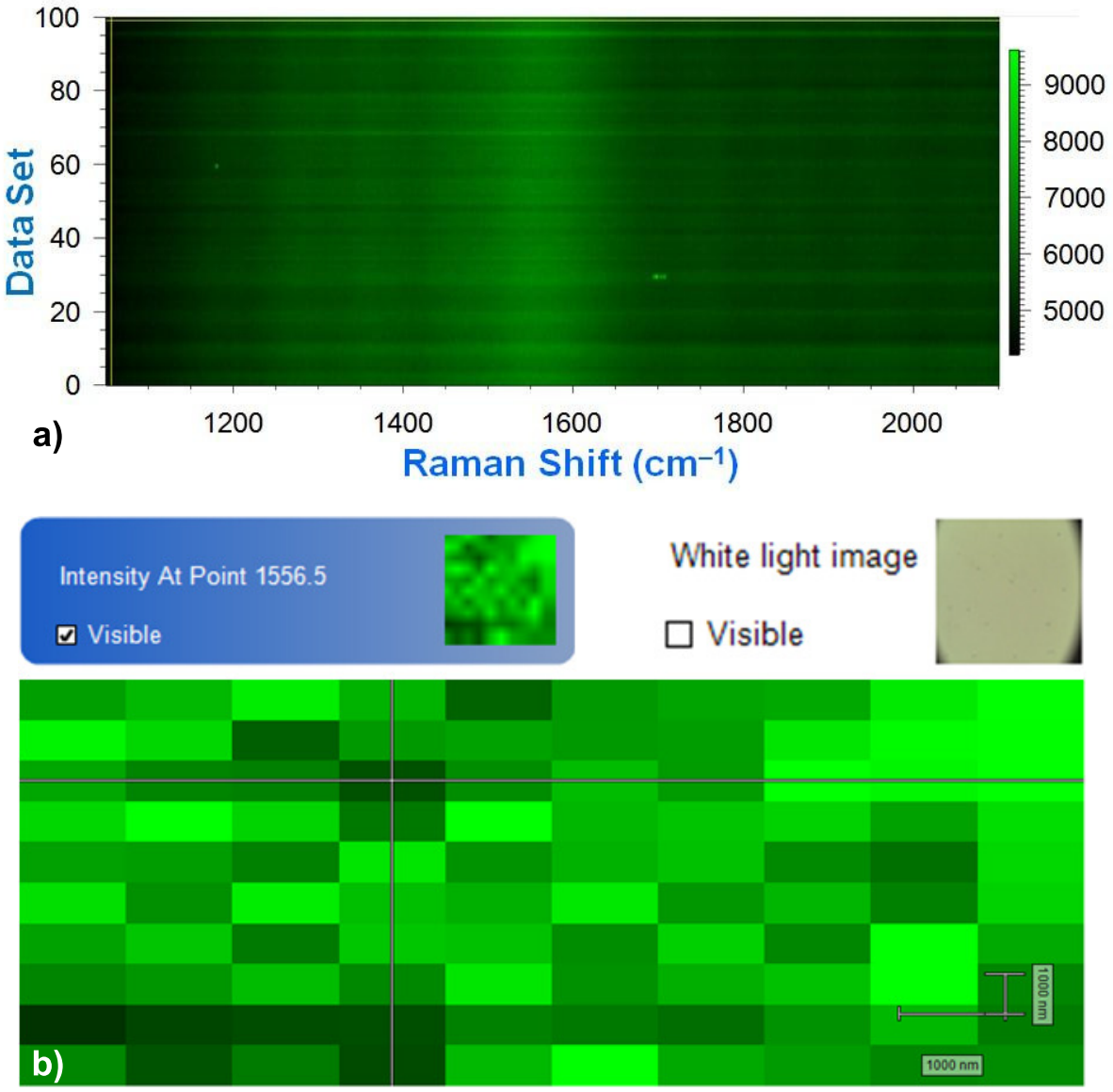

Figure 4-11. Raman microscopy mapping of nanotube-doped multilayers: a) line mapping of the region covers D- and G-bands, b) area mapping of an arbitrary wavelength in the G-band region.

4.3.5. Surface Morphology

DLS provided solvent swollen diameter of dispersed complexes but SEM provides direct information on actual size of particles. Figure 4-12 shows the morphology of medium-form films at 50K magnification. Although energy of incoming beam kept as low as possible, films were rapidly etched in higher magnifications (recall Chapter 2 above). So, we probably missed small bundles (~7 tubules per bundle). But, FE-SEM studies are still informative to compare the relative abundance of SWCNTs in resulting films. First, free polymers/molecules inevitably exist in dispersions and non-CNT regions exist in multilayer films. As a result, surface coverage of SWCNTs differs in different compositions. We previously claimed on the

success of TA over PVPon as a stabilizing agent based on OAS results. FE-SEM images (compare "b" and "c" in Figure 4-12) also provide further evidence on the success of TA. It seems, TA not only disperse higher concentration of particles, also help to enrich SWCNT in film structure (note that optical absorption of PVPon-SWCNT and TA-SWCNT comparable but approximately three time more particles are observed in composition-c (PVPon/TA-SWCNT) comparing composition-b (PVPon-SWCNT/TA) case. This might be due to higher aggregate sizes of PVPon-SWCNT colloids comparing TA-SWCNT colloids. Also, the image of $(PVPon\text{-}SWCNT/TA\text{-}SWCNT)_n$ seems as the superimposed version of $(PVPon\text{-}SWCNT/TA)_n$, and $(PVPon/TA\text{-}SWCNT)_n$. It is also important to emphasize that, tubules seems to overlap each other in composition-C. This might be a visualization of percolative network formation in this structure. On the other hand, composition-C seems contain more than the superimposition of composition-A and -B which might be showing SWCNT-SWCNT interactions and enrichment of SWCNT on the surface during spin-assembly.

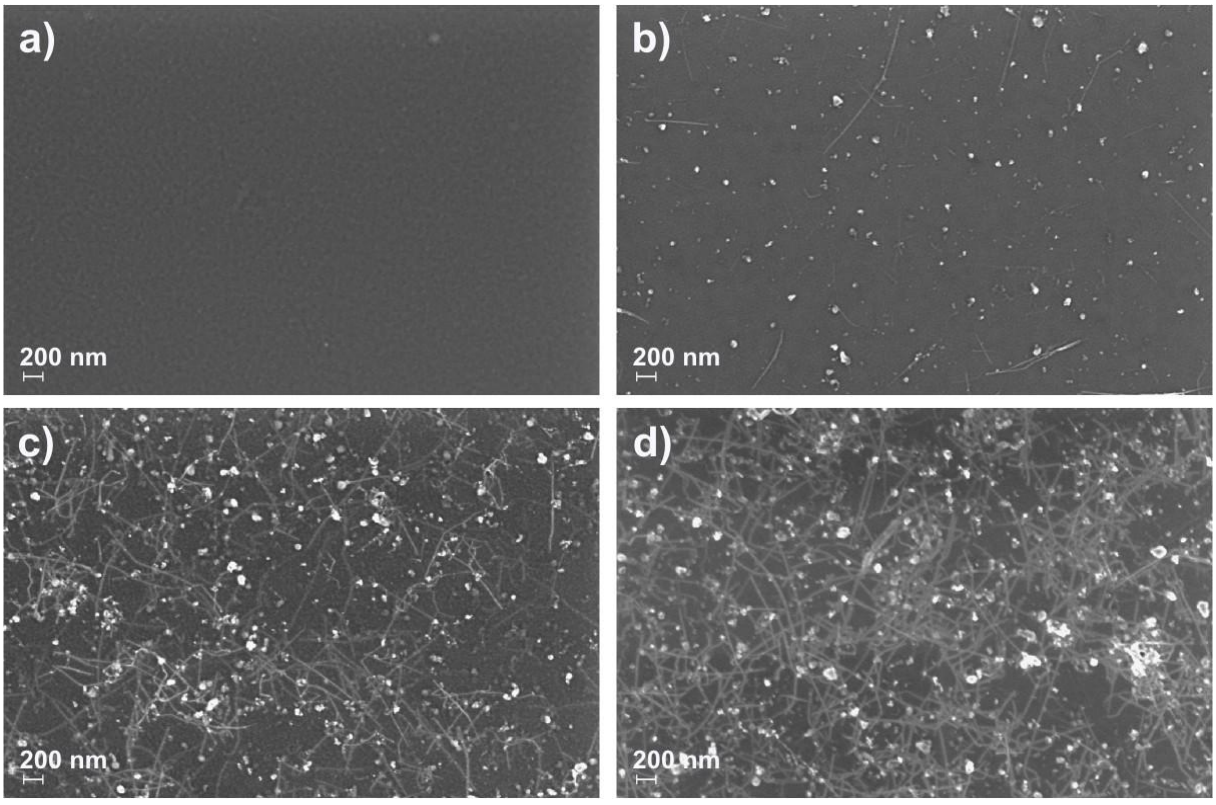

Figure 4-12. Field-emission electron micrographs of different medium-form films showing relative success of mediators used: (a) Control (PVPon/TA) of 10.0, b) composition-A (PVPon-SWCNT/TA) of 9.5, c) composition-B (PVPon/TA-SWCNT) of 10.0, and composition-C, d) composition-D (PVPon-SWCNT/TA-SWCNT) of 10.0 bilayers.

In the first part of FE-SEM observations of medium-form films demonstrated the relative success of TA comparing PVPon. Below, we show the FE-SEM images of small- and large-form images (see Figure 4-13). Other than SWCNT complexes, a variety of bead-like particles are seen in electron micrographs. Those particles could be some residual catalysts, airborne fine particles, titanium probe residues and non-CNT CNPs stabilized in the system via dispersing agents (ultracentrifugation might not be enough to remove all). PVPon is reported to assembly in water [519,781-782]. Also, its association with anions (i.e. PVPon-I) and its usage in nanoparticle formation of metal cations are very-well-known. We characterized the raw SWCNTs and fabricated large-form LbL films using XPS. XPS results of SWCNTs (see Appendix-H) showed no catalyst and XPS results of SWCNT-doped multilayers showed only C, O, and N (data not shown). Thus, observed non-SWCNT particles are less likely to be contaminants, but are likely to be CNPs present in the powder and formed during ultrasonication. On the other hand, there is a trade-off between increasing SWCNT concentration and eliminating non-CNT particles in resulting dispersion. In fact, more extreme process conditions (viz. prolonged sonication) would be applied to increase the amount of individualized tubules and more efficient centrifugation (viz. higher speed, longer application) would be performed up to a point. In addition to this, non-CNT particles comes from the powder form of SWCNTs would be eliminated by applying specific purification routines.

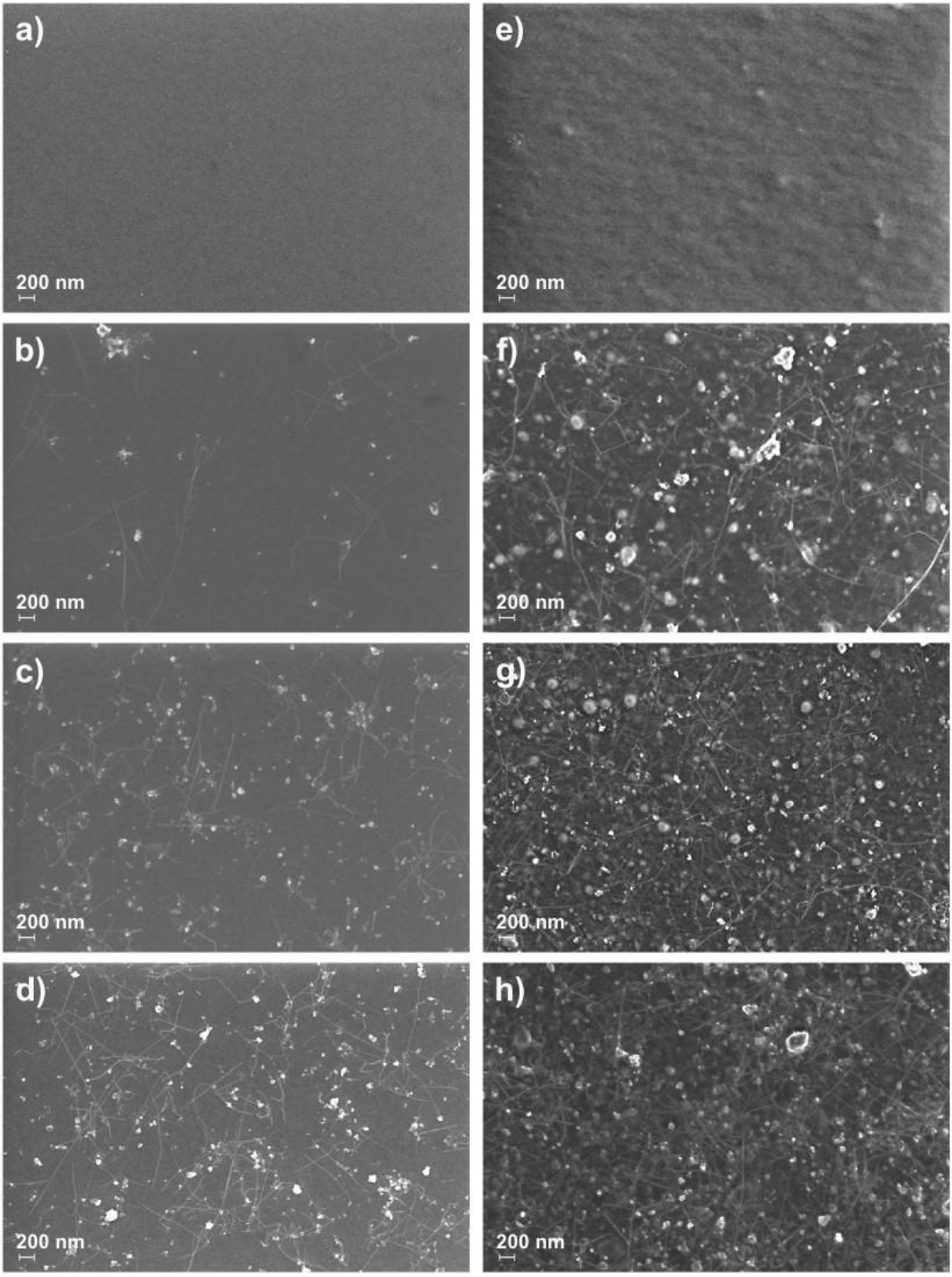

Figure 4-13. Field-emission electron micrographs of particle-free and single-wall carbon nanotube doped layer-by-layer films – Small- and large-form films: Control (PVPon/TA) of a) 3.0, and e) 25.0; composition-A (PVPon-SWCNT/TA) of b) 2.5, and f) 24.5; composition-B (PVPon/TA-SWCNT) of c) 3.0, and g) 25.0; composition-C (PVPon-SWCNT/TA-SWCNT) of d) 3.0, and h) 25.0 bilayers.

4.3.6. Surface Morphology and Roughness Analysis

FE-SEM provided valuable insights on global properties such as abundance and homogeneity of tubules. To monitor finer details such as individual tubules and surface roughness we performed AFM studies. AFM provided direct evidence on the presence of highly individualized SWCNTs and surface roughness of films.[57] Diameters of complexes (PVPon-SWCNT and TA-SWCNT) are expected to be slightly above 2-3 nanometers for individual tubules due to adsorption of dispersing agents. As expected, approximately 2-3 nanometer wide tubules are seen in Figure 4-14 (below). SWCNTs embedded on top layer are well recognizable, but underneath layers also contain SWCNTs and in some regions those tubules are hardly seen.

[57] For the sake of clarity, here we only provide the images of undoped and (PVPon-SWCNT/TA-SWCNT)$_n$ composition.

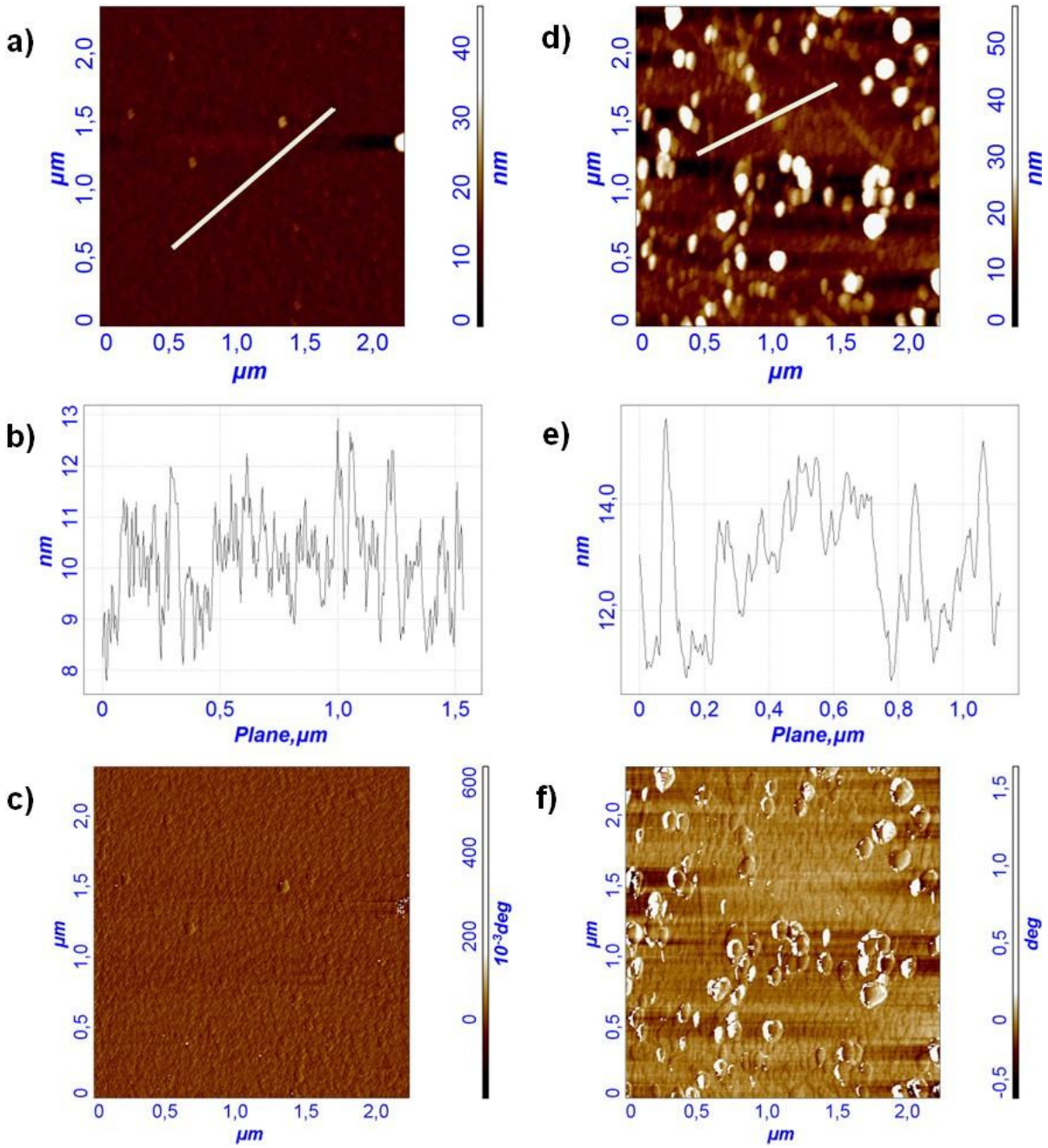

Figure 4-14. The presence of individual single-wall carbon nanotubes on the top layer of multilayer films: a) Height image and b) line profile, and c) phase image of control sample (PVPon/TA); d) Height image and e) line profile, and f) phase image of composition-C (PVPon-SWCNT/TA-SWCNT).

Surface roughness is an essential parameter for many applications and it seems possible to tailor surface roughness of resulting films. We observed the influence of nanoparticle inclusion on surface roughness (Table 4-2). Higher the amount of tubules, higher the surface roughness (recall FE-SEM results). To further visualize roughness effect, we plotted frequencies of height counts (see Figure 4-15). We observed bimodal character for each film (a third shoulder is also apparent in double-loaded architecture). By increasing

tubule content; peaks upshift, broaden and hence total frequencies are suppressed (follow the arrow).

Table 4-2 Influence of nanotube-doping on root mean square surface roughness levels of multilayer films.

Film Compositions	RMS Roughness (nm)
Control Sample: $(PVPon/TA)_{3.0}$	1.24 ± 0.31
Composition-A: $(PVPon\text{-}SWCNT/TA)_{2.5}$	3.09 ± 0.28
Composition-B: $(PVPon/TA\text{-}SWCNT)_{3.0}$	5.52 ± 0.28
Composition-C: $(PVPon\text{-}SWCNT/TA\text{-}SWCNT)_{3.0}$	7.03 ± 1.51

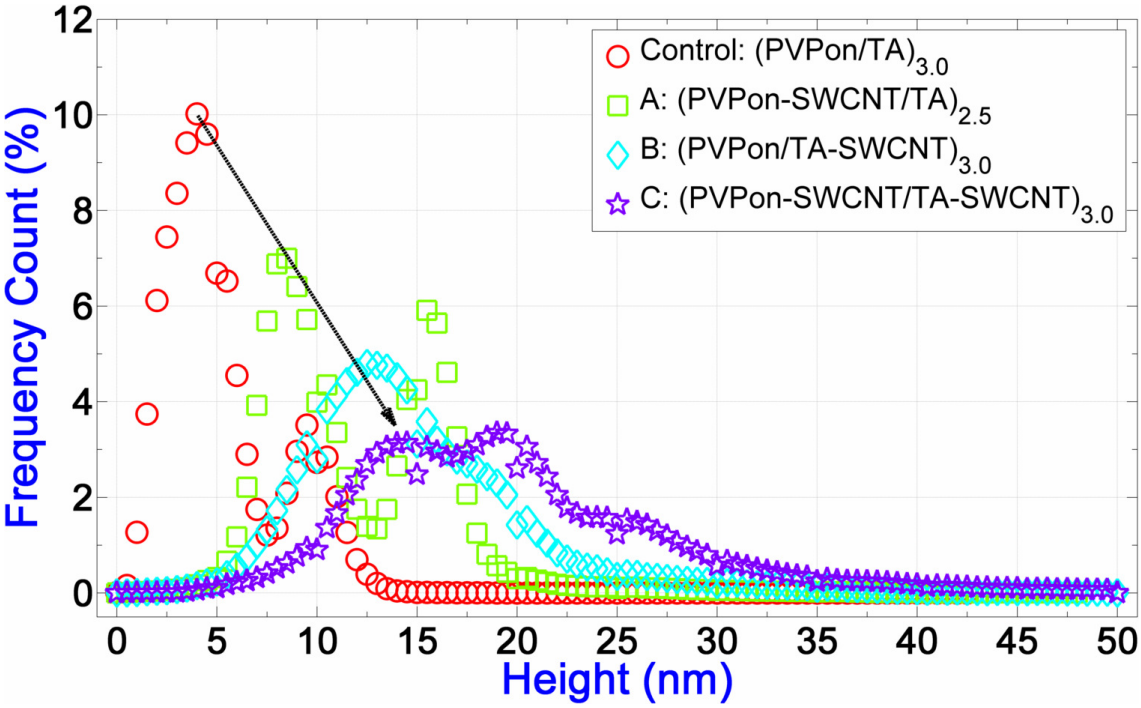

Figure 4-15. Frequency count analysis of filtered roughness data of single-wall carbon nanotube doped films (Arrow demarcates both the shift in first peaks and the decrease in relative frequencies of maxima points).

FE-SEM and AFM studies together showed that, SWCNT-doped multilayers considerably rough comparing undoped surfaces. In our previous study we showed the importance of film-fluid contact time on growth and dissolution characteristics of spin-assembled *hb*-multilayers. It has been theoretically and experimentally shown that, liquid thin films retain longer on rough surfaces in during spin-coating [783]. In this study, we focused on the fabrication of SWCNT-doped multilayers. However, the influence of film-fluid contact time is of worthy to investigate and the results of such a study might explain observed extreme stabilities one step further.

4.3.7. Water Wettability

In the first sense, water wettabilities of bare films are quite high considering the affinity[58] of PVPon and TA towards water. Probably, H-bonding sites of both PVPon and TA are occupied by the complexation of PVPon and TA in *hb*-multilayers. So, when the complex is formed, water molecules experience hydrophobic backbones of PVPon chains and aromatic surfaces of TAs more. Considering the inclusion of hydrophobic of SWCNTs in film structure, it would be reasonable to observe decreased water wettability [784]. However, the general tendency is an increase probably mainly due to high surface coverage of SWCNTs with hydrophilic dispersants (see Figure 4-16). Also, when we consider wettabilities of doped architectures, two interesting details can be emphasized. Top layer TA films (b cases, i.e. C-A2) are less wettable comparing top layer PVPon films (a case, i.e. C-A1). In addition, higher the tubule content (recall FE-SEM results above), higher the difference of contact angle values between "a" and "b" cases. Roughness effect,[59] saturation of H-bonding sites, and surface coverage of tubules[60] likely coexist and this interplay overcomplicates the picture.

[58] Water contact angle of the spin coated PVPon and TA films are around 17.7 ± 0.3° and 13.5 ± 1.6° respectively (PVPon and TA dissolved in ethanol as 1.0 g/L, films were spun at 2000 rpm and nitrogen gas flow is used for drying).

[59] Below 90°C, increased surface roughness generally decreases contact angle values.

[60] A portion of SWCNT surfaces might still be unfunctionalized (unoccupied) with dispersing agents.

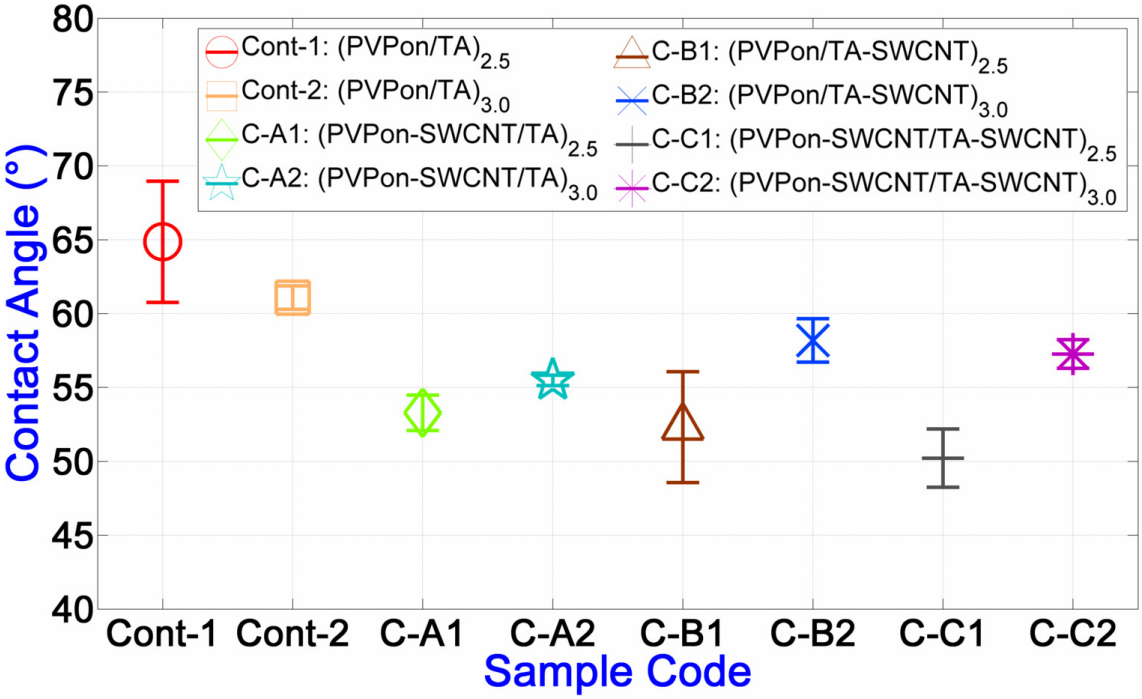

Figure 4-16. Water wettability analysis of single-wall carbon nanotube doped films.

Water wettability behavior of our films might be important for possible (bio)electronic applications. Chemical functionalization (i.e. oxidation) or ionic dispersant assisted stabilization of CNTs limit the electronic device applications because counter ions cause unwanted shortcuts [785]. Also, exclusion of salt from film structure reduce water pairing affinity of resulting films which is desirable for electronic applications [166]. Our films are salt- and polyelectrolyte-free (note that TA is in its unionized form), and hence are promising candidates for SWCNT-doped electronic films.

4.4. CONCLUSIONS

We have developed a noncovalent strategy to fabricate SWCNT-doped nanocomposites. SWCNTs were ultrasonically debundled in the presence of dispersant solutions and SWCNT-SWCNT interactions were shielded through different noncovalent interactions. Prepared dispersions were simultaneously and separately exploited to fabricate SWCNT incorporated nanocomposites. We demonstrated that PVPon- and TA-functionalized SWCNTs can simultaneously be incorporated in *hb*-LbL multilayers. Our results show that SWCNTs acts as an active component of film structure and contribute to film stability. Fabricated nanoarchitectures are not only interesting due to fundamental science point of view. Due to the easily spreading nature of bacterial infectious diseases, a bulk of research is devoted to

introduce new antibacterial surfaces. Combination of a protein-repellent (anti-fouling) polymer (PVPon [786-787]) with natural (TA) and synthetic (SWCNT) antimicrobial agents is highly promising as an antimicrobial system. Similarly, SWCNTs are promising nanocarriers for novel pharmaceutical applications. Further effort is needed to evaluate the advantages and limitations of proposed multilayer films as biomedical nanomaterials. We have no doubt that, hydrophobic agents can be loaded on pi-surfaces of CNTs and those particles can be employed in film assembly (we have preliminary results on eosin loading, data not shown). But, efficient drug loading on SWCNTs does not ensure effective delivery when SWCNTs are coagulated. As far as we see, this problem is the only handicap of proposed strategy. In a parallel study, we overcame this problem by switching from PVPon to PLU (see Appendix-O) and further stabilizing the noncovalently functionalized nanoparticles with crosslinked encapsulates. Both the idea introduced and the experimental routines shown might potentially be used for the design of other nanoparticle-doped *hb*-multilayers. We believe our approach can be adapted to other pi-conjugated nanoparticles such as CFSs, and boron nitride nanomaterials by small modifications.

Chapter 5: GENERAL CONCLUSIONS and FUTURE PERSPECTIVE

There is a growing scientific awareness and simultaneously commercial attention upon the importance of nanocomposite materials. Especially, nanocomposites of organic polymers and inorganic nanoparticles are of interest, where nanoparticles serve as functional nanofillers in polymeric matrices. Among inorganic nanoparticles used, carbonaceous nanoparticles and their counterparts are highly promising for advanced material applications. Unmatched physical, chemical, and biological properties of these nanoparticles provide multifunctionality to their polymeric hosts. Therefore, elegant processing conditions are required to tailor nanoparticles for greater applications. From this perspective, we focused on the incorporation of inorganic nanomaterials in LbL assembled *hb*-multilayers. We designed a versatile *hb*-multilayer platform which can be adjusted to LbL films with a wide span of nanoparticles. Below, general conclusions of this study and our future perspectives are available.

5.1. GENERAL CONCLUSIONS

A variety of CNT-embedded thin films and multilayers are available in the literature. However, exploitation of CNTs and related pi-conjugated nanoparticles in *hb*-multilayers was rather untouched. Here, we showed a fully supramolecular approach to incorporate pi-conjugated nanoparticles in *hb*-multilayer nanocomposites. First of all, our findings underline how promising *hb*-LbL platform is to fabricate NP-doped nanocomposites. In addition, PVPon and TA are conventionally employed drug excipients and SWCNTs are raising stars of nanoformulation trend in pharmaceutical research. Our contribution is not only scientifically interesting, but also potentially applicable in real life. Proposed nanocomposites are also promising for a variety of different applications from antimicrobial surfaces and tissue engineering applications to electronics, optics and solar cells.

Incorporation of nanoparticles in bulk matrices can be inevitable to improve material performance, but it requires the usage of nanoparticles in high amounts reach a percolated network [361,766]. Our results suggested that, when both components of LbL pairs are loaded with (SW)CNTs a percolative network might be obtained using noncovalent functionalization and LbL techniques which increases the stability of resulting materials. Indeed, from a very

fundamental point of view, (PVPon-SWCNT/TA-SWCNT)$_n$ system might be considered as a new and simple example of currently speculated [788] highly robust supramolecular assemblies. In addition, this strategy may serve as the pathway to design new hybrid LbL architectures using different pi-conjugated nanoparticles together (e.g. (PVPon-BNFL/TA-MWCNT)).

5.2. FUTURE PERSPECTIVE

Optimization in processing conditions of supramolecular strategies is a complex task. Since, it directly determines final performance of end-products. Virtually any process we demonstrated can be improved. Especially, noncovalent preparation of nanocolloids requires attention. Actual and relative concentrations of dispersants and nanoparticles can be changed. Parameters (e.g. exposure time, applied power etc.) of ultrasonication steps can be further optimized. LbL side of our supramolecular approach can also be modified. We have showed spin-LbL is useful for our chemical systems whereas dip-LbL is not convenient. However, we did not check spray-LbL. We expect spray-LbL can also successfully build up nanoparticle-doped systems. We currently plan to design a spin-spray setup similar to an early report [194] and study this topic.

Engineers are always pushed to develop applicable, reproducible, modifiable, and if possible, scalable processes. It seems the only soft spot of spin process is its vulnerability in scale-up. Spray-LbL may solve the scale-up problem of our system in the future. In this case, large volumes of dispersions will be needed. In bath sonication studies, we empirically optimized the position of sample tubes in bath, and the volume of energy transfer media (viz. water). In parallel, we optimized the level of liquid volume in tube for horn sonication. Accordingly we modified a commercial ultrasonic cleaner through attaching a fixed position cell for samples and a set of cooling helices. However, a complete picture of optimization was both beyond the objective of this study and out of our expertise. The locations, numbers, and power of transducers should be well studied for efficient mass production of SWCNT dispersions. Geometry of both bath- and horn-type sonicators should also be tailored to achieve highly efficient largescale “debundler reactor”s to reach affordable industrial applications. Also, we believe that hydrodynamic cavitation obtained by fluid flow in venturi tubes or in orifice plates have a potential to reduce energy cost of the ultrasonic debundling of CNTs [789-791].

Molecular interactions between dispersants and CNTs are highly complex and require

a deep understanding. According to our results, presence of salt ions triggers the coagulation of dispersed CNTs. We are also in agreements with previous reports which show the positive effect of elevated pH on TA-CNT systems. This is evidently due to polyelectrolyte nature of TAs and the dilemma arises at this point. We understand the destabilization of PVPon-SWCNT colloids upon salt addition (also see Appendix-P). But, pi-pi interactions known to be compete with cation-pi interactions in aqueous phase [792]. Binding energy of pi-pi interactions vary significantly from system to system, and Na^+-SWCNT would be stronger than pi-pi interactions between TA and SWCNT. Also, the presence of water in CNT dispersions overcomplicates the picture. So, further experimental and theoretical investigations are needed to fully understand the complex nature of those systems. At this point, computational chemistry approaches may provide useful insights. Monogalloyl form of the TA (pentagalloylglucopyranose) can be exploited as a model of TAs since it is relatively simple.

Proposed LbL system is also highly promising for another critical application. We applied the core idea of this thesis to a fine crystal namely brochantite.[61] Brochantite was earlier shown to be most abundant and active ingredient of Bordeaux mixture which is one of most widely used antifungal agent in agricultural. Current formulations of Bordeaux mixture and related products greatly suffer from rain wash-off. We embedded brochantite crystals in water-resistant multilayer films on surfaces based on the strategies developed here. We believe this approach may prevent excessive usage of antifungal particles trough increasing their tenacity on plant surfaces.

Fundamentals of our approach are mainly appeared in industry. It is surely more but to name a few in historical order; TAs from tanning industry, L-B/S from General Electric Company (1920s to 1930s), PVPon from BASF (in late 1930s by Reppe), LbL self-assembly from DuPont Company (1960s), C clusters from Exxon Research and Engineering Corporation (1984)I and SWCNTs from NEC Corporation and IBM (1993). We believe this is not a coincidence and supports the industrial importance of our strategy. In industry, engineers are frequently forced/directed to develop formulations using well known ingredients if available. Our way that exploits commercially available materials to fabricate

[61] Presented as "Karahan, H. E., Kaş, R., Birer, Ö., & Demirel, A. L. (2011, June). Fabrication of H-bonded multilayers containing polymer-stabilized basic copper(II) sulphate fine crystals and a natural organic matter. Poster and abstract in *ICMAT 2011*, *Symposium B: Synthesis and Architecture of Nanomaterials*, Singapore. Best Poster Award winning study."

advance nanocoatings is one move ahead of fancy formulations which are common in the literature. Thus, we believe our design will be improved and tailored to specific applications by other researchers in near future.

Self-assembly occurs in nature in a dynamic manner to sustain life at a cellular level [793-794]. The interplay of intermolecular interactions is critical in self-assembly, and inspires today's nanotechnology [795-797]. In current nanotechnology, it is hard to make use of self-assembly as Nature did. But, nanotechnology surely emulates the Nature. We hope that our findings can be combined with synthetic biology approaches in a close future to create advanced multilayer architectures.

APPENDICES

Appendix-A: *Citation Report of Layer-by-Layer and Carbon Nanotube Fields*

For the last ten years, citation statistics of major related fields were given in Figure App-1 below. Data is collected from citation reports of Web of Science (data is gathered from the official page of Thomson Reuters, please visit www.webofknowledge.com). From the tendancies, logarithmic expansion of CNT field is clear. Also, *hb*-LbL field keeps growing whereas LbL field seems rather steady in overall. These statistics underline the importance of our contributions.

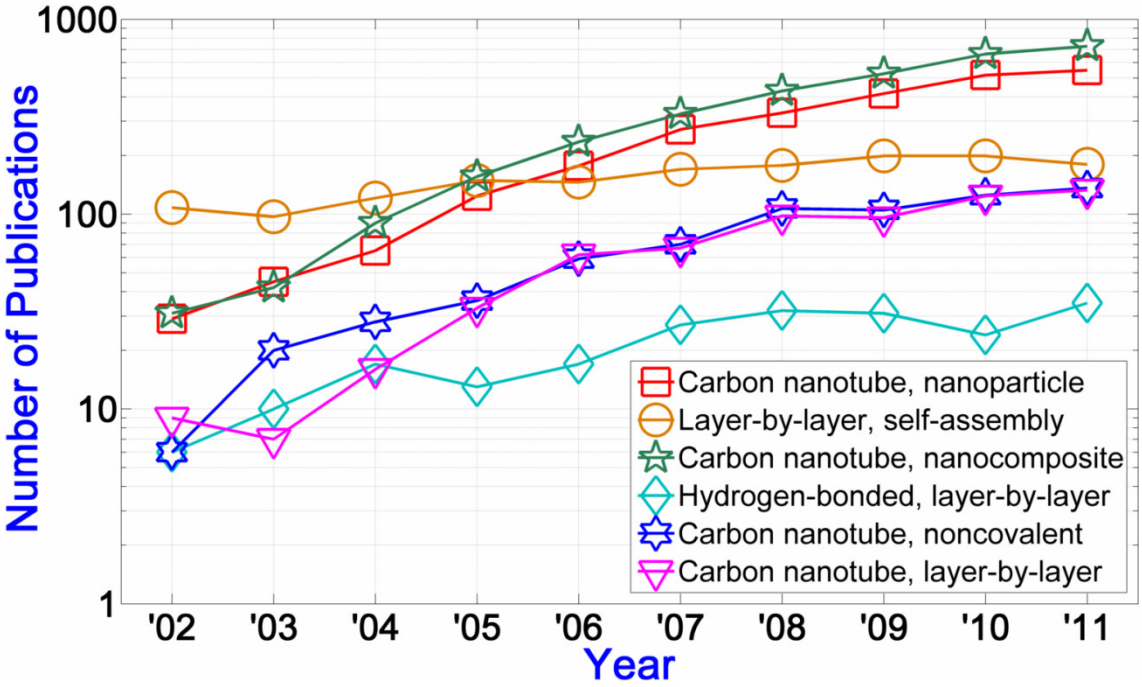

Figure App-1. Citation dynamics of last ten years of major related fields (Used keywords are seen in the legend).

Appendix-B: *Concise Comparison of Multilayer Film Growth Techniques*

Generally, different groups select one of the three major multilayer film growing techniques depending on many factors. But, the reasons behind the selection are not always emphasized. Here, we provide a brief comparison of multilayer film fabrication techniques to provide an

idea on the comparison of multilayer fabrication techniques (see Table App-1). Driving force of multilayer assembly, equipment requirements, realized applications, and major advantages/disadvantages of three major techniques were summarized.

Table App-1. "Compare at-a-glance" chart for major techniques for the fabrication of multilayer nanofilms.

	L-B/S	**SAM**	**LbL**
Driving force of assembly	*Film formation*: Hydrophobic effects (reduction of liquid surface tension) and mechanical enforcement; *Film growth*: Originally vdW.	*First layer*: Surface chemisorptions; *Film growth*: Originally covalent assembly (H-bonding interactions are also shown).	Originally, surface physisorption and *es*-assembly. Then, extended to any type of chemical and physical bonding (primarily H-bondings).
Device Need	Langmuir trough	Beaker-tweezer	*Dip*: Beaker-tweezer *Spin*: Spin coater *Spray*: Mister (spray)
Real (in market) applications	*To our knowledge, not available*	Different specialized coatings (please visit www.aculon.com and www.asemblon.com)	Elastic conductors (MetalRubber®) by NanoSonic Inc. [798], Contact lens coating by CIBA-Vision® [799], food packaging Yasa-sheet by Shiratori NanoTechnology [800], synthetic vaccines by Artificial Cell Technologies, Inc. (please visit www.artificialcelltech.com), LbL-functionalized custom beads by Surflay Nanotec GmbH (please visit www.surflay.com)
Advantages (A) and disadvantages (D)	*A*: Precise control of the monolayer thickness, homogeneous deposition; *D*: Cost is high, building block are limited, substrate selection is restricted deposition is slow	*A*: Ideal model systems, functional substrates can be produced; *D*: Cost is high, not practical for multilayer production, building blocks are limited	*Please refer to Chapter 1 for information.*

Appendix-C: *Geodesic Dome of Fuller*

Considering the geometric resemblance of CNB structures and geodesic domes, CNBs were named as "(buckminster)fullerene" after Buckminster Fuller who is the architect of a famous geodesic dome (refer [323,326]). Geodesic domes are interesting pieces of architecture in the intersection of art, mathematics, and science. Even Wikipedia provides a satisfactory survey on properties and historical development of geodesic domes. Curios readers are directed to following the related Wikipedia entry (http://en.wikipedia.org/wiki/Geodesic_dome).

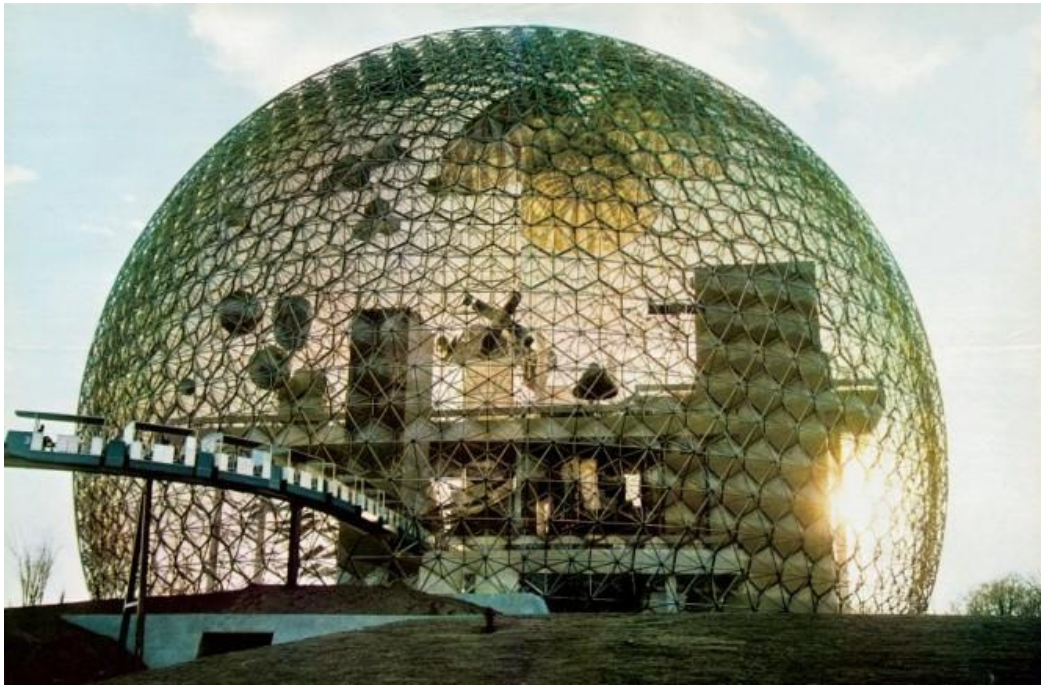

Figure App-2. A famous geodesic dome of architect Richard Buckminster Fuller (The Pavilion, Montreal Biosphere, established in 1967, Canada).[62]

Appendix-D: *Bath- and Horn-Type Ultrasonication Setups*

In this study, we have employed two different sonication devices which are bath-, and horn-type sonicators. Essential specifications of the ultrasonic bath device (Ultrasons-H Code: 3000838, see Figure App-3 and App-4) was as follows: i) Volume (maximum) – 6 L, ii) size – H-15/W-30/D-14, iii) frequency – 50/60 Hz, and iv) power – 720 W. Main specifications of ultrasonic horn (SONOPULS HD 3100, see Figure App-5) was also as follows: i) Processing frequency – 20 Hz, and ii) amplitude: 10–100% (controllable).

[62] Retrieved September 04, 2010, from the http://blogs.nationalgeographic.com/blogs/intelligenttravel/17553fuller_pavilion.jpg

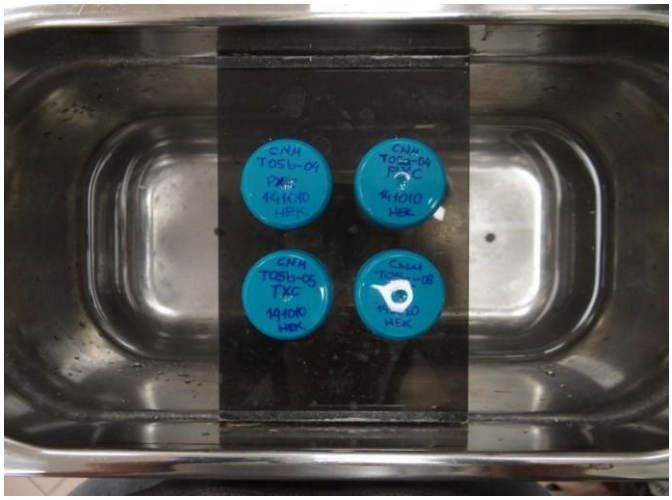

Figure App-3. Positioning dispersion vessels in ultrasonic-bath – top view.

Figure App-4. Positioning dispersion vessels in ultrasonic-bath – side view.

Figure App-5. Immersion of ultrasonic horn in dispersion vessel (Note that the vessel is located inside a cooling jacket and sample is dark which denotes dispersion of carbon nanotubes).

Appendix-E: ***Layer-by-Layer Dip-Assembly of Polyvinylpyrrolidone and Tannic Acid***

In the early stages of our investigations, we were planning to dip-assemble PVPon/TA-SWCNT multilayers at pH 5.00. We studied BPEI-free dip-LbL of PVPon/TA pair and observed an erratic growth at pH 5.00 (see Figure App-6). At that time, we did not check the effect of BPEI and switched from dip-assembly to spin-assembly. However, we subsequently studied film growth at pH 4.50 using BPEI and observed clear exponential growth (see Figure App-7). This difference might be originated from the first dissociation of TA around pH 5.00 or BPEI might be favoring multilayer deposition considerably.

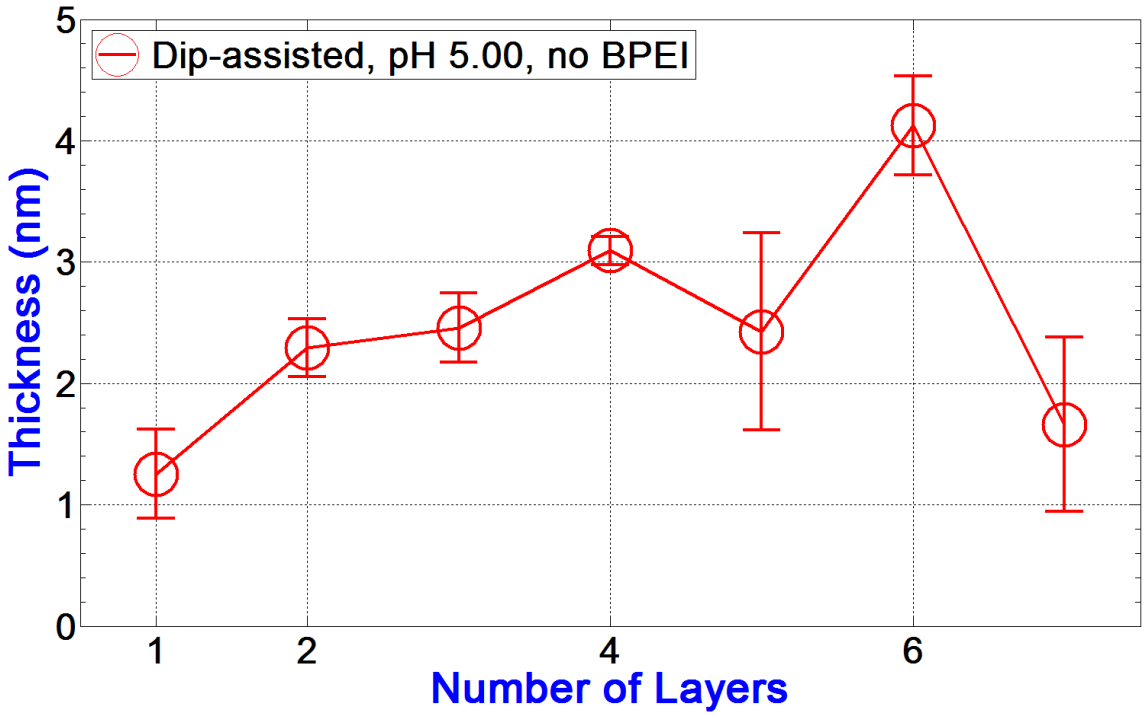

Figure App-6. Erratic growth of dip-assembled multilayer at pH 5.00 without the usage of anchoring layer.

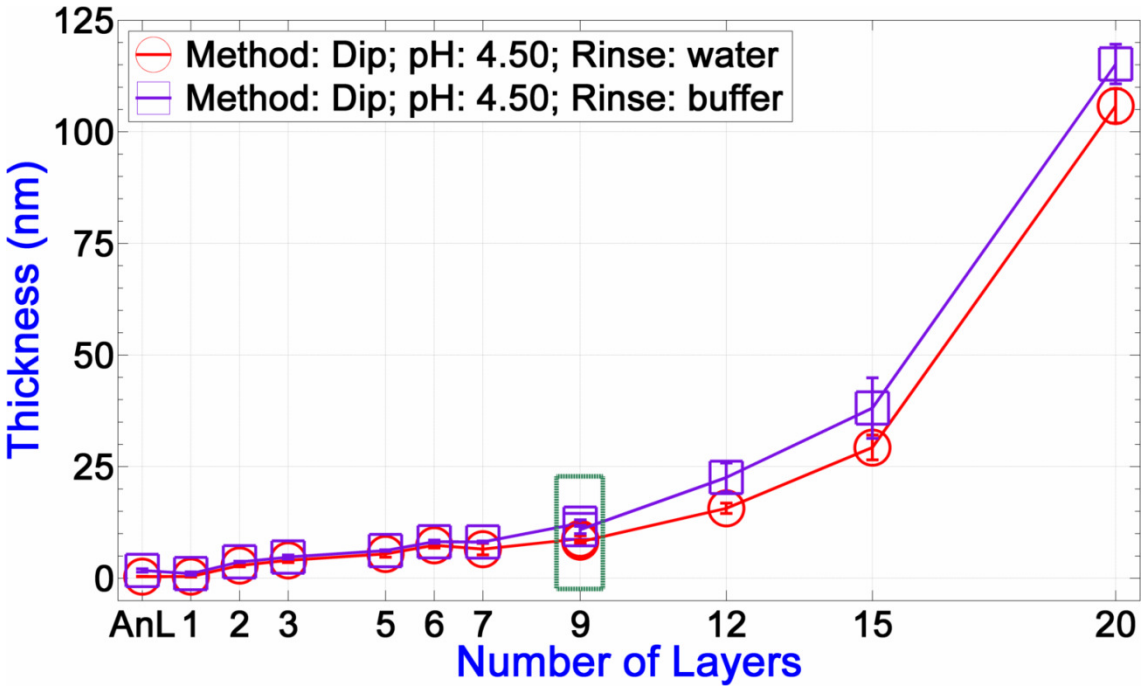

Figure App-7. Exponential growth of dip-assembled multilayers assembled at pH 4.50.

Similar to pH 4.50, PVPon/TA multilayers enters exponential growth regime around fifth to seventh bilayer when dip-assembly is performed at pH 2.00 (see Figure App-8). However, spin-LbL of salt-added and pH-adjusted solutions exhibited straight linear growth as we observed in spin-LbL of BPEI- and buffer-free multilayers. Several different points are worth emphasizing in these results. First, it is interesting to note the difference that, the effect of rinsing media on final film thickness is higher in spin-LbL comparing dip-LbL. Second, both in spin- and dip-LbL BPEI layer is desorbed by PVPon adsorption which probably cause a mixed BPEI/PVPon anchoring layer. Lastly, zigzag character is still obvious in dip-LbL although overall behavior found to be exponential (please concentrate on “a” curve in the figure).

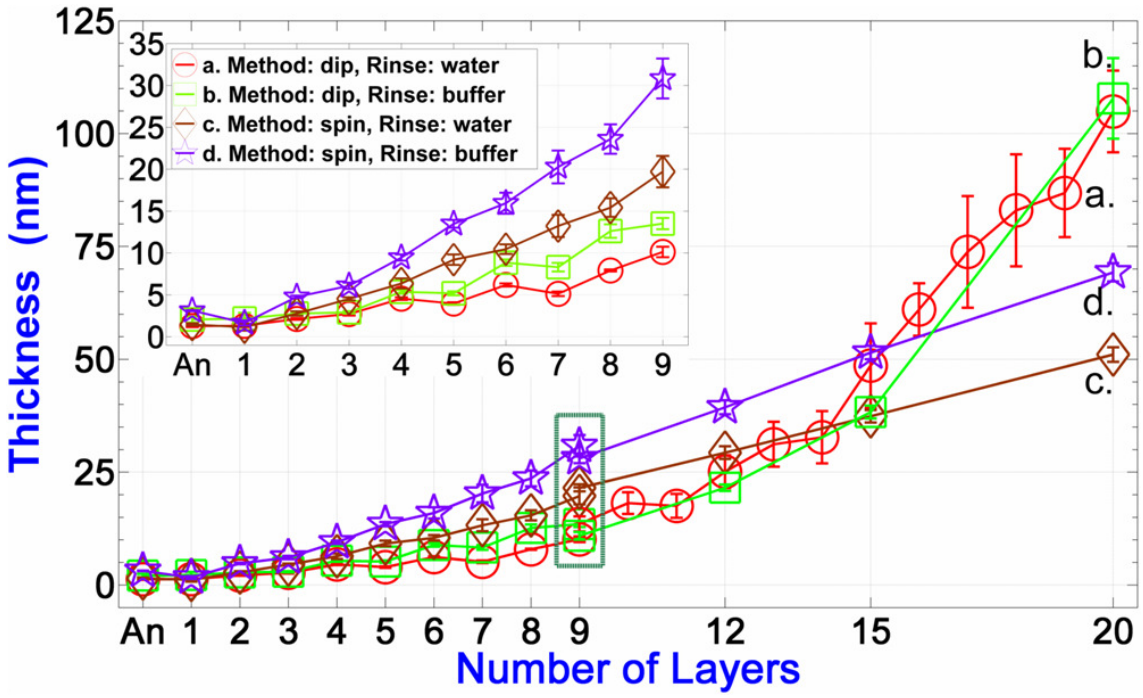

Figure App-8. Comparison of the growth profiles of dip- and spin-assembled multilayers (An: anchoring).

Zigzag-like exponential character of dip-LbL and suppression of this character by spin-LbL were shown above. This behavioral difference seemed to be controlled by liquid-film contact time which is a couple of seconds in spin-LbL, but in the order of minutes for dip-LbL. To check this hypothesis, we deposited dip-LbL films by reducing the deposition time from 5 min to 1 min (see Figure App-9). We observed exponential growth with a slight increase in thickness in initial steps comparing the growth profiles in Figure App-8. This might be indicating the suppression of material desorption which is observed zigzag growth but thickness measurements were not performed continuously.

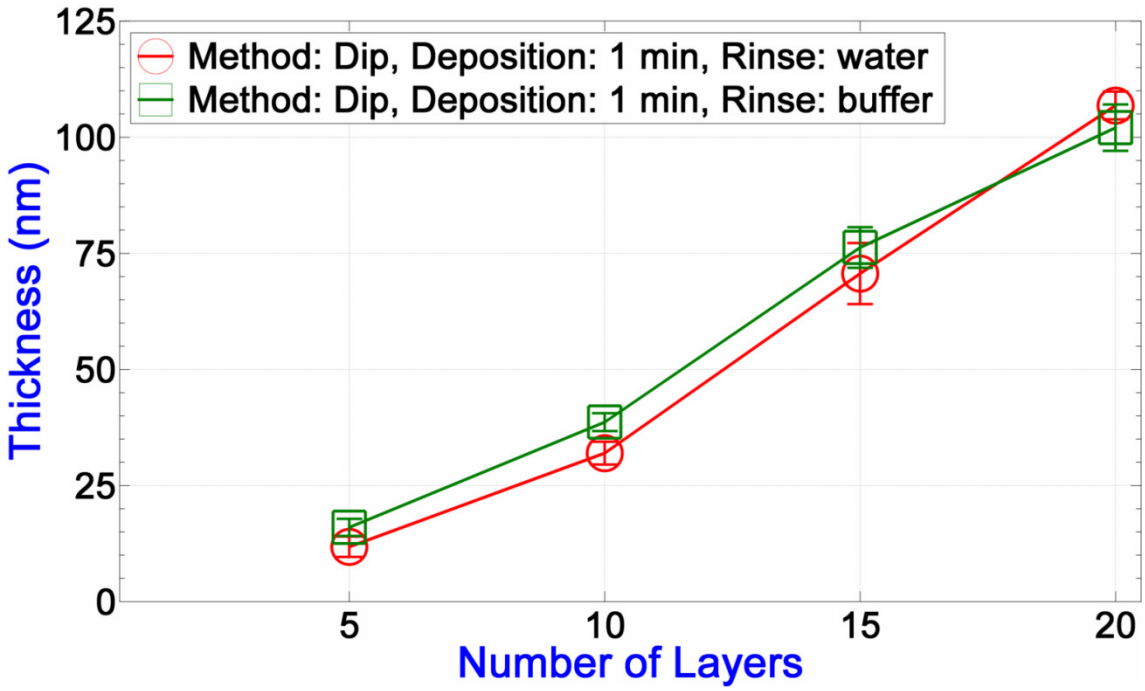

Figure App-9. Dip-assisted multilayer growth at low film-solution contact time.

Above, we provided the data on exponential growth of dip-assisted (BPEI)(PVPon/TA)$_n$ films. But, the effect of pH-adjustment (which is coupled with ionic strength variations) and the usage of anchoring layer were missing. To rule out the possible arguments against the comparison of electrolyte- and BPEI-free spin-multilayers with dip-LbL, we also studied dip-assembly of electrolyte- or/and BPEI-free multilayers. Regardless of pH-adjustment, ionic strength of rinsing liquid, and the usage of anchoring layer; again exponential growth was observed (see Figure App-10). As expected, a slight difference in thickness was recorded in buffer rinsing. Also, we observed film stripping in BPEI-added pH-Nat (see curve "d") whereas no sign of film destabilization was observed in BPEI-free case ("c"). This shows that BPEI layer has a profound effect on the chacater of multilayer assembly. Also, BPEI seems decreasing stability of resulting multilayer films.

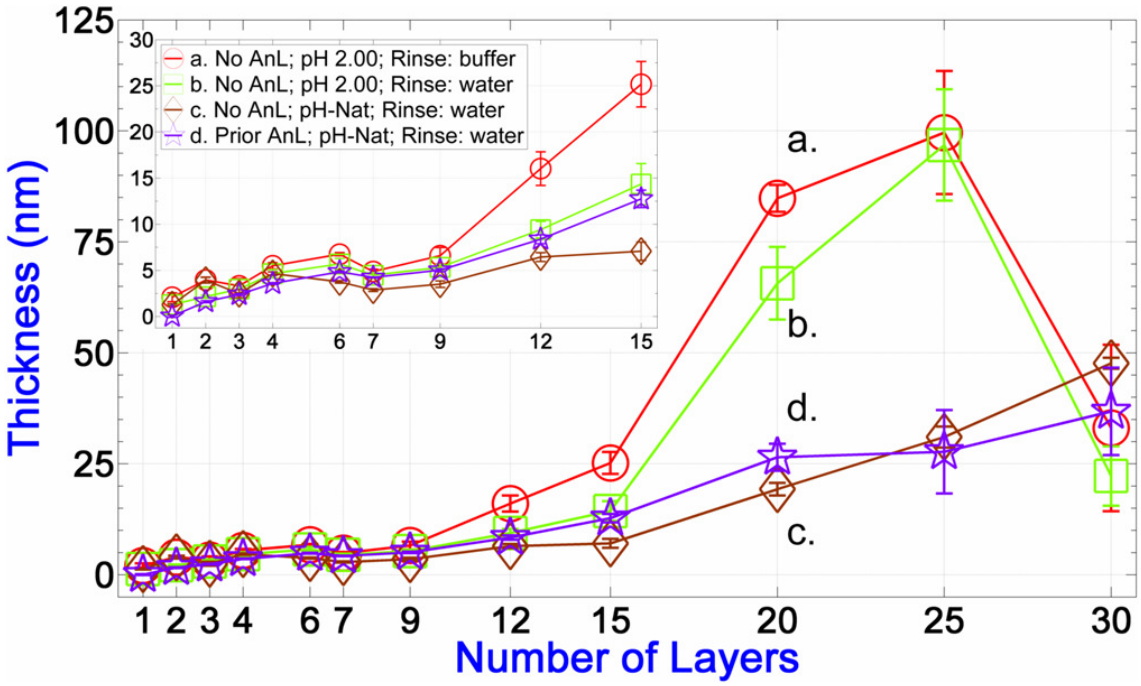

Figure App-10. The effects of anchoring layer, rinsing media, and pH-adjustment on dip-assisted assembly of multilayer.

Appendix-F: *Summary of Literature Data Available on Multilayer Growth and pH-Dependent Dissolution of Polyvinylpyrrolidone and Tannic Acid Layer-by-Layer Pair*

The LbL pair employed in this study was originally reported by Erel and Sukhishvili [122]. In their detailed report, growth and pH-dependent dissolution of this system is elaborately shown. Below, essential data provided in aforementioned article is seen (Figure App-11 and App-12) which we frequently referred in our discussions.

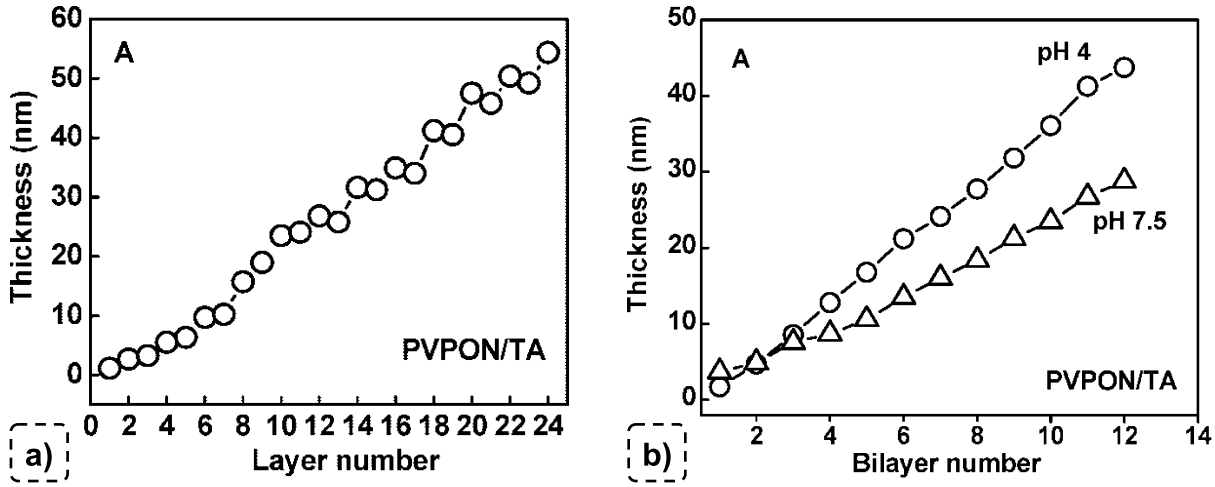

Figure App-11. Literature data on multilayer assembly profile of polyvinylpyrrolidone and tannic acid reported by Erel and Sukhishvili: a) pH 2.00 (thickness measurement performed in each layer), and b) higher pH values (thickness measurement performed in each bilayer).

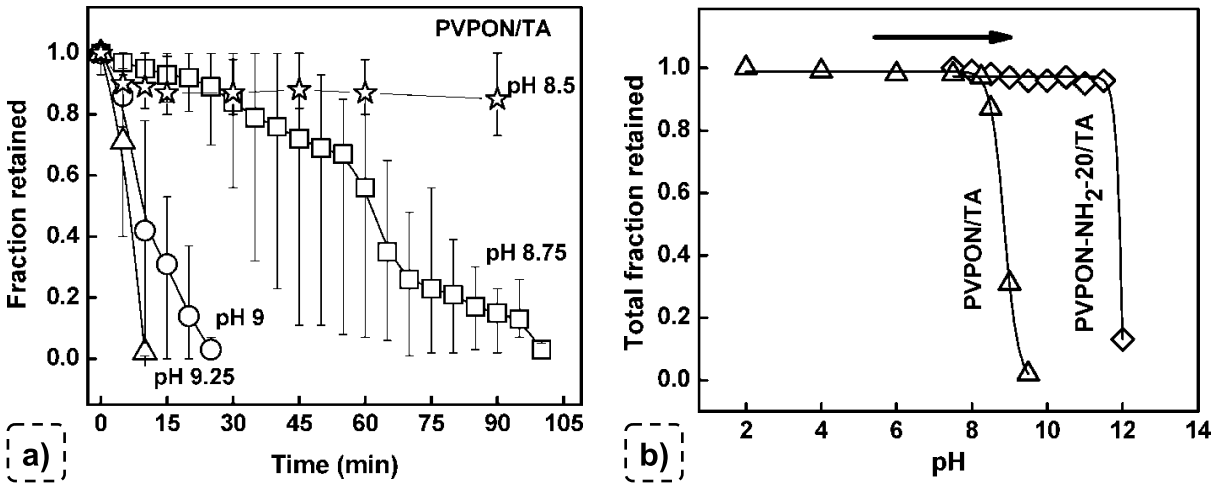

Figure App-12. Literature data on pH-dependent dissolution profile of multilayers of polyvinylpyrrolidone and tannic acid reported by Erel and Sukhishvili: a) Effect of time study (six bilayer films exposed to different pH values in a time-dependent manner), critical dissolution pH study (six bilayer film for different pH values in a sequential manner) experiments.

Appendix-G: *Effect of Electrolytes in Exponential Growth of Spin-Assisted Multilayers Deposited at a Contact Time Typical to Dip-Assembly*

In Chapter 2, we observed the possible importance of film-fluid contact time on multilayer growth. Then, we applied this concept to our further investigations and we grounded the importance of this parameter in growth and dissolution behaviors of PVPon/TA multilayers in Chapter 3. On the way we design the experiments in Chapter 3, we performed long film-fluid contact time experiments in spin-LbL to test our hypothesis. Besides, we were curious about the effect of rinsing media.[63] Thus, to get an idea on possible complications of rinsing media and we also tested the effect of rinsing media. In this set of experiment, we increased fluid-film contact time from 10-20 seconds to 300 seconds which is typical [122,653,667-670] for dip-assembly of PVPon/TA. We first grew multilayer films up to ten bilayers at pH 2.00 and tested the effect of rinsing media (see from "a" to "c" in Figure App-13). As a result of pre-incubation (dipping-like prior step before spinning), we observed thicker films. However, observed increases in thickness values were below our expectations. Thus, we assembled another multilayer at pH 2.00 with buffer rinsing and monitored the film growth at each step (not a continuous assembly process was performed, film growth was interrupted with ellipsometric measurements at each step, see curve "a" in the figure). We observed a clear

[63] When we switched from pH-adjusted assembly to pH-Nat case, we also switched from buffer solution (0.01 M phosphate buffer) to water.

exponential growth which presumably started to stagnate at thirteenth layer. In fact, during the assembly of sample "a" and "b", we observed dramatic color changes between the centre and edges of samples starting around seven bilayer deposition (color is a simple indicator of film thickness). It is not surprising that, error bars of "a" and "b" are high. On the other hand, sample "a" seemed to be far from growth stagnation and film destruction at tenth bilayer. As a result, those results clearly show that in spin-LbL, film deposition is not only controlled by spinning rate; fluid-film contact time is also important. This conclusion opened up the way for us to investigate the effect of spinning rate and fluid-film contact time on multilayer growth and pH-triggered dissolution in detail (see Chapter 3).

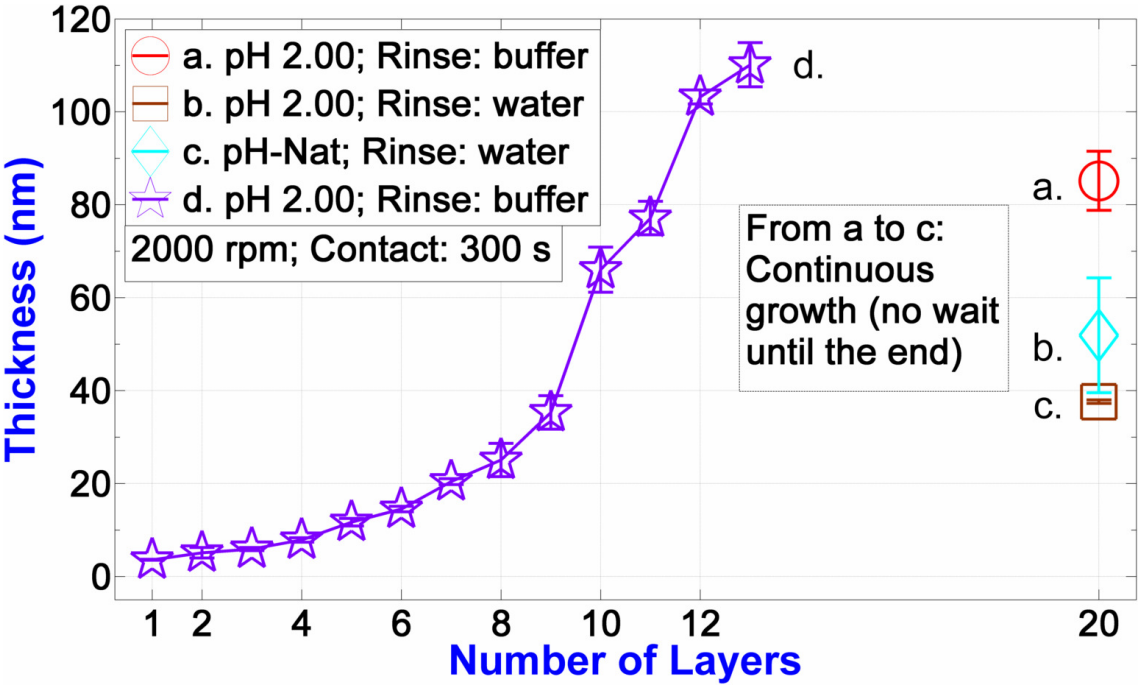

Figure App-13. Effect of film-fluid contact time on growth behavior spin-assisted multilayers.

We have also observed exponential growth in spin-assembly when high contact time was applied and thickness measurement were done discontinuously (see Figure App-14). No film stagnation was observed which is genrally followed by film "stripping". Also, final film thickness remained below continuous growth which is a sign of kinetic nature of growth.

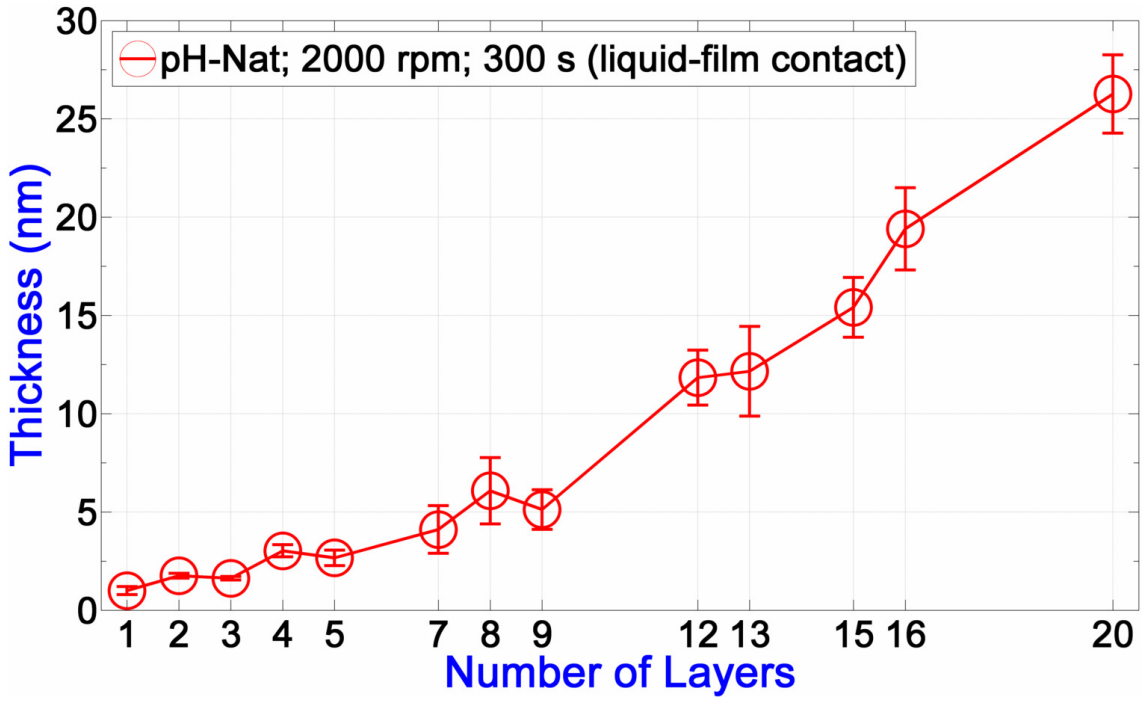

Figure App-14. Exponential growth of spin-grown multilayers at high film-fluid contact time.

Appendix-H: *X-Ray Photoelectron Spectra of Used Single-Wall Carbon Nanotube Sample*

SWCNTs in this study were used procured from Thomas Swan & Corporation Ltd. (England) under the brand name of Elicarb™ SW. According to the information provided by manufacturer, this sample is unfunctionalized and purified. Indeed, an XPS (Thermo Scientific K-Alpha, Thermo Fisher Scientific, Inc., USA) survey spectrum of this sample shows no signature of elements other than C and O (see Figure App-15 below and refer [801] for peak assignments). During purification process, hydroxyl and carboxyl functionalities can be attached to CNT surfaces. However, this level of O impurity is not considered as surface functionalization, because this level surface modification is virtually ineffective on the dispersion of SWCNTs. On the other hand, chemical functionalities may alter optical properties of SWCNTs significantly (recall Chapter 1 above).

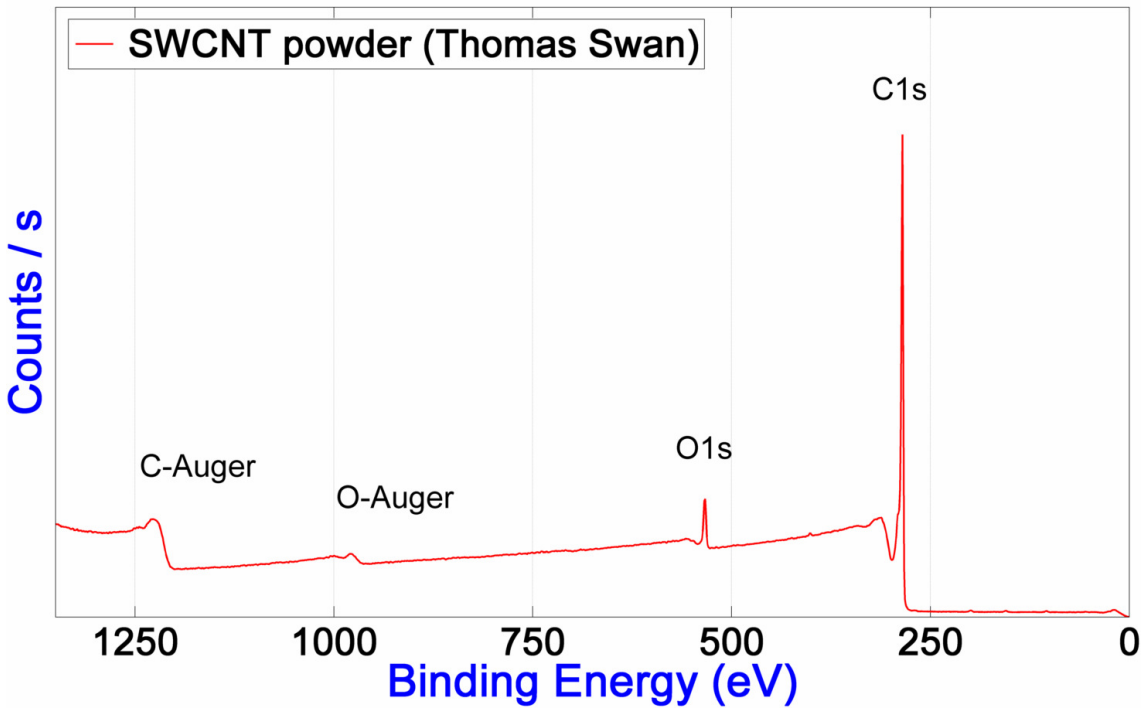

Figure App-15. X-ray photoelectron spectra of unfunctionalized single-wall carbon nanotube sample used in this study (Elicarb™ Thomas Swan, England).

Appendix-I: *Spray-Multilayers of Polyvinylpyrrolidone and Tannic Acid*

We have already compared dip- and spin-LbL multilayers of PVPon/TA pair. The most essential outcome of these studies was the observation of multilayer growth profile changes depending on the film deposition method. We mainly attributed observed variation to film-fluid contact time changes of different methods. Spin-LbL of low contact time ended up with linear-like growth whereas spin-LbL of high liquid contact showed and dip-LbL (normally high contact time) exhibited obvious exponential growth. So, we decided to check the behavior of spray-LbL. Before spray-LbL, we dip-modified Si substrates with pH 7.50 BPEI (0.5 g/L) to form anchoring layer. Then, we applied mists of assembly solutions and rinsing media (once in each step) in a sequential manner and multilayers were dried using N_2 flow at each step just after (~10-15 s) the mist application. First, we optimized distance of nozzles (regular cosmetic spray nozzles of 50 mL under the brand name of Watsons) and substrates for good surface coverage (data not shown). At 15 cm distance (note that this value may change from system to system, see [175]), we observed perfectly linear growth (other distances – 5, 10, 20 cm – were also linear but some irregularities observed). Then, we studied the effect of pH adjustment (from pH-Nat to pH 2.00) and rinsing media (water vs. buffer) as we already did for spin- and dip-assembly. As can be seen from Figure App-16 below, bilayer

thickness of spray-multilayers remained even below spin-LbL for both pH-Nat and pH 2.00 cases. We believe this observation supports film-fluid[64] contact time on growth behavior. A more detailed investigation will be performed and pH-triggered dissolution profile will be studied as well.

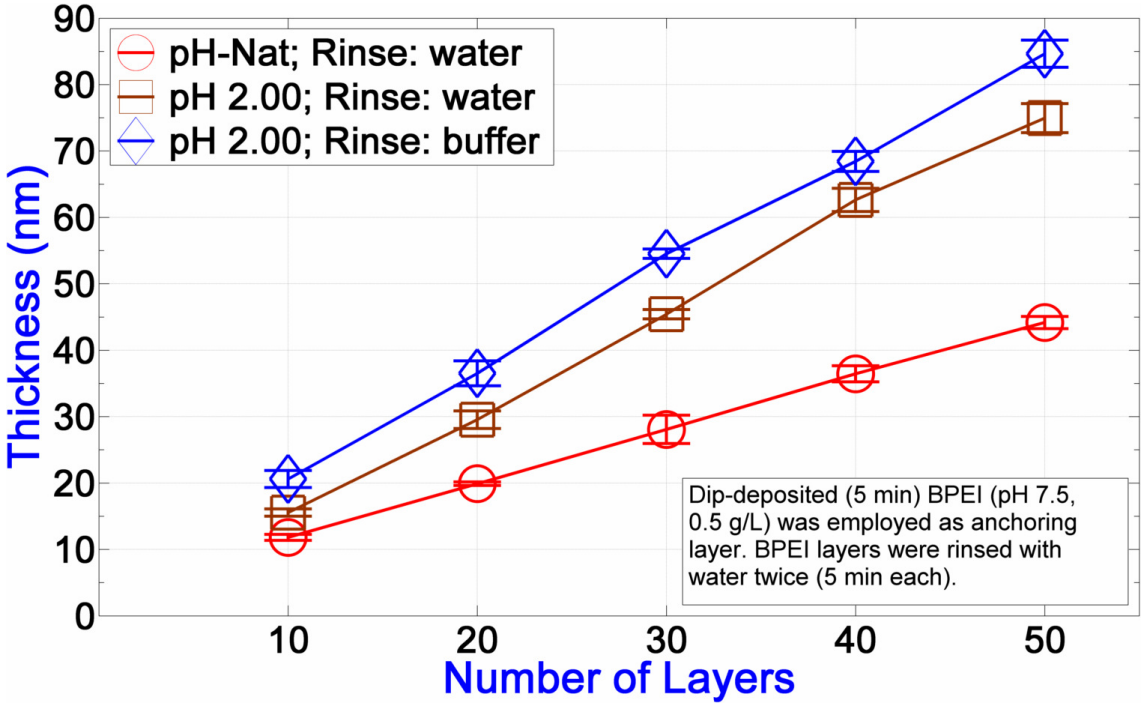

Figure App-16. Spray-assisted multilayer growth of pH 2.00 and native pH solutions (note that nozzle-substrate distance is fixed to 15 cm which is the optimized distance in our system, data not shown).

Appendix-J: *pH-Stability Comparison of Dip- and Spin-Assembled Multilayers*

Observed variations in growth of spin- and dip-LbL films suggested us a possible difference in pH stability. So, we tested pH-dependent stability of dip- and spin-assisted bare (no carbon nanotube addition) films and observed pH-stability variations between dip- and spin-assembled multilayers (see Figure App-17). In accordance with the mechanisms explained in Chapter 3, dip-LbL films are more stable than spin-LbL. The reason is probably originated from the timescale of pH-dissolution experiment which is considerably fast in this case. As we explained above in Chapter 3, fast dissolution hinders the equilibration of spin-multilayers and although dip-LbL films less hierarchical (Note that dip-LbL films have more time to reach a more favorable equilibrium during deposition).

[64] Here it would be better to name as mist, but for consistency we preferred to keep our nomenclature the same.

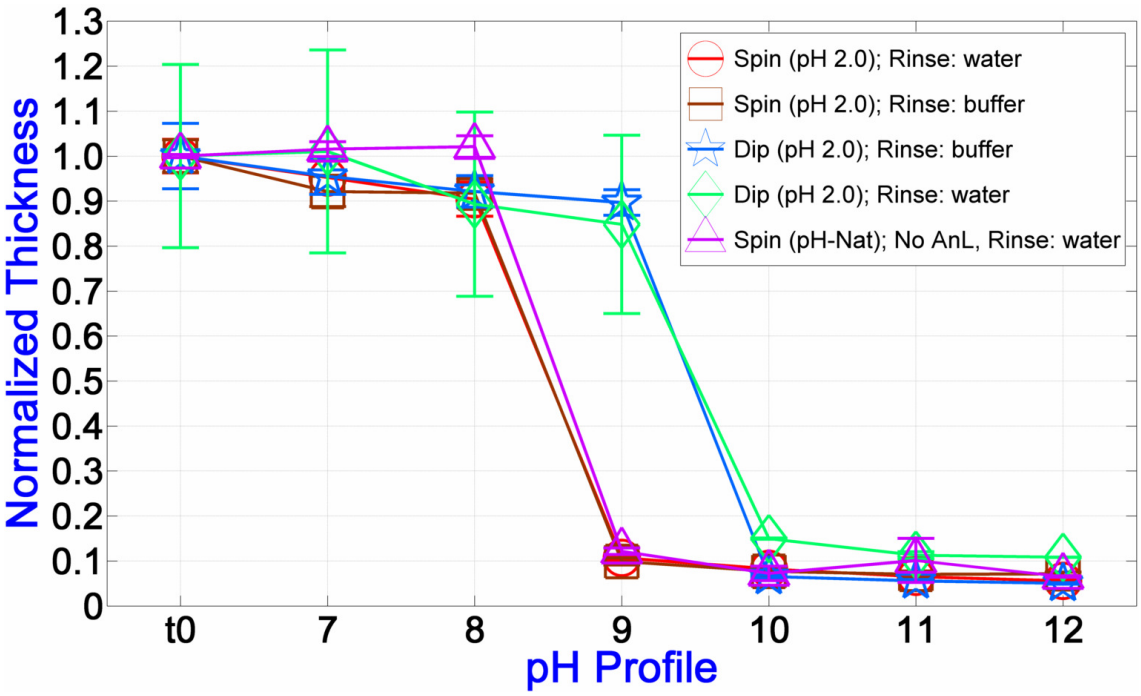

Figure App-17. Comparison of the pH-stability of- spin and dip-assembled multilayers.

However, we have also compared the dissolution of dip- and spin-assembled multilayer with QCM. QCM utilize Sauerbrey equation which correlates the mass change on a resonating plate with the changes of resonance frequency of oscillation ("$\Delta f = -C_f \times \Delta m$" where "$C_f$" is known to system-specific sensitivity factor). In Figure App-18, we first observe the swelling of spin-LbL film before dissolution. At pH-Nat of phosphate buffer (~4.80), a rapid water uptake takes place in the first couple seconds. Then, the rate of water uptake decreases. Water uptake rate increase at pH ~7.00 (we skip pH 6.00) showed a dramatic mass reduction at the very beginning of pH 9.00 which corresponds to rapid dissolution of film (critical dissolution pH is in between pH 8.00 and 9.00). Then, a slow dissolution takes place until pH 12.00. Finally, probably the first couple of layers (1 to 3 we guess) attracted by the substrate [802] are dissolved at pH 12. It is very clear that dip-LbL exhibits a different behavior than spin-LbL (see Figure App-19). First, the major difference is the deep well observed at pH ~9.00 which is an indication of film disintegration (Note that spin-LbL film dissolved at pH ~8.00). We attribute this behavior to the dramatic change in viscoelastic behavior of dip-assembled film just before the disintegration. In addition, it seems that dip-LbL films are dissolved in two different pH values. We consider this behavior as a consequence of exponential growth: The first part corresponds to exponential region and the second one belongs to initial zigzag-like part. In this case, exponential part is less stable than spin-LbL films, but zigzag-part of dip-LbL films are more stable than spin-LbL films.

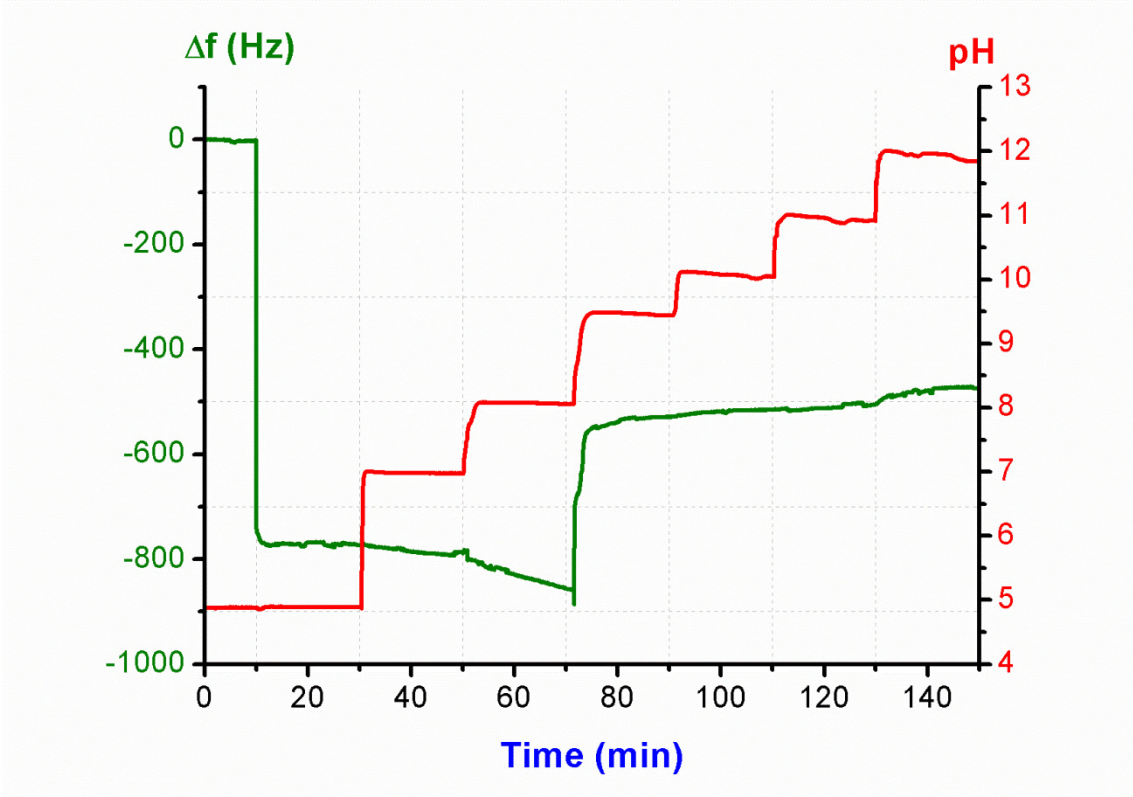

Figure App-18. pH-triggered dissolution of spin-assembled multilayer studied with quartz crystal microbalance.

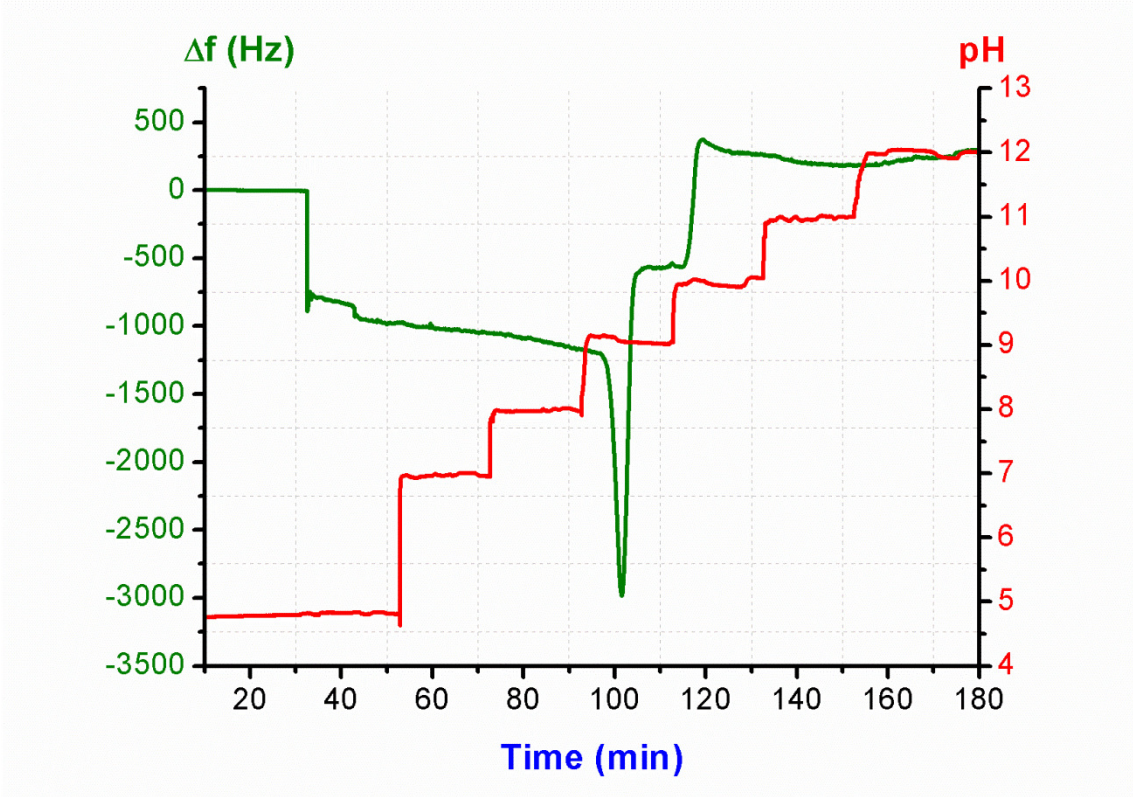

Figure App-19. pH-triggered dissolution of dip-assembled multilayer studied with quartz crystal microbalance.

Appendix-K: *Component-Induced Disintegration of Layer-by-Layer Films*

Kovacevic et al. correlated the instability of dip-LbL multilayers with the mobility of molecules [211]. In our previous study (Chapter 3), we showed evidence on high mobility of molecules in PVPon/TA multilayers. We believe kinetically trapped spin-LbL PVPon/TA multilayers are likely to be mobile enough to restructure themselves in more favorable states. Indeed, according to Kovacevic et al., there are three practical way to dissolve polymer complexes at constant temperature: i) pH perturbation (for pH responsive systems), ii) incubation in high ionic strength salt solution (mainly for polyelectrolyte systems), and iii) incubation in low ionic strength polymer solutions. In LbL complexes, complexation usually takes place in such a way that decomplexation remains minor. However, we observed a clear decomplexation of PVPon/TA when exposed to PVPon solutions. We consider PVPon-induced dissolution in relation to exponential growth tendency of PVPon/TA pair. We imagine PVPon chains try to diffuse inside the film and restructure it. During this process, the branching points TA molecules with PVPon chains dynamically exchanged between PVPon chains. Hence, loosely-anchored PVPon chains evolve in film structure. As a result, during desorption of loosely-bound PVPon chains, some TA molecules dissolve too and film disintegrates. We first serendipitously observed PVPon-induced dissolution and then a simple experiment is devised. We first assembled 4.5 bilayer films using dipping (5 min deposition + 2×5 min rinsing) and spinning (2000 rpm) on BPEI-modified (pH 7.50) substrates using pH 2.00 buffered solutions (0.01 M phosphate buffer). For rinsing, we used buffer solutions or water. Finally, PVPon-induced disintegration studies were performed employing the PVPon solutions used for assembly. Regardless of the rinsing routine and film deposition method, films disintegrated with an exponentially decreasing rate (see Figure App-20). In overall, dip-multilayers seemed to be more resistant against PVPon exposure. On the other hand, we regard kinetic reversibility and zigzag growth as related phenomena. Schlenoff's Group has investigated the effect of chain M_w on kinetic irreversibility of *es*-multilayers and has showed that "stripping" of chains can be favored using higher M_w polymers [803]. Thus, we anticipate that PVPon-induced destabilization of PVPon/TA multilayers can be suppressed by using higher M_w PVPon. Indeed, Schmidt and Hammond have been assembled PVPon/TA multilayers using higher M_w PVPon [667] and we believed that their results exhibit the suppression of component-induced destabilization (recall Chapter 2 for further discussions).

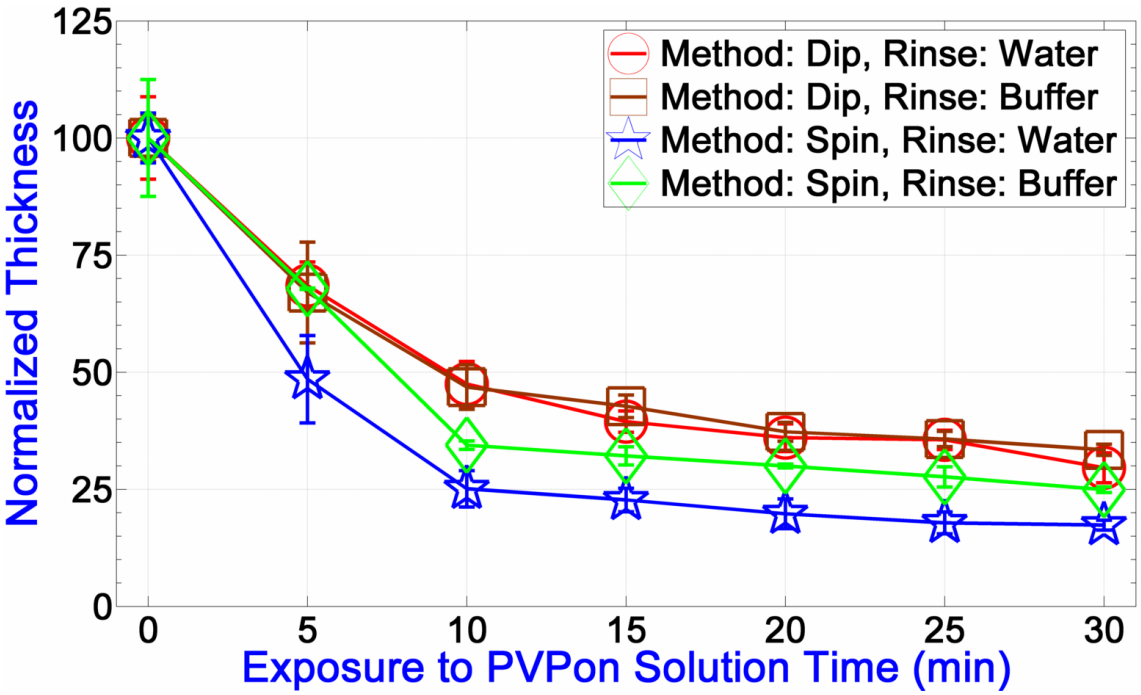

Figure App-20. Time-dependent dissolution of multilayer films triggered by polyvinylpyrrolidone exposure.

Appendix-L: *The Effect of Solution pH on the Formation of Quinones in Tannic Acid*

TA undergoes auto-oxidation in time which can be tracked by eye due to color formation. Oxidation of TA molecules is also a pH-dependent process. At high pH values, deprotonated hydroxyl groups became quinonic and TA solutions turn into yellow (see Figure App-21).

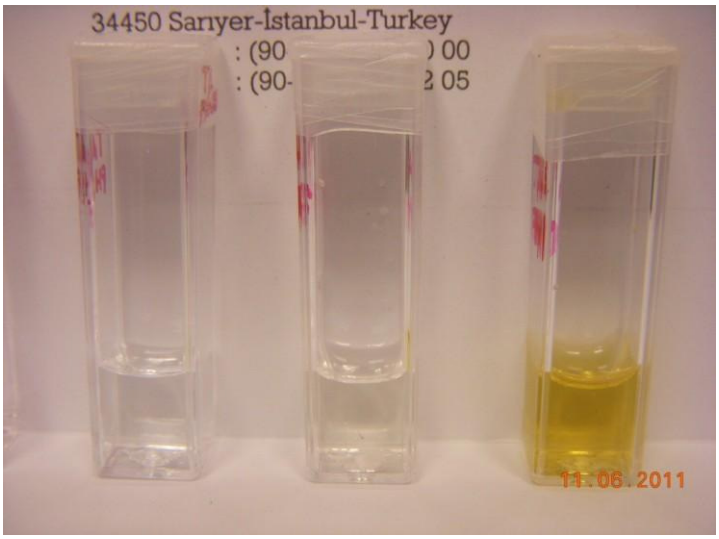

Figure App-21. Effect of solution pH on coloring of tannic acid which denotes oxidation and quinone formation**:** From left to right; pH 2.00, 6.00 and 10.00 (note that pH 6.00 sample is slightly yellowish).

Appendix-M: ***Infrared Spectra of Dispersing Agents and Nanotube Colloids in Solid Their Form***

We have checked[65] the chemical functionalities present on SWCNT powders and possible chemical effects of ultrasound on SWCNTs and dispersing agents using FT-IR (see Figure App-22 and App-23). We observed no significant change in before- and after-ultrasound spectra of both PVPon and TA. Modified SWCNT powders (PVPon-SWCNT and TA-SWCNT) also exhibited other significant characters other than the sum up of dispersing agents and SWCNTs. On the other hand, it should be noted that, the presence of carboxyl groups (–COOH) on SWCNTs was verified with this analysis (note the peak at ~1720 cm^{-1} which is attributed to the C=O stretching of carboxyl groups [804]). On the other hand, we should emphasize that, observed carboxyl functionalities might be suppressing the features expected in OAS studies and it might also be contributing to water dispersibility. But, it is clear that this level of carboxyl groups is not enough for dispersant-free dispersion. Thus, we can still consider utilized SWCNTs as "pristine" (recall Subsection 1.2.5.3).

[65] The parameters chosen for FT-IR studies were: i. Scan range [cm^{-1}]: 4000-600, ii. Spectral resolution [cm^{-1}]: 4, and iii. Number of scan: 128.

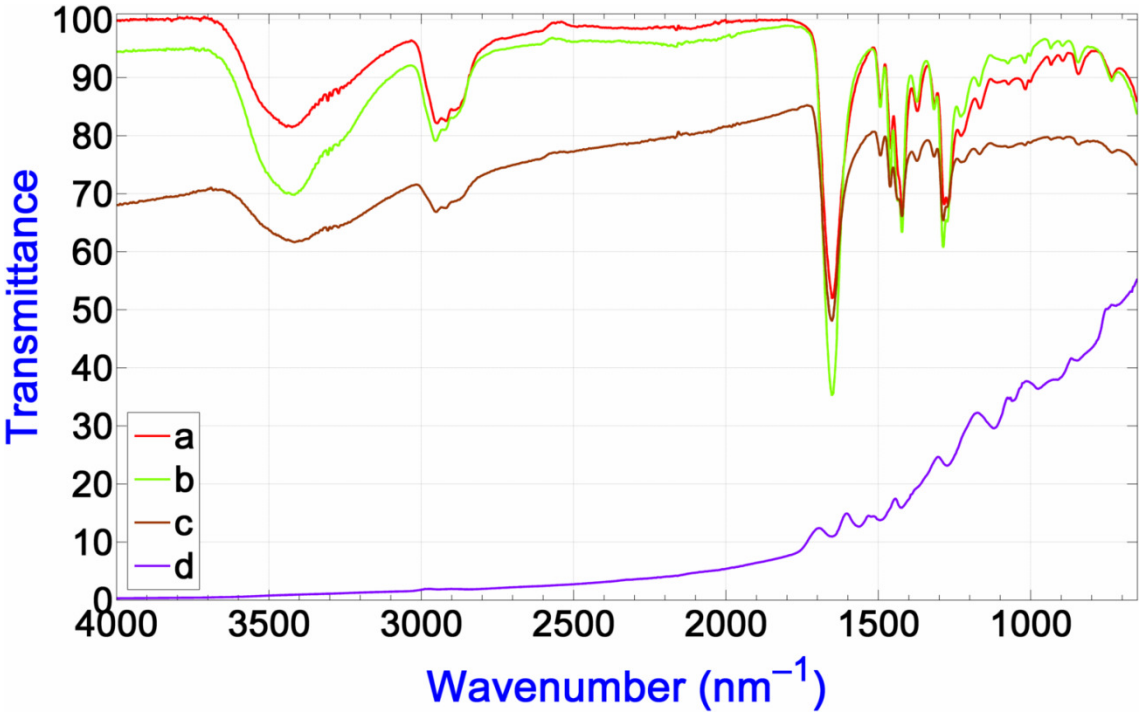

Figure App-22. Evaluation of ultrasonic irritation of poly(*N*-vinyl-2-pyrrolidone): a) Fresh PVPon powder, b) ultrasound-applied and aged PVPon, c) lyophilized powder of PVPon-SWCNT dispersion, and d) pristine SWCNT powder (Thomas Swan).

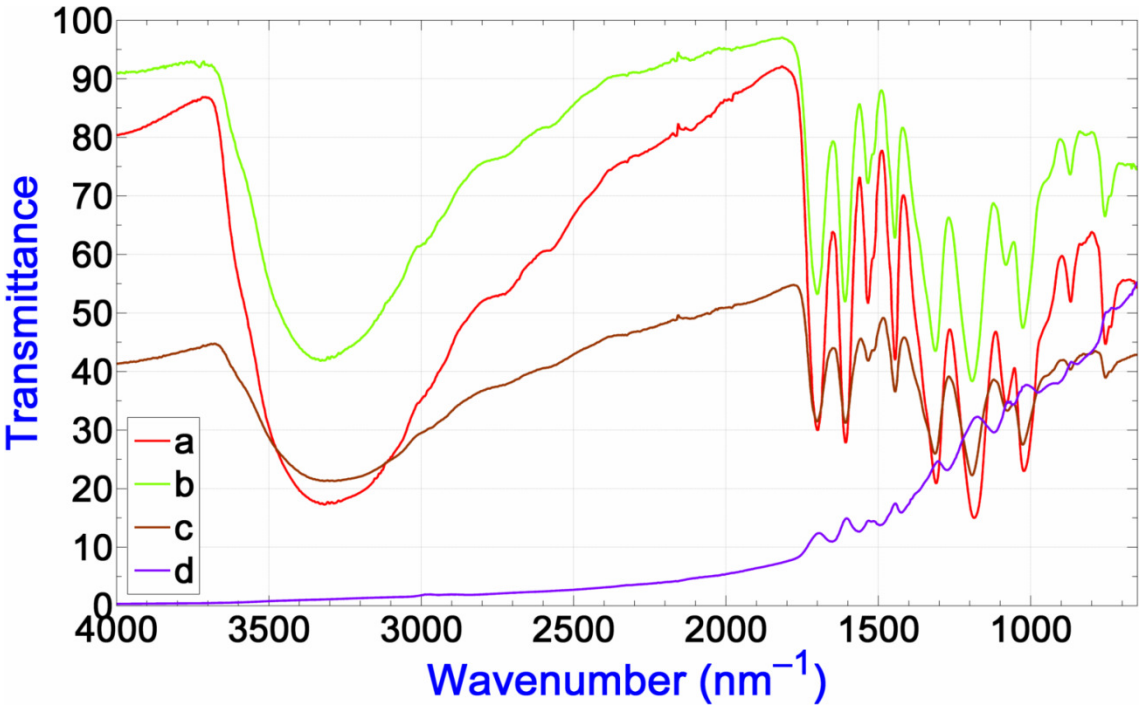

Figure App-23. Evaluation of ultrasonic irritation of tannic acid: a) Fresh TA powder, b) ultrasound-applied and aged TA, c) lyophilized powder of TA-SWCNT dispersion, and d) pristine SWCNT powder (Thomas Swan).

Appendix-N: ***pH-Stability of Long Term Aged Spin-Assembled Multilayers***

In Chapter 4, Figure 4-10 shows pH-dependent disintegration of undoped and nanotube-doped multilayer films up to pH 10.0. That graph clearly showed that undoped/fresh control sample (control-2) and composition-C are highly pH-resistant. After a couple of months we continued to pH-disintegration experiment beyond pH 10.0 using the sampe samples. We were expecting to observe better pH-stability of composition-C and we were planning to determine the critical dissolution pH of Control-2. We did observe enhanced pH-stability in composition-C, but complete dissolution of control-2 was totally unexpected (see Figure App-24). It seems that, the CNT-CNT interactions are enough to hold the multilayer intact at high pH values. In addition, composition-B also exhibited a slightly better stability compared to samples other than composition-C. This might be due to retardation of oxidation in TA molecules in the presence of SWCNTs.

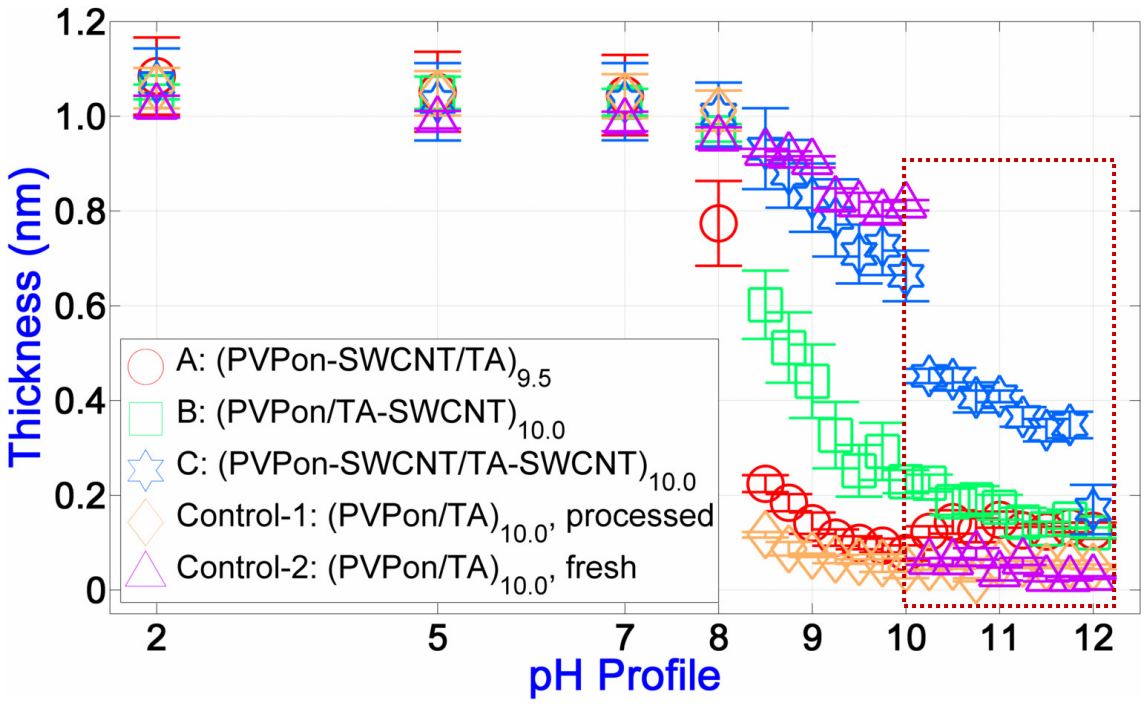

Figure App-24. pH-Stability of long-term aged multilayers shows enhanced stability of nanotube-doped films.

Appendix-O: ***Layer-by-Layer Spin-Assembly of Pluronic F-127 and Tannic Acid***

We studied dip- and spin-LbL of PLU/TA pair and observed that spin-LbL does not ensure perfectly linear growth in TA-based *hb*-multilayers. Indeed, dip-LbL (data not shown) and BPEI-free spin-LbL of PLU/TA multilayers grew erratic. However, we could achieve multilayer complexation between pH-Nat solutions of PLU and TA when BPEI is used as

precursor layer (see Figure App-25). We also checked the effect of quiescent rinsing time before spinning which are denoted as long (60 s) and short (3-5 s) in the figure below. Independent from the rinsing time, we observed zigzag-like growing multilayers. This observation rules out the possibility that spin-LbL gives linear growth irrespective to the LbL pair. In addition, PLU is also a successful dispersing agent for SWCNTs and we have then exploited this system for the incorporation of SWCNTs in *hb*-multilayers (data now shown).

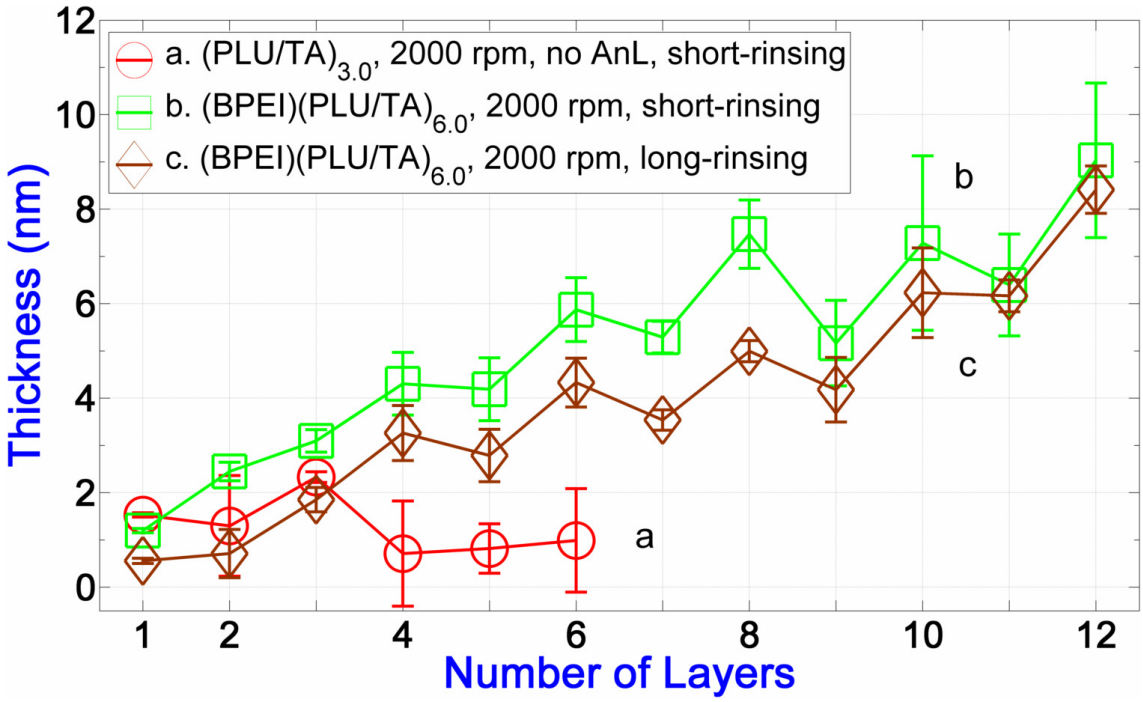

Figure App-25. Zigzag growth in spin-assisted deposition of layer-by-layer films.

Appendix-P: *Effect of pH on Polyvinylpyrrolidone-aided Dispersion of Carbon Nanotubes*

Smalley's Group reported PVPon-SWCNT dispersion (total concentration < 1.4 g/L) to salt out at 135 ± 20 mM NaCl [337]. But, no previous report provides information on pH response of PVPon-CNP systems. So, we checked SWCNT dispersion efficiency of PVPon as a function solution pH (see Figure App-26). Compared to buffer-free PVPon-SWCNT systems (see Chapter 3), all of pH adjusted (0.01 M phosphate buffer and required amount of NaOH) batches (P3-P4-P5) apparently dispersed low quantities of SWCNTs. In these experiments, adverse effect of buffering system appeared better than TA-SWCNT system. We did not aim to fully understand pH-dependent behavior of this system, but it is interesting to observe better dispersion at pH 10.00 comparing pH 2.00. The reason behind might be highly complex. We believe screening of particle charges of PVPon might be increasing hydrophobic interactions and possible conformational changes might also be contributing.

But, in any case, added salts hinder PVPon-stabilization of SWCNTs.

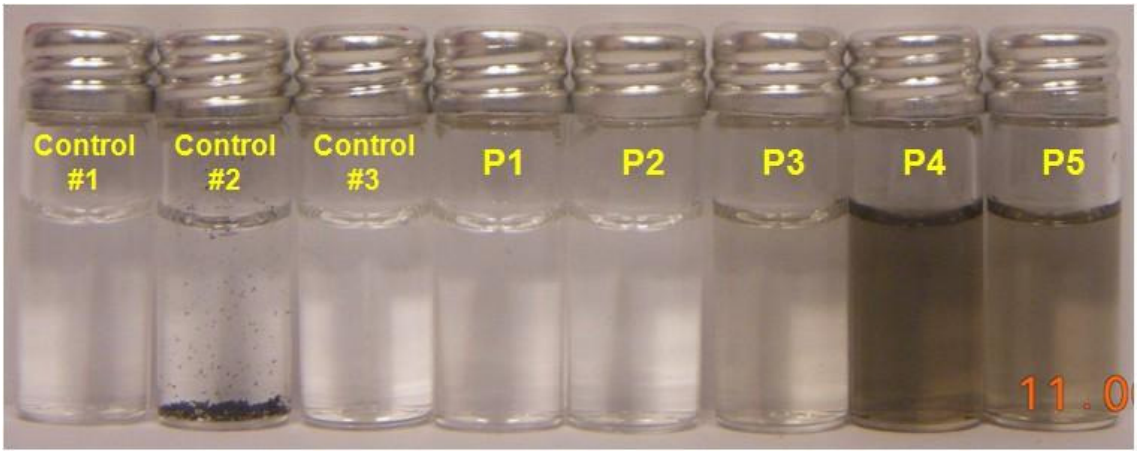

Figure App-26. Effect of pH adjustment on poly(*N*-vinyl-2-pyrrolidone) aided dispersion of single-wall carbon nanotubes (Control#1: DI-H_2O; Control#2: Sonicated SWCNTs in DI-H_2O; Control#3: Fresh PVPon; P1: Sonicated PVPon, P2: Aged PVPon; P3 to P5 are pH 2.00, 6.00, and 10.00 dispersions respectively).

Appendix-Q: *Thermogravimetric Analysis of Nanotube Dispersions*

From the image below it is seen that approximately 40% of TA-SWCNT powder is SWCNTs (see Figure App-27).[66] That observation shows that, our OAS studies underestimate the concentration of SWCNTs in dispersions. Similarly, approximately %20 of PVPon-SWCNT dispersions seems to be SWCNT (data not shown).

[66] Experiment was performed under Ar environment. In the studied temperature range, mass reduction of raw SWCNT powder was ~ 5% (data not shown).

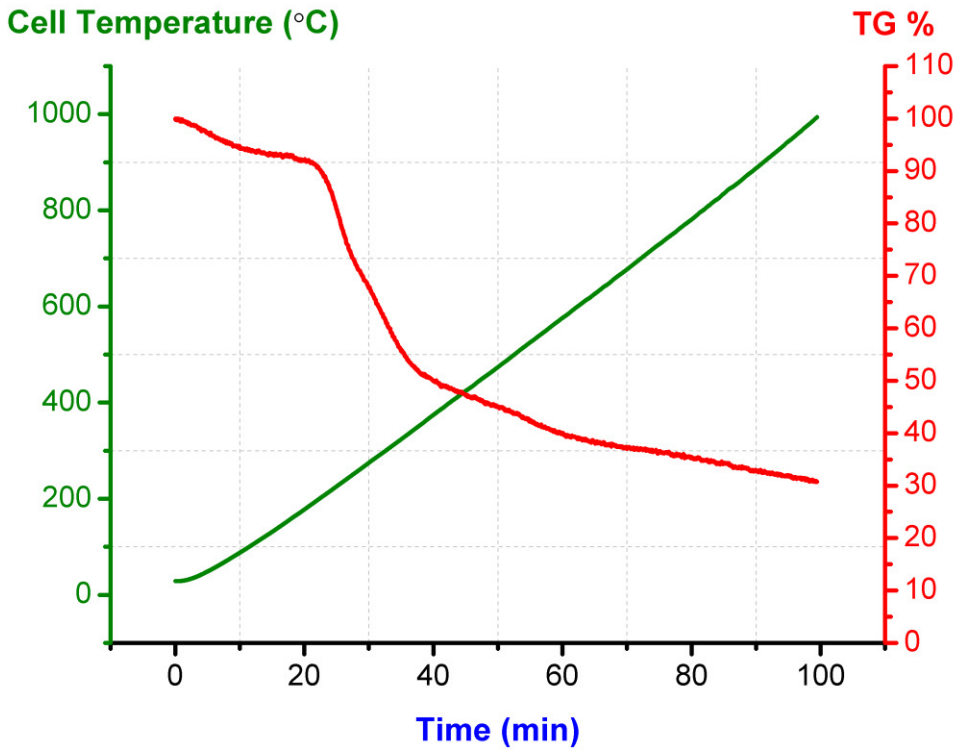

Figure App-27. Thermogravimetric analysis of tannic acid stabilized single-wall carbon nanotubes.

BIBLIOGRAPHY[67]

[1] C. N. R. Rao, "Dimensions of Chemical Science," in *Current Trends in Science - Platinum Jubilee Special*, N. Mukunda, Ed. Indian Academy of Sciences, 2009, pp. 7–8.

[2] M. C. T. Fyfe and J. F. Stoddart, "Synthetic supramolecular chemistry," *Accounts of Chemical Research*, vol. 30, no. 10, pp. 393–401, 1997.

[3] G. M. Whitesides, J. P. Mathias, and C. T. Seto, "Molecular self-assembly and nanochemistry: A chemical strategy for the synthesis of nanostructures," *Science*, vol. 254, no. 5036, pp. 1312–1319, 1991.

[4] J. W. Steed, D. R. Turner, and K. J. Wallace, *Core Concepts in Supramolecular Chemistry and Nanochemistry*, vol. 129, no. 46. John Wiley & Sons, Ltd., 2007, pp. 1–27.

[5] G. A. Ozin, "Nanochemistry: Synthesis in diminishing dimensions," *Advanced Materials*, vol. 4, no. 10, pp. 612–649, 1992.

[6] B. D. Summ and N. I. Ivanova, "The use of objects and methods of colloid chemistry in nanochemistry," *Russian Chemical Reviews*, vol. 69, no. 11, pp. 911–923, 2000.

[7] M. A. Cohen Stuart, "Supramolecular perspectives in colloid science," *Colloid and Polymer Science*, vol. 286, no. 8–9, pp. 855–864, 2008.

[8] H. Weller, "Quantum size colloids: from size-dependent properties of discrete particles to self-organized superstructures," *Current Opinion in Colloid and Interface Science*, vol. 3, no. 2, pp. 194–199, 1998.

[9] M. Rosoff, Ed., *Nano-Surface Chemistry*. Marcel Dekker, Inc., 2002, pp. 213–242.

[10] M. A. van Hove, "From surface science to nanotechnology," *Catalysis Today*, vol. 113, no. 3–4, pp. 133–140, 2006.

[11] S. Zhang, "Emerging biological materials through molecular self-assembly," *Biotechnology Advances*, vol. 20, no. 5–6, pp. 321–339, 2002.

[12] A. B. Descalzo, R. Martínez-Máñez, F. Sancenón, K. Hoffmann, and K. Rurack, "The supramolecular chemistry of organic-inorganic hybrid materials," *Angewandte Chemie International Edition in English*, vol. 45, no. 36, pp. 5924–5948, 2006.

[13] K. Ariga, J. P. Hill, and Q. Ji, "Layer-by-layer assembly as a versatile bottom-up nanofabrication technique for exploratory research and realistic application," *Physical Chemistry Chemical Physics*, vol. 9, no. 19, pp. 2319–2340, May 2007.

[14] J.-M. Lehn, "From matter to life: Chemistry?!," *Resonance*, vol. 1, no. 3, pp. 39–53, Mar. 1996.

[15] G. R. Desiraju, "Chemistry beyond the molecule," *Nature*, vol. 412, no. 6845, pp. 397–400, Jul. 2001.

[16] D. G. Castner and B. D. Ratner, "Biomedical surface science: Foundations to frontiers," *Surface Science*, vol. 500, no. 1–3, pp. 28–60, Mar. 2002.

[17] S. E. McNeil, "Nanotechnology for the biologist," *Journal of Leukocyte Biology*, vol. 78, no. 3, pp. 585–594, 2005.

[18] T. Fernandes-Alnemri et al., "The pyroptosome: a supramolecular assembly of ASC dimers mediating inflammatory cell death via caspase-1 activation.," *Cell Death and Differentiation*, vol. 14, no. 9, pp. 1590–1604, Sep. 2007.

[67] Prepared following the instructions in IEEE Citation Reference which is available online: www.ieee.org/documents/ieeecitationref.pdf

[19] S. W. Fox, “Spontaneous generation, the origin of life, and self assembly,” *Biosystems*, vol. 2, no. 5, pp. 235–240, Nov. 1968.

[20] H. Kuhn, “Self-organization of molecular systems and evolution of the genetic apparatus,” *Angewandte Chemie International Edition in English*, vol. 11, no. 9, pp. 798–820, Sep. 1972.

[21] M. Eigen, “Selforganization of matter and the evolution of biological macromolecules,” *Die Naturwissenschaften*, vol. 58, no. 10, pp. 465–523, Oct. 1971.

[22] P.-A. Monnard, C. L. Apel, A. Kanavarioti, and D. W. Deamer, “Influence of ionic inorganic solutes on self-assembly and polymerization processes related to early forms of life: Implications for a prebiotic aqueous medium,” *Astrobiology*, vol. 2, no. 2, pp. 139–152, Jan. 2002.

[23] D. Deamer, J. P. Dworkin, S. A. Sandford, M. P. Bernstein, and L. J. Allamandola, “The first cell membranes,” *Astrobiology*, vol. 2, no. 4, pp. 371–381, Jan. 2002.

[24] D. Deamer, S. Singaram, S. Rajamani, V. Kompanichenko, and S. Guggenheim, “Self-assembly processes in the prebiotic environment,” *Philosophical Transactions of the Royal Society B: Biological Sciences*, vol. 361, no. 1474, pp. 1809–1818, Oct. 2006.

[25] S. T. Nguyen, D. L. Gin, J. T. Hupp, and X. Zhang, “Supramolecular chemistry: Functional structures on the mesoscale,” *Proceedings of the National Academy of Sciences of the United States of America*, vol. 98, no. 21, pp. 11849–11850, 2001.

[26] J.-M. Lehn, “Toward complex matter: Supramolecular chemistry and self-organization,” *Proceedings of the National Academy of Sciences of the United States of America*, vol. 99, no. 8, pp. 4763–4768, 2002.

[27] G. M. Whitesides et al., “Noncovalent synthesis: Using physical-organic chemistry to make aggregates,” *Accounts of Chemical Research*, vol. 28, no. 1, pp. 37–44, 1995.

[28] J. N. Israelachvili, “Thermodynamic Principles of Self-Assembly,” in *Intermolecular and Surface Forces*, Third Edit., Elsevier Inc., 1992, pp. 503–534.

[29] G. M. Whitesides and B. Grzybowski, “Self-assembly at all scales,” *Science*, vol. 295, no. 5564, pp. 2418–2421, 2002.

[30] L. C. Palmer, Y. S. Velichko, M. O. de la Cruz, and S. I. Stupp, “Supramolecular self-assembly codes for functional structures,” *Philosophical Transactions of the Royal Society A: Mathematical, Physical and Engineering Sciences*, vol. 365, no. 1855, pp. 1417–1433, 2007.

[31] F. M. Harold, “Molecules into cells: Specifying spatial architecture,” *Microbiology and Molecular Biology Reviews*, vol. 69, no. 4, pp. 544–564, 2005.

[32] K. Ariga and T. Kunitake, *Supramolecular Chemistry – Fundamentals and Applications*, English Ed. Springer-Verlag Heidelberg, 2006.

[33] J. H. E. Cartwright and A. G. Checa, “The dynamics of nacre self-assembly,” *Journal of the Royal Society Interface*, vol. 4, no. 14, pp. 491–504, 2007.

[34] J.-M. Lehn, “Toward self-organization and complex matter,” *Science*, vol. 295, no. 5564, pp. 2400–2403, 2002.

[35] I. W. Hamley, “Nanotechnology with soft materials,” *Angewandte Chemie International Edition in English*, vol. 42, no. 15, pp. 1692–1712, 2003.

[36] F. M. Menger, “Supramolecular chemistry and self-assembly,” *Proceedings of the National Academy of Sciences of the United States of America*, vol. 99, no. 8, pp. 4818–4822, 2002.

[37] R. P. Feynman, “There’s plenty of room at the bottom,” *Engineering and Science*, vol. 23, no. 5, pp. 22–36, 1960.

[38] K. Okamoto, P. Chithra, G. J. Richards, J. P. Hill, and K. Ariga, “Self-assembly of optical molecules with supramolecular concepts,” *International Journal of Molecular Sciences*, vol. 10, no. 5, pp. 1950–1966, May 2009.

[39] K. Ariga, X. Hu, S. Mandal, and J. P. Hill, “By what means should nanoscaled materials be constructed: molecule, medium, or human?,” *Nanoscale*, vol. 2, no. 2, pp. 198–214, 2010.

[40] J. H. Hah et al., “Converging lithography by combination of electrostatic layer-by-layer self-assembly and 193 nm photolithography: Top-down meets bottom-up,” *Journal of Vacuum Science and Technology B: Microelectronics and Nanometer Structures*, vol. 24, no. 5, pp. 2209–2213, 2006.

[41] A. H. Marcus, D. M. Hussey, N. A. Diachun, and M. D. Fayer, “Nanodomain formation in a liquid polymer blend: The initial stages of phase separation,” *The Journal of Chemical Physics*, vol. 103, no. 18, pp. 8189–8200, 1995.

[42] I. Akiba, H. Masunaga, K. Sasaki, K. Shikasho, and K. Sakurai, “Nanostructured polymer blend formed from poly(N-vinylpyrrolidone) and end-functional polystyrene,” *Polymer*, vol. 45, no. 17, pp. 5761–5764, 2004.

[43] L. Zhang, “Self-assembled intrinsic nanoscale phase separation in polymers,” *Europhysics Letters*, vol. 93, no. 5, p. 58002, 2011.

[44] J. Peng, Y. Han, W. Knoll, and D. H. Kim, “Development of nanodomain and fractal morphologies in solvent annealed block copolymer thin films,” *Macromolecular Rapid Communications*, vol. 28, no. 13, pp. 1422–1428, 2007.

[45] E. A. Stefanescu, C. Daranga, and C. Stefanescu, “Insight into the broad field of polymer nanocomposites: From carbon nanotubes to clay nanoplatelets, via metal nanoparticles,” *Materials*, vol. 2, no. 4, pp. 2095–2153, 2009.

[46] L. S. Schadler, L. C. Brinson, and W. G. Sawyer, “Polymer nanocomposites: A small part of the story,” *Journal of the Minerals, Metals and Materials Society*, vol. 59, no. 3, pp. 53–60, May 2007.

[47] D. R. Baer, “Enhancing coating functionality using nanoscience and nanotechnology,” *Progress in Organic Coatings*, vol. 47, no. 3–4, pp. 342–356, 2003.

[48] M. M. de Villiers, D. P. Otto, S. J. Strydom, and Y. M. Lvov, “Introduction to nanocoatings produced by layer-by-layer (LbL) self-assembly,” *Advanced Drug Delivery Reviews*, vol. 63, no. 9, pp. 701–715, 2011.

[49] A. P. R. Johnston, C. Cortez, A. S. Angelatos, and F. Caruso, “Layer-by-layer engineered capsules and their applications,” *Current Opinion in Colloid and Interface Science*, vol. 11, no. 4, pp. 203–209, 2006.

[50] S. A. Sukhishvili, “Responsive polymer films and capsules via layer-by-layer assembly,” *Current Opinion in Colloid and Interface Science*, vol. 10, no. 1–2, pp. 37–44, 2005.

[51] L. Zhang and T. J. Webster, “Nanotechnology and nanomaterials: Promises for improved tissue regeneration,” *Nano Today*, vol. 4, no. 1, pp. 66–80, 2009.

[52] P. Sanguansri and M. A. Augustin, “Nanoscale materials development – a food industry perspective,” *Trends in Food Science &Technology*, vol. 17, no. 10, pp. 547–556, 2006.

[53] S. Parveen, R. Misra, and S. K. Sahoo, “Nanoparticles: a boon to drug delivery, therapeutics, diagnostics and imaging,” *Nanomedicine: Nanotechnology, Biology, and Medicine*, vol. xx, no. xx, p. xxx–xxx, 2011.

[54] C. N. R. Rao and A. K. Cheetham, “Materials Science at the Nanoscale,” in *Nanomaterials Handbook*, Y. Gogotsi, Ed. Taylor & Francis Group, LLC, 2006, pp. 1–12.

[55] O. V. Salata, “Applications of nanoparticles in biology and medicine,” *Journal of Nanobiotechnology*, vol. 2, no. 3, pp. 1–6, 2004.

[56] M. A. Lemley, “Patenting nanotechnology,” *Stanford Law Review*, vol. 58, no. 2, pp. 601–630, 2005.

[57] J. Weiss, P. Takhistov, and D. J. McClements, “Functional materials in food nanotechnology,” *Journal of Food Science*, vol. 71, no. 9, pp. R107–R116, 2006.

[58] Y. Dang, Y. Zhang, L. Fan, H. Chen, and M. C. Roco, “Trends in worldwide nanotechnology patent applications: 1991 to 2008,” *Journal of Nanoparticle Research*, vol. 12, no. 3, pp. 687–706, 2010.

[59] A. P. Alivisatos, “Semiconductor clusters, nanocrystals, and quantum dots,” *Science*, vol. 271, no. 5251, pp. 933–937, 1996.

[60] A. P. Alivisatos, “Perspectives on the physical chemistry of semiconductor nanocrystals,” *Journal of Physical Chemistry*, vol. 3654, no. 95, pp. 13226–13239, 1996.

[61] M.-C. Daniel and D. Astruc, “Gold nanoparticles: Assembly, supramolecular chemistry, quantum-size-related properties, and applications toward biology, catalysis, and nanotechnology,” *Chemical Reviews*, vol. 104, no. 1, pp. 293–346, 2004.

[62] M. A. El-Sayed, “Small is different: Shape-, size-, and composition-dependent properties of

some colloidal semiconductor nanocrystals," *Accounts of Chemical Research*, vol. 37, no. 5, pp. 326–333, May 2004.

[63] H. Yu, J. Li, R. A. Loomis, P. C. Gibbons, L.-W. Wang, and W. E. Buhro, "Cadmium selenide quantum wires and the transition from 3D to 2D confinement," *Journal of the American Chemical Society*, vol. 125, no. 52, pp. 16168–16169, 2003.

[64] C. Burda, X. Chen, R. Narayanan, and M. A. El-Sayed, "Chemistry and properties of nanocrystals of different shapes," *Chemical Reviews*, vol. 105, no. 4, pp. 1025–1102, 2005.

[65] S. Acharya, J. P. Hill, and K. Ariga, "Soft Langmuir-Blodgett technique for hard nanomaterials," *Advanced Materials*, vol. 21, no. 29, pp. 2959–2981, 2009.

[66] C. T. Sun and H. Zhang, "Size-dependent elastic moduli of platelike nanomaterials," *Journal of Applied Physics*, vol. 93, no. 2, pp. 1212–1218, 2003.

[67] S. K. Sohaebuddin, P. T. Thevenot, D. Baker, J. W. Eaton, and L. Tang, "Nanomaterial cytotoxicity is composition, size, and cell type dependent," *Particle and Fibre Toxicology*, vol. 7, no. 22, pp. 1–17, 2010.

[68] V. Pokropivny and V. Skorokhod, "New dimensionality classifications of nanostructures," *Physica E: Low-dimensional Systems and Nanostructures*, vol. 40, no. 7, pp. 2521–2525, May 2008.

[69] V. Pokropivny and V. Skorokhod, "Classification of nanostructures by dimensionality and concept of surface forms engineering in nanomaterial science," *Materials Science and Engineering: C*, vol. 27, no. 5–8, pp. 990–993, 2007.

[70] C. N. R. Rao and A. K. Cheetham, "Science and technology of nanomaterials: current status and future prospects," *Journal of Materials Chemistry*, vol. 11, no. 12, pp. 2887–2894, 2001.

[71] E. Matijevic, "Preparation and properties of uniform size colloids," *Chemistry of Materials*, vol. 5, no. 4, pp. 412–426, 1993.

[72] E. Matijevic, "Monodispersed metal (hydrous) oxides-A fascinating field of colloid science," *Accounts of Chemical Research*, vol. 14, no. 1, pp. 22–29, 1981.

[73] V. A. Bykov, "Langmuir-Blodgett films and nanotechnology," *Biosensor and Bioelectronics*, vol. 11, no. 9, pp. 923–932, 1996.

[74] J. C. Huie, "Guided molecular self-assembly: a review of recent efforts," *Smart Materials and Structures*, vol. 12, no. 2, pp. 264–271, 2003.

[75] G. Decher and J. B. Schlenoff, Eds., *Multilayer Thin Films: Sequential Assembly of Nanocomposite Materials*, vol. 1. Wiley-VCH Verlag GmbH & Co. KGaA, 2002, pp. 1–527.

[76] E. Ruiz-Hitzky, M. Darder, P. Aranda, and K. Ariga, "Advances in biomimetic and nanostructured biohybrid materials," *Advanced Materials*, vol. 22, no. 3, pp. 323–336, 2010.

[77] K. Ariga, J. P. Hill, and Q. Ji, "Biomaterials and biofunctionality in layered macromolecular assemblies," *Macromolecular Bioscience*, vol. 8, no. 11, pp. 981–990, 2008.

[78] G. Decher, M. Eckle, J. Schmitt, and B. Struth, "Layer-by-layer assembled multicomposite films," *Current Opinion in Colloid and Interface Science*, vol. 3, no. 1, pp. 32–39, Feb. 1998.

[79] L. Wang, F. Tang, and K. Ozawa, "Layer-by-layer assembled thin films of inorganic nanomaterials: fabrication and photo-electrochemical properties," *International Journal of Surface Science and Engineering*, vol. 3, no. 1–2, pp. 44–63, 2009.

[80] D. T. Haynie, L. Zhang, W. Zhao, and J. S. Rudra, "Protein-inspired multilayer nanofilms: science, technology and medicine," *Nanomedicine: Nanotechnology, Biology, and Medicine*, vol. 2, no. 3, pp. 150–157, 2006.

[81] I. Langmuir, "The constitution and fundamental properties of solids and liquids," *Journal of the American Chemical Society*, vol. 39, no. 9, pp. 1848–1906, 1917.

[82] I. Langmuir, "The mechanism of the surface phenomena of flotation," *Transactions of the Faraday Society*, vol. 15, pp. 62–74, 1920.

[83] K. B. Blodgett, "Films built by depositing successive monomolecular layers on a solid surface," *Journal of the American Chemical Society*, vol. 57, no. 6, pp. 1007–1022, 1935.

[84] I. Langmuir and V. J. Schaefer, "The effect of dissolved salts on insoluble monolayers," *Journal of the American Chemical Society*, vol. 59, no. 11, pp. 2400–2414, 1937.

[85] I. Langmuir and V. J. Schaefer, "Monolayers and multilayers of chlorophyll," *Journal of the*

American Chemical Society, vol. 59, no. 10, pp. 2075–2076, 1937.

[86] I. Langmuir and V. J. Schaefer, "Improved methods of conditioning surfaces for adsorption," *Journal of the American Chemical Society*, vol. 59, no. 9, pp. 1762–1763, 1937.

[87] I. Langmuir and V. J. Schaefer, "Salted-out protein films," *Journal of the American Chemical Society*, vol. 60, no. 11, pp. 2803–2810, 1938.

[88] H. Kuhn, "Versuche zur Herstellung einfacher organisierter Systeme von Molekülen," *Pure and Applied Chemistry*, vol. 11, no. 3–4, p. 345, 1965.

[89] H. Kuhn and D. Möbius, "Systems of monomolecular layers-Assembling and physico-chemical behavior," *Angewandte Chemie International Edition in English*, vol. 10, no. 9, pp. 620–637, Sep. 1971.

[90] J. J. Kirkland, "Porous thin-layer modified glass bead supports for gas liquid chromatography," *Analytical Chemistry*, vol. 37, no. 12, pp. 1458–1461, Nov. 1965.

[91] R. K. Iler, "Multilayers of colloidal particles," *Journal of Colloid and Interface Science*, vol. 21, no. 6, pp. 569–594, 1966.

[92] R. K. Iler, "Adsorption of colloidal silica on alumina and of colloidal alumina on silica," *Journal of the American Ceramic Society*, vol. 47, no. 4, pp. 194–198, 1964.

[93] G. Decher and J.-D. Hong, "Buildup of ultrathin multilayer films by a self-assembly process, 1. Consecutive adsorption of anionic and cationic bipolar amphiphiles on charged surfaces," *Makromolekulare Chemie. Macromolecular Symposia*, vol. 46, no. 1, pp. 321–327, 1991.

[94] G. Decher and J. D. Hong, "Buildup of ultrathin multilayer films by a self-assembly process: II. Consecutive adsorption of anionic and cationic bipolar amphiphiles and polyelectrolytes on charged surfaces," *Berichte der Bunsengesellschaft für physikalische Chemie*, vol. 95, no. 11, pp. 1430–1434, 1991.

[95] G. Decher, J.-D. Hong, and J. Schmitt, "Buildup of ultrathin multilayer films by a self-assembly process: III. Consecutively alternating adsorption of anionic and cationic polyelectrolytes on charged surfaces," *Thin Solid Films*, vol. 210–211, no. 2, pp. 831–835, 1992.

[96] G. Decher and J. Schmitt, "Fine-tuning of the film thickness of ultrathin multilayer films composed of consecutively alternating layers of anionic and cationic polyelectrolytes," *Progress in Colloid and Polymer Science*, vol. 89, pp. 160–164, 1992.

[97] Y. Lvov, G. Decher, and H. Möhwald, "Assembly, structural characterization, and thermal behavior of layer-by-layer deposited ultrathin films of poly (vinyl sulfate) and poly (allylamine)," *Langmuir*, vol. 9, no. 2, pp. 481–486, 1993.

[98] Y. Lvov, G. Decher, and G. Sukhorukov, "Assembly of thin films by means of successive deposition of alternate layers of DNA and poly(allylamine)," *Macromolecules*, vol. 26, no. 20, pp. 5396–5399, 1993.

[99] G. Decher, Y. Lvov, and J. Schmitt, "Proof of multilayer structural organization in self-assembled polycation-polyanion molecular films," *Thin Solid Films*, vol. 244, no. 1–2, pp. 772–777, May 1994.

[100] J. L. Lutkenhaus and P. T. Hammond, "Electrochemically enabled polyelectrolyte multilayer devices: from fuel cells to sensors," *Soft Matter*, vol. 3, no. 7, pp. 804–816, 2007.

[101] E. Kharlampieva, V. Kozlovskaya, and S. A. Sukhishvili, "Layer-by-layer hydrogen-bonded polymer films: From fundamentals to applications," *Advanced Materials*, vol. 21, no. 30, pp. 3053–3065, Aug. 2009.

[102] M. Sato and M. Sano, "van der Waals layer-by-layer construction of a carbon nanotube 2D network," *Langmuir*, vol. 21, no. 24, pp. 11490–11494, Nov. 2005.

[103] M. Matsusaki, H. Ajiro, T. Kida, T. Serizawa, and M. Akashi, "Layer-by-layer assembly through weak interactions and their biomedical applications," *Advanced Materials*, vol. 24, no. 4, pp. 454–474, Jan. 2012.

[104] Y. Shimazaki, M. Mitsuishi, S. Ito, and M. Yamamoto, "Preparation of the layer-by-layer deposited ultrathin film based on the charge-transfer interaction," *Langmuir*, vol. 13, no. 6, pp. 1385–1387, Mar. 1997.

[105] Y. Shimazaki, M. Mitsuishi, S. Ito, and M. Yamamoto, "Preparation and characterization of the

layer-by-layer deposited ultrathin film based on the charge-transfer interaction in organic solvents," *Langmuir*, vol. 14, no. 10, pp. 2768–2773, May 1998.

[106] Y. Shimazaki, M. Mitsuishi, S. Ito, and M. Yamamoto, "Alternate adsorption of polymers on a gold surface through the charge-transfer interaction," *Macromolecules*, vol. 32, no. 24, pp. 8220–8223, Nov. 1999.

[107] E. Kharlampieva, I. Erel-Unal, and S. A. Sukhishvili, "Amphoteric surface hydrogels derived from hydrogen-bonded multilayers: Reversible loading of dyes and macromolecules," *Langmuir*, vol. 23, no. 1, pp. 175–181, Jan. 2007.

[108] D. E. Bergbreiter and K.-S. Liao, "Covalent layer-by-layer assembly—an effective, forgiving way to construct functional robust ultrathin films and nanocomposites," *Soft Matter*, vol. 5, no. 1, p. 23, 2009.

[109] C. J. Ochs, G. K. Such, Y. Yan, M. P. van Koeverden, and F. Caruso, "Biodegradable click capsules with engineered drug-loaded multilayers," *ACS Nano*, vol. 4, no. 3, pp. 1653–1663, Mar. 2010.

[110] H. G. M. van de Steeg, M. A. Cohen Stuart, A. de Keizer, and B. H. Bijsterbosch, "Polyelectrolyte adsorption: A subtle balance of forces," *Langmuir*, vol. 8, no. 10, pp. 2538–2546, Oct. 1992.

[111] N. G. Hoogeveen, M. A. Cohen Stuart, G. J. Fleer, and M. R. Böhmer, "Formation and stability of multilayers of polyelectrolytes," *Langmuir*, vol. 12, no. 15, pp. 3675–3681, Jan. 1996.

[112] S. T. Dubas and J. B. Schlenoff, "Factors controlling the growth of polyelectrolyte multilayers," *Macromolecules*, vol. 32, no. 24, pp. 8153–8160, 1999.

[113] W. B. Stockton and M. F. Rubner, "Molecular-level processing of conjugated polymers. 4. Layer-by-layer manipulation of polyaniline via hydrogen-bonding interactions," *Macromolecules*, vol. 30, no. 9, pp. 2717–2725, May 1997.

[114] L. Wang, Z. Wang, X. Zhang, J. Shen, L. Chi, and H. Fuchs, "A new approach for the fabrication of an alternating multilayer film of poly(4-vinylpyridine) and poly(acrylic acid) based on hydrogen bonding," *Macromolecular Rapid Communications*, vol. 18, no. 6, pp. 509–514, 1997.

[115] J. F. Quinn, A. P. R. Johnston, G. K. Such, A. N. Zelikin, and F. Caruso, "Next generation, sequentially assembled ultrathin films: beyond electrostatics," *Chemical Society Reviews*, vol. 36, no. 5, pp. 707–718, May 2007.

[116] N. A. Kotov, "Layer-by-layer self-assembly: The contribution of hydrophobic interactions," *NanoStructured Materials*, vol. 12, no. 5–8, pp. 789–796, 1999.

[117] S. L. Clark and P. T. Hammond, "The role of secondary interactions in selective electrostatic multilayer deposition," *Langmuir*, vol. 16, no. 26, pp. 10206–10214, Dec. 2000.

[118] T. Serizawa, S. Kamimura, N. Kawanishi, and M. Akashi, "Layer-by-layer assembly of poly(vinyl alcohol) and hydrophobic polymers based on their physical adsorption on surfaces," *Langmuir*, vol. 18, no. 22, pp. 8381–8385, Oct. 2002.

[119] A. Guyomard, G. Muller, and K. Glinel, "Buildup of multilayers based on amphiphilic polyelectrolytes," *Macromolecules*, vol. 38, no. 13, pp. 5737–5742, 2005.

[120] P. Bertrand, A. Jonas, A. Laschewsky, and R. Legras, "Ultrathin polymer coatings by complexation of polyelectrolytes at interfaces: suitable materials, structure and properties," *Macromolecular Rapid Communications*, vol. 21, no. 7, pp. 319–348, Apr. 2000.

[121] M. J. McShane and Y. M. Lvov, "Layer-by-Layer Electrostatic Self-Assembly of Polyelectrolyte," *Dekker Encyclopedia of Nanoscience and Nanotechnology*, vol. 20, no. 4. Taylor Francis Group, LLC, pp. 1823–1840, Feb-2009.

[122] I. Erel-Unal and S. A. Sukhishvili, "Hydrogen-bonded multilayers of a neutral polymer and a polyphenol," *Macromolecules*, vol. 41, no. 11, pp. 3962–3970, 2008.

[123] I. Erel, H. Schlaad, and A. L. Demirel, "Effect of structural isomerism and polymer end group on the pH-stability of hydrogen-bonded multilayers," *Journal of Colloid and Interface Science*, vol. 361, no. 2, pp. 477–482, Sep. 2011.

[124] I. Erel, H. E. Karahan, C. Tuncer, V. Bütün, and A. L. Demirel, "Hydrogen-bonded multilayers of micelles of a dually responsive dicationic block copolymer," *Soft Matter*, vol. 8, no. 3, pp.

827–836, 2012.
[125] M. Kolasińska, R. Krastev, and P. Warszyński, “Characteristics of polyelectrolyte multilayers: Effect of PEI anchoring layer and posttreatment after deposition,” *Journal of Colloid and Interface Science*, vol. 305, no. 1, pp. 46–56, Jan. 2007.
[126] E. Lojou and P. Bianco, “Key role of the anchoring PEI layer on the electrochemistry of redox proteins at carbon electrodes Consequences on assemblies involving proteins and clay,” *Electrochimica Acta*, vol. 52, no. 25, pp. 7307–7314, Sep. 2007.
[127] A. Trybała, L. Szyk-Warszyńska, and P. Warszyński, “The effect of anchoring PEI layer on the build-up of polyelectrolyte multilayer films at homogeneous and heterogeneous surfaces,” *Colloids and Surfaces A: Physicochemical and Engineering Aspects*, vol. 343, no. 1–3, pp. 127–132, Jul. 2009.
[128] P. Tryoen-Tóth et al., “Viability, adhesion, and bone phenotype of osteoblast-like cells on polyelectrolyte multilayer films,” *Journal of Biomedical Materials Research*, vol. 60, no. 4, pp. 657–667, Jun. 2002.
[129] C. Brunot, L. Ponsonnet, C. Lagneau, P. Farge, C. Picart, and B. Grosgogeat, “Cytotoxicity of polyethyleneimine (PEI), precursor base layer of polyelectrolyte multilayer films,” *Biomaterials*, vol. 28, no. 4, pp. 632–640, Feb. 2007.
[130] V. Moby, A. Kadi, N. de Isla, J. F. Stoltz, and P. Menu, “Polyelectrolyte multilayer films: Effect of the initial anchoring layer on the cell growth,” *Bio-Medical Materials and Engineering*, vol. 18, no. 4–5, pp. 199–204, Jan. 2008.
[131] E. Kharlampieva and S. A. Sukhishvili, “Hydrogen-bonded layer-by-layer polymer films,” *Journal of Macromolecular Science, Part C: Polymer Reviews*, vol. 46, no. 4, pp. 377–395, Dec. 2006.
[132] N. Sardar, M. Kamil, Kabir-ud-Din, and M. S. Ali, “Solution behavior of nonionic polymer hydroxypropylmethyl cellulose: Effect of salts on the energetics at the cloud point,” *Journal of Chemical and Engineering Data*, vol. 56, no. 4, pp. 984–987, 2011.
[133] P. Tatar Güner, A. Mikó, F. F. Schweinberger, and A. L. Demirel, “Self-assembled poly(2-ethyl-2-oxazoline) fibers in aqueous solutions,” *Polymer Chemistry*, pp. 2–4, 2012.
[134] M. Nagvekar, F. Tihminlioglu, and R. P. Danner, “Colligative properties of polyelectrolyte solutions,” *Fluid Phase Equilibria*, vol. 145, no. 1, pp. 15–41, Mar. 1998.
[135] A. V. Dobrynin and M. Rubinstein, “Theory of polyelectrolytes in solutions and at surfaces,” *Progress in Polymer Science*, vol. 30, no. 11, pp. 1049–1118, Nov. 2005.
[136] M. R. Böhmer, O. A. Evers, and J. M. H. M. Scheutjens, “Weak polyelectrolytes between two surfaces: adsorption and stabilization,” *Macromolecules*, vol. 23, no. 8, pp. 2288–2301, Apr. 1990.
[137] A. W. P. Vermeer, F. A. M. Leermakers, and L. K. Koopal, “Adsorption of weak polyelectrolytes on surfaces with a variable charge. Self-consistent-field calculations,” *Langmuir*, vol. 13, no. 16, pp. 4413–4421, Aug. 1997.
[138] S. A. Sukhishvili and S. Granick, “Layered, erasable, ultrathin polymer films,” *Journal of the American Chemical Society*, vol. 122, no. 39, pp. 9550–9551, Oct. 2000.
[139] S. A. Sukhishvili and S. Granick, “Layered, erasable polymer multilayers formed by hydrogen-bonded sequential self-assembly,” *Macromolecules*, vol. 35, no. 1, pp. 301–310, Jan. 2002.
[140] G. S. Manning, “Limiting laws and counterion condensation in polyelectrolyte solutions I. Colligative properties,” *The Journal of Chemical Physics*, vol. 51, no. 3, p. 924 (10pp), 1969.
[141] G. S. Manning, “Limiting laws and counterion condensation in polyelectrolyte solutions II. Self-diffusion of the small ions,” *The Journal of Chemical Physics*, vol. 51, no. 3, p. 934 (5pp), 1969.
[142] G. S. Manning, “Limiting laws and counterion condensation in polyelectrolyte solutions. III. An analysis based on the Mayer ionic solution theory,” *The Journal of Chemical Physics*, vol. 51, no. 8, p. 3249 (4pp), 1969.
[143] Y. Zhang and P. S. Cremer, “Interactions between macromolecules and ions: The Hofmeister series,” *Current Opinion in Chemical Biology*, vol. 10, no. 6, pp. 658–663, Dec. 2006.
[144] M. Salomäki, P. Tervasmäki, S. Areva, and J. Kankare, “The Hofmeister anion effect and the

growth of polyelectrolyte multilayers," *Langmuir*, vol. 20, no. 9, pp. 3679–3683, Apr. 2004.
[145] J. B. Schlenoff, A. H. Rmaile, and C. B. Bucur, "Hydration contributions to association in polyelectrolyte multilayers and complexes: Visualizing hydrophobicity," *Journal of the American Chemical Society*, vol. 130, no. 41, pp. 13589–13597, Oct. 2008.
[146] J. E. Wong, H. Zastrow, W. Jaeger, and R. von Klitzing, "Specific ion versus electrostatic effects on the construction of polyelectrolyte multilayers," *Langmuir*, vol. 25, no. 24, pp. 14061–14070, Dec. 2009.
[147] J. B. Schlenoff and S. T. Dubas, "Mechanism of polyelectrolyte multilayer growth: Charge overcompensation and distribution," *Macromolecules*, vol. 34, no. 3, pp. 592–598, 2001.
[148] S. T. Dubas and J. B. Schlenoff, "Swelling and smoothing of polyelectrolyte multilayers by salt," *Langmuir*, vol. 17, no. 25, pp. 7725–7727, 2001.
[149] R. Steitz, W. Jaeger, and R. von Klitzing, "Influence of charge density and ionic strength on the multilayer formation of strong polyelectrolytes," *Langmuir*, vol. 17, no. 15, pp. 4471–4474, 2001.
[150] T. Serizawa, M. Yamaguchi, and M. Akashi, "Alternating bioactivity of polymeric layer-by-layer assemblies: Anticoagulation vs procoagulation of human blood," *Biomacromolecules*, vol. 3, no. 4, pp. 724–731, 2002.
[151] Z. Xu, C. Hu, and H. Guoxin, "Layer-by-layer self-assembly of multilayer films based on humic acid," *Thin Solid Films*, vol. 519, no. 13, pp. 4324–4328, Apr. 2011.
[152] D. Yoo, S. S. Shiratori, and M. F. Rubner, "Controlling bilayer composition and surface wettability of sequentially adsorbed multilayers of weak polyelectrolytes," *Macromolecules*, vol. 31, no. 13, pp. 4309–4318, Jun. 1998.
[153] S. S. Shiratori and M. F. Rubner, "pH-Dependent thickness behavior of sequentially adsorbed layers of weak polyelectrolytes," *Macromolecules*, vol. 33, no. 11, pp. 4213–4219, May 2000.
[154] S. T. Dubas and J. B. Schlenoff, "Polyelectrolyte multilayers containing a weak polyacid: Construction and deconstruction," *Macromolecules*, vol. 34, no. 11, pp. 3736–3740, May 2001.
[155] J. Choi and M. F. Rubner, "Influence of the degree of ionization on weak polyelectrolyte multilayer assembly," *Macromolecules*, vol. 38, no. 1, pp. 116–124, Jan. 2005.
[156] S. Boddohi, C. E. Killingsworth, and M. J. Kipper, "Polyelectrolyte multilayer assembly as a function of pH and ionic strength using the polysaccharides chitosan and heparin," *Biomacromolecules*, vol. 9, no. 7, pp. 2021–2028, Jul. 2008.
[157] M. Lösche, J. Schmitt, G. Decher, W. G. Bouwman, and K. Kjaer, "Detailed structure of molecularly thin polyelectrolyte multilayer films on solid substrates as revealed by neutron reflectometry," *Macromolecules*, vol. 31, no. 25, pp. 8893–8906, Dec. 1998.
[158] H.-J. Butt, K. Graf, and M. Kappl, "Surface modification," in *Physics and Chemistry of Interfaces*, WILEY-VCH Verlag GmbH & Co. KGaA, 2003, pp. 206–222.
[159] L. J. Kirwan, G. Papastavrou, M. Borkovec, and S. H. Behrens, "Imaging the coil-to-globule conformational transition of a weak polyelectrolyte by tuning the polyelectrolyte charge density," *Nano Letters*, vol. 4, no. 1, pp. 149–152, Jan. 2004.
[160] S. Wang, S. Granick, and J. Zhao, "Charge on a weak polyelectrolyte," *The Journal of Chemical Physics*, vol. 129, no. 24, p. 241102 (4pp), Dec. 2008.
[161] G. Decher, "Fuzzy nanoassemblies: Toward layered polymeric multicomposites," *Science*, vol. 277, no. 5330, pp. 1232–1237, 1997.
[162] T. R. Farhat and J. B. Schlenoff, "Ion transport and equilibria in polyelectrolyte multilayers," *Langmuir*, vol. 17, no. 4, pp. 1184–1192, Feb. 2001.
[163] H. W. Jomaa and J. B. Schlenoff, "Salt-induced polyelectrolyte interdiffusion in multilayered films: A neutron reflectivity study," *Macromolecules*, vol. 38, no. 20, pp. 8473–8480, Oct. 2005.
[164] R. von Klitzing, J. E. Wong, W. Jaeger, and R. Steitz, "Short range interactions in polyelectrolyte multilayers," *Current Opinion in Colloid and Interface Science*, vol. 9, no. 1–2, pp. 158–162, 2004.
[165] J. B. Schlenoff, H. Ly, and M. Li, "Charge and mass balance in polyelectrolyte multilayers," *Journal of the American Chemical Society*, vol. 120, no. 30, pp. 7626–7634, Aug. 1998.

[166] T. Farhat, G. Yassin, S. T. Dubas, and J. B. Schlenoff, "Water and ion pairing in polyelectrolyte multilayers," *Langmuir*, vol. 15, no. 20, pp. 6621–6623, Sep. 1999.
[167] H. H. Rmaile and J. B. Schlenoff, "'Internal pKa's' in polyelectrolyte multilayers: Coupling protons and salt," *Langmuir*, vol. 18, no. 22, pp. 8263–8265, Oct. 2002.
[168] J. A. Jaber and J. B. Schlenoff, "Counterions and water in polyelectrolyte multilayers: A tale of two polycations," *Langmuir*, vol. 23, no. 2, pp. 896–901, Jan. 2007.
[169] G. Ibarz, L. Dähne, E. Donath, and H. Möhwald, "Smart micro- and nanocontainers for storage, transport, and release," *Advanced Materials*, vol. 13, no. 17, pp. 1324–1327, Sep. 2001.
[170] J. J. Bikerman, "On the formation and structure of multilayers," *Proceedings of the Royal Society of London. Series A, Mathematical and Physical Sciences*, vol. 170, no. 940, pp. 130–144, 1939.
[171] M. Schönhoff, "Self-assembled polyelectrolyte multilayers," *Current Opinion in Colloid and Interface Science*, vol. 8, no. 1, pp. 86–95, 2003.
[172] B. S. Shim et al., "Nanostructured thin films made by dewetting method of layer-by-layer assembly," *Nano Letters*, vol. 7, no. 11, pp. 3266–3273, Nov. 2007.
[173] Y. H. Ko, Y. H. Kim, J. Park, K. T. Nam, J. H. Park, and P. J. Yoo, "Electric-field-assisted layer-by-layer assembly of weakly charged polyelectrolyte multilayers," *Macromolecules*, vol. 44, no. 8, pp. 2866–2872, Apr. 2011.
[174] J. B. Schlenoff, S. T. Dubas, and T. Farhat, "Sprayed polyelectrolyte multilayers," *Langmuir*, vol. 16, no. 26, pp. 9968–9969, 2000.
[175] A. Izquierdo, S. S. Ono, J.-C. Voegel, P. Schaaf, and G. Decher, "Dipping versus spraying: Exploring the deposition conditions for speeding up layer-by-layer assembly," *Langmuir*, vol. 21, no. 16, pp. 7558–7567, 2005.
[176] O. Félix, Z. Zheng, F. Cousin, and G. Decher, "Are sprayed LbL-films stratified? A first assessment of the nanostructure of spray-assembled multilayers by neutron reflectometry," *Comptes Rendus Chimie*, vol. 12, no. 1–2, pp. 225–234, Jan. 2009.
[177] J. Cho, K. Char, J.-D. Hong, and K.-B. Lee, "Fabrication of highly ordered multilayer films using a spin self-assembly method," *Advanced Materials*, vol. 13, no. 14, pp. 1076–1078, 2001.
[178] P. A. Chiarelli, M. S. Johal, J. L. Casson, J. B. Roberts, J. M. Robinson, and H.-L. Wang, "Controlled fabrication of polyelectrolyte multilayer thin films using spin-assembly," *Advanced Materials*, vol. 13, no. 15, pp. 1167–1171, 2001.
[179] A. G. Emslie, F. T. Bonner, and L. G. Peck, "Flow of a viscous liquid on a rotating disk," *Journal of Applied Physics*, vol. 29, no. 5, p. 858, 1958.
[180] B. D. Washo, "Rheology and modeling of the spin coating process," *IBM Journal of Research and Development*, vol. 21, no. 2, pp. 190–198, Mar. 1977.
[181] T. J. Rehg and B. G. Higgins, "The effects of inertia and interfacial shear on film flow on a rotating disk," *Physics of Fluids*, vol. 31, no. 6, p. 1360, 1988.
[182] D. E. Bornside, C. W. Macosko, and L. E. Scriven, "Spin coating: One-dimensional model," *Journal of Applied Physics*, vol. 66, no. 11, p. 5185, 1989.
[183] T. Ohara, Y. Matsumoto, and H. Ohashi, "The film formation dynamics in spin coating," *Physics of Fluids A: Fluid Dynamics*, vol. 1, no. 12, pp. 1949–1959, 1989.
[184] D. B. Hall, P. Underhill, and J. M. Torkelson, "Spin coating of thin and ultrathin polymer films," *Polymer Engineering and Science*, vol. 38, no. 12, pp. 2039–2045, Dec. 1998.
[185] D. W. Schubert and T. Dunkel, "Spin coating from a molecular point of view: its concentration regimes, influence of molar mass and distribution," *Materials Research Innovations*, vol. 7, no. 5, pp. 314–321, Oct. 2003.
[186] K. Norrman, A. Ghanbari-Siahkali, and N. B. Larsen, "Studies of spin-coated polymer films," *Annual Reports Section "C" (Physical Chemistry)*, vol. 101, pp. 174–201, 2005.
[187] J. Cho et al., "Quantitative analysis on the adsorbed amount and structural characteristics of spin self-assembled multilayer films," *Polymer*, vol. 44, no. 18, pp. 5455–5459, Aug. 2003.
[188] S.-S. Lee, K.-B. Lee, and J.-D. Hong, "Evidence for spin coating electrostatic self-assembly of

polyelectrolytes," *Langmuir*, vol. 19, no. 18, pp. 7592–7596, Sep. 2003.
[189] C. J. Lefaux, J. A. Zimberlin, A. V. Dobrynin, and P. T. Mather, "Polyelectrolyte spin assembly: Influence of ionic strength on the growth of multilayered thin films," *Journal of Polymer Science Part B: Polymer Physics*, vol. 42, no. 19, pp. 3654–3666, Oct. 2004.
[190] J. Seo, J. L. Lutkenhaus, J. Kim, P. T. Hammond, and K. Char, "Effect of the layer-by-layer (LbL) deposition method on the surface morphology and wetting behavior of hydrophobically modified PEO and PAA LbL films," *Langmuir*, vol. 24, no. 15, pp. 7995–8000, 2008.
[191] E. Kharlampieva, V. Kozlovskaya, J. Chan, J. F. Ankner, and V. V. Tsukruk, "Spin-assisted layer-by-layer assembly: Variation of stratification as studied with neutron reflectivity," *Langmuir*, vol. 25, no. 24, pp. 14017–14024, Dec. 2009.
[192] B. S. Dandapat and S. Maity, "Effects of air-flow and evaporation on the development of thin liquid film over a rotating annular disk," *International Journal of Non-Linear Mechanics*, vol. 44, no. 8, pp. 877–882, Oct. 2009.
[193] V. Cregan and S. B. G. O'Brien, "A note on spin-coating with small evaporation," *Journal of Colloid and Interface Science*, vol. 314, no. 1, pp. 324–328, 2007.
[194] M. H. Merrill and C. T. Sun, "Fast, simple and efficient assembly of nanolayered materials and devices," *Nanotechnology*, vol. 20, no. 7, p. 075606 (7pp), 2009.
[195] A. Nabok, "Structural Study of Organic/Inorganic Nanocomposites," in *Organic and Inorganic Nanostructures*, Artech House, Incorporated, 2005.
[196] V. V. Tsukruk, V. N. Bliznyuk, D. Visser, A. L. Campbell, T. J. Bunning, and W. W. Adams, "Electrostatic deposition of polyionic monolayers on charged surfaces," *Macromolecules*, vol. 30, no. 21, pp. 6615–6625, Oct. 1997.
[197] C. Picart et al., "Buildup mechanism for poly(l-lysine)/hyaluronic acid films onto a solid surface," *Langmuir*, vol. 17, no. 23, pp. 7414–7424, Nov. 2001.
[198] P. Lavalle et al., "Comparison of the structure of polyelectrolyte multilayer films exhibiting a linear and an exponential growth regime: An in situ atomic force microscopy study," *Macromolecules*, vol. 35, no. 11, pp. 4458–4465, May 2002.
[199] C. Picart et al., "Molecular basis for the explanation of the exponential growth of polyelectrolyte multilayers," *Proceedings of the National Academy of Sciences of the United States of America*, vol. 99, no. 20, pp. 12531–12535, 2002.
[200] D. T. Haynie, E. Cho, and P. Waduge, "'In and out diffusion' hypothesis of exponential multilayer film buildup revisited," *Langmuir*, vol. 27, no. 9, pp. 5700–5704, May 2011.
[201] L. Kolarik, D. N. Furlong, H. Joy, C. Struijk, and R. Rowe, "Building assemblies from high molecular weight polyelectrolytes," *Langmuir*, vol. 15, no. 23, pp. 8265–8275, Nov. 1999.
[202] J. Ruths, F. Essler, G. Decher, and H. Riegler, "Polyelectrolytes I: Polyanion/polycation multilayers at the air/monolayer/water interface as elements for quantitative polymer adsorption studies and preparation of hetero-superlattices on solid surfaces," *Langmuir*, vol. 16, no. 23, pp. 8871–8878, Nov. 2000.
[203] P. Bieker and M. Schönhoff, "Linear and exponential growth regimes of multilayers of weak polyelectrolytes in dependence on pH," *Macromolecules*, vol. 43, no. 11, pp. 5052–5059, Jun. 2010.
[204] I. Choi, R. Suntivich, F. A. Plamper, C. V. Synatschke, A. H. E. Müller, and V. V. Tsukruk, "pH-Controlled exponential and linear growing modes of layer-by-layer assemblies of star polyelectrolytes," *Journal of the American Chemical Society*, vol. 133, no. 24, pp. 9592–9606, Jun. 2011.
[205] C. Porcel, P. Lavalle, G. Decher, B. Senger, J.-C. Voegel, and P. Schaaf, "Influence of the polyelectrolyte molecular weight on exponentially growing multilayer films in the linear regime," *Langmuir*, vol. 23, no. 4, pp. 1898–1904, Mar. 2007.
[206] C. Porcel et al., "From exponential to linear growth in polyelectrolyte multilayers," *Langmuir*, vol. 22, no. 9, pp. 4376–4383, Apr. 2006.
[207] M. Lundin, E. Blomberg, and R. D. Tilton, "Polymer dynamics in layer-by-layer assemblies of chitosan and heparin," *Langmuir*, vol. 26, no. 5, pp. 3242–3451, Mar. 2010.
[208] J. J. Cerdà, B. Qiao, and C. Holm, "Understanding polyelectrolyte multilayers: an open

challenge for simulations," *Soft Matter*, vol. 5, no. 22, pp. 4412–4425, 2009.
[209] J. J. Cerdà, B. Qiao, and C. Holm, "Modeling strategies for polyelectrolyte multilayers," *The European Physical Journal Special Topics*, vol. 177, no. 1, pp. 129–148, Oct. 2009.
[210] K. Ariga, Y. Lvov, and T. Kunitake, "Assembling alternate dye-polyion molecular films by electrostatic layer-by-layer adsorption," *Journal of the American Chemical Society*, vol. 119, no. 9, pp. 2224–2231, Mar. 1997.
[211] D. Kovacevic, S. van der Burgh, A. de Keizer, and M. A. Cohen Stuart, "Kinetics of formation and dissolution of weak polyelectrolyte multilayers: Role of salt and free polyions," *Langmuir*, vol. 18, no. 14, pp. 5607–5612, Jul. 2002.
[212] L. Richert et al., "Layer by layer buildup of polysaccharide films: physical chemistry and cellular adhesion aspects," *Langmuir*, vol. 20, no. 2, pp. 448–458, Jan. 2004.
[213] T. Shutava, M. Prouty, D. Kommireddy, and Y. Lvov, "pH responsive decomposable layer-by-layer nanofilms and capsules on the basis of tannic acid," *Macromolecules*, vol. 38, no. 7, pp. 2850–2858, Apr. 2005.
[214] O. Svensson, L. Lindh, M. Cárdenas, and T. Arnebrant, "Layer-by-layer assembly of mucin and chitosan–Influence of surface properties, concentration and type of mucin," *Journal of Colloid and Interface Science*, vol. 299, no. 2, pp. 608–616, Jul. 2006.
[215] C. C. Buron, F. Membrey, C. Filiâtre, and A. Foissy, "A new approach to determine the mean thickness and refractive index of polyelectrolyte multilayer using optical reflectometry," *Colloids and Surfaces A: Physicochemical and Engineering Aspects*, vol. 289, no. 1–3, pp. 163–171, Oct. 2006.
[216] T. G. Shutava, S. S. Balkundi, and Y. M. Lvov, "(-)-Epigallocatechin gallate/gelatin layer-by-layer assembled films and microcapsules.," *Journal of Colloid and Interface Science*, vol. 330, no. 2, pp. 276–83, Feb. 2009.
[217] J. Zhu, B. S. Shim, M. Di Prima, and N. A. Kotov, "Transparent conductors from carbon nanotubes LBL-assembled with polymer dopant with π-π electron transfer," *Journal of the American Chemical Society*, vol. 133, no. 19, pp. 7450–7460, May 2011.
[218] A. Rothen, "The ellipsometer, an apparatus to measure thicknesses of thin surface films," *Review of Scientific Instruments*, vol. 16, no. 2, p. 26 (5pp), 1945.
[219] K. Vedam, "Spectroscopic ellipsometry: a historical overview," *Thin Solid Films*, vol. 313–314, no. 1–2, pp. 1–9, Feb. 1998.
[220] R. M. A. Azzam, "The intertwined history of polarimetry and ellipsometry," *Thin Solid Films*, vol. 519, no. 9, pp. 2584–2588, Feb. 2011.
[221] J. A. Woollam, C. Bungay, J. Hilfiker, and T. Tiwald, "VUV and IR spectroellipsometric studies of polymer surfaces," *Nuclear Instruments and Methods in Physics Research Section B: Beam Interactions with Materials and Atoms*, vol. 208, pp. 35–39, Aug. 2003.
[222] J. M. M. de Nijs and A. van Silfhout, "Systematic and random errors in rotating-analyzer ellipsometry," *Journal of the Optical Society of America A: Optics, Image Science, and Vision*, vol. 5, no. 6, pp. 773–781, 1988.
[223] R. W. Collins and Y.-T. Kim, "Ellipsometry for thin-film and surface analysis," *Analytical Chemistry*, vol. 62, no. 17, p. 887A–890A, Sep. 1990.
[224] B. Johs and C. M. Herzinger, "Quantifying the accuracy of ellipsometer systems," *Physica Status Solidi (C) - Current Topics in Solid State Physics*, vol. 5, no. 5, pp. 1031–1035, May 2008.
[225] H. Fujiwara, *Spectroscopic Ellipsometry: Principles and Applications*. John Wiley & Sons Ltd, 2007.
[226] T. A. Mykhaylyk, N. L. Dmitruk, S. D. Evans, I. W. Hamley, and J. R. Henderson, "Comparative characterisation by atomic force microscopy and ellipsometry of soft and solid thin films," *Surface and Interface Analysis*, vol. 39, no. 7, pp. 575–581, 2007.
[227] X. Ming et al., "Accurate determination of film thickness by low-angle X-ray reflection," *Chinese Physics*, vol. 9, no. 11, pp. 833–836, 2000.
[228] A. Gibaud and S. Hazra, "X-ray reflectivity and diffuse scattering," *Current Science*, vol. 78, no. 12, pp. 1467–1477, Feb. 2000.

[229] P. Podsiadlo et al., “Highly ductile multilayered films by layer-by-layer assembly of oppositely charged polyurethanes for biomedical applications,” *Langmuir*, vol. 25, no. 24, pp. 14093–14099, Dec. 2009.

[230] S. N. Magonov and D. H. Reneker, “Characterization of polymer surfaces with atomic force microscopy,” *Annual Review of Materials Science*, vol. 27, no. 1, pp. 175–222, Aug. 1997.

[231] G. Binnig, C. F. Quate, and C. Gerber, “Atomic force microscope,” *Physical Review Letters*, vol. 56, no. 9, pp. 930–933, 1986.

[232] G. Meyer and N. M. Amer, “Novel optical approach to atomic force microscopy,” *Applied Physics Letters*, vol. 53, no. 12, p. 1045 (3pp), 1988.

[233] K. D. Jandt, “Atomic force microscopy of biomaterials surfaces and interfaces,” *Surface Science*, vol. 491, no. 3, pp. 303–332, Oct. 2001.

[234] M. E. Greene, C. R. Kinser, D. E. Kramer, L. S. C. Pingree, and M. C. Hersam, “Application of scanning probe microscopy to the characterization and fabrication of hybrid nanomaterials,” *Microscopy Research and Technique*, vol. 64, no. 5–6, pp. 415–434, Aug. 2004.

[235] J. L. Hutter and J. Bechhoefer, “Calibration of atomic-force microscope tips,” *Review of Scientific Instruments*, vol. 64, no. 7, pp. 1868–1873, 1993.

[236] J. E. Sader, J. W. M. Chon, and P. Mulvaney, “Calibration of rectangular atomic force microscope cantilevers,” *Review of Scientific Instruments*, vol. 70, no. 10, pp. 3967–3969, 1999.

[237] W. R. Bowen and N. Hilal, *Atomic Force Microscopy in Process Engineering: Introduction to AFM for Improved Processes and Products*, vol. 1, no. 6. Butterworth Heinemann, 2009, pp. 624–649.

[238] B. Cappella and G. Dietler, “Force-distance curves by atomic force microscopy,” *Surface Science Reports*, vol. 34, no. 1–3, pp. 1–3, 5–104, Jan. 1999.

[239] M. Lösche, “Protein monolayers at interfaces,” *Current Opinion in Solid State and Materials Science*, vol. 2, no. 5, pp. 546–556, 1997.

[240] B. Kasemo, “Biological surface science,” *Current Opinion in Solid State and Materials Science*, vol. 3, no. 5, pp. 451–459, Oct. 1998.

[241] M. T. Thompson, M. C. Berg, I. S. Tobias, M. F. Rubner, and K. J. Van Vliet, “Tuning compliance of nanoscale polyelectrolyte multilayers to modulate cell adhesion,” *Biomaterials*, vol. 26, no. 34, pp. 6836–6845, Dec. 2005.

[242] M. T. Thompson, M. C. Berg, I. S. Tobias, J. A. Lichter, M. F. Rubner, and K. J. Van Vliet, “Biochemical functionalization of polymeric cell substrata can alter mechanical compliance,” *Biomacromolecules*, vol. 7, no. 6, pp. 1990–1995, Jun. 2006.

[243] D. E. Discher, P. Janmey, and Y.-L. Wang, “Tissue cells feel and respond to the stiffness of their substrate.,” *Science*, vol. 310, no. 5751, pp. 1139–1143, Nov. 2005.

[244] V. Vogel and M. Sheetz, “Local force and geometry sensing regulate cell functions.,” *Nature Reviews Molecular Cell Biology*, vol. 7, no. 4, pp. 265–275, Apr. 2006.

[245] B. Bhushan and X. Li, “Nanomechanical characterisation of solid surfaces and thin films,” *International Materials Reviews*, vol. 48, no. 3, pp. 125–164, Jun. 2003.

[246] A.-Y. Jee and M. Lee, “Comparative analysis on the nanoindentation of polymers using atomic force microscopy,” *Polymer Testing*, vol. 29, no. 1, pp. 95–99, Feb. 2010.

[247] N. A. Burnham, R. J. Colton, and H. M. Pollock, “Interpretation of force curves in force microscopy,” *Nanotechnology*, vol. 4, no. 2, pp. 64–80, 1993.

[248] M. S. Bobji and S. K. Biswas, “Estimation of hardness by nanoindentation of rough surfaces,” *Journal of Materials Research*, vol. 13, no. 11, pp. 3227–3233, Nov. 1998.

[249] E. Riedo, J. Chevrier, F. Comin, and H. Brune, “Nanotribology of carbon based thin films: the influence of film structure and surface morphology,” *Surface Science*, vol. 477, no. 1, pp. 25–34, Apr. 2001.

[250] H.-J. Butt, B. Cappella, and M. Kappl, “Force measurements with the atomic force microscope: Technique, interpretation and applications,” *Surface Science Reports*, vol. 59, no. 1–6, pp. 1–152, Oct. 2005.

[251] O. Mermut, J. Lefebvre, D. G. Gray, and C. J. Barrett, “Structural and mechanical properties of

polyelectrolyte multilayer films studied by AFM," *Macromolecules*, vol. 36, no. 23, pp. 8819–8824, Nov. 2003.

[252] L. Richert, A. J. Engler, D. E. Discher, and C. Picart, "Elasticity of native and cross-linked polyelectrolyte multilayer films," *Biomacromolecules*, vol. 5, no. 5, pp. 1908–1916, 2004.

[253] X. Dai, Y. Zhang, Y. Guan, S. Yang, and J. Xu, "Mechanical properties of polyelectrolyte multilayer self-assembled films," *Thin Solid Films*, vol. 474, no. 1–2, pp. 159–164, Mar. 2005.

[254] Y. Lvov, G. Decher, H. Haas, H. Möhwald, and A. Kalachev, "X-ray analysis of ultrathin polymer films self-assembled onto substrates," *Physica B: Condensed Matter*, vol. 198, no. 1–3, pp. 89–91, 1994.

[255] D. Korneev, Y. Lvov, G. Decher, J. Schmitt, and S. Yaradaikin, "Neutron reflectivity analysis of self-assembled film superlattices with alternate layers of deuterated and hydrogenated polysterenesulfonate and polyallylamine," *Physica B: Condensed Matter*, vol. 213–214, pp. 954–956, Aug. 1995.

[256] K. Lowack and C. A. Helm, "Molecular mechanisms controlling the self-assembly process of polyelectrolyte multilayers," *Macromolecules*, vol. 31, no. 3, pp. 823–833, 1998.

[257] G. Decher, B. Lehr, K. Lowack, Y. Lvov, and J. Schmitt, "New nanocomposite films for biosensors: layer-by-layer adsorbed films of polyelectrolytes, proteins or DNA," *Biosensors and Bioelectronics*, vol. 9, no. 9–10, pp. 677–684, Jan. 1994.

[258] Z. Tang, Y. Wang, P. Podsiadlo, and N. A. Kotov, "Biomedical applications of layer-by-layer assembly: From biomimetics to tissue engineering," *Advanced Materials*, vol. 18, no. 24, pp. 3203–3224, Dec. 2006.

[259] J. A. Lichter, K. J. Van Vliet, and M. F. Rubner, "Design of antibacterial surfaces and interfaces: Polyelectrolyte multilayers as a multifunctional platform," *Macromolecules*, vol. 42, no. 22, pp. 8573–8586, Nov. 2009.

[260] T. Boudou, T. Crouzier, K. Ren, G. Blin, and C. Picart, "Multiple functionalities of polyelectrolyte multilayer films: new biomedical applications," *Advanced Materials*, vol. 22, no. 4, pp. 441–467, Jan. 2010.

[261] V. K. Vendra, L. Wu, and S. Krishnan, "Polymer thin films for biomedical applications," in *Nanostructured Thin Films and Surfaces.*, vol. 5, C. S. S. R. Kumar, Ed. Weinheim, Germany: WILEY-VCH Verlag GmbH & Co. KGaA, 2010, pp. 1–54.

[262] M. Gao, X. Zhang, B. Yang, and J. Shen, "A monolayer of PbI2 nanoparticles adsorbed on MD-LB film," *Journal of the Chemical Society, Chemical Communications*, no. 19, pp. 2229–2230, 1994.

[263] V. Krstic, G. S. Duesberg, J. Muster, M. Burghard, and S. Roth, "Langmuir−Blodgett films of matrix-diluted single-walled carbon nanotubes," *Chemistry of Materials*, vol. 10, no. 9, pp. 2338–2340, Sep. 1998.

[264] L. Hu, D. S. Hecht, and G. Grüner, "Carbon nanotube thin films: Fabrication, properties, and applications," *Chemical Reviews*, vol. 110, no. 10, pp. 5790–5844, 2010.

[265] M. Gao, M. Gao, X. Zhang, Y. Yang, B. Yang, and J. Shen, "Constructing PbI2 nanoparticles into a multilayer structure using the molecular deposition (MD) method," *Journal of the Chemical Society, Chemical Communications*, no. 24, pp. 2777–2778, 1994.

[266] E. R. Kleinfeld and G. S. Ferguson, "Stepwise formation of multilayered nanostructural films from macromolecular precursors," *Science*, vol. 265, no. 5170, pp. 370–373, Jul. 1994.

[267] S. W. Keller, H.-N. Kim, and T. E. Mallouk, "Layer-by-Layer Assembly of intercalation compounds and heterostructures on surfaces: Toward molecular‘ beaker’ epitaxy," *Journal of the American Chemical Society*, vol. 116, no. 19, pp. 8817–8818, Sep. 1994.

[268] N. A. Kotov, I. Dekany, and J. H. Fendler, "Layer-by-layer self-assembly of polyelectrolyte-semiconductor nanoparticle composite films," *The Journal of Physical Chemistry*, vol. 99, no. 35, pp. 13065–13069, Aug. 1995.

[269] D. L. Feldheim, K. C. Grabar, M. J. Natan, and T. E. Mallouk, "Electron transfer in self-assembled inorganic polyelectrolyte/metal nanoparticle heterostructures," *Journal of the American Chemical Society*, vol. 118, no. 32, pp. 7640–7641, Jan. 1996.

[270] Y. Lvov, K. Ariga, M. Onda, I. Ichinose, and T. Kunitake, "Alternate assembly of ordered

multilayers of SiO2 and other nanoparticlesn and polyions," *Langmuir*, vol. 13, no. 23, pp. 6195–6203, Nov. 1997.

[271] Y. Liu, A. Wang, and R. O. Claus, "Layer-by-layer electrostatic self-assembly of nanoscale Fe3O4 particles and polyimide precursor on silicon and silica surfaces," *Applied Physics Letters*, vol. 71, no. 16, p. 2265 (3pp), 1997.

[272] J. Schmitt et al., "Metal nanoparticle/polymer superlattice films: Fabrication and control of layer structure," *Advanced Materials*, vol. 9, no. 1, pp. 61–65, Jul. 1997.

[273] N. A. Kotov, S. Magonov, and E. Tropsha, "Layer-by-layer self-assembly of alumosilicate-polyelectrolyte composites: Mechanism of deposition, crack resistance, and perspectives for novel membrane materials," *Chemistry of Materials*, vol. 10, no. 3, pp. 886–895, Mar. 1998.

[274] K. Ariga, Y. Lvov, I. Ichinose, and T. Kunitake, "Ultrathin films of inorganic materials (SiO2 nanoparticle, montmorillonite microplate, and molybdenum oxide) prepared by alternate layer-by-layer assembly with organic polyions," *Applied Clay Science*, vol. 15, no. 1–2, pp. 137–152, Sep. 1999.

[275] Z. Tang, N. A. Kotov, S. Magonov, and B. Ozturk, "Nanostructured artificial nacre," *Nature Materials*, vol. 2, no. 6, pp. 413–418, Jun. 2003.

[276] P. Podsiadlo et al., "Layer-by-layer assembly of nacre-like nanostructured composites with antimicrobial properties," *Langmuir*, vol. 21, no. 25, pp. 11915–11921, Dec. 2005.

[277] P. Podsiadlo et al., "Ultrastrong and stiff layered polymer nanocomposites," *Science*, vol. 318, no. 5847, pp. 80–83, Oct. 2007.

[278] A. K. Kaushik et al., "The role of nanoparticle layer separation in the finite deformation response of layered polyurethane-clay nanocomposites," *Macromolecules*, vol. 42, no. 17, pp. 6588–6595, Sep. 2009.

[279] A. A. Mamedov, N. A. Kotov, M. Prato, D. M. Guldi, J. P. Wicksted, and A. Hirsch, "Molecular design of strong single-wall carbon nanotube/polyelectrolyte multilayer composites," *Nature Materials*, vol. 1, no. 3, pp. 190–194, 2002.

[280] E. Jan and N. A. Kotov, "Successful differentiation of mouse neural stem cells on layer-by-layer assembled single-walled carbon nanotube composite," *Nano Letters*, vol. 7, no. 5, pp. 1123–1128, May 2007.

[281] N. A. Kotov, "Ordered layered assemblies of nanoparticles," *MRS Bulletin*, vol. 26, no. 12, pp. 992–997, May 2001.

[282] S. Srivastava and N. A. Kotov, "Composite layer-by-layer (LBL) assembly with inorganic nanoparticles and nanowires," *Accounts of Chemical Research*, vol. 41, no. 12, pp. 1831–1841, 2008.

[283] P. Podsiadlo, B. S. Shim, and N. A. Kotov, "Polymer/clay and polymer/carbon nanotube hybrid organic–inorganic multilayered composites made by sequential layering of nanometer scale films," *Coordination Chemistry Reviews*, vol. 253, no. 23–24, pp. 2835–2851, Dec. 2009.

[284] E. Hao and T. Lian, "Layer-by-layer assembly of CdSe nanoparticles based on hydrogen bonding," *Langmuir*, vol. 16, no. 21, pp. 7879–7881, Oct. 2000.

[285] E. Hao and T. Lian, "Buildup of polymer/Au nanoparticle multilayer thin films based on hydrogen bonding," *Chemistry of Materials*, vol. 12, no. 11, pp. 3392–3396, Nov. 2000.

[286] S. Yang et al., "Composite thin film by hydrogen-bonding assembly of polymer brush and poly(vinylpyrrolidone)," *Langmuir*, vol. 22, no. 1, pp. 338–343, 2006.

[287] G. S. Irmukhametova, B. J. Fraser, J. L. Keddie, G. A. Mun, and V. V. Khutoryanskiy, "Hydrogen-bonding-driven self-assembly of PEGylated organosilica nanoparticles with poly(acrylic acid) in aqueous solutions and in layer-by-layer deposition at solid surfaces," *Langmuir*, vol. 28, no. 1, pp. 299–306, Jan. 2012.

[288] B. S. Shim et al., "Multiparameter structural optimization of single-walled carbon nanotube composites: toward record strength, stiffness, and toughness.," *ACS Nano*, vol. 3, no. 7, pp. 1711–1722, Jul. 2009.

[289] B. S. Shim, Z. Tang, V. Sinani, and N. A. Kotov, "Layer-by-layer assembly of single-wall carbon nanotube polymeric nanocomposites: Structural control and material properties," in *The 2005 Annual Meeting - 5th Topical Conference on Nanoscale Science and Engineering*, 2005.

[290] B. S. Shim, Z. Tang, M. P. Morabito, A. Agarwal, H. Hong, and N. A. Kotov, "Integration of conductivity, transparency, and mechanical strength into highly homogeneous layer-by-layer composites of single-walled carbon nanotubes for optoelectronics," *Chemistry of Materials*, vol. 19, no. 23, pp. 5467–5474, 2007.

[291] A. Ishibashi, Y. Yamaguchi, H. Murakami, and N. Nakashima, "Layer-by-layer assembly of RNA/single-walled carbon nanotube nanocomposites," *Chemical Physics Letters*, vol. 419, no. 4–6, pp. 574–577, Feb. 2006.

[292] N. Nakashima, "Solubilization of single-walled carbon nanotubes with condensed aromatic compounds," *Science and Technology of Advanced Materials*, vol. 7, no. 7, pp. 609–616, Oct. 2006.

[293] T. Henning and F. Salama, "Carbon in the universe," *Science*, vol. 282, no. 5397, pp. 2204–2210, Dec. 1998.

[294] W. Bains, "Many chemistries could be used to build living systems," *Astrobiology*, vol. 4, no. 2, pp. 137–167, Jan. 2004.

[295] T. Henning and M. Schnaiter, "Carbon - From space to laboratory," *Earth, Moon, and Planets*, vol. 80, no. 1–3, pp. 179–207, 1998.

[296] E. H. L. Falcao and F. Wudl, "Carbon allotropes: Beyond graphite and diamond," *Journal of Chemical Technology and Biotechnology*, vol. 82, no. 6, pp. 524–531, 2007.

[297] K. S. Novoselov et al., "Electric field effect in atomically thin carbon films," *Science*, vol. 306, no. 5696, pp. 666–669, Oct. 2004.

[298] S. Iijima, "Helical microtubules of graphitic carbon," *Nature*, vol. 354, pp. 56–58, 1991.

[299] R. B. Heimann, S. E. Evsyukov, and Y. Koga, "Carbon allotropes: a suggested classification scheme based on valence orbital hybridization," *Carbon*, vol. 35, no. 10–11, pp. 1654–1658, 1997.

[300] J. Robertson, "Diamond-like amorphous carbon," *Materials Science and Engineering: R: Reports*, vol. 37, no. 4–6, pp. 129–281, May 2002.

[301] M. Moniruzzaman and K. I. Winey, "Polymer nanocomposites containing carbon nanotubes," *Macromolecules*, vol. 39, no. 16, pp. 5194–5205, Aug. 2006.

[302] E. Joselevich, "Electronic structure and chemical reactivity of carbon nanotubes: A chemist's view," *ChemPhysChem: A European Journal of Chemical Physics and Physical Chemistry*, vol. 5, no. 5, pp. 619–624, May 2004.

[303] D. Ugarte, "Curling and closure of graphitic networks under electron-beam irradiation," *Nature*, vol. 359, pp. 707–709, 1992.

[304] M. S. Dresselhaus, G. Dresselhaus, and R. Saito, "Carbon fibers based on C60 and their symmetry," *Physical Review B*, vol. 45, no. 11, pp. 6234–6242, Mar. 1992.

[305] M. S. Dresselhaus, G. Dresselhaus, and R. Saito, "Physics of carbon nanotubes," *Carbon*, vol. 33, no. 7, pp. 883–891, 1995.

[306] S. Weber, *Steffen Weber's Crystallography Picture Book: Nanotubes & Nanocones*. Available at Official Website of JCrystalSoft, 2004.

[307] S. Weber, *Steffen Weber's Crystallography Picture Book: Fullerenes*. Available at Official Website of JCrystalSoft, 2004.

[308] M. Reibold, P. Paufler, A. A. Levin, W. Kochmann, N. Pätzke, and D. C. Meyer, "Materials: Carbon nanotubes in an ancient Damascus sabre," *Nature*, vol. 444, p. 286, Nov. 2006.

[309] J. D. Verhoeven, a. H. Pendray, and W. E. Dauksch, "The key role of impurities in ancient damascus steel blades," *Journal of the Minerals, Metals and Materials Society*, vol. 50, no. 9, pp. 58–64, Sep. 1998.

[310] L. Milgrom, "Carbon nanotubes: Saladin's secret weapon," *Chemistry World*, 2006.

[311] A. W. Hull, "A new method of X-ray crystal analysis," *Physical Review*, vol. 10, no. 6, pp. 661–696, Dec. 1917.

[312] L. Pauling, "The structure and properties of graphite and boron nitride," *Proceedings of the National Academy of Sciences of the United States of America*, vol. 56, no. 6, pp. 1646–1652, 1966.

[313] L. Pauling, "The structure of the chlorites," *Proceedings of the National Academy of Sciences*,

vol. 16, no. 9, pp. 578–582, Sep. 1930.
[314] L. V. Radushkevich and V. M. Lukyanovich, “About the structure of carbon formed by thermal decomposition of carbon monoxide on iron substrate [in Russian],” *Zhurnal Fizicheskoi Khimii [currently, Russian Journal of Physical Chemistry A. Focus on Chemistry]*, vol. 26, pp. 88–95, 1952.
[315] M. Monthioux and V. Kuznetsov, “Who should be given the credit for the discovery of carbon nanotubes?,” *Carbon*, vol. 44, no. 9, pp. 1621–1623, Aug. 2006.
[316] W. R. Davis, R. J. Slawson, and G. R. Rigby, “An unusual form of carbon,” *Nature*, vol. 171, pp. 756–756, Apr. 1953.
[317] J. A. E. Gibson, “Early nanotubes?,” *Nature*, vol. 359, no. 6394, pp. 369–369, Oct. 1992.
[318] H. P. Boehm, “The first observation of carbon nanotubes,” *Carbon*, vol. 35, no. 4, pp. 581–584, 1997.
[319] R. Bacon, “Growth, structure, and properties of graphite whiskers,” *Journal of Applied Physics*, vol. 31, no. 2, pp. 283–231, 1960.
[320] D. Colbert and R. Smalley, “Past, Present and Future of Fullerene Nanotubes: Buckytubes,” in *Perspectives of Fullerene Nanotechnology*, First Edit., E. Ōsawa, Ed. Kluwer Academic Publishers, 2002, pp. 3–10.
[321] W. Bollmann and J. Spreadborough, “Action of graphite as a lubricant,” *Nature*, vol. 186, pp. 29–30, Apr. 1960.
[322] E. Osawa, “Superaromaticity [in Japanese],” *Kagaku*, vol. 25, no. 9, pp. 854–863, 1970.
[323] H. W. Kroto, A. W. Allaf, and P. S. Balm, “C60: Buckminsterfullerene,” *Chemical Reviews*, vol. 91, no. 6, pp. 1213–1235, 1992.
[324] A. Oberlin, M. Endo, and T. Koyama, “Filamentous growth of carbon through benzene decomposition,” *Journal of Crystal Growth*, vol. 32, no. 3, pp. 335–349, Mar. 1976.
[325] E. A. Rohlfing, D. M. Cox, and A. Kaldor, “Production and characterization of supersonic carbon cluster beams,” *The Journal of Chemical Physics*, vol. 81, no. 7, p. 3322 (9pp), 1984.
[326] H. W. Kroto, J. R. Heath, S. C. O’Brien, R. F. Curl, and R. E. Smalley, “C60: Buckminsterfullerene,” *Nature*, vol. 318, pp. 162–163, 1985.
[327] W. Kratschmer, L. D. Lamb, K. Fostiropoulos, and D. R. Huffman, “Solid C60: a new form of carbon,” *Nature*, vol. 347, pp. 354–358, 1990.
[328] R. Taylor, J. P. Hare, A. K. Abdul-Sada, and H. W. Kroto, “Isolation, separation and characterisation of the fullerenes C60 and C70: the third form of carbon,” *Journal of the Chemical Society, Chemical Communications*, no. 20, pp. 1423–1425, 1990.
[329] S. Wang and P. R. Buseck, “Packing of C60 molecules and related fullerenes in crystals: a direct view,” *Chemical Physics Letters*, vol. 182, no. 1, pp. 1–4, Jul. 1991.
[330] T. Andersson, K. Nilsson, M. Sundahl, G. Westman, and O. Wennerström, “C60 embedded in gama-cyclodextrin: a water-soluble fullerene,” *Journal of the Chemical Society, Chemical Communications*, no. 8, p. 604, 1992.
[331] S. Iijima and T. Ichihashi, “Single-shell carbon nanotubes of 1-nm diameter,” *Nature*, vol. 363, pp. 603–605, 1993.
[332] D. S. Bethune et al., “Cobalt-catalysed growth of carbon nanotubes with single-atomic-layer walls,” *Nature*, vol. 363, pp. 605–607, 1993.
[333] T. Guo, P. Nikolaev, A. Thess, D. T. Colbert, and R. E. Smalley, “Catalytic growth of single-walled nanotubes by laser vaporization,” *Chemical Physics Letters*, vol. 243, no. 1–2, pp. 49–54, 1995.
[334] A. Thess et al., “Crystalline ropes of metallic carbon nanotubes,” *Science*, vol. 273, no. 5274, pp. 483–487, Jul. 1996.
[335] J.-M. Bonard et al., “Purification and size-selection of carbon nanotubes,” *Advanced Materials*, vol. 9, no. 10, pp. 827–831, 1997.
[336] B. Z. Tang and H. Xu, “Preparation, alignment, and optical properties of soluble poly(phenylacetylene)-wrapped carbon nanotubes,” *Macromolecules*, vol. 32, no. 8, pp. 2569–2576, Apr. 1999.
[337] M. J. O’Connell et al., “Reversible water-solubilization of single-walled carbon nanotubes by

polymer wrapping," *Chemical Physics Letters*, vol. 342, no. 3–4, pp. 265–271, 2001.
[338] P. G. Collins, M. S. Arnold, and P. Avouris, "Engineering carbon nanotubes and nanotube circuits using electrical breakdown," *Science*, vol. 292, no. 5517, pp. 706–709, Apr. 2001.
[339] R. J. Chen, Y. Zhang, D. Wang, and H. Dai, "Noncovalent sidewall functionalization of single-walled carbon nanotubes for protein immobilization," *Journal of the American Chemical Society*, vol. 123, no. 16, pp. 3838–3839, 2001.
[340] N. Nakashima, Y. Tomonari, and H. Murakami, "Water-soluble single-walled carbon nanotubes via noncovalent sidewall-functionalization with a pyrene-carrying ammonium ion," *Chemistry Letters*, vol. 31, no. 6, pp. 638–638, 2002.
[341] R. Tenne, L. Margulis, M. Genut, and G. Hodes, "Polyhedral and cylindrical structures of tungsten disulphide," *Nature*, vol. 360, pp. 444–446, Dec. 1992.
[342] N. G. Chopra et al., "Boron nitride nanotubes," *Science*, vol. 269, no. 5226, p. 966967, 1995.
[343] E. Joselevich, H. Dai, J. Liu, K. Hata, and A. H. Windle, "Carbon nanotube synthesis and organization," in *Carbon Nanotubes: Advanced Topics in the Synthesis, Structure, Properties, and Applications*, vol. 164, no. 2008, Berlin Heidelberg: Springer-Verlag, 2008, pp. 101–164.
[344] S. Karthikeyan, P. Mahalıngam, and M. Karthik, "Large scale synthesis of carbon nanotubes," *E-Journal of Chemistry*, vol. 6, no. 1, pp. 1–12, Jul. 2009.
[345] L. C. Qin, D. Zhou, A. R. Krauss, and D. M. Gruen, "Growing carbon nanotubes by microwave plasma-enhanced chemical vapor deposition," *Applied Physics Letters*, vol. 72, no. 26, pp. 3437–3439, 1998.
[346] M. J. Bronikowski, P. A. Willis, D. T. Colbert, K. A. Smith, and R. E. Smalley, "Gas-phase production of carbon single-walled nanotubes from carbon monoxide via the HiPco process: A parametric study," *Journal of Vacuum Science & Technology A: Vacuum, Surfaces, and Films*, vol. 19, no. 4, p. 1800, 2001.
[347] T. W. Ebbesen and P. M. Ajayan, "Large-scale synthesis of carbon nanotubes," *Nature*, vol. 358, no. 6383, pp. 220–222, 1992.
[348] C. Journet et al., "Large-scale production of single-walled carbon nanotubes by the electric-arc technique," *Nature*, vol. 388, no. 6644, pp. 756–757, 1997.
[349] C. D. Scott, S. Arepalli, P. Nikolaev, and R. E. Smalley, "Growth mechanisms for single-wall carbon nanotubes in a laser-ablation process," *Applied Physics A: Materials Science & Processing*, vol. 72, no. 5, pp. 573–580, May 2001.
[350] H. Dai, A. G. Rinzler, P. Nikolaev, A. Thess, D. T. Colbert, and R. E. Smalley, "Single-wall nanotubes produced by metal-catalyzed disproportionation of carbon monoxide," *Chemical Physics Letters*, vol. 260, no. 3–4, pp. 471–475, Sep. 1996.
[351] B. Kitiyanan, W. E. Alvarez, J. H. Harwell, and D. E. Resasco, "Controlled production of single-wall carbon nanotubes by catalytic decomposition of CO on bimetallic Co–Mo catalysts," *Chemical Physics Letters*, vol. 317, no. 3–5, pp. 497–503, Feb. 2000.
[352] S. Bandow, A. M. Rao, K. A. Williams, A. Thess, R. E. Smalley, and P. C. Eklund, "Purification of single-wall carbon nanotubes by microfiltration," *The Journal of Physical Chemistry B*, vol. 101, no. 44, pp. 8839–8842, Oct. 1997.
[353] H. Hu, B. Zhao, M. E. Itkis, and R. C. Haddon, "Nitric acid purification of single-walled carbon nanotubes," *The Journal of Physical Chemistry B*, vol. 107, no. 50, pp. 13838–13842, 2003.
[354] L. Bai, X. Ma, J. Liu, X. Sun, D. Zhao, and D. G. Evans, "Rapid separation and purification of nanoparticles in organic density gradients," *Journal of the American Chemical Society*, vol. 132, no. 7, pp. 2333–2337, 2010.
[355] M. Hanauer, S. Pierrat, I. Zins, A. Lotz, and C. Sönnichsen, "Separation of nanoparticles by gel electrophoresis according to size and shape," *Nano Letters*, vol. 7, no. 9, pp. 2881–2885, 2007.
[356] A. G. Rinzler et al., "Large-scale purification of single-wall carbon nanotubes: process, product, and characterization," *Applied Physics A: Materials Science & Processing*, vol. 67, no. 1, pp. 29–37, Jul. 1998.
[357] K. B. Shelimov, R. O. Esenaliev, A. G. Rinzler, C. B. Huffman, and R. E. Smalley, "Purification of single-wall carbon nanotubes by ultrasonically assisted filtration," *Chemical*

Physics Letters, vol. 282, no. 5–6, pp. 429–434, Jan. 1998.

[358] P. Hou, C. Liu, and H. Cheng, "Purification of carbon nanotubes," *Carbon*, vol. 46, no. 15, pp. 2003–2025, Dec. 2008.

[359] P. Chaturvedi, P. Verma, A. Singh, P. K. Chaudhary, and P. K. Basu, "Carbon nanotube–Purification and sorting protocols," *Defence Science Journal*, vol. 58, no. 5, pp. 591–599, 2008.

[360] C. Backes and A. Hirsch, "Noncovalent functionalization of carbon nanotubes," in *Chemistry of Nanocarbons*, vol. 113, T. Akasaka, F. Wudl, and S. Nagase, Eds. Chichester, UK: John Wiley & Sons, Ltd, 2010, pp. 1–48.

[361] M. J. Green, N. Behabtu, M. Pasquali, and W. W. Adams, "Nanotubes as polymers," *Polymer*, vol. 50, no. 21, pp. 4979–4997, 2009.

[362] S. D. Bergin et al., "Large populations of individual nanotubes in surfactant-based dispersions without the need for ultracentrifugation," *The Journal of Physical Chemistry C*, vol. 112, no. 4, pp. 972–977, Jan. 2008.

[363] M. C. Hersam, "Progress towards monodisperse single-walled carbon nanotubes," *Nature Nanotechnology*, vol. 3, no. 7, pp. 387–394, Jul. 2008.

[364] C.-H. Liu and H.-L. Zhang, "Chemical approaches towards single-species single-walled carbon nanotubes," *Nanoscale*, vol. 2, no. 10, pp. 1901–1918, Oct. 2010.

[365] O. Jost et al., "Diameter grouping in bulk samples of single-walled carbon nanotubes from optical absorption spectroscopy," *Applied Physics Letters*, vol. 75, no. 15, pp. 2217–2219, 1999.

[366] S. M. Bachilo, L. Balzano, J. E. Herrera, F. Pompeo, D. E. Resasco, and R. B. Weisman, "Narrow (n,m)-distribution of single-walled carbon nanotubes grown using a solid supported catalyst," *Journal of the American Chemical Society*, vol. 125, no. 37, pp. 11186–7, Sep. 2003.

[367] G. Lolli, L. Zhang, L. Balzano, N. Sakulchaicharoen, Y. Tan, and D. E. Resasco, "Tailoring (n,m) structure of single-walled carbon nanotubes by modifying reaction conditions and the nature of the support of CoMo catalysts," *The Journal of Physical Chemistry B*, vol. 110, no. 5, pp. 2108–2115, Feb. 2006.

[368] M. He et al., "Predominant (6,5) single-walled carbon nanotube growth on a copper-promoted iron catalyst," *Journal of the American Chemical Society*, vol. 132, no. 40, pp. 13994–13996, Oct. 2010.

[369] G. S. Duesberg, M. Burghard, J. Muster, G. Philipp, and S. Roth, "Separation of carbon nanotubes by size exclusion chromatography," *Chemical Communications*, no. 3, pp. 435–436, 1998.

[370] D. Chattopadhyay, S. Lastella, S. Kim, and F. Papadimitrakopoulos, "Length separation of zwitterion-functionalized single wall carbon nanotubes by GPC," *Journal of the American Chemical Society*, vol. 124, no. 5, pp. 728–729, Feb. 2002.

[371] J. A. Fagan et al., "Centrifugal length separation of carbon nanotubes," *Langmuir*, vol. 24, no. 24, pp. 13880–13889, Dec. 2008.

[372] D. A. Heller, R. M. Mayrhofer, S. Baik, Y. V. Grinkova, M. L. Usrey, and M. S. Strano, "Concomitant length and diameter separation of single-walled carbon nanotubes," *Journal of the American Chemical Society*, vol. 126, no. 44, pp. 14567–14573, Nov. 2004.

[373] M. S. Arnold, S. I. Stupp, and M. C. Hersam, "Enrichment of single-walled carbon nanotubes by diameter in density gradients," *Nano Letters*, vol. 5, no. 4, pp. 713–718, Apr. 2005.

[374] H. Yang, S. C. Wang, P. Mercier, and D. L. Akins, "Diameter-selective dispersion of single-walled carbon nanotubes using a water-soluble, biocompatible polymer," *Chemical Communications*, no. 13, pp. 1425–1457, Apr. 2006.

[375] D. Chattopadhyay, I. Galeska, and F. Papadimitrakopoulos, "A route for bulk separation of semiconducting from metallic single-wall carbon nanotubes," *Journal of the American Chemical Society*, vol. 125, no. 11, pp. 3370–3375, Mar. 2003.

[376] Y. Maeda et al., "Large-scale separation of metallic and semiconducting single-walled carbon nanotubes," *Journal of the American Chemical Society*, vol. 127, no. 29, pp. 10287–10290, Jul. 2005.

[377] M. S. Arnold, A. A. Green, J. F. Hulvat, S. I. Stupp, and M. C. Hersam, “Sorting carbon nanotubes by electronic structure using density differentiation,” *Nature Nanotechnology*, vol. 1, no. 1, pp. 60–5, Oct. 2006.

[378] A. L. Antaris, J.-W. T. Seo, A. A. Green, and M. C. Hersam, “Sorting single-walled carbon nanotubes by electronic type using nonionic, biocompatible block copolymers,” *ACS Nano*, vol. 4, no. 8, pp. 4725–4732, Aug. 2010.

[379] P. Zhao, E. Einarsson, R. Xiang, Y. Murakami, and S. Maruyama, “Controllable expansion of single-walled carbon nanotube dispersions using density gradient ultracentrifugation,” *The Journal of Physical Chemistry C*, vol. 114, no. 11, pp. 4831–4834, Mar. 2010.

[380] R. Krupke, F. Hennrich, H. v. Löhneysen, and M. M. Kappes, “Separation of metallic from semiconducting single-walled carbon nanotubes,” *Science*, vol. 301, no. 5631, pp. 344–347, Jul. 2003.

[381] S. K. Doorn, “Single-walled carbon nanotubes: Separation using capillary electrophoresis,” in *Dekker Encyclopedia of Nanoscience and Nanotechnology*, Marcel Dekker, Inc., 2004, pp. 3617–3628.

[382] Y. Lian et al., “Spectroscopic study on the centrifugal fractionation of soluble single-walled carbon nanotubes,” *Carbon*, vol. 43, no. 13, pp. 2750–2759, Nov. 2005.

[383] A. A. Green and M. C. Hersam, “Ultracentrifugation of single-walled nanotubes,” *Materials Today*, vol. 10, no. 12, pp. 59–60, Dec. 2007.

[384] N. Komatsu and F. Wang, “A comprehensive review on separation methods and techniques for single-walled carbon nanotubes,” *Materials*, vol. 3, no. 7, pp. 3818–3844, Jun. 2010.

[385] M. Zheng et al., “Structure-based carbon nanotube sorting by sequence-dependent DNA assembly,” *Science*, vol. 302, no. 5650, pp. 1545–1548, Nov. 2003.

[386] M. Zheng et al., “DNA-assisted dispersion and separation of carbon nanotubes,” *Nature Materials*, vol. 2, no. 5, pp. 338–342, May 2003.

[387] A. Nish, J.-Y. Hwang, J. Doig, and R. J. Nicholas, “Highly selective dispersion of single-walled carbon nanotubes using aromatic polymers,” *Nature Nanotechnology*, vol. 2, no. 10, pp. 640–646, Oct. 2007.

[388] M. Deza, M. Dutour, and P. W. Fowler, “Zigzags, railroads, and knots in fullerenes,” *Journal of Chemical Information and Computer Sciences*, vol. 44, no. 4, pp. 1282–1293, 2004.

[389] F. Cozzi, W. H. Powell, and C. Thilgen, “Numbering of Fullerenes (IUPAC Recommendations 2005),” *Pure and Applied Chemistry*, vol. 77, no. 5, pp. 843–923, 2005.

[390] W. A. de Heer, “Recent developments in carbon nanotubes,” *Current Opinion in Solid State and Materials Science*, vol. 4, no. 4, pp. 355–359, Aug. 1999.

[391] M. Terrones, “Science and technology of the twenty-first century: Synthesis, properties, and applications of carbon nanotubes,” *Annual Review of Materials Research*, vol. 33, no. 1, pp. 419–501, Aug. 2003.

[392] N. Hamada, S.-I. Sawada, and A. Oshiyama, “New one-dimensional conductors: Graphitic microtubules,” *Physical Review Letters*, vol. 68, no. 10, pp. 1579–1581, Mar. 1992.

[393] R. Saito, M. Fujita, G. Dresselhaus, and M. S. Dresselhaus, “Electronic structure of chiral graphene tubules,” *Applied Physics Letters*, vol. 60, no. 18, pp. 2204–2206, Oct. 1992.

[394] X. Peng et al., “Optically active single-walled carbon nanotubes.,” *Nature Nanotechnology*, vol. 2, no. 6, pp. 361–365, Jun. 2007.

[395] E. T. Thostenson, Z. Ren, and T.-W. Chou, “Advances in the science and technology of carbon nanotubes and their composites: a review,” *Composites Science and Technology*, vol. 61, no. 13, pp. 1899–1912, Oct. 2001.

[396] T. Ando, “The electronic properties of graphene and carbon nanotubes,” *NPG Asia Materials*, vol. 1, no. 1, pp. 17–21, Oct. 2009.

[397] S. Melchor and J. a Dobado, “CoNTub: An algorithm for connecting two arbitrary carbon nanotubes,” *Journal of Chemical Information and Computer Sciences*, vol. 44, no. 5, pp. 1639–1646, 2004.

[398] P. R. Wallace, “The band theory of graphite,” *Physical Review*, vol. 71, no. 9, pp. 622–634, May 1947.

[399] J. W. Mintmire, B. I. Dunlap, and C. T. White, “Are fullerene tubules metallic?,” *Physical Review Letters*, vol. 68, no. 5, pp. 631–634, Feb. 1992.

[400] T. W. Odom, J.-L. Huang, P. Kim, and C. M. Lieber, “Structure and electronic properties of carbon nanotubes,” *The Journal of Physical Chemistry B*, vol. 104, no. 13, pp. 2794–2809, Apr. 2000.

[401] H. Kataura et al., “Optical properties of single-walled carbon nanotubes,” *Synthetic Metals*, vol. 103, no. 1–3, pp. 2555–2558, Oct. 1999.

[402] R. B. Weisman, “Fluorimetric characterization of single-walled carbon nanotubes.,” *Analytical and Bioanalytical Chemistry*, vol. 396, no. 3, pp. 1015–1023, Feb. 2010.

[403] R. B. Weisman, S. M. Bachilo, and D. Tsyboulski, “Fluorescence spectroscopy of single-walled carbon nanotubes in aqueous suspension,” *Applied Physics A: Materials Science & Processing*, vol. 78, no. 8, pp. 1111–1116, May 2004.

[404] T. M. Krygowski and M. K. Cyrański, “Structural aspects of aromaticity,” *Chemical Reviews*, vol. 101, no. 5, pp. 1385–1420, May 2001.

[405] J. Aihara, T. Yamabe, and H. Hosoya, “Aromatic character of graphite and carbon nanotubes,” *Synthetic Metals*, vol. 64, no. 2–3, pp. 309–313, Jun. 1994.

[406] P. R. Bandaru, “Electrical Properties and Applications of Carbon Nanotube Structures,” *Journal of Nanoscience and Nanotechnology*, vol. 7, no. 4, pp. 1239–1267, Apr. 2007.

[407] I. Stavarache et al., “Electrical behavior of multi-walled carbon nanotube network embedded in amorphous silicon nitride,” *Nanoscale Research Letters*, vol. 6, no. 1, pp. 88–94, Jan. 2011.

[408] S. M. Bachilo, M. S. Strano, C. Kittrell, R. H. Hauge, R. E. Smalley, and R. B. Weisman, “Structure-assigned optical spectra of single-walled carbon nanotubes.,” *Science*, vol. 298, no. 5602, pp. 2361–2366, Dec. 2002.

[409] A. Hagen and T. Hertel, “Quantitative analysis of optical spectra from individual single-wall carbon nanotubes,” *Nano Letters*, vol. 3, no. 3, pp. 383–388, Mar. 2003.

[410] R. B. Weisman and S. M. Bachilo, “Dependence of optical transition energies on structure for single-walled carbon nanotubes in aqueous suspension: An empirical Kataura plot,” *Nano Letters*, vol. 3, no. 9, pp. 1235–1238, Sep. 2003.

[411] D. Robertson, D. Brenner, and J. Mintmire, “Energetics of nanoscale graphitic tubules,” *Physical Review B*, vol. 45, no. 21, pp. 12592–12595, Jun. 1992.

[412] R. Saito, M. Fujita, G. Dresselhaus, and M. S. Dresselhaus, “Electronic structure of graphene tubules based on C60,” *Physical Review B*, vol. 46, no. 3, pp. 1804–1811, Jul. 1992.

[413] J. W. Mintmire and C. T. White, “Universal density of states for carbon nanotubes,” *Physical Review Letters*, vol. 81, no. 12, pp. 2506–2509, Sep. 1998.

[414] R. Saito, G. Dresselhaus, and M. S. Dresselhaus, “Trigonal warping effect of carbon nanotubes,” *Physical Review B*, vol. 61, no. 4, pp. 2981–2990, 2000.

[415] J. W. G. Wildöer, L. C. Venema, A. G. Rinzler, R. E. Smalley, and C. Dekker, “Electronic structure of atomically resolved carbon nanotubes,” *Nature*, vol. 391, no. 6662, pp. 59–62, 1998.

[416] T. W. Odom, J.-L. Huang, P. Kim, and C. M. Lieber, “Atomic structure and electronic properties of single-walled carbon nanotubes,” *Nature*, vol. 391, no. 6662, pp. 62–64, 1998.

[417] T. W. Odom, J.-L. Huang, P. Kim, M. Ouyang, and C. M. Lieber, “Scanning tunneling microscopy and spectroscopy studies of single wall carbon nanotubes,” *Journal of Materials Research*, vol. 13, no. 9, pp. 2380–2388, 1998.

[418] P. Kim, T. W. Odom, J.-L. Huang, and C. M. Lieber, “Electronic density of states of atomically resolved single-walled carbon nanotubes: Van Hove singularities and end states,” *Physical Review Letters*, vol. 82, no. 6, pp. 1225–1228, Feb. 1999.

[419] M. J. O’Connell et al., “Band gap fluorescence from individual single-walled carbon nanotubes,” *Science*, vol. 297, no. 5581, pp. 593–596, Jul. 2002.

[420] L. Van Hove, “The occurrence of singularities in the elastic frequency distribution of a crystal,” *Physical Review*, vol. 89, no. 6, pp. 1189–1193, Mar. 1953.

[421] E. G. Wilson, “Electronic excitations of a conjugated polymer crystal,” *Journal of Physics C: Solid State Physics*, vol. 8, no. 5, pp. 727–742, Mar. 1975.

[422] J. Hu, T. W. Odom, and C. M. Lieber, “Chemistry and physics in one dimension: Synthesis and properties of nanowires and nanotubes,” *Accounts of Chemical Research*, vol. 32, no. 5, pp. 435–445, May 1999.

[423] J. Kono et al., “Ultra-fast optical spectroscopy of micelle-suspended single-walled carbon nanotubes,” *Applied Physics A: Materials Science & Processing*, vol. 78, no. 8, pp. 1093–1098, May 2004.

[424] J.-C. Charlier, “Defects in carbon nanotubes,” *Accounts of Chemical Research*, vol. 35, no. 12, pp. 1063–1069, Dec. 2002.

[425] M. Zhang and J. Li, “Carbon nanotube in different shapes,” *Materials Today*, vol. 12, no. 6, pp. 12–18, Jun. 2009.

[426] R. S. Ruoff, “Time, temperature, and load: The flaws of carbon nanotubes,” *Proceedings of the National Academy of Sciences of the United States of America*, vol. 103, no. 18, pp. 6779–6780, May 2006.

[427] R. H. Baughman, A. A. Zakhidov, and W. A. de Heer, “Carbon nanotubes--the route toward applications,” *Science*, vol. 297, no. 5582, pp. 787–792, Aug. 2002.

[428] M. Endo, M. S. Strano, and P. M. Ajayan, “Potential applications of carbon Nanotubes,” in *Carbon Nanotubes: Advanced Topics in the Synthesis, Structure, Properties, and Applications*, vol. 62, Berlin Heidelberg: Springer-Verlag, 2008, pp. 13–62.

[429] Z. Liu, S. Tabakman, K. Welsher, and H. Dai, “Carbon nanotubes in biology and medicine: In vitro and in vivo detection, imaging and drug delivery,” *Nano Research*, vol. 2, no. 2, pp. 85–120, Feb. 2009.

[430] K. Kostarelos, A. Bianco, and M. Prato, “Promises, facts and challenges for carbon nanotubes in imaging and therapeutics,” *Nature Nanotechnology*, vol. 4, no. 10, pp. 627–633, Oct. 2009.

[431] J. M. Schnorr and T. M. Swager, “Emerging applications of carbon nanotubes,” *Chemistry of Materials*, vol. 23, no. 3, pp. 646–657, Feb. 2011.

[432] B. Fiedler, F. H. Gojny, M. H. G. Wichmann, M. C. M. Nolte, and K. Schulte, “Fundamental aspects of nano-reinforced composites,” *Composites Science and Technology*, vol. 66, no. 16, pp. 3115–3125, Dec. 2006.

[433] B. J. Ash, A. Eitan, and L. S. Schadler, “Polymer nanocomposites with particle and carbon nanotube fillers,” in *Dekker Encyclopedia of Nanoscience and Nanotechnology*, J. A. Schwarz and C. I. Contescu, Eds. Dekker Dekker, In., 2004.

[434] A. M. K. Esawi and M. M. Farag, “Carbon nanotube reinforced composites: Potential and current challenges,” *Materials and Design*, vol. 28, no. 9, pp. 2394–2401, 2007.

[435] W. Luther and G. Bachmann, Eds., “nano.DE-Report 2009: Status quo of nanotechnology in Germany,” Federal Ministry of Education and Research, Department “Nanomaterials; New Materials,” Bonn, Berlin, Germany, 2009.

[436] W. B. Choi et al., “Fully sealed, high-brightness carbon-nanotube field-emission display,” *Applied Physics*, vol. 75, no. 20, pp. 3129–3131, 1999.

[437] K. Jiang, J. Wang, Q. Li, L. Liu, C. Liu, and S. Fan, “Superaligned carbon nanotube arrays, films, and yarns: A road to applications,” *Advanced Materials*, vol. 23, no. 9, pp. 1154–1161, Mar. 2011.

[438] S. Liu et al., “Sharper and faster ‘nano darts’ kill more bacteria: A study of antibacterial pristine single-walled carbon nanotube,” *ACS Nano*, vol. 3, no. 12, pp. 3891–3902, 2009.

[439] V. Raffa et al., “Can the properties of carbon nanotubes influence their internalization by living cells?,” *Carbon*, vol. 46, no. 12, pp. 1600–1610, Oct. 2008.

[440] J. Cheng et al., “Reversible accumulation of PEGylated single-walled carbon nanotubes in the mammalian nucleus,” *ACS Nano*, vol. 2, no. 10, pp. 2085–2094, Oct. 2008.

[441] C. P. Firme and P. R. Bandaru, “Toxicity issues in the application of carbon nanotubes to biological systems,” *Nanomedicine: Nanotechnology, Biology, and Medicine*, vol. 6, no. 2, pp. 245–256, Apr. 2010.

[442] S. Pogodin and V. A. Baulin, “Can a carbon nanotube pierce through a phospholipid bilayer?,” *ACS Nano*, vol. 4, no. 9, pp. 5293–5300, Sep. 2010.

[443] Z. Liu, X. Sun, N. Nakayama-Ratchford, and H. Dai, “Supramolecular chemistry on water-

soluble carbon nanotubes for drug loading and delivery," *ACS Nano*, vol. 1, no. 1, pp. 50–56, Aug. 2007.

[444] Z. Liu et al., "Supramolecular stacking of doxorubicin on carbon nanotubes for in vivo cancer therapy," *Angewandte Chemie International Edition in English*, vol. 48, no. 41, pp. 7668–7672, Jan. 2009.

[445] E. Heister et al., "Triple functionalisation of single-walled carbon nanotubes with doxorubicin, a monoclonal antibody, and a fluorescent marker for targeted cancer therapy," *Carbon*, vol. 47, no. 9, pp. 2152–2160, 2009.

[446] J. Shi, A. R. Votruba, O. C. Farokhzad, and R. Langer, "Nanotechnology in drug delivery and tissue engineering: From discovery to applications," *Nano Letters*, vol. 10, no. 9, pp. 3223–3230, Sep. 2010.

[447] A. Di Crescenzo, D. Velluto, J. A. Hubbell, and A. Fontana, "Biocompatible dispersions of carbon nanotubes: a potential tool for intracellular transport of anticancer drugs," *Nanoscale*, vol. 3, no. 3, pp. 925–928, Mar. 2011.

[448] S. Y. Madani, N. Naderi, O. Dissanayake, A. Tan, and A. M. Madani Seifalian, "A new era of cancer treatment: carbon nanotubes as drug delivery tools," *International Journal of Nanomedicine*, vol. 6, pp. 2963–2979, Nov. 2011.

[449] N. W. Shi Kam, T. C. Jessop, P. A. Wender, and H. Dai, "Nanotube molecular transporters: Internalization of carbon nanotube-protein conjugates into mammalian cells," *Journal of the American Chemical Society*, vol. 126, no. 22, pp. 6850–1, Jun. 2004.

[450] N. W. Shi Kam, M. O'Connell, J. A. Wisdom, and H. Dai, "Carbon nanotubes as multifunctional biological transporters and near-infrared agents for selective cancer cell destruction," *Proceedings of the National Academy of Sciences of the United States of America*, vol. 102, no. 33, pp. 11600–11605, Aug. 2005.

[451] N. V. Konduru et al., "Phosphatidylserine targets single-walled carbon nanotubes to professional phagocytes in vitro and in vivo," *PloS ONE*, vol. 4, no. 2, pp. e4398–e4399, Jan. 2009.

[452] Z. Liu, S. M. Tabakman, Z. Chen, and H. Dai, "Preparation of carbon nanotube bioconjugates for biomedical applications," *Nature Protocols*, vol. 4, no. 9, pp. 1372–82, Jan. 2009.

[453] M. K. Gheith et al., "Stimulation of neural cells by lateral currents in conductive layer-by-layer films of single-walled carbon nanotubes," *Advanced Materials*, vol. 18, no. 22, pp. 2975–2979, Nov. 2006.

[454] N. W. Shi Kam, E. Jan, and N. A. Kotov, "Electrical stimulation of neural stem cells mediated by humanized carbon nanotube composite made with extracellular matrix protein," *Nano Letters*, vol. 9, no. 1, pp. 273–278, Jan. 2009.

[455] J. Holy, E. Perkins, and X. Yu, "Adhesion, proliferation and differentiation of pluripotent stem cells on multi-walled carbon nanotubes," *IET Nanobiotechnology*, vol. 5, no. 2, pp. 41–46, Jun. 2011.

[456] A. Verma and F. Stellacci, "Effect of surface properties on nanoparticle-cell interactions," *Small*, vol. 6, no. 1, pp. 12–21, Jan. 2010.

[457] J. M. Wörle-Knirsch, K. Pulskamp, and H. F. Krug, "Oops they did it again! Carbon nanotubes hoax scientists in viability assays," *Nano Letters*, vol. 6, no. 6, pp. 1261–1268, Jun. 2006.

[458] H.-X. Ren, X. Chen, J.-H. Liu, N. Gu, and X.-J. Huang, "Toxicity of single-walled carbon nanotube: How we were wrong?," *Materials Today*, vol. 13, no. 1–2, pp. 6–8, Jan. 2010.

[459] B. Fadeel and A. E. Garcia-Bennett, "Better safe than sorry: Understanding the toxicological properties of inorganic nanoparticles manufactured for biomedical applications," *Advanced Drug Delivery Reviews*, vol. 62, no. 3, pp. 362–374, Mar. 2010.

[460] S. Kang, M. Herzberg, D. F. Rodrigues, and M. Elimelech, "Antibacterial effects of carbon nanotubes: Size does matter!," *Langmuir*, vol. 24, no. 13, pp. 6409–6413, 2008.

[461] C. Yang, J. Mamouni, Y. Tang, and L. Yang, "Antimicrobial activity of single-walled carbon nanotubes: Length effect," *Langmuir*, vol. 26, no. 20, pp. 16013–16019, 2010.

[462] S. Aslan, C. Z. Loebick, S. Kang, M. Elimelech, L. D. Pfefferle, and P. R. Van Tassel, "Antimicrobial biomaterials based on carbon nanotubes dispersed in poly (lactic-co-glycolic

acid),” *Nanoscale*, vol. 2, no. 9, pp. 1789–1794, Sep. 2010.

[463] C. D. Vecitis, K. R. Zodrow, S. Kang, and M. Elimelech, “Electronic-structure-dependent bacterial cytotoxicity of single-walled carbon nanotubes,” *ACS Nano*, vol. 4, no. 9, pp. 5471–5479, 2010.

[464] S. S. Karajanagi, A. A. Vertegel, R. S. Kane, and J. S. Dordick, “Structure and function of enzymes adsorbed onto single-walled carbon nanotubes,” *Langmuir*, vol. 20, no. 26, pp. 11594–11599, 2004.

[465] J. Zhong et al., “Bio–nano interaction of proteins adsorbed on single-walled carbon nanotubes,” *Carbon*, vol. 47, no. 4, pp. 967–973, Apr. 2009.

[466] A. D. Maynard, P. A. Baron, M. Foley, A. A. Shvedova, E. R. Kisin, and V. Castranova, “Exposure to carbon nanotube material: Aerosol release during the handling of unrefined single-walled carbon nanotube material,” *Journal of Toxicology and Environmental Health, Part A*, vol. 67, no. 1, pp. 87–107, Jan. 2004.

[467] P. Wick et al., “The degree and kind of agglomeration affect carbon nanotube cytotoxicity,” *Toxicology letters*, vol. 168, no. 2, pp. 121–131, Jan. 2007.

[468] C. Buzea, I. I. Pacheco, and K. Robbie, “Nanomaterials and nanoparticles: Sources and toxicity,” *Biointerphases*, vol. 2, no. 4, pp. MR17–MR71, 2007.

[469] J. Kayat, V. Gajbhiye, R. K. Tekade, and N. K. Jain, “Pulmonary toxicity of carbon nanotubes: a systematic report,” *Nanomedicine: Nanotechnology, Biology, and Medicine*, vol. 7, no. 1, pp. 40–49, Feb. 2011.

[470] P. Cherukuri et al., “Mammalian pharmacokinetics of carbon nanotubes using intrinsic near-infrared fluorescence,” *Proceedings of the National Academy of Sciences of the United States of America*, vol. 103, no. 50, pp. 18882–18886, Dec. 2006.

[471] R. Wang et al., “SWCNT PEG-eggs: Single-walled carbon nanotubes in biocompatible shell-crosslinked micelles,” *Carbon*, vol. 45, no. 12, pp. 2388–2393, Oct. 2007.

[472] Y. Lin et al., “Advances toward bioapplications of carbon nanotubes,” *Journal of Materials Chemistry*, vol. 14, no. 4, pp. 527–541, 2004.

[473] S. Kang, M. Pinault, L. D. Pfefferle, and M. Elimelech, “Single-walled carbon nanotubes exhibit strong antimicrobial activity,” *Langmuir*, vol. 23, no. 17, pp. 8670–8673, 2007.

[474] P. Asuri, S. S. Karajanagi, R. S. Kane, and J. S. Dordick, “Polymer-nanotube-enzyme composites as active antifouling films,” *Small*, vol. 3, no. 1, pp. 50–53, Jan. 2007.

[475] V. K. K. Upadhyayula and V. Gadhamshetty, “Appreciating the role of carbon nanotube composites in preventing biofouling and promoting biofilms on material surfaces in environmental engineering: A review,” *Biotechnology Advances*, vol. 28, no. 6, pp. 802–816, 2010.

[476] D. Nepal, S. Balasubramanian, A. L. Simonian, and V. A. Davis, “Strong antimicrobial coatings: Single-walled carbon nanotubes armored with biopolymers,” *Nano Letters*, vol. 8, no. 7, pp. 1896–1901, 2008.

[477] D. W. Schaefer and R. S. Justice, “How nano are nanocomposites?,” *Macromolecules*, vol. 40, no. 24, pp. 8501–8517, Nov. 2007.

[478] J. Aihara, “Lack of superaromaticity in carbon nanotubes,” *The Journal of Physical Chemistry*, vol. 98, no. 39, pp. 9773–9776, Sep. 1994.

[479] K. Balasubramanian and M. Burghard, “Chemically functionalized carbon nanotubes,” *Small*, vol. 1, no. 2, pp. 180–192, Feb. 2005.

[480] S. Banerjee, T. Hemraj-Benny, and S. S. Wong, “Covalent surface chemistry of single-walled carbon nanotubes,” *Advanced Materials*, vol. 17, no. 1, pp. 17–29, Jan. 2005.

[481] E. T. Mickelson, C. B. Huffman, A. G. Rinzler, R. E. Smalley, R. H. Hauge, and J. L. Margrave, “Fluorination of single-wall carbon nanotubes,” *Chemical Physics Letters*, vol. 296, no. 1–2, pp. 188–194, Oct. 1998.

[482] J. Chen et al., “Solution properties of single-walled carbon nanotubes,” *Science*, vol. 282, no. 5386, pp. 95–98, Oct. 1998.

[483] M. Holzinger et al., “Sidewall functionalization of carbon nanotubes,” *Angewandte Chemie International Edition in English*, vol. 40, no. 21, pp. 4002–4005, Nov. 2001.

[484] D.-H. Jung, Y. K. Ko, and H.-T. Jung, “Aggregation behavior of chemically attached poly(ethylene glycol) to single-walled carbon nanotubes (SWNTs) ropes,” *Materials Science and Engineering: C*, vol. 24, no. 1–2, pp. 117–121, Jan. 2004.

[485] H. Kong et al., “Poly(N-isopropylacrylamide)-coated carbon nanotubes: Temperature-sensitive molecular nanohybrids in water,” *Macromolecules*, vol. 37, no. 18, pp. 6683–6686, Sep. 2004.

[486] J. Chen, H. Liu, W. A. Weimer, M. D. Halls, D. H. Waldeck, and G. C. Walker, “Noncovalent engineering of carbon nanotube surfaces by rigid, functional conjugated polymers,” *Journal of the American Chemical Society*, vol. 124, no. 31, pp. 9034–9035, 2002.

[487] K. D. Ausman, R. Piner, O. Lourie, R. S. Ruoff, and M. Korobov, “Organic solvent dispersions of single-walled carbon nanotubes: Toward solutions of pristine nanotubes,” *The Journal of Physical Chemistry B*, vol. 104, no. 38, pp. 8911–8915, Sep. 2000.

[488] J. L. Bahr, E. T. Mickelson, M. J. Bronikowski, R. E. Smalley, and J. M. Tour, “Dissolution of small diameter single-wall carbon nanotubes in organic solvents?,” *Chemical Communications*, no. 2, pp. 193–194, 2001.

[489] C.-Y. Hu, Y.-J. Xu, S.-W. Duo, R.-F. Zhang, and M.-S. Li, “Non-covalent functionalization of carbon nanotubes with surfactants and polymers,” *Journal of the Chinese Chemical Society*, vol. 56, no. 2, pp. 234–239, 2009.

[490] J. Goldfarb and S. Rodriguez, “Aqueous solutions of polyvinylpyrrolidone,” *Die Makromolekulare Chemie*, vol. 116, no. 1, pp. 96–106, 1968.

[491] T. Tadros, “Polymeric surfactants in disperse systems,” *Advances in Colloid and Interface Science*, vol. 147–148, pp. 281–99, 2009.

[492] L. Türker, A. Güner, F. Yigit, and O. Güven, “Spectrophotometric behavior of polyvinylpyrrolidone in aqueous and nonaqueous media (I),” *Colloid & Polymer Science*, vol. 268, no. 4, pp. 337–344, Apr. 1990.

[493] A. Güner, “Properties of aqueous salt solutions of polyvinylpyrrolidone. I. Viscosity characteristics,” *Journal of Applied Polymer Science*, vol. 62, no. 5, pp. 785–788, Oct. 1996.

[494] A. Dan, S. Ghosh, and S. P. Moulik, “The solution behavior of poly(vinylpyrrolidone): Its clouding in salt solution, solvation by water and isopropanol, and interaction with sodium dodecyl sulfate,” *The Journal of Physical Chemistry B*, vol. 112, no. 12, pp. 3617–3624, Mar. 2008.

[495] I. I. Khairullin, Y.-H. Chen, and L.-P. Hwang, “Evidence for electron charge transfer in the polyvinylpyrrolidone-C60 system as seen from ESR spectra,” *Chemical Physics Letters*, vol. 275, no. 1–2, pp. 1–6, Aug. 1997.

[496] L. V. Vinogradova et al., “Water-soluble complexes of C60 fullerene with poly(N-vinylpyrrolidone),” *Polymer Science, Series A: Polymer Physics*, vol. 40, no. 11, pp. 1152–1159, 1998.

[497] C. Yu-Huei, I. I. Khairullin, S. Mei-Po, and H. Lian-Pin, “Electron spin resonance and infrared spectroscopy study of the polyvinylpyrrolidone-C60 composite,” *Fullerene Science and Technology*, vol. 7, no. 5, pp. 807–823, Sep. 1999.

[498] C. Ungurenasu and A. Airinei, “Highly stable C60/poly(vinylpyrrolidone) charge-transfer complexes afford new predictions for biological applications of underivatized fullerenes,” *Journal of Medicinal Chemistry*, vol. 43, no. 16, pp. 3186–3188, Aug. 2000.

[499] J. N. Smith, J. Meadows, and P. A. Williams, “Adsorption of polyvinylpyrrolidone onto polystyrene latices and the effect on colloid stability,” *Langmuir*, vol. 12, no. 16, pp. 3773–3778, Jan. 1996.

[500] N. Shinyashiki, A. Spanoudaki, and W. Yamamoto, “Segmental relaxation of hydrophilic poly(vinylpyrrolidone) in chloroform studied by broadband dielectric spectroscopy,” *Macromolecules*, vol. 44, no. 7, pp. 2140–2148, Apr. 2011.

[501] H. P. Frank, S. Barkin, and F. R. Eirich, “The interaction of polyvinylpyrrolidone with some azo dyes,” *The Journal of Physical Chemistry*, vol. 61, no. 10, pp. 1375–1380, 1957.

[502] P. Molyneux and H. P. Frank, “The interaction of polyvinylpyrrolidone with aromatic compounds in aqueous solution. Part I. Thermodynamics of the binding equilibria and interaction forces,” *Journal of the American Chemical Society*, vol. 83, no. 15, pp. 3169–3174,

Jul. 1961.

[503] P. Molyneux and H. P. Frank, “The interaction of polyvinylpyrrolidone with aromatic compounds in aqueous solution. Part II. The effect of the interaction on the molecular size of the polymer,” *Journal of the American Chemical Society*, vol. 83, no. 15, pp. 3175–3180, 1961.

[504] P. Molyneux and H. P. Frank, “The interaction of polyvinylpyrrolidone with aromatic compounds in aqueous solution. III. A model for the molecular expansions caused by anionic cosolutes,” *Journal of the American Chemical Society*, vol. 86, no. 22, pp. 4753–4757, Nov. 1964.

[505] P. Molyneux and M. Cornarakis-Lentzos, “The interaction of polyvinylpyrrolidone with aromatic compounds in aqueous solution. Part IV. Evaluation of the co-operativity parameter, and the methylene-group contribution to the binding strength, for the alkyl parahydroxybenzoates,” *Colloid and Polymer Science*, vol. 257, no. 8, pp. 855–873, Aug. 1979.

[506] D. Baskaran, J. W. Mays, and M. S. Bratcher, “Noncovalent and nonspecific molecular interactions of polymers with multiwalled carbon nanotubes,” *Chemistry of Materials*, vol. 17, no. 13, pp. 3389–3397, Jun. 2005.

[507] A. Beigbeder et al., “CH-π interactions as the driving force for silicone-based nanocomposites with exceptional properties,” *Advanced Materials*, vol. 20, no. 5, pp. 1003–1007, Mar. 2008.

[508] G. R. Desiraju, “Hydrogen bridges in crystal engineering: Interactions without borders,” *Accounts of Chemical Research*, vol. 35, no. 7, pp. 565–73, Jul. 2002.

[509] S. Tsuzuki and A. Fujii, “Nature and physical origin of CH/π interaction: significant difference from conventional hydrogen bonds,” *Physical Chemistry Chemical Physics*, vol. 10, no. 19, pp. 2584–2594, May 2008.

[510] M. Maresca, A. Derghal, C. Carravagna, S. Dudin, and J. Fantini, “Controlled aggregation of adenine by sugars: physicochemical studies, molecular modelling simulations of sugar–aromatic CH–π stacking interactions, and biological significance,” *Physical Chemistry Chemical Physics*, vol. 10, no. 19, pp. 2581–2583, May 2008.

[511] A. Star, D. W. Steuerman, J. R. Heath, and J. F. Stoddart, “Starched carbon nanotubes,” *Angewandte Chemie International Edition in English*, vol. 41, no. 14, pp. 2508–2512, Jul. 2002.

[512] O.-K. Kim, J. Je, J. W. Baldwin, S. Kooi, P. E. Pehrsson, and L. J. Buckley, “Solubilization of single-wall carbon nanotubes by supramolecular encapsulation of helical amylose,” *Journal of the American Chemical Society*, vol. 125, no. 15, pp. 4426–4427, Apr. 2003.

[513] M. Numata et al., “Inclusion of cut and as-grown single-walled carbon nanotubes in the helical superstructure of schizophyllan and curdlan (ß-1,3-glucans),” *Journal of the American Chemical Society*, vol. 127, no. 16, pp. 5875–5884, Apr. 2005.

[514] J. M. H. M. Scheutjens and G. J. Fleer, “Statistical theory of the adsorption of interacting chain molecules. 1. Partition function, segment density distribution, and adsorption isotherms,” *The Journal of Physical Chemistry*, vol. 83, no. 12, pp. 1619–1635, Jun. 1979.

[515] J. M. H. M. Scheutjens and G. J. Fleer, “Statistical theory of the adsorption of interacting chain molecules. 2. Train, loop, and tail size distribution,” *The Journal of Physical Chemistry*, vol. 84, no. 2, pp. 178–190, Jan. 1980.

[516] M. A. Cohen Stuart, “Adsorbed polymers in colloidal systems: from statics to dynamics,” *Polymer Journal*, vol. 23, no. 5, pp. 669–682, 1991.

[517] M. A. Cohen Stuart, “Flexible polymers at a solid-liquid interface: The adsorption of polyvinyl pyrrolidone onto silica,” Wageningen UR, 1980.

[518] K. Ishiduki and K. Esumi, “The effect of pH on adsorption of poly(acrylic acid) and poly(vinylpyrrolidone) on alumina from their binary mixtures,” *Langmuir*, vol. 13, no. 6, pp. 1587–1591, Mar. 1997.

[519] P. Qiu and C. Mao, “Biomimetic branched hollow fibers templated by self-assembled fibrous polyvinylpyrrolidone structures in aqueous solution.,” *ACS Nano*, vol. 4, no. 3, pp. 1573–1579, Mar. 2010.

[520] M. E. Hughes, E. Brandin, and J. A. Golovchenko, “Optical absorption of DNA-carbon

nanotube structures," *Nano Letters*, vol. 7, no. 5, pp. 1191–1194, May 2007.
[521] X. Wang, Y. Liu, W. Qiu, and D. Zhu, "Immobilization of tetra-tert-butylphthalocyanines on carbon nanotubes: a first step towards the development of new nanomaterials," *Journal of Materials Chemistry*, vol. 12, no. 6, pp. 1636–1639, May 2002.
[522] H. Murakami, T. Nomura, and N. Nakashima, "Noncovalent porphyrin-functionalized single-walled carbon nanotubes in solution and the formation of porphyrin–nanotube nanocomposites," *Chemical Physics Letters*, vol. 378, no. 5–6, pp. 481–485, Sep. 2003.
[523] G. Nakamura, K. Narimatsu, Y. Niidome, and N. Nakashima, "Green tea solution individually solubilizes single-walled carbon nanotubes," *Chemistry Letters*, vol. 36, no. 9, pp. 1140–1141, 2007.
[524] Y. Chen, Y. D. Lee, H. Vedala, B. L. Allen, and A. Star, "Exploring the chemical sensitivity of a carbon nanotube/green tea composite," *ACS Nano*, vol. 4, no. 11, pp. 6854–6862, Nov. 2010.
[525] Y. Liu et al., "Debundling of single-walled carbon nanotubes by using natural polyelectrolytes," *Nanotechnology*, vol. 18, no. 36, p. 365702 (6pp), 2007.
[526] H. Hyung, J. D. Fortner, J. B. Hughes, and J.-H. Kim, "Natural organic matter stabilizes carbon nanotubes in the aqueous phase," *Environmental Science & Technology*, vol. 41, no. 1, pp. 179–184, Jan. 2007.
[527] I. Schwyzer, R. Kaegi, L. Sigg, A. Magrez, and B. Nowack, "Influence of the initial state of carbon nanotubes on their colloidal stability under natural conditions," *Environmental Pollution*, vol. 159, no. 6, pp. 1641–1648, Jun. 2011.
[528] D. Lin and B. Xing, "Tannic acid adsorption and its role for stabilizing carbon nanotube suspensions," *Environmental Science & Technology*, vol. 42, no. 16, pp. 5917–5923, 2008.
[529] D. Lin, N. Liu, K. Yang, L. Zhu, Y. Xu, and B. Xing, "The effect of ionic strength and pH on the stability of tannic acid-facilitated carbon nanotube suspensions," *Carbon*, vol. 47, no. 12, pp. 2875–2882, 2009.
[530] E. Matuyama, "Ultrasonic grinding of natural graphite," *Nature*, vol. 207, no. 5002, pp. 1189–1190, Sep. 1965.
[531] B.-S. Kim, H.-I. Lee, Y. Min, Z. Poon, and P. T. Hammond, "Hydrogen-bonded multilayer of pH-responsive polymeric micelles with tannic acid for surface drug delivery," *Chemical Communications*, no. 28, pp. 4194–4196, Jul. 2009.
[532] Y. Tomonari, H. Murakami, and N. Nakashima, "Solubilization of single-walled carbon nanotubes by using polycyclic aromatic ammonium amphiphiles in water—Strategy for the design of high-performance solubilizers," *Chemistry - A European Journal*, vol. 12, no. 15, pp. 4027–4034, May 2006.
[533] R. Gaudreault, T. G. M. van de Ven, and M. A. Whitehead, "Molecular modeling of poly(ethylene oxide) model cofactors; 1,3,6-tri-O-galloyl-ß-D-glucose and corilagin," *Journal of Molecular Modeling*, vol. 8, no. 3, pp. 73–80, 2002.
[534] X. Guo, H. Shao, W. Hu, W. Gao, and X. Chen, "Tannin and polyacrylic acid polarity and structure influence on the performance of polyvinylchloride ultrafiltration membrane," *Desalination*, vol. 250, no. 2, pp. 740–744, Jan. 2010.
[535] C. Morin, D. Simon, and P. Sautet, "Density-functional study of the adsorption and vibration spectra of benzene molecules on Pt(111)," *The Journal of Physical Chemistry B*, vol. 107, no. 13, pp. 2995–3002, Apr. 2003.
[536] K. E. Wise, C. Park, E. J. Siochi, and J. S. Harrison, "Stable dispersion of single wall carbon nanotubes in polyimide: the role of noncovalent interactions," *Chemical Physics Letters*, vol. 391, no. 4–6, pp. 207–211, Jun. 2004.
[537] E. Edri and O. Regev, "pH effects on BSA-dispersed carbon nanotubes studied by spectroscopy-enhanced composition evaluation techniques," *Analytical Chemistry*, vol. 80, no. 11, pp. 4049–4054, Jun. 2008.
[538] S. M. Hauge and J. J. Willaman, "Effect of pH on adsorption by carbons," *Industrial and Engineering Chemistry*, vol. 19, no. 8, pp. 943–953, Aug. 1927.
[539] G. Mueller, C. J. Radke, and J. M. Prausnitz, "Adsorption of weak organic electrolytes from aqueous solution on activated carbon. Effect of pH," *The Journal of Physical Chemistry*, vol.

84, no. 4, pp. 369–376, Feb. 1980.
[540] S. Ramesh et al., “Dissolution of pristine single walled carbon nanotubes in superacids by direct protonation,” *The Journal of Physical Chemistry B*, vol. 108, no. 26, pp. 8794–8798, Jul. 2004.
[541] A. N. G. Parra-Vasquez et al., “Spontaneous dissolution of ultralong single- and multiwalled carbon nanotubes,” *ACS Nano*, vol. 4, no. 7, pp. 3969–3978, Jul. 2010.
[542] A. Pénicaud, P. Poulin, A. Derré, E. Anglaret, and P. Petit, “Spontaneous dissolution of a single-wall carbon nanotube salt,” *Journal of the American Chemical Society*, vol. 127, no. 1, pp. 8–9, Jan. 2005.
[543] S. Fogden, C. A. Howard, R. K. Heenan, N. T. Skipper, and M. S. P. Shaffer, “Scalable method for the reductive dissolution, purification, and separation of single-walled carbon nanotubes.,” *ACS Nano*, vol. 6, no. 1, pp. 54–62, Jan. 2012.
[544] M. Nadler, T. Mahrholz, U. Riedel, C. Schilde, and A. Kwade, “Preparation of colloidal carbon nanotube dispersions and their characterisation using a disc centrifuge,” *Carbon*, vol. 46, no. 11, pp. 1384–1392, Sep. 2008.
[545] A. T. Seyhan, M. Tanoglu, and K. Schulte, “Mode I and mode II fracture toughness of E-glass non-crimp fabric/carbon nanotube (CNT) modified polymer based composites,” *Engineering Fracture Mechanics*, vol. 75, no. 18, pp. 5151–5162, Dec. 2008.
[546] P.-C. Ma, N. A. Siddiqui, G. Marom, and J.-K. Kim, “Dispersion and functionalization of carbon nanotubes for polymer-based nanocomposites: A review,” *Composites Part A: Applied Science and Manufacturing*, vol. 41, no. 10, pp. 1345–1367, Oct. 2010.
[547] K. S. Suslick, “Sonochemistry,” *Science*, vol. 247, no. 4949, pp. 1439–45, Mar. 1990.
[548] L. H. Thompson and L. K. Doraiswamy, “Sonochemistry: Science and engineering,” *Industrial & Engineering Chemistry Research*, vol. 38, no. 4, pp. 1215–1249, Apr. 1999.
[549] M. E. Fitzgerald, V. Griffing, and J. Sullivan, “Chemical effects of ultrasonics—‘Hot spot’ chemistry,” *The Journal of Chemical Physics*, vol. 25, no. 5, pp. 926–934, 1956.
[550] K. S. Suslick, D. A. Hammerton, and R. E. Cline, “Sonochemical hot spot,” *Journal of the American Chemical Society*, vol. 108, no. 18, pp. 5641–5642, Sep. 1986.
[551] K. S. Suslick, “The chemical effects of ultrasound,” *Scientific American*, vol. 260, no. 2, pp. 80–86, 1989.
[552] K. S. Suslick and G. J. Price, “Applications of ultrasound to materials chemistry,” *Annual Review of Materials Science*, vol. 29, no. 1, pp. 295–326, Aug. 1999.
[553] J. H. Bang and K. S. Suslick, “Applications of ultrasound to the synthesis of nanostructured materials,” *Advanced Materials*, vol. 22, no. 10, pp. 1039–1059, Mar. 2010.
[554] S. J. Doktycz and K. S. Suslick, “Interparticle collisions driven by ultrasound,” *Science*, vol. 247, no. 4946, pp. 1067–1069, Mar. 1990.
[555] E. B. Flint and K. S. Suslick, “The temperature of cavitation,” *Science*, vol. 253, no. 5026, pp. 1397–1399, Sep. 1991.
[556] P. J. Westervelt, “The theory of steady rotational flow generated by a sound field,” *The Journal of the Acoustical Society of America*, vol. 25, no. 1, pp. 60–67, 1953.
[557] W. L. Nyborg, “Acoustic streaming due to attenuated plane waves,” *The Journal of the Acoustical Society of America*, vol. 25, no. 1, pp. 68–75, 1953.
[558] J. Kolb and W. L. Nyborg, “Small-scale acoustic streaming in liquids,” *The Journal of the Acoustical Society of America*, vol. 28, no. 6, pp. 1237–1242, 1956.
[559] W. L. Nyborg, “Acoustic streaming near a boundary,” *The Journal of the Acoustical Society of America*, vol. 30, no. 4, pp. 329–339, 1958.
[560] S. A. Elder, “Cavitation microstreaming,” *The Journal of the Acoustical Society of America*, vol. 31, no. 1, pp. 54–64, 1959.
[561] C. P. Lee and T. G. Wang, “Outer acoustic streaming,” *The Journal of the Acoustical Society of America*, vol. 88, no. 5, pp. 2367–2375, 1990.
[562] M. S. Strano et al., “The role of surfactant adsorption during ultrasonication in the dispersion of single-walled carbon nanotubes,” *Journal of Nanoscience and Nanotechnology*, vol. 3, no. 1, pp. 81–86, Feb. 2003.

[563] Q. Cheng, S. Debnath, E. Gregan, and H. J. Byrne, "Ultrasound-assisted SWNTs dispersion: Effects of sonication parameters and solvent properties," *The Journal of Physical Chemistry C*, vol. 114, no. 19, pp. 8821–8827, May 2010.

[564] P. R. Gogate, "Cavitational reactors for process intensification of chemical processing applications: A critical review," *Chemical Engineering and Processing: Process Intensification*, vol. 47, no. 4, pp. 515–527, Apr. 2008.

[565] T. Yamamoto et al., "Improved bath sonication method for dispersion of individual single-walled carbon nanotubes using new triphenylene-based surfactant," *Japanese Journal of Applied Physics*, vol. 47, no. 4, pp. 2000–2004, Apr. 2008.

[566] N. Grossiord, O. Regev, J. Loos, J. Meuldijk, and C. E. Koning, "Time-dependent study of the exfoliation process of carbon nanotubes in aqueous dispersions by using UV-visible spectroscopy," *Analytical Chemistry*, vol. 77, no. 16, pp. 5135–5139, Aug. 2005.

[567] B. Krause, M. Mende, P. Pötschke, and G. Petzold, "Dispersability and particle size distribution of CNTs in an aqueous surfactant dispersion as a function of ultrasonic treatment time," *Carbon*, vol. 48, no. 10, pp. 2746–2754, Aug. 2010.

[568] Y. G. Adewuyi, "Sonochemistry: Environmental science and engineering applications," *Industrial & Engineering Chemistry Research*, vol. 40, no. 22, pp. 4681–4715, Oct. 2001.

[569] S. Majumdar, P. S. Kumar, and A. B. Pandit, "Effect of liquid-phase properties on ultrasound intensity and cavitational activity," *Ultrasonics Sonochemistry*, vol. 5, no. 3, pp. 113–118, Nov. 1998.

[570] P. R. Gogate, P. A. Tatake, P. M. Kanthale, and A. B. Pandit, "Mapping of sonochemical reactors: Review, analysis, and experimental verification," *AIChE Journal*, vol. 48, no. 7, pp. 1542–1560, Jul. 2002.

[571] P. R. Gogate and A. B. Pandit, "Sonochemical reactors: scale up aspects," *Ultrasonics Sonochemistry*, vol. 11, no. 3–4, pp. 105–117, May 2004.

[572] A. Kumar, T. Kumaresan, A. B. Pandit, and J. B. Joshi, "Characterization of flow phenomena induced by ultrasonic horn," *Chemical Engineering Science*, vol. 61, no. 22, pp. 7410–7420, Nov. 2006.

[573] A. Kumar, P. R. Gogate, and A. B. Pandit, "Mapping the efficacy of new designs for large scale sonochemical reactors," *Ultrasonics Sonochemistry*, vol. 14, no. 5, pp. 538–544, Jul. 2007.

[574] V. S. Sutkar and P. R. Gogate, "Design aspects of sonochemical reactors: Techniques for understanding cavitational activity distribution and effect of operating parameters," *Chemical Engineering Journal*, vol. 155, no. 1–2, pp. 26–36, Dec. 2009.

[575] V. S. Sutkar and P. R. Gogate, "Mapping of cavitational activity in high frequency sonochemical reactor," *Chemical Engineering Journal*, vol. 158, no. 2, pp. 296–304, Apr. 2010.

[576] S. R. Soudagar and S. D. Samant, "Semiquantitative characterization of ultrasonic cleaner using a novel piezoelectric pressure intensity measurement probe," *Ultrasonics Sonochemistry*, vol. 2, no. 1, pp. S49–S53, Jan. 1995.

[577] D. Kobayashi, H. Matsumoto, and C. Kuroda, "Effect of reactor's positions on polymerization and degradation in an ultrasonic field," *Ultrasonics Sonochemistry*, vol. 15, no. 3, pp. 251–256, Mar. 2008.

[578] J. Chen, M. J. Dyer, and M.-F. Yu, "Cyclodextrin-mediated soft cutting of single-walled carbon nanotubes," *Journal of the American Chemical Society*, vol. 123, no. 25, pp. 6201–6202, Jun. 2001.

[579] A. D. Walmsley and A. R. Williams, "Measurement of cavitational activity within ultrasonic baths," *Journal of Dentistry*, vol. 19, no. 1, pp. 62–66, Feb. 1991.

[580] S. S. Karajanagi, H. Yang, P. Asuri, E. Sellitto, J. S. Dordick, and R. S. Kane, "Protein-assisted solubilization of single-walled carbon nanotubes," *Langmuir*, vol. 22, no. 4, pp. 1392–1395, Feb. 2006.

[581] F. Guittonneau, A. Abdelouas, B. Grambow, and S. Huclier, "The effect of high power ultrasound on an aqueous suspension of graphite," *Ultrasonics Sonochemistry*, vol. 17, no. 2,

pp. 391–398, Feb. 2010.

[582] K. L. Lu, R. M. Lago, Y. K. Chen, M. L. H. Green, P. J. F. Harris, and S. C. Tsang, “Mechanical damage of carbon nanotubes by ultrasound,” *Carbon*, vol. 34, no. 6, pp. 814–816, 1996.

[583] D. Nepal, D. S. Kim, and K. E. Geckeler, “A facile and rapid purification method for single-walled carbon nanotubes,” *Carbon*, vol. 43, no. 3, pp. 660–662, 2005.

[584] J. E. Decker et al., “Sample preparation protocols for realization of reproducible characterization of single-wall carbon nanotubes,” *Metrologia*, vol. 46, no. 6, pp. 682–692, Dec. 2009.

[585] A. I. Vorob’eva, “Equipment and techniques for carbon nanotube research,” *Physics-Uspekhi*, vol. 53, no. 3, pp. 257–277, Jun. 2010.

[586] M. Alexander and D. G. Dalgleish, “Dynamic light scattering techniques and their applications in food science,” *Food Biophysics*, vol. 1, no. 1, pp. 2–13, Feb. 2006.

[587] V. Filipe, A. Hawe, and W. Jiskoot, “Critical evaluation of Nanoparticle Tracking Analysis (NTA) by NanoSight for the measurement of nanoparticles and protein aggregates,” *Pharmaceutical Research*, vol. 27, no. 5, pp. 796–810, May 2010.

[588] S. Badaire, P. Poulin, M. Maugey, and C. Zakri, “In situ measurements of nanotube dimensions in suspensions by depolarized dynamic light scattering,” *Langmuir*, vol. 20, no. 24, pp. 10367–10370, Nov. 2004.

[589] J. Rodriguez-Fernandez, J. Perez-Juste, L. M. Liz-Marzan, and P. R. Lang, “Dynamic light scattering of short Au rods with low aspect ratios,” *Journal of Physical Chemistry C*, vol. 111, no. 13, pp. 5020–5025, Apr. 2007.

[590] D. G. Dalgleish and F. R. Hallett, “Dynamic light scattering: applications to food systems,” *Food Research International*, vol. 28, no. 3, pp. 181–193, Jan. 1995.

[591] Y. K. Moon, J. Lee, J. K. Lee, T. K. Kim, and S. H. Kim, “Synthesis of length-controlled aerosol carbon nanotubes and their dispersion stability in aqueous solution,” *Langmuir*, vol. 25, no. 3, pp. 1739–1743, Feb. 2009.

[592] A. R. Petosa, D. P. Jaisi, I. R. Quevedo, M. Elimelech, and N. Tufenkji, “Aggregation and deposition of engineered nanomaterials in aquatic environments: Role of physicochemical interactions,” *Environmental Science & Technology*, vol. 44, no. 17, pp. 6532–6549, Sep. 2010.

[593] K. L. Chen, B. A. Smith, W. P. Ball, and D. H. Fairbrother, “Assessing the colloidal properties of engineered nanoparticles in water: case studies from fullerene C60 nanoparticles and carbon nanotubes,” *Environmental Chemistry*, vol. 7, no. 1, p. 10, 2010.

[594] A. Delgado and E. Matijevié, “Particle size distribution of inorganic colloidal dispersions: A comparison of different techniques,” *Particle & Particle Systems Characterization*, vol. 8, no. 1–4, pp. 128–135, Sep. 1991.

[595] H.-J. Butt, K. Graf, and M. Kappl, “Surface forces,” in *Physics and Chemistry of Interfaces*, WILEY-VCH Verlag GmbH & Co. KGaA, 2003, pp. 80–117.

[596] V. Tandon, S. K. Bhagavatula, W. C. Nelson, and B. J. Kirby, “Zeta potential and electroosmotic mobility in microfluidic devices fabricated from hydrophobic polymers: 1. The origins of charge,” *Electrophoresis*, vol. 29, no. 5, pp. 1092–101, Mar. 2008.

[597] Z. Sun, V. Nicolosi, D. Rickard, S. D. Bergin, D. Aherne, and J. N. Coleman, “Quantitative Evaluation of Surfactant-stabilized Single-walled Carbon Nanotubes: Dispersion Quality and Its Correlation with Zeta Potential,” *Journal of Physical Chemistry C*, vol. 112, no. 29, pp. 10692–10699, Jul. 2008.

[598] L. Jiang, L. Gao, and J. Sun, “Production of aqueous colloidal dispersions of carbon nanotubes,” *Journal of Colloid and Interface Science*, vol. 260, no. 1, pp. 89–94, Apr. 2003.

[599] H. Hu et al., “Influence of the zeta potential on the dispersability and purification of single-walled carbon nanotubes,” *The Journal of Physical Chemistry B*, vol. 109, no. 23, pp. 11520–11524, Jun. 2005.

[600] D. Douroumis, D. G. Fatouros, N. Bouropoulos, K. Papagelis, and D. Tasis, “Colloidal stability of carbon nanotubes in an aqueous dispersion of phospholipid,” *International Journal of*

Nanomedicine, vol. 2, no. 4, pp. 761–6, Jan. 2007.

[601] B. White, S. Banerjee, S. O'Brien, N. J. . Turro, and I. P. Herman, "Zeta-potential measurements of surfactant-wrapped individual single-walled carbon nanotubes," *Journal of Physical Chemistry C*, vol. 111, no. 37, pp. 13684–13690, Sep. 2007.

[602] S. Park and K. Hamad-Schifferli, "Evaluation of hydrodynamic size and zeta-potential of surface-modified Au nanoparticle-DNA conjugates via Ferguson analysis," *Journal of Physical Chemistry C*, vol. 112, no. 20, pp. 7611–7616, May 2008.

[603] S. Park, N. Sinha, and K. Hamad-Schifferli, "Effective size and zeta potential of nanorods by Ferguson analysis," *Langmuir*, vol. 26, no. 16, pp. 13071–13075, Aug. 2010.

[604] E. Heister et al., "Higher dispersion efficacy of functionalized carbon nanotubes in chemical and biological environments," *ACS Nano*, vol. 4, no. 5, pp. 2615–2626, May 2010.

[605] M. Sano, A. Kamino, and S. Shinkai, "Critical coagulation of Langmuir monolayers: 2D Schulze−Hardy rule," *The Journal of Physical Chemistry B*, vol. 104, no. 44, pp. 10339–10347, Nov. 2000.

[606] M. Sano, J. Okamura, and S. Shinkai, "Colloidal nature of single-walled carbon nanotubes in electrolyte solution: The Schulze−Hardy rule," *Langmuir*, vol. 17, no. 22, pp. 7172–7173, Oct. 2001.

[607] N. B. Saleh, L. D. Pfefferle, and M. Elimelech, "Aggregation kinetics of multiwalled carbon nanotubes in aquatic systems: Measurements and environmental implications," *Environmental Science & Technology*, vol. 42, no. 21, pp. 7963–7969, Nov. 2008.

[608] J. Workman, "Ultraviolet, visible, and near-infrared spectrometry," in *Applied Spectroscopy: A Compact Reference for Practitioners*, J. Workman and A. W. Springsteen, Eds. New York: Academic Press, 1998, pp. 29–48.

[609] B. Valeur, "Absorption of UV–visible light," in *Molecular Fluorescence: Principles and Applications*, Wiley-VCH Verlag GmbH & Co. KGaA, 2001, pp. 20–32.

[610] J. Workman, "Optical spectrometers," in *Applied Spectroscopy: A Compact Reference for Practitioners*, J. Workman and A. W. Springsteen, Eds. New York: Academic Press, 1998, pp. 3–28.

[611] D. Breuer, "Molecular spectroscopy in the ultraviolet and visible range," in *The MAK-Collection for Occupational Health and Safety: Part III: Air Monitoring Methods*, vol. 10, H. Parlar and H. Greim, Eds. Weinheim: WILEY-VCH Verlag GmbH & Co. KGaA, 2007, pp. 39–53.

[612] R. Hoffmann, "How chemistry and physics meet in the solid state," *Angewandte Chemie International Edition in English*, vol. 26, no. 9, pp. 846–878, 1987.

[613] A. Gavezzotti, "Supramolecular interactions: Energetic considerations," in *Making Crystals by Design: Methods, Techniques and Applications*, D. Braga and F. Grepioni, Eds. Weinheim, Germany: Wiley-VCH Verlag GmbH & Co. KGaA, 2007, pp. 1–24.

[614] Y. Lian et al., "Assignment of the fine structure in the optical absorption spectra of soluble single-walled carbon nanotubes," *The Journal of Physical Chemistry B*, vol. 107, no. 44, pp. 12082–12087, Nov. 2003.

[615] Y. Miyata, K. Yanagi, Y. Maniwa, and H. Kataura, "Optical properties of metallic and semiconducting single-wall carbon nanotubes," *Physica Status Solidi (B)*, vol. 245, no. 10, pp. 2233–2238, Oct. 2008.

[616] V. A. Karachevtsev, A. M. Plokhotnichenko, M. V. Karachevtsev, and V. S. Leontiev, "Decrease of carbon nanotube UV light absorption induced by π–π-stacking interaction with nucleotide bases," *Carbon*, vol. 48, no. 13, pp. 3682–3691, Nov. 2010.

[617] C. G. Salzmann, B. T. T. Chu, G. Tobias, S. A. Llewellyn, and M. L. H. Green, "Quantitative assessment of carbon nanotube dispersions by Raman spectroscopy," *Carbon*, vol. 45, no. 5, pp. 907–912, Apr. 2007.

[618] A. Ikeda, T. Hamano, K. Hayashi, and J.-I. Kikuchi, "Water-solubilization of nucleotides-coated single-walled carbon nanotubes using a high-speed vibration milling technique," *Organic Letters*, vol. 8, no. 6, pp. 1153–1156, Mar. 2006.

[619] B. Zhao, M. E. Itkis, S. Niyogi, H. Hu, J. Zhang, and R. C. Haddon, "Study of the extinction

coefficients of single-walled carbon nanotubes and related carbon materials," *The Journal of Physical Chemistry B*, vol. 108, no. 24, pp. 8136–8141, Jun. 2004.

[620] B. J. Landi, H. J. Ruf, C. M. Evans, C. D. Cress, and R. P. Raffaelle, "Purity assessment of single-wall carbon nanotubes, using optical absorption spectroscopy.," *The Journal of Physical Chemistry B*, vol. 109, no. 20, pp. 9952–9965, May 2005.

[621] S. Jeong, K. Kim, K. An, S. Lee, and Y. Lee, "Optical absorption spectroscopy for determining carbon nanotube concentration in solution," *Synthetic Metals*, vol. 157, no. 13–15, pp. 570–574, Jul. 2007.

[622] F. Schöppler et al., "Molar extinction coefficient of single-wall carbon nanotubes," *The Journal of Physical Chemistry C*, vol. 115, no. 30, pp. 14682–14686, Aug. 2011.

[623] J. Zhao, C. Jiang, Y. Fan, M. Burghard, T. Basché, and A. Mews, "Diameter-dependent combination modes in individual single-walled carbon nanotubes," *Nano Letters*, vol. 2, no. 8, pp. 823–826, Aug. 2002.

[624] M. S. Strano, S. K. Doorn, E. H. Haroz, C. Kittrell, R. H. Hauge, and R. E. Smalley, "Assignment of (n,m) Raman and optical Features of metallic single-walled carbon nanotubes," *Nano Letters*, vol. 3, no. 8, pp. 1091–1096, Aug. 2003.

[625] M. S. Dresselhaus, A. Jorio, and R. Saito, "Characterizing graphene, graphite, and carbon nanotubes by Raman spectroscopy," *Annual Review of Condensed Matter Physics*, vol. 1, no. 1, pp. 89–108, Aug. 2010.

[626] A. C. Dillon, P. A. Parilla, J. L. Alleman, T. Gennett, K. M. Jones, and M. J. Heben, "Systematic inclusion of defects in pure carbon single-wall nanotubes and their effect on the Raman D-band," *Chemical Physics Letters*, vol. 401, no. 4–6, pp. 522–528, Jan. 2005.

[627] M. S. Dresselhaus, G. Dresselhaus, and M. Hofmann, "The big picture of Raman scattering in carbon nanotubes," *Vibrational Spectroscopy*, vol. 45, no. 2, pp. 71–81, Nov. 2007.

[628] A. Tiberj and J. Camassel, "Raman imaging in semiconductor physics: Applications to microelectronic materials and devices," in *Raman Imaging*, A. Zoubir, Ed. Berlin Heidelberg: Springer-Ve rlag, 2012.

[629] G. Romero, E. Rojas, I. Estrela-Lopis, E. Donath, and S. E. Moya, "Spontaneous confocal Raman microscopy-a tool to study the uptake of nanoparticles and carbon nanotubes into cells," *Nanoscale Research Letters*, vol. 6, no. 1, p. 429(4pp), Jan. 2011.

[630] C. M. Voge and J. P. Stegemann, "Carbon nanotubes in neural interfacing applications," *Journal of Neural Engineering*, vol. 8, no. 1, p. 011001, Feb. 2011.

[631] S. K. Vashist, D. Zheng, G. Pastorin, K. Al-Rubeaan, J. H. T. Luong, and F.-S. Sheu, "Delivery of drugs and biomolecules using carbon nanotubes," *Carbon*, vol. 49, no. 13, pp. 4077–4097, Nov. 2011.

[632] S. W. Lee, B.-S. Kim, S. Chen, Y. Shao-Horn, and P. T. Hammond, "Layer-by-layer assembly of all carbon nanotube ultrathin films for electrochemical applications," *Journal of the American Chemical Society*, vol. 131, no. 2, pp. 671–679, Jan. 2009.

[633] M. N. Hyder, S. W. Lee, F. Ç. Cebeci, D. J. Schmidt, Y. Shao-Horn, and P. T. Hammond, "Layer-by-layer assembled polyaniline nanofiber/multiwall carbon nanotube thin film electrodes for high-power and high-energy storage applications," *ACS Nano*, vol. 5, no. 11, pp. 8552–61, Nov. 2011.

[634] R. K. Gupta and E. Haslam, "Vegetable tannins – Structure and biosynthesis," in *Polyphenols in Cereals and Legumes*, J. H. Hulse, Ed. Ottawa, Ont., Canada: IDRC, 1980, pp. 15–24.

[635] E. Haslam, "Natural polyphenols (vegetable tannins) as drugs: Possible modes of action," *Journal of Natural Products*, vol. 59, no. 2, pp. 205–215, Feb. 1996.

[636] K. Fukuchi et al., "Inhibition of herpes simplex virus infection by tannins and related compounds," *Antiviral Research*, vol. 11, no. 5–6, pp. 285–297, Jun. 1989.

[637] M. Nishizawa et al., "Anti-AIDS agents, 1. Isolation and characterization of four new tetragalloylquinic acids as a new class of HIV reverse transcriptase inhibitors from tannic acid," *Journal of Natural Products*, vol. 52, no. 4, pp. 762–768, Jul. 1989.

[638] H. Akiyama, K. Fujii, O. Yamasaki, T. Oono, and K. Iwatsuki, "Antibacterial action of several tannins against Staphylococcus aureus," *The Journal of Antimicrobial Chemotherapy*, vol. 48,

no. 4, pp. 487–491, 2001.

[639] H. Mukhtar, M. Das, W. A. Khan, Z. Y. Wang, D. P. Bik, and D. R. Bickers, "Exceptional activity of tannic acid among naturally occurring plant phenols in protecting against 7, 12-dimethylbenz(a)anthracene-, benzo(a)pyrene-, 3-methylcholanthrene-, and N-methyl-N-nitrosourea-induced skin tumorigenesis in mice," *Cancer Research*, vol. 48, no. 9, pp. 2361–2365, 1988.

[640] X. Chen et al., "Tannic acid is an inhibitor of CXCL12 (SDF-1alpha)/CXCR4 with antiangiogenic activity," *Clinical Cancer Research*, vol. 9, no. 8, pp. 3115–3123, 2003.

[641] J. Zhang, L. Li, S.-H. Kim, A. E. Hagerman, and J. Lü, "Anti-cancer, anti-diabetic and other pharmacologic and biological activities of penta-galloyl-glucose," *Pharmaceutical Research*, vol. 26, no. 9, pp. 2066–2080, Sep. 2009.

[642] D. A. Kocisko, G. S. Baron, R. Rubenstein, J. Chen, S. Kuizon, and B. Caughey, "New inhibitors of scrapie-associated prion protein formation in a library of 2,000 drugs and natural products," *Journal of Virology*, vol. 77, no. 19, pp. 10288–10294, 2003.

[643] K. Ono, K. Hasegawa, H. Naiki, and M. Yamada, "Anti-amyloidogenic activity of tannic acid and its activity to destabilize Alzheimer's beta-amyloid fibrils in vitro," *Biochimica et Biophysica Acta*, vol. 1690, no. 3, pp. 193–202, Nov. 2004.

[644] Y. Porat, A. Abramowitz, and E. Gazit, "Inhibition of amyloid fibril formation by polyphenols: structural similarity and aromatic interactions as a common inhibition mechanism," *Chemical Biology & Drug Design*, vol. 67, no. 1, pp. 27–37, Jan. 2006.

[645] S. S. Alison, "On the use and administration of tannic acid in various diseases," *London Journal of Medicine*, vol. 2, no. 13, pp. 1–9, 1850.

[646] A. E. Hagerman et al., "High molecular weight plant polyphenolics (tannins) as biological antioxidants," *Journal of Agricultural and Food Chemistry*, vol. 46, no. 5, pp. 1887–1892, May 1998.

[647] Y. Li et al., "Natural anti-diabetic compound 1,2,3,4,6-penta-O-galloyl-D-glucopyranose binds to insulin receptor and activates insulin-mediated glucose transport signaling pathway," *Biochemical and Biophysical Research Communications*, vol. 336, no. 2, pp. 430–437, 2005.

[648] P. Pithayanukul, P. Ruenraroengsak, R. Bavovada, N. Pakmanee, R. Suttisri, and S. Saen-oon, "Inhibition of Naja kaouthia venom activities by plant polyphenols," *Journal of Ethnopharmacology*, vol. 97, no. 3, pp. 527–533, Mar. 2005.

[649] B. Nair, "Final report on the safety assessment of polyvinylpyrrolidone (PVP)," *International Journal of Toxicology*, vol. 17, no. 4 suppl, pp. 95–130, Jan. 1998.

[650] S. Baritaki, G. Tzanakakis, and J. Alifragis, "Light scattering and in vitro biocompatibility studies of poly (vinyl pyrrolidone) derivatives with amino-acid-dependent groups," *Journal of Biomedical Materials Research*, vol. 63, no. 6, pp. 830–837, Jan. 2002.

[651] SCF (Scientific Committee on Food), "Opinion of the Scientific Committee on Food on the safety of N-vinyl-2-pyrrolidone residues in polyvinylpyrrolidone and polyvinylpolypyrrolidone (insoluble polyvinylpyrrolidone) when used as food additives," 2002.

[652] EFSA Panel on Food Additives and Nutrient Sources added to Food (ANS), "Scientific opinion on the safety of polyvinylpyrrolidone-vinyl acetate copolymer for the proposed uses as a food additive," *EFSA Journal*, vol. 8, no. 12, pp. 1948–1976, 2010.

[653] V. Kozlovskaya et al., "Hydrogen-bonded LbL shells for living cell surface engineering," *Soft Matter*, vol. 7, no. 6, p. 2364, 2011.

[654] N. Nakashima, S. Okuzono, H. Murakami, T. Nakai, and K. Yoshikawa, "DNA dissolves single-walled carbon nanotubes in water," *Chemistry Letters*, vol. 32, no. 5, pp. 456–457, 2003.

[655] C. Backes, C. D. Schmidt, K. Rosenlehner, F. Hauke, J. N. Coleman, and A. Hirsch, "Nanotube surfactant design: The versatility of water-soluble perylene bisimides," *Advanced Materials*, vol. 22, no. 7, pp. 788–802, Feb. 2010.

[656] M. W. Forney and J. C. Poler, "Significantly enhanced single-walled carbon nanotube dispersion stability in mixed solvent systems," *The Journal of Physical Chemistry C*, vol. 115, no. 21, pp. 10531–10536, Jun. 2011.

[657] S. Niyogi, C. G. Densmore, and S. K. Doorn, "Electrolyte tuning of surfactant interfacial

behavior for enhanced density-based separations of single-walled carbon nanotubes," *Journal of the American Chemical Society*, vol. 131, no. 3, pp. 1144–1153, Jan. 2009.

[658] M. E. Itkis, D. E. Perea, R. Jung, S. Niyogi, and R. C. Haddon, "Comparison of analytical techniques for purity evaluation of single-walled carbon nanotubes," *Journal of the American Chemical Society*, vol. 127, no. 10, pp. 3439–3448, Mar. 2005.

[659] S. Attal, R. Thiruvengadathan, and O. Regev, "Determination of the concentration of single-walled carbon nanotubes in aqueous dispersions using UV-visible absorption spectroscopy," *Analytical Chemistry*, vol. 78, no. 23, pp. 8098–8104, Dec. 2006.

[660] D. I. Kreller, G. Gibson, W. Novak, G. W. Van Loon, and J. H. Horton, "Competitive adsorption of phosphate and carboxylate with natural organic matter on hydrous iron oxides as investigated by chemical force microscopy," *Colloids and Surfaces A: Physicochemical and Engineering Aspects*, vol. 212, no. 2–3, pp. 249–264, Jan. 2003.

[661] S. A. Simon et al., "Increased adhesion between neutral lipid bilayers: Interbilayer bridges formed by tannic acid," *Biophysical Journal*, vol. 66, no. 6, pp. 1943–1958, Jun. 1994.

[662] S. L. Cumberland and G. F. Strouse, "Analysis of the nature of oxyanion adsorption on gold nanomaterial surfaces," *Langmuir*, vol. 18, no. 1, pp. 269–276, Jan. 2002.

[663] T. Bond, E. H. Goslan, S. A. Parsons, and B. Jefferson, "Disinfection by-product formation of natural organic matter surrogates and treatment by coagulation, MIEX and nanofiltration," *Water research*, vol. 44, no. 5, pp. 1645–1653, Mar. 2010.

[664] R. Osawa and T. P. Walsh, "Effects of acidic and alkaline treatments on tannic acid and its binding property to protein," *Journal of Agricultural and Food Chemistry*, vol. 41, no. 5, pp. 704–707, May 1993.

[665] T. J. Kim, J. L. Silva, M. K. Kim, and Y. S. Jung, "Enhanced antioxidant capacity and antimicrobial activity of tannic acid by thermal processing," *Food Chemistry*, vol. 118, no. 3, pp. 740–746, Feb. 2010.

[666] N. Spreti, A. Bartoletti, P. Di Profio, R. Germani, and G. Savelli, "Effects of ionic and zwitterionic surfactants on the stabilization of bovine catalase," *Biotechnology Progress*, vol. 11, no. 1, pp. 107–111, 1995.

[667] D. J. Schmidt and P. T. Hammond, "Electrochemically erasable hydrogen-bonded thin films," *Chemical Communications*, vol. 46, no. 39, pp. 7358–7360, Oct. 2010.

[668] V. Kozlovskaya, E. Kharlampieva, I. Drachuk, D. Cheng, and V. V. Tsukruk, "Responsive microcapsule reactors based on hydrogen-bonded tannic acid layer-by-layer assemblies," *Soft Matter*, vol. 6, no. 15, pp. 3596–3608, 2010.

[669] J. L. Carter, I. Drachuk, S. Harbaugh, N. Kelley-Loughnane, M. Stone, and V. V. Tsukruk, "Truly nonionic polymer shells for the encapsulation of living cells," *Macromolecular Bioscience*, vol. 11, no. 9, pp. 1244–1253, Sep. 2011.

[670] M. O. Lisunova, I. Drachuk, O. A. Shchepelina, K. D. Anderson, and V. V. Tsukruk, "Direct probing of micromechanical properties of hydrogen-bonded layer-by-layer microcapsule shells with different chemical compositions," *Langmuir*, vol. 27, no. 17, pp. 11157–11165, Sep. 2011.

[671] D. J. Schmidt and P. T. Hammond, "Supplemental Information on 'Electrochemically erasable hydrogen-bonded thin films'," *Chemical Communications*, pp. 1–9, Oct. 2010.

[672] P. Schaaf, J.-C. Voegel, L. Jierry, and F. Boulmedais, "Spray-assisted polyelectrolyte multilayer buildup: from step-by-step to single-step polyelectrolyte film constructions," *Advanced Materials*, vol. 24, no. 8, pp. 1001–1016, Feb. 2012.

[673] L. M. Clayton et al., "Transparent poly(methyl methacrylate)/single-walled carbon nanotube (PMMA/SWNT) composite films with increased dielectric constants," *Advanced Functional Materials*, vol. 15, no. 1, pp. 101–106, Jan. 2005.

[674] Y. N. Yamakoshi, T. Yagami, K. Fukuhara, S. Sueyoshi, and N. Miyata, "Solubilization of fullerenes into water with polyvinylpyrrolidone applicable to biological tests," *Journal of the Chemical Society, Chemical Communications*, no. 4, p. 517, 1994.

[675] M. L. Sushko, H. Tenhu, and S. I. Klenin, "Static and dynamic light scattering study of strong intermolecular interactions in aqueous solutions of PVP/C60 complexes," *Polymer*, vol. 43, no.

9, pp. 2769–2775, Apr. 2002.
[676] E. Tarassova, V. Aseyev, H. Tenhu, and S. Klenin, “Poly(vinyl pyrrolidone)—C70 complexes in aqueous solutions,” *Polymer*, vol. 44, no. 17, pp. 4863–4870, Aug. 2003.
[677] E. Tarassova, V. Aseyev, A. Filippov, and H. Tenhu, “Structure of poly(vinyl pyrrolidone) – C70 complexes in aqueous solutions,” *Polymer*, vol. 48, no. 15, pp. 4503–4510, Jul. 2007.
[678] W. Guan, C. Wu, and H. Lu, “Synthesis of polyvinylpyrrolidone-coated carbon nanotubes [in Chinese],” *Huazhong Keji Daxue Xuebao, Ziran Kexueban*, vol. 30, pp. 114–116, 2002.
[679] V. C. Moore et al., “Individually suspended single-walled carbon nanotubes in various surfactants,” *Nano Letters*, vol. 3, no. 10, pp. 1379–1382, Oct. 2003.
[680] T. Hasan, V. Scardaci, P. Tan, A. G. Rozhin, W. I. Milne, and A. C. Ferrari, “Stabilization and ‘debundling’ of single-wall carbon nanotube dispersions in N-Methyl-2-pyrrolidone (NMP) by polyvinylpyrrolidone (PVP),” *Journal of Physical Chemistry C*, vol. 111, no. 34, pp. 12594–12602, Aug. 2007.
[681] T. J. Simmons, S.-H. Lee, T.-J. Park, D. P. Hashim, P. M. Ajayan, and R. J. Linhardt, “Antiseptic single wall carbon nanotube bandages,” *Carbon*, vol. 47, no. 6, pp. 1561–1564, May 2009.
[682] A. B. Bourlinos, V. Georgakilas, R. Zboril, T. A. Steriotis, A. K. Stubos, and C. Trapalis, “Aqueous-phase exfoliation of graphite in the presence of polyvinylpyrrolidone for the production of water-soluble graphenes,” *Solid State Communications*, vol. 149, no. 47–48, pp. 2172–2176, Dec. 2009.
[683] Q. Huang et al., “Donor–acceptor nanoensembles based on boron nitride nanotubes,” *Advanced Materials*, vol. 19, no. 7, pp. 934–938, Apr. 2007.
[684] G. Decher, “Layer-by-layer assembly (putting molecules to work),” in *Multilayer Thin Films: Sequential Assembly of Nanocomposite Materials*, 2nd Ed., G. Decher and J. B. Schlenoff, Eds. Weinheim, Germany: Wiley-VCH Verlag GmbH & Co. KGaA, 2012, pp. 1–22.
[685] V. V. Khutoryanskiy, “Hydrogen-bonded interpolymer complexes as materials for pharmaceutical applications,” *International Journal of Pharmaceutics*, vol. 334, no. 1–2, pp. 15–26, Apr. 2007.
[686] J. F. Quinn and F. Caruso, “Facile tailoring of film morphology and release properties using layer-by-layer assembly of thermoresponsive materials,” *Langmuir*, vol. 20, no. 1, pp. 20–22, Jan. 2004.
[687] I. Erel-Unal and S. A. Sukhishvili, “Hydrogen-bonded hybrid multilayers: Film architecture controls release of macromolecules,” *Macromolecules*, vol. 41, no. 22, pp. 8737–8744, 2008.
[688] B.-S. Kim, R. C. Smith, Z. Poon, and P. T. Hammond, “MAD (multiagent delivery) nanolayer: delivering multiple therapeutics from hierarchically assembled surface coatings,” *Langmuir*, vol. 25, no. 24, pp. 14086–14092, Dec. 2009.
[689] G. K. Such, A. P. R. Johnston, and F. Caruso, “Engineered hydrogen-bonded polymer multilayers: from assembly to biomedical applications,” *Chemical Society Reviews*, vol. 40, no. 1, pp. 19–29, Jan. 2011.
[690] P. T. Hammond, “Building biomedical materials layer-by-layer,” *Materials Today*, vol. 15, no. 5, pp. 196–206, May 2012.
[691] H. Hong, R. Steitz, S. Kirstein, and D. Davidov, “Superlattice structures in poly(phenylenevinylene)-based self-assembled films,” *Advanced Materials*, vol. 10, no. 14, pp. 1104–1108, Oct. 1998.
[692] S.-S. Lee, J.-D. Hong, C. H. Kim, K. Kim, J. P. Koo, and K.-B. Lee, “Layer-by-layer deposited multilayer assemblies of ionene-type polyelectrolytes based on the spin-coating method,” *Macromolecules*, vol. 34, no. 16, pp. 5358–5360, Jul. 2001.
[693] A. Shukla, S. N. Avadhany, J. C. Fang, and P. T. Hammond, “Tunable vancomycin releasing surfaces for biomedical applications,” *Small*, vol. 6, no. 21, pp. 8–10, 2010.
[694] P. A. Chiarelli, M. S. Johal, D. J. Holmes, J. L. Casson, J. M. Robinson, and H.-L. Wang, “Polyelectrolyte spin-assembly,” *Langmuir*, vol. 18, no. 1, pp. 168–173, 2002.
[695] H. Jang and S. Kim, “Spin-coated ultrathin multilayers and their micropatterning using microfluidic channels,” *Korea-Australia Rheology Journal*, vol. 15, no. 1, pp. 1–7, 2003.

[696] J. Cho and K. Char, “Effect of layer integrity of spin self-assembled multilayer films on surface wettability,” *Langmuir*, vol. 20, no. 10, pp. 4011–4016, May 2004.

[697] P. A. Patel, A. V. Dobrynin, and P. T. Mather, “Combined effect of spin speed and ionic strength on polyelectrolyte spin assembly,” *Langmuir*, vol. 23, no. 25, pp. 12589–12597, Dec. 2007.

[698] M. Raposo, R. S. Pontes, L. H. C. Mattoso, and O. N. Oliveira, “Kinetics of adsorption of poly(o-methoxyaniline) self-assembled films,” *Macromolecules*, vol. 30, no. 20, pp. 6095–6101, Oct. 1997.

[699] P. J. Yoo et al., “Spontaneous assembly of viruses on multilayered polymer surfaces,” *Nature Materials*, vol. 5, no. 3, pp. 234–240, Mar. 2006.

[700] P. J. Yoo, N. S. Zacharia, J. Doh, K. T. Nam, A. M. Belcher, and P. T. Hammond, “Controlling surface mobility in interdiffusing polyelectrolyte multilayers,” *ACS Nano*, vol. 2, no. 3, pp. 561–571, Mar. 2008.

[701] P. T. Hammond, “Engineering materials layer-by-layer: Challenges and opportunities in multilayer assembly,” *AIChE Journal*, vol. 57, no. 11, pp. 2928–2940, 2011.

[702] B.-H. Sohn, T.-H. Kim, and K. Char, “Process-dependent photocatalytic properties of polymer thin films containing TiO2 nanoparticles: Dip vs spin self-assembly methods,” *Langmuir*, vol. 18, no. 21, pp. 7770–7772, Oct. 2002.

[703] Y. M. Lee et al., “Spin-assembled layer-by-layer films of weakly charged polyelectrolyte multilayer,” *Journal of Nanoscience and Nanotechnology*, vol. 9, no. 12, pp. 1–6, 2009.

[704] C. J. Lawrence, “The mechanics of spin coating of polymer films,” *Physics of Fluids*, vol. 31, no. 10, p. 2786, 1988.

[705] R. Yonkoski and D. Soane, “Model for spin coating in microelectronic applications,” *Journal of applied physics*, vol. 72, no. 2, p. 725, 1992.

[706] P. G. De Gennes, P. Pincus, R. M. Velasco, and F. Brochard, “Remarks on polyelectrolyte conformation,” *Journal de Physique*, vol. 37, no. 12, pp. 1461–1473, 1976.

[707] M. Rubinstein, R. Colby, and A. Dobrynin, “Dynamics of semidilute polyelectrolyte solutions,” *Physical Review Letters*, vol. 73, no. 20, pp. 2776–2779, Nov. 1994.

[708] A. Dobrynin, R. Colby, and M. Rubinstein, “Scaling theory of polyelectrolyte solutions,” *Macromolecules*, pp. 1859–1871, 1995.

[709] B. Madhan, A. Dhathathreyan, V. Subramanian, and T. Ramasami, “Investigations on geometrical features in induced ordering of collagen by small molecules,” *Journal of Chemical Sciences*, vol. 115, no. 5–6, pp. 751–766, Oct. 2003.

[710] M. S. Johal et al., “Polyelectrolyte trilayer combinations using spin-assembly and ionic self-assembly,” *Langmuir*, vol. 21, no. 23, pp. 8876–8881, 2003.

[711] B. Reisfeld, S. G. Bankoff, and S. H. Davis, “The dynamics and stability of thin liquid films during spin coating. I. Films with constant rates of evaporation or absorption,” *Journal of Applied Physics*, vol. 70, no. 10, pp. 5258–5266, 1991.

[712] A. Weill and E. Dechenaux, “The spin-coating process mechanism related to polymer solution properties,” *Polymer Engineering and Science*, vol. 28, no. 15, pp. 945–948, Aug. 1988.

[713] S. Walheim, M. Böltau, J. Mlynek, G. Krausch, and U. Steiner, “Structure formation via polymer demixing in spin-cast films,” *Macromolecules*, vol. 30, no. 17, pp. 4995–5003, Aug. 1997.

[714] F. Ilhan, L. Diamondis, L. Gautreau, and V. M. Rotello, “Kinetic trapping of host–guest complexes in a polymeric matrix,” *Chemical Communications*, no. 6, pp. 447–448, 2000.

[715] J. Yu, D. Hu, and P. F. Barbara, “Unmasking electronic energy transfer of conjugated polymers by suppression of O2 quenching,” *Science*, vol. 289, no. 5483, pp. 1327–1330, Aug. 2000.

[716] M. Stamm and J.-U. Sommer, “Polymer-nanoparticle films: Entropy and enthalpy at play,” *Nature Materials*, vol. 6, no. 4, pp. 260–261, Apr. 2007.

[717] G. Reiter and S. Napolitano, “Possible origin of thickness-dependent deviations from bulk properties of thin polymer films,” *Journal of Polymer Science Part B: Polymer Physics*, vol. 48, no. 24, pp. 2544–2547, Dec. 2010.

[718] P. Wang and J. T. Koberstein, “Morphology of immiscible polymer blend thin films prepared

by spin-coating," *Macromolecules*, vol. 37, no. 15, pp. 5671–5681, Jul. 2004.
[719] R. S. Krishnan et al., "Self-assembled multilayers of nanocomponents," *Nano Letters*, vol. 7, no. 2, pp. 484–489, Feb. 2007.
[720] Z. Feldötö, I. Varga, and E. Blomberg, "Influence of salt and rinsing protocol on the structure of PAH/PSS polyelectrolyte multilayers," *Langmuir*, vol. 26, no. 22, pp. 17048–17057, Nov. 2010.
[721] C. M. Andres and N. A. Kotov, "Inkjet deposition of layer-by-layer assembled films," *Journal of the American Chemical Society*, vol. 132, no. 41, pp. 14496–14502, Oct. 2010.
[722] R. Maoz, J. Sagiv, H. Möhwald, and P. Quint, "Hydrogen-bonded multilayers of self-assembling silanes: structure elucidation by combined Fourier transform infra-red spectroscopy and X-ray scattering techniques," *Supramolecular Science*, vol. 2, no. 1, pp. 9–24, 1995.
[723] A. B. Artyukhin, O. Bakajin, P. Stroeve, and A. Noy, "Layer-by-Layer electrostatic self-assembly of polyelectrolyte nanoshells on individual carbon nanotube templates," *Langmuir*, vol. 20, no. 4, pp. 1442–1448, Feb. 2004.
[724] H. Paloniemi et al., "Water-soluble full-length single-wall carbon nanotube polyelectrolytes: Preparation and characterization," *The Journal of Physical Chemistry B*, vol. 109, no. 18, pp. 8634–8642, May 2005.
[725] H. Paloniemi et al., "Layer-by-layer electrostatic self-assembly of single-wall carbon nanotube polyelectrolytes," *Langmuir*, vol. 22, no. 1, pp. 74–83, Jan. 2006.
[726] J. M. Hughes, H. Cathcart, and J. N. Coleman, "Dispersion and exfoliation of nanotubes with synthetic oligonucleotides: Variation of dispersion efficiency and oligo-nanotube interaction with base type," *The Journal of Physical Chemistry C*, vol. 114, no. 27, pp. 11741–11747, Jul. 2010.
[727] M. F. Islam, E. Rojas, D. M. Bergey, A. T. Johnson, and A. G. Yodh, "High weight fraction surfactant solubilization of single-wall carbon nanotubes in water," *Nano Letters*, vol. 3, no. 2, pp. 269–273, Feb. 2003.
[728] O. Matarredona, H. Rhoads, Z. Li, J. H. Harwell, L. Balzano, and D. E. Resasco, "Dispersion of single-walled carbon nanotubes in aqueous solutions of the anionic surfactant NaDDBS," *The Journal of Physical Chemistry B*, vol. 107, no. 48, pp. 13357–13367, Dec. 2003.
[729] A. J. Blanch, C. E. Lenehan, and J. S. Quinton, "Optimizing surfactant concentrations for dispersion of single-walled carbon nanotubes in aqueous solution," *The Journal of Physical Chemistry B*, vol. 114, no. 30, pp. 9805–9811, Aug. 2010.
[730] H. Hyung and J.-H. Kim, "Natural organic matter (NOM) adsorption to multi-walled carbon nanotubes: Effect of NOM characteristics and water quality parameters," *Environmental Science & Technology*, vol. 42, no. 12, pp. 4416–4421, 2008.
[731] R. Rastogi, R. Kaushal, S. K. Tripathi, A. L. Sharma, I. Kaur, and L. M. Bharadwaj, "Comparative study of carbon nanotube dispersion using surfactants," *Journal of Colloid and Interface Science*, vol. 328, no. 2, pp. 421–428, Dec. 2008.
[732] B. Koh, J. B. Park, X. Hou, and W. Cheng, "Comparative dispersion studies of single-walled carbon nanotubes in aqueous solution," *The Journal of Physical Chemistry B*, vol. 115, no. 11, pp. 2627–33, Mar. 2011.
[733] M. F. Lin and D. S. Chuu, "π plasmons in carbon nanotube bundles," *Physical Review B*, vol. 57, no. 16, pp. 10183–10187, Apr. 1998.
[734] S. Reich, C. Thomsen, and P. Ordejón, "Electronic band structure of isolated and bundled carbon nanotubes," *Physical Review B*, vol. 65, no. 15, pp. 1–11, Mar. 2002.
[735] A. G. Ryabenko, T. V. Dorofeeva, and G. I. Zvereva, "UV–VIS–NIR spectroscopy study of sensitivity of single-wall carbon nanotubes to chemical processing and Van-der-Waals SWNT/SWNT interaction. Verification of the SWNT content measurements by absorption spectroscopy," *Carbon*, vol. 42, no. 8–9, pp. 1523–1535, 2004.
[736] A. Naumov, S. Ghosh, D. A. Tsyboulski, S. M. Bachilo, and R. B. Weisman, "Analyzing absorption backgrounds in single-walled carbon nanotube spectra," *ACS Nano*, vol. 5, no. 3, pp. 1639–1648, 2011.
[737] A. Star et al., "Preparation and properties of polymer-wrapped single-walled carbon

nanotubes," *Angewandte Chemie International Edition in English*, vol. 40, no. 9, pp. 1721–1725, 2001.

[738] D. Simien, J. A. Fagan, W. Luo, J. F. Douglas, K. Migler, and J. Obrzut, "Influence of nanotube length on the optical and conductivity properties of thin single-wall carbon nanotube networks," *ACS Nano*, vol. 2, no. 9, pp. 1879–1884, Sep. 2008.

[739] J. L. Hernandez-López, E. R. Alvizo-Páez, S. E. Moya, and J. Ruiz-García, "Trapping, pattern formation, and ordering of polyelectrolyte/single-wall carbon nanotube complexes at the air/water and air/solid interfaces," *The Journal of Physical Chemistry B*, vol. 110, no. 46, pp. 23179–23191, Nov. 2006.

[740] Y. Yan, J. Cui, P. Pötschke, and B. Voit, "Dispersion of pristine single-walled carbon nanotubes using pyrene-capped polystyrene and its application for preparation of polystyrene matrix composites," *Carbon*, vol. 48, no. 9, pp. 2603–2612, Aug. 2010.

[741] A. Buso, L. Balbo, M. Giomo, G. Farnia, and G. Sandonà, "Electrochemical removal of tannins from aqueous solutions," *Industrial & Engineering Chemistry Research*, vol. 39, no. 2, pp. 494–499, Feb. 2000.

[742] Y. Nagata, K. Hirai, H. Bandow, and Y. Maeda, "Decomposition of hydroxybenzoic and humic acids in water by ultrasonic irradiation," *Environmental Science & Technology*, vol. 30, no. 4, pp. 1133–1138, Jan. 1996.

[743] J. D. Seymour and R. B. Gupta, "Oxidation of aqueous pollutants using ultrasound: Salt-induced enhancement," *Industrial & Engineering Chemistry Research*, vol. 36, no. 9, pp. 3453–3457, Sep. 1997.

[744] P. R. Gogate, S. Mujumdar, J. Thampi, A. M. Wilhelm, and A. B. Pandit, "Destruction of phenol using sonochemical reactors: scale up aspects and comparison of novel configuration with conventional reactors," *Separation and Purification Technology*, vol. 34, no. 1–3, pp. 25–34, Jan. 2004.

[745] E. Taylor, B. B. Cook, and M. A. Tarr, "Dissolved organic matter inhibition of sonochemical degradation of aqueous polycyclic aromatic hydrocarbons," *Ultrasonics Sonochemistry*, vol. 6, no. 4, pp. 175–183, Sep. 1999.

[746] Z. Laughrey, E. Bear, R. Jones, and M. A. Tarr, "Aqueous sonolytic decomposition of polycyclic aromatic hydrocarbons in the presence of additional dissolved species," *Ultrasonics Sonochemistry*, vol. 8, no. 4, pp. 353–357, Oct. 2001.

[747] B. M. I. van der Zande, J. K. G. Dhont, M. R. Böhmer, and A. P. Philipse, "Colloidal dispersions of gold rods characterized by dynamic light scattering and electrophoresis," *Langmuir*, vol. 16, no. 2, pp. 459–464, Jan. 2000.

[748] S. N. Katekhaye and P. R. Gogate, "Intensification of cavitational activity in sonochemical reactors using different additives: Efficacy assessment using a model reaction," *Chemical Engineering and Processing: Process Intensification*, vol. 50, no. 1, pp. 95–103, Jan. 2011.

[749] K. Ghosh and M. Schnitzer, "Macromolecular structures of humic substances," *Soil Science*, vol. 129, no. 5, p. 266, 1980.

[750] A. Piccolo, S. Nardi, and G. Concheri, "Macromolecular changes of humic substances induced by interaction with organic acids," *European Journal of Soil Science*, vol. 47, no. 3, pp. 319–328, Sep. 1996.

[751] E. Chibowski, M. Espinosa-Jiménez, A. Ontiveros-Ortega, and E. Giménez-Martin, "Surface free energy, adsorption and zeta potential in leacril/tannic acid system," *Langmuir*, vol. 14, no. 18, pp. 5237–5244, Sep. 1998.

[752] P. Conte and A. Piccolo, "Conformational arrangement of dissolved humic substances. Influence of solution composition on association of humic molecules," *Environmental Science & Technology*, vol. 33, no. 10, pp. 1682–1690, May 1999.

[753] S. C. B. Myneni, J. T. Brown, G. A. Martinez, and W. Meyer-Ilse, "Imaging of humic substance macromolecular structures in water and soils," *Science*, vol. 286, no. 5443, pp. 1335–1337, Nov. 1999.

[754] B. Varga, G. Kiss, I. Galambos, A. Gelencsér, J. Hlavay, and Z. Krivácsy, "Secondary structure of humic acids. Can micelle-like conformation be proved by aqueous size exclusion chromatography?," *Environmental Science & Technology*, vol. 34, no. 15, pp. 3303–3306,

Aug. 2000.
[755] S. L. de Moraes and M. O. O. Rezende, “Behavior of humic acid as a micellar phase in micellar electrokinetic chromatography (MEKC),” *Microchimica Acta*, vol. 151, no. 1–2, pp. 115–122, Jul. 2005.
[756] H.-C. Lin, P.-C. Chen, T.-J. Cheng, and R. L. C. Chen, “Formation of tannin–albumin nano-particles at neutral pH as measured by light scattering techniques,” *Analytical Biochemistry*, vol. 325, no. 1, pp. 117–120, Feb. 2004.
[757] L. Wu, “Thermal effects on liquid film dynamics in spin coating,” *Sensors and Actuators A: Physical*, vol. 134, no. 1, pp. 140–145, 2007.
[758] C. S. Peyratout and L. Dähne, “Tailor-made polyelectrolyte microcapsules: From multilayers to smart containers,” *Angewandte Chemie International Edition in English*, vol. 43, no. 29, pp. 3762–3783, Jul. 2004.
[759] M. McDonald, I. Mila, and A. Scalbert, “Precipitation of metal ions by plant polyphenols: Optimal conditions and origin of precipitation,” *Journal of Agricultural and Food Chemistry*, vol. 44, no. 2, pp. 599–606, Jan. 1996.
[760] R. V. Barbehenn and M. M. Martin, “Formation of insoluble and colloidally dispersed tannic acid complexes in the midgut fluid ofManduca sexta (Lepidoptera: Sphingidae): An explanation for the failure of tannic acid to cross the peritrophic envelopes of lepidopteran larvae,” *Archives of Insect Biochemistry and Physiology*, vol. 39, no. 3, pp. 109–117, 1998.
[761] S. Koda, H. Mori, K. Matsumoto, and H. Nomura, “Ultrasonic degradation of water-soluble polymers,” *Polymer*, vol. 35, no. 1, pp. 30–33, Jan. 1994.
[762] A. Henglein, “Chemical effects of continuous and pulsed ultrasound in aqueous solutions,” *Ultrasonics Sonochemistry*, vol. 2, no. 2, pp. S115–S121, Jan. 1995.
[763] T. Aarthi, M. S. Shaama, and G. Madras, “Degradation of water soluble polymers under combined ultrasonic and ultraviolet radiation,” *Industrial & Engineering Chemistry Research*, vol. 46, no. 19, pp. 6204–6210, Sep. 2007.
[764] M. T. Taghizadeh and A. Bahadori, “Degradation kinetics of poly (vinyl-pyrrolidone) under ultrasonic irradiation,” *Journal of Polymer Research*, vol. 16, no. 5, pp. 545–554, Dec. 2008.
[765] A. Mehrdad, “Ultrasonic degradation of polyvinyl pyrrolidone in mixed water/acetone,” *Journal of Applied Polymer Science*, vol. 120, no. 6, pp. 3701–3708, Jun. 2011.
[766] J. N. Coleman et al., “Percolation-dominated conductivity in a conjugated-polymer-carbon-nanotube composite,” *Physical Review B*, vol. 58, no. 12, pp. R7492–R7495, 1998.
[767] L. Hu, D. S. Hecht, and G. Grüner, “Percolation in transparent and conducting carbon nanotube networks,” *Nano Letters*, vol. 4, no. 12, pp. 2513–2517, Dec. 2004.
[768] F. S. Gittleson, D. J. Kohn, X. Li, and A. D. Taylor, “Improving the assembly speed, quality, and tunability of thin conductive multilayers,” *ACS Nano*, vol. 6, no. 5, pp. 3703–3711, May 2012.
[769] C. A. Hunter and J. K. M. Sanders, “The nature of π-π interactions,” *Journal of the American Chemical Society*, vol. 112, no. 14, pp. 5525–5534, Jul. 1990.
[770] C. A. Hunter, “Arene—arene interactions: Electrostatic or charge transfer?,” *Angewandte Chemie International Edition in English*, vol. 32, no. 11, pp. 1584–1586, Nov. 1993.
[771] S. Grimme, “Do special noncovalent π-π stacking interactions really exist?,” *Angewandte Chemie International Edition in English*, vol. 47, no. 18, pp. 3430–3484, Jan. 2008.
[772] T. Tang, J. Qu, K. Müllen, and S. E. Webber, “Molecular layer-by-layer self-assembly of water-soluble perylene diimides through π-π and electrostatic interactions,” *Langmuir*, vol. 22, no. 1, pp. 26–28, Jan. 2006.
[773] S. E. Burke and C. J. Barrett, “Acid-base equilibria of weak polyelectrolytes in multilayer thin films,” *Langmuir*, vol. 19, no. 8, pp. 3297–3303, Apr. 2003.
[774] S. E. Burke and C. J. Barrett, “pH-Responsive properties of multilayered poly(L-lysine)/hyaluronic acid surfaces,” *Biomacromolecules*, vol. 4, no. 6, pp. 1773–1783, 2003.
[775] P. Mignon, S. Loverix, F. De Proft, and P. Geerlings, “Influence of stacking on hydrogen bonding: Quantum chemical study on pyridine−benzene model complexes,” *The Journal of Physical Chemistry A*, vol. 108, no. 28, pp. 6038–6044, Jul. 2004.

[776] P. Mignon, S. Loverix, J. Steyaert, and P. Geerlings, “Influence of the pi-pi interaction on the hydrogen bonding capacity of stacked DNA/RNA bases,” *Nucleic Acids Research*, vol. 33, no. 6, pp. 1779–1789, Jan. 2005.

[777] Y. Miyata, K. Mizuno, and H. Kataura, “Purity and defect characterization of single-wall carbon nanotubes using Raman spectroscopy,” *Journal of Nanomaterials*, vol. 2011, no. Cvd, pp. 1–7, 2011.

[778] B. L. Allen et al., “Biodegradation of single-walled carbon nanotubes through enzymatic catalysis,” *Nano Letters*, vol. 8, no. 11, pp. 3899–3903, Nov. 2008.

[779] B. L. Allen et al., “Mechanistic investigations of horseradish peroxidase-catalyzed degradation of single-walled carbon nanotubes,” *Journal of the American Chemical Society*, vol. 131, no. 47, pp. 17194–205, Dec. 2009.

[780] X. Liu, R. H. Hurt, and A. B. Kane, “Biodurability of single-walled carbon nanotubes depends on surface functionalization,” *Carbon*, vol. 48, no. 7, pp. 1961–1969, Jun. 2010.

[781] T. Sun and H. E. King, “Aggregation behavior in the semidilute poly(N-vinyl-2-pyrrolidone)/water system,” *Macromolecules*, vol. 29, no. 9, pp. 3175–3181, Jan. 1996.

[782] P. Sakellariou, “Theta temperature of poly(N-vinyl pyrrolidone) in water,” *Polymer*, vol. 33, no. 6, pp. 1339–1342, Jan. 1992.

[783] F. Ma, “Flow of a thin film over a rough rotating disk,” *Probabilistic Engineering Mechanics*, vol. 9, no. 1–2, pp. 39–45, Jan. 1994.

[784] M. Schönhoff et al., “Hydration and internal properties of polyelectrolyte multilayers,” *Colloids and Surfaces A: Physicochemical and Engineering Aspects*, vol. 303, no. 1–2, pp. 14–29, 2007.

[785] S. Meuer, L. Braun, T. Schilling, and R. Zentel, “α-Pyrene polymer functionalized multiwalled carbon nanotubes: Solubility, stability and depletion phenomena,” *Polymer*, vol. 50, no. 1, pp. 154–160, 2009.

[786] S. Robinson and P. A. Williams, “Inhibition of protein adsorption onto silica by polyvinylpyrrolidone,” *Langmuir*, vol. 18, no. 23, pp. 8743–8748, 2002.

[787] C. R. Kinnane et al., “Low-fouling poly(N-vinyl pyrrolidone) capsules with engineered degradable properties,” *Biomacromolecules*, vol. 10, no. 10, pp. 2839–2846, Oct. 2009.

[788] B. Rybtchinski, “Adaptive supramolecular nanomaterials based on strong noncovalent interactions,” *ACS Nano*, vol. 5, no. 9, pp. 6791–6818, Sep. 2011.

[789] V. S. Moholkar, P. Senthil Kumar, and A. B. Pandit, “Hydrodynamic cavitation for sonochemical effects,” *Ultrasonics Sonochemistry*, vol. 6, no. 1–2, pp. 53–65, Mar. 1999.

[790] V. S. Moholkar and A. B. Pandit, “Modeling of hydrodynamic cavitation reactors: a unified approach,” *Chemical Engineering Science*, vol. 56, no. 21–22, pp. 6295–6302, Nov. 2001.

[791] P. R. Gogate and A. B. Pandit, “A review and assessment of hydrodynamic cavitation as a technology for the future,” *Ultrasonics Sonochemistry*, vol. 12, no. 1–2, pp. 21–7, Jan. 2005.

[792] M. Keiluweit and M. Kleber, “Molecular-level interactions in soils and sediments: The role of aromatic π-systems,” *Environmental Science & Technology*, vol. 43, no. 10, pp. 3421–3429, May 2009.

[793] D. Marenduzzo, K. Finan, and P. R. Cook, “The depletion attraction: an underappreciated force driving cellular organization,” *The Journal of Cell Biology*, vol. 175, no. 5, pp. 681–686, Dec. 2006.

[794] J. Spitzer and B. Poolman, “The role of biomacromolecular crowding, ionic strength, and physicochemical gradients in the complexities of life’s emergence,” *Microbiology and Molecular Biology Reviews*, vol. 73, no. 2, pp. 371–388, Jun. 2009.

[795] S. Zhang, T. Holmes, C. Lockshin, and A. Rich, “Spontaneous assembly of a self-complementary oligopeptide to form a stable macroscopic membrane,” *Proceedings of the National Academy of Sciences of the United States of America*, vol. 90, no. 8, pp. 3334–3348, Apr. 1993.

[796] S. Gilead and E. Gazit, “Self-organization of short peptide fragments: From amyloid fibrils to nanoscale supramolecular assemblies,” *Supramolecular Chemistry*, vol. 17, no. 1–2, pp. 87–92, 2005.

[797] A. Lakshmanan and C. A. E. Hauser, “Ultrasmall peptides self-assemble into diverse nanostructures: morphological evaluation and potential implications.,” *International Journal of Molecular Sciences*, vol. 12, no. 9, pp. 5736–5746, Jan. 2011.

[798] L. Allen, “A limber future,” *Popular Science*, no. 36, pp. 1–2, 2004.

[799] L. C. Winterton, J. M. Lally, M. Rubner, and Y. Qiu, “Single-dip process for achieving a layer-by-layer-like coating,” U.S. Patent US6793973B22004.

[800] J. Gorman, “Layered approach: A simple technique for making thin coatings is poised to shift from curiosity to commodity,” *Science News*, vol. 164, no. 6, p. 91, Aug. 2003.

[801] T. I. T. Okpalugo, P. Papakonstantinou, H. Murphy, J. McLaughlin, and N. M. D. Brown, “High resolution XPS characterization of chemical functionalised MWCNTs and SWCNTs,” *Carbon*, vol. 43, no. 1, pp. 153–161, Jan. 2005.

[802] G. Ladam, P. Schaad, J. C. Voegel, P. Schaaf, G. Decher, and F. Cuisinier, “In situ determination of the structural properties of initially deposited polyelectrolyte multilayers,” *Langmuir*, vol. 16, no. 3, pp. 1249–1255, Feb. 2000.

[803] Z. Sui, D. Salloum, and J. B. Schlenoff, “Effect of molecular weight on the construction of polyelectrolyte multilayers: Stripping versus sticking,” *Langmuir*, vol. 19, no. 6, pp. 2491–2495, Mar. 2003.

[804] T. Ramanathan, F. T. Fisher, R. S. Ruoff, and L. C. Brinson, “Amino-functionalized carbon nanotubes for binding to polymers and biological systems,” *Chemistry of Materials*, vol. 17, no. 6, pp. 1290–1295, Mar. 2005.

VITA

Hüseyin Enis KARAHAN was born in 1985 in Dicle (Diyarbakir, Turkey). He started his high school period in Zonguldak Science High School and he graduated from Eyüboğlu Science High School (2003). He received his first BSc degree in Chemical Engineering from İstanbul Technical University, İstanbul, in September of 2008 with a design project on H_2 production from coal, and a graduation project on blending of water-borne polyurethanes with chitosan. The following year (2009), he obtained his double major degree from Molecular Biology and Genetics Department of the same university with a graduation project on identification of polyphenol oxidase genes of an industrially important fungus. During undergraduate times, he worked in different companies including an R&D department of a textile company which is specialized in polyurethane membranes and foams (2007-2008). In his undergraduate period, he also held a five month student assistantship position in Molecular Biology. He enrolled to Master Program of Material Science and Engineering at Koç University in 2009. He worked as a teaching and research assistant in Chemistry Department of Koç University (2009-2012). He served in general, organic and analytical chemistry student laboratories; and he also lectured in problem sessions in general chemistry. His research activities in Koç University covered a broad spectrum of materials science including self-assembly of polymers, noncovalent modification of nanoparticles, fabrication of multilayer films, designing of organic-inorganic nanocomposites, and ultrasound-assisted synthesis of inorganic particles to name a few. Out of those activities, he had 8 conference presentations, and 1 publication to his credit and a series of publications are in progress for submission.

L’arte non è mai finita, solo abbandonato.

[Art is never finished, only abandoned.]

Leonardo di ser Piero da VINCI (1452 – 1519)